Michael Schmischke

Interpretable Approximation of High-Dimensional Data based on the ANOVA Decomposition

Michael Schmischke

Interpretable Approximation of High-Dimensional Data based on the ANOVA Decomposition

TECHNISCHE UNIVERSITÄT
CHEMNITZ

Universitätsverlag Chemnitz
2022

Impressum

Bibliografische Information der Deutschen Nationalbibliothek

Die Deutsche Nationalbibliothek verzeichnet diese Publikation in der Deutschen Nationalbibliografie; detaillierte bibliografische Angaben sind im Internet über https://www.dnb.de abrufbar.

Titelgrafik: Michael Schmischke
Satz/Layout: Michael Schmischke

Technische Universität Chemnitz/Universitätsbibliothek
Universitätsverlag Chemnitz
09107 Chemnitz
https://www.tu-chemnitz.de/ub/univerlag

Herstellung:
Bookwire GmbH Frankfurt am Main

Print on Demand
Gedruckt auf FSC-zertifiziertem Papier

ISBN 978-3-96100-164-4

https://nbn-resolving.de/urn:nbn:de:bsz:ch1-qucosa2-791415

Interpretable Approximation of High-Dimensional Data based on the ANOVA Decomposition

von der Fakultät für Mathematik
der Technischen Universität Chemnitz
genehmigte

Dissertation

zur Erlangung des akademischen Grades

doctor rerum naturalium
(Dr. rer. nat.)

vorgelegt von
Michael Schmischke, M. Sc.

Tag der Einreichung: 03. Februar 2022

Betreuer: Prof. Dr. Daniel Potts, Technische Universität Chemnitz

Gutachter: Prof. Dr. Daniel Potts, Technische Universität Chemnitz
Prof. Dr. Michael Gnewuch, Universität Osnabrück
Prof. Dr. Ingo Steinwart, Universität Stuttgart

Tag der Öffentlichen Prüfung: 11. Mai 2022

Contents

1 Introduction

We are living in a digital age where the amount of data humanity is creating increases constantly. On average, the stunning amount of 1 134 000 terabytes or 1.134 exabytes is generated globally each day. This number is expected to rise to about 463 exabytes per day in 2025. In the area of machine learning, we create models based on data we have available with the goal to make predictions for unknown cases. Today, the applications are rising inflationary and these models are present in our everyday life as never before with data sets becoming ever more high-dimensional. These models may bring advancement even for crucial tasks such as the prevention of forest fires in a world influenced by climate change.

In a supervised learning setting, we have labeled data available for training a model that is able to predict the labels on future data. This is the setting we focus on in this work. Here, we have a close relationship to approximation theory since we may assume that an unknown underlying function maps each data point to its label. It is this function that we want to learn or approximate. In the classical function approximation sense, our data are nodes in the domain and the label is represented by the value of the function at the respective node.

When we consider the approximation of a function with high dimension, the most fundamental issue is the curse of dimensionality, as Richard Bellman first described it, see [Bel72]. The curse says that with increasing dimension, we need an exponentially increasing amount of data to achieve reasonable accuracy. For a rigorous mathematical formulation of the curse, we refer to [NW08]. It quickly prevents the application of straightforward methods for approximation when the dimension rises. For a single problem with spatial dimension 40 and two points in each dimension, we have $2^{40} \approx 2 \cdot 10^{12}$ which is not going to be feasible, even with the huge amount of data we have today. Therefore, it is a necessity to find ways around this curse, e.g., by making further assumptions that fit the problem.

Moreover, the question of interpretability in the context of explainable artificial intelligence is gaining significant traction. We want to know how the predictions come to pass and which attributes are the most influential. This gives us not only a possibility to make modifications trying to achieve a certain outcome, but also to discard the measurement of unimportant attributes that may be expensive. Many well-known and proven methods in machine learning, e.g., support vector machines, neural networks, and decision trees, cf. [SC08, HTF13, Agg15], do not intrinsically allow for interpretation. However, there is rather current research on the interpretability of these methods, see e.g. [MSM18, Sam19]. Moreover, we have approaches from statistics with regard to interpretability like the estimation of mutual information, see [KSG04, Ros14].

We focus solely on a scenario with *scattered data* in this work, i.e., the nodes are either drawn randomly or they are given to us in applications. We refer to [Wen04] for a an overview of this topic and [Buh03] with a special focus on kernel methods with radial basis function kernels. In the case of *active learning* or *black-box approximation*, it would be possible to choose a sampling scheme for a function. For active learning, we have seen the development of many reliable methods such as sparse grids, cf. [Heg03, BG04, GH14], or rank-1 lattices, see e.g. [SJ94, Käm13, KPV15, CKNS20]. A rank-1 lattice represents a sampling scheme with a simple structure that transforms the evaluation of a high-dimensional

function to the computation of a single fast Fourier transform. They have been used in the integration as well as the approximation of functions where the lattice is generated by an efficient component-by-component construction, see e.g. [CN07].

In this work, we present a method for the approximation of high-dimensional functions and data that is built around the concept of interpretability. *What are the requirements on this method?* The first requirement is straightforward that the method should produce an approximation that is close to the original function, in the case of function approximation, or generalizes well to new data. As the second requirement, we want to be able to evaluate the approximation fast on a large number of new nodes or data points. Those two requirements are nothing surprising and every machine learning method should fulfill them. However, we add interpretability as the third requirement, i.e., the ability to determine how the variables interact and how important their contribution is. This provides us with a powerful tool to analyze and understand the data set. Using, e.g., an attribute ranking, we may identify important and unimportant variables. As the fourth and final requirement, we want to have the ability to incorporate the information we gained through this interpretation to improve the model.

Our method consists of three major components which we introduce in the following. The fist crucial component of the method is the multivariate classical *analysis of variance (ANOVA)* decomposition, cf. [CMO97, RFA99, Gri06, LO06, Hol11] and [Owe13, Appendix A] for an overview. The ANOVA decomposition is an important model in the analysis of dimension interactions of multivariate, high-dimensional functions. It decomposes a d-variate function f into 2^d ANOVA terms $f_{\boldsymbol{u}}$ as

$$f = \sum_{\boldsymbol{u} \subseteq \{1,2,\dots,d\}} f_{\boldsymbol{u}}$$

where each term is uniquely identified by a subset of the coordinate indices $\{1, 2, \dots, d\}$. The decomposition has shown to be a useful tool in the study of the success of certain quadrature methods for the integration of high- and infinite-dimensional functions, see [Nie92, BG04, GH10, BG14, GKS16, KNP+17]. The directly related global

sensitivity indices or Sobol indices, cf. [Sob90, Sob01, LO06], provide the necessary means for interpretation. They assign each ANOVA term a value of how much they relatively contribute to the variance of the function. We investigate the connection of the classical ANOVA decomposition to orthonormal bases in weighted Lebesgue spaces L_2 and show interesting relationships to the support of the index of the basis coefficients.

Our approach around the curse of dimensionality is also motivated by the decomposition. In fact, we assume sparsity in the ANOVA decomposition related to the concept of superposition dimension. In other words, we remove ANOVA terms where more than $d_s < d$ variables interact such that

$$f \approx \sum_{\substack{\boldsymbol{u} \subseteq \{1,2,\dots,d\} \\ |\boldsymbol{u}| \leq d_s}} f_{\boldsymbol{u}}.$$

This is a sensible assumptions for functions of certain smoothness types, e.g., dominating-mixed smoothness, cf. [PS21a], but also for data sets from applications. Here, the *sparsity-of-effects* principle tells us that many real world systems are dominated by a small number of low-complexity interactions, see e.g. [WH11, HSS+21]. This technique is also related to low-dimensional structures and active subspace methods [FSV12, CDW14, CEHW17] as well as random features [RR08, CJJ12, YLM+12, LTOS19, HSS+21]. The method of sparse random features in [HSS+21] goes into a similar direction with the difference that weights or basis functions are drawn at random and a different optimization problem is considered. The ShRIMP method has also recently combined this approach with iterative magnitude pruning, cf. [XSSW21].

Discrete transformations such as the discrete Fourier transform, the discrete cosine transform, and others are of great importance in a variety of applications from applied mathematics and other sciences. They are the basis for algorithms like the fast Fourier transform (FFT) and the fast cosine transform (FCT), cf. [Bri88, PPST18]. The FFT itself is certainly one of the most important algorithms today. The non-equispaced fast Fourier transform (NFFT) and the non-equispaced

fast cosine transform (NFCT) represent extensions of this concept that allow for non-equispaced spatial nodes, cf. [KKP09, PPST18, KKP]. The complexity of these algorithms depends on the size of the index set which grows exponentially in the dimension for many common examples. In relation to the sparse ANOVA decomposition, we propose a form of index set, the grouped index set, that fits this decomposition. The second component of our approximation method are the grouped transformations from [BPS22]. They represent an extension of NFFT and NFCT in order to perform fast transformations with grouped index sets and non-equispaced nodes. The basis for the method is to break down one high-dimensional transformation into multiple low-dimensional transformations. In addition, it is possible to compute these transformations simultaneously which enables us to use parallelization.

Finally, we combine the previous ideas and approximate our function via solving a least-squares problem of the form

$$\min_{\hat{f}} \left\| \boldsymbol{y} - \boldsymbol{F}\hat{\boldsymbol{f}} \right\|_{\ell_2}^2$$

which represents our third and final component. We employ the iterative LSQR algorithm, cf. [PS82, Bjö96], in a matrix-free variant. The system matrix $\boldsymbol{F}$ itself is never explicitly constructed, but the fast grouped transformation algorithms serve as an *oracle* function that delivers the result of matrix-vector multiplications with $\boldsymbol{F}$ and its adjoint. We also incorporate regularization into the problem that additionally allows us to use a priori information about the smoothness of the function if it is given. Furthermore, we analyze the condition of the matrices based on the matrix Chernoff bound by Tropp, see [Tro11], as well as the errors of the method with two approaches. To this end, we assume randomly generated nodes according to a distribution corresponding to the underlying function space and make use of concentration inequalities. First, we consider the worst-case error for classes of functions in smoothness spaces and show probabilistic error bounds. The results are an extension of [KUV21, MU21] in our setting. The error for individual function approximation is considered as the second setting with the help of Bernstein's inequality, cf. [SC08,

Chapter 6]. In the case of sparse grids as sampling schemes, such errors have been discussed in [Boh17]. For hyperbolic wavelet regression, this has recently been considered in [LPU21].

In order to demonstrate the applicability of the method, we perform numerical experiments with synthetic and real data. Synthetic data represents the approximation of a given function where the nodes as data points are generated randomly in the domain and the function is evaluated at these points. In the case of real data, we apply our method to publicly available regression data sets. In both settings, we compare our results to benchmark data from published articles.

Outline of the Thesis

Chapter 2: The Classical ANOVA Decomposition

Chapter 2 is concerned with the introduction of the classical ANOVA decomposition and its properties. In Section 2.1, we discuss weighted Lebesgue spaces and orthonormal systems as well as some of the surrounding important theory as preliminaries. Section 2.1.1 lies emphasis on the spaces that characterize smoothness through the decay of the basis coefficients such as Sobolev type spaces and weighted Wiener spaces. Examples for spaces with complete orthonormal systems that will be important for our method are provided in Section 2.1.2. The approximation of functions by partial sums is briefly discussed in Section 2.1.3.

The main goal of Section 2.2 is to expand the results of [PS21a] for periodic functions, and [PS22a] for the Chebyshev system. In these works, we proposed a new Fourier approach to understanding the ANOVA decomposition. Here, we aim to generalize this approach to the setting of complete orthonormal systems in weighted Lebesgue spaces. We introduce the integral projection and the ANOVA terms leading to the classical ANOVA decomposition. Specifically, we investigate the relationship between the decomposition and the basis coefficients culminating in Lemma 2.14 and Lemma 2.17. Moreover, we show that functions inherit their smoothness, i.e., the decay properties of the basis

coefficients, to projections and ANOVA terms in Theorem 2.21 and Theorem 2.22.

Section 2.3 is concerned with the interpretability of the ANOVA decomposition using Sobol indices. We discuss notions of effective dimension and specifically how the superposition dimension as one such notion may lead to sparsity in the decomposition. This motivates the introduction of the truncated ANOVA decomposition. Here, we are able to find a relationship to the basis coefficients in Lemma 2.24 and a direct formula in Theorem 2.25. In order to connect the smoothness of the function to the concept of low-dimensional interactions, we use a previously proposed worst-case version of the superposition dimension for the Sobolev type space. In this setting, Lemma 2.28 connects this worst-case version with the truncation error of the truncated ANOVA decomposition. Theorem 2.29 and Theorem 2.30 provide general bounds for this truncation error. When considering the important special case of dominating-mixed and isotropic smoothness, we have the bounds in Corollary 2.32 and Corollary 2.33 which imply that the worst-case superposition dimension is low for this class of functions.

Chapter 3: Fast Multiplication with Grouped Transformations

In Chapter 3, we introduce the grouped transformations from [BPS22] in a general setting. Section 3.1 provides the foundation for this by reiterating on the non-equispaced discrete Fourier transform (NDFT) and the non-equispaced discrete cosine transform (NDCT) as well as their fast algorithms NFFT and NFCT.

Section 3.2 is concerned with the grouped transformations making a distinction between the periodic and non-periodic case. In Section 3.2.1, we relate the sparsity in the ANOVA decomposition to a specific structure in index sets, culminating in Definition 3.3, the grouped index set, and the analysis of its properties. Section 3.2.2 introduces the details of the grouped transformation. Specifically, we go into detail about the matrix structure and how to decompose the high-dimensional transformation into multiple low-dimensional transformations. As a

result, we obtain Algorithm 3.1 and its counterpart for the adjoint multiplication Algorithm 3.2. The algorithm is implemented as a publicly available package for the programming language Julia which is addressed in Section 3.2.3.

Chapter 4: High-Dimensional Explainable ANOVA Approximation

Chapter 4 combines the classical ANOVA decomposition and the grouped transformations into our approximation method. In Section 4.1, we discuss how the method uses LSQR to solve a least-squares problem with the goal to determine approximations of the basis coefficients of our unknown function. In the case of a real data set, we refer to the unknown underlying function that maps input to output. Here, the relationship between the number of nodes and the number of basis functions for the approximation is crucial. We distinguish between the overdetermined and the underdetermined case. In an overdetermined setting, Theorem 4.2 and Corollary 4.3 provide upper and lower bounds on the spectral norm of the Moore-Penrose of our system matrix. In the case of an underdetermined setting, we introduce regularization that is capable of incorporating a priori information about the decay of the basis coefficients, i.e., the smoothness of the function.

Section 4.2 introduces the method with its interpretation capabilities that allow us to perform a refitting, i.e., using structural information to obtain a better approximation. This is summarized in Algorithm 4.1. In Section 4.2.1, we go into detail about different strategies for detecting important ANOVA terms and recognizing the potential sparsity in the decomposition. Specifically, we propose a new method for obtaining attribute rankings. Section 4.3 is concerned with approximation errors, i.e., the worst-case error for functions from smoothness spaces and the individual approximation error. Theorem 4.10 considers the worst-case error bound for L_2 in Sobolev type spaces while Theorem 4.11 gives us a bound in weighted Wiener spaces. We consider the bounds in the context of functions of dominating-mixed smoothness as an important special case. Theorem 4.12 and Theorem 4.13 give bounds on the indi-

vidual approximation error for L_2 and L_∞ with the help of Bernstein's inequality. However, this may again grant insight for functions in smoothness spaces when we are unaware of the L_∞ worst-case error, see Corollary 4.14 and Corollary 4.15. Additional information on the importance of ANOVA terms can be incorporated using Theorem 4.16 and Theorem 4.17. The method and all the related tools are implemented in a publicly available package for the programming language Julia.

Chapter 5: Numerical Experiments with Synthetic Data

Chapter 5 is concerned with demonstrating the applicability of our method for function approximation, i.e., as data we have nodes in the domain drawn i.i.d. at random according to the corresponding distribution. The function is then evaluated at these nodes and for some experiments we add Gaussian noise. As benchmark function, we use a 9-dimensional periodic function in Section 5.1 which is a sum of products of univariate B-splines, see also [PV16] where a similar function appears. We also consider a related 8-dimensional non-periodic function in Section 5.2. As a final example, we use the well-known Friedman 1, Friedman 2, and Friedman 3 functions in Section 5.3, see e.g. [MLH03, BGM09, BDL11]. We apply different methods from Section 4.2.1 for the detection of important ANOVA terms and use refitting to obtain our approximations. For the Friedman functions, we compare our results to popular machine learning methods and mutual information estimation as a different form of attribute ranking.

Chapter 6: Numerical Experiments with Real Data

In Chapter 6, we perform experiments with our method on real data sets that are publicly available. Here, we rely on data sets from the UCI repository [DG17] and from the website [Tor]. The data sets include forest fire prevention, house energy prediction, air-foil self-noise prediction, and house price prediction. Moreover, we consider a data set about the control action on the ailerons of an F16 airplane.

The strategies from Section 4.2.1 are applied to detect importance information about the attributes and their interactions. All results are compared to published benchmark experiments with well-known machine learning methods.

Chapter 7: Conclusion

We summarize the main results of this work in Chapter 7.

Publications

Parts of this work were already published in the following articles:

- D. Potts, and M. Schmischke
  Approximation of high-dimensional periodic functions with Fourier-based methods
  SIAM Journal on Numerical Analysis 59 (5), 2393-2429, 2021
  Citation: [PS21a]

- D. Potts, and M. Schmischke
  Interpretable approximation of high-dimensional data
  SIAM Journal on Mathematics of Data Science 3 (4), 1301–1323, 2021
  Citation: [PS21b]

- D. Potts, and M. Schmischke
  Learning multivariate functions with low-dimensional structures using polynomial bases
  Journal of Computational and Applied Mathematics 403, 113821, 2022
  Citation: [PS22a]

- D. Potts, and M. Schmischke
  Interpretable transformed ANOVA approximation on the example of the prevention of forest fires

Frontiers in Applied Mathematics and Statistics 8, 795250, 2022
Citation: [PS22b]

- D. Potts, F. Bartel, and M. Schmischke
Grouped transformations and regularization in high-dimensional explainable ANOVA approximation
SIAM Journal on Scientific Computing (accepted), 2022
Citation: [BPS22]

Acknowledgments

First of all, I want to express my most sincere gratitude to my advisor Prof. Dr. Daniel Potts. He offered continuous support through many fruitful discussions and gave valuable impulses for my work. I highly valued this mentorship throughout the years that sometimes transcended mathematics. I also want to thank Prof. Dr. Tino Ullrich with his vast knowledge for giving his advice and insights on many topics. For her meticulous proofreading of large parts of this work, I am very grateful to my colleague and research group leader Dr. Franziska Nestler. The environment in our working group as well as at the faculty of mathematics as a whole is unique in a very positive sense. I am very grateful for having such great and helpful colleagues. I am going to remember many discussions during our daily coffee break fondly for the rest of my life.

Moreover, I thank my parents Angela and Jens for making it possible for me to study mathematics at all. Their support throughout the years allowed this work to happen at all and I will be eternally grateful for that. Since the time as a PhD student is in many ways not always easy, I thank my girlfriend Kseniya Akhalaya for supporting me every day.

I was partly supported by the BMBF as a member of the junior research group SALE (fast algorithms for explainable recommendation systems) with the grant number 01|S20053A. The exchange throughout the different projects within the group was very enlightening and motivating to me.

2

The Classical ANOVA Decomposition

The **analysis of variance (ANOVA)** decomposition, see e.g. [CMO97, RFA99, Gri06, LO06, Hol11], represents an important model in the analysis of dimension interactions of multivariate, high-dimensional functions. It was also a major tool in understanding the reason behind the success of quadrature methods for high-dimensional integration [Nie92, BG04, GH10] as well as infinite-dimensional integration [BG14, GKS16, KNP+17]. The ANOVA decomposition decomposes a d-variate function in 2^d ANOVA terms where each term belongs to a subset of coordinate indices $[d] \coloneqq \{1, 2, \dots, d\}$. Each single term depends only on the variables in the corresponding subset and the number of these variables is the order of the ANOVA term. In this chapter, we study the classical ANOVA decomposition for functions in weighted Lebesgue spaces with orthonormal bases - periodic and non-periodic - and how it acts on the frequency domain. The decomposition is referred to as *classical* because we choose an integral projection operator. In this setting, we discuss relationships between ANOVA terms and the support of the basis indices as subsets of $\mathbb{Z}^d$. Moreover, we prove formulas for the representation of ANOVA terms and projections. The chapter is based on results from [PS21a] for periodic functions and

[PS22a] for non-periodic functions.

In Section 2.1, we discuss weighted Lebesgue spaces and necessary functional analytic foundations for our theory. Smoothness spaces based on the decay of basis coefficients are considered as well. The ANOVA decomposition will be introduced in Section 2.2 and we study its behavior with regard to orthonormal bases in weighted Lebesgue spaces. Lemma 2.14 and Lemma 2.17 based on [PS21a] show how the projection operator and the ANOVA terms are represented in the frequency domain. Moreover, we show in Theorem 2.21 and Theorem 2.22 that functions in our setting inherit their smoothness to the projections and the ANOVA terms. In Section 2.3, we discuss the important interpretability properties of the decomposition with regard to effective dimensions and certain truncation ideas. These will be particularly relevant for the explainable approximation method in Chapter 4. We also provide a connection between the truncated decomposition and the basis expansion of the function in Lemma 2.24.

The worst-case superposition dimension relates the smoothness of the function in form of a Sobolev type space to the superposition dimension. In Lemma 2.28, we show the connection to the L_2 truncation error in the Sobolev type space. Subsequently, we discuss the worst-case ANOVA truncation error in L_2 in Theorem 2.29 and L_∞ in Theorem 2.30. As an important example, we consider product and order-dependent weights, see [KSS12, GKN$^+$14, KN16, GKN$^+$18], of functions with isotropic and dominating-mixed smoothness, cf. [GH14, KPV15, BKUV17], an derive Corollary 2.32 and Corollary 2.33.

2.1 Weighted Lebesgue Spaces and Orthonormal Systems

In this section, we discuss weighted Lebesgue spaces and their important properties as well as complete orthonormal systems and basis expansions. Together with the idea of product spaces we lay the foundation for our later considerations of the ANOVA decomposition in Section 2.2. We use the well-known book by Werner [Wer18] as our

reference for functional analysis and [CK04] for Lebesgue spaces in particular. We also consider Sobolev spaces, see e.g. [Ada03], in the variant of Sobolev type spaces, cf. [KMU16], and weighted Wiener spaces, see [BD73, KLT21], which relate the smoothness of a function to the decay of its basis coefficients.

In the following, we define the Lebesgue function spaces and the corresponding sequence spaces.

Definition 2.1. *Let $p \in [1, \infty]$, $\mathbb{D} \in \{\mathbb{T}, [-1, 1], [0, 1], \mathbb{R}\}$, and $\omega \colon \mathbb{D}^d \to (0, \infty)$ a probability measure with*

$$\int_{\mathbb{D}^d} \omega(\boldsymbol{x}) \, \mathrm{d}\boldsymbol{x} = 1$$

*where $\mathbb{T} \cong \mathbb{R}/\mathbb{Z}$ is the torus. We define the **weighted Lebesgue spaces** with spatial dimension $d \in \mathbb{N}$ as*

$$\mathrm{L}_p(\mathbb{D}^d, \omega) \coloneqq \left\{ f \colon \mathbb{D}^d \to \mathbb{C} \quad \text{measurable} \colon \int_{\mathbb{D}^d} |f(\boldsymbol{x})|^p \ \omega(\boldsymbol{x}) \, \mathrm{d}\boldsymbol{x} < \infty \right\}$$

for $p < \infty$ and

$$\mathrm{L}_\infty(\mathbb{D}^d) \coloneqq \left\{ f \colon \mathbb{D}^d \to \mathbb{C} \quad \text{measurable} \colon \operatorname*{ess\,supp}_{\boldsymbol{x} \in \mathbb{D}^d} |f(\boldsymbol{x})| < \infty \right\}.$$

For the weight function $\omega \equiv 1$, we write

$$\mathrm{L}_p(\mathbb{D}^d) \coloneqq \mathrm{L}_p(\mathbb{D}^d, 1).$$

The corresponding norms are given by

$$\begin{aligned} \|f\|_{\mathrm{L}_p(\mathbb{D}^d, \omega)} &\coloneqq \left(\int_{\mathbb{D}^d} |f(\boldsymbol{x})|^p \ \mathrm{d}\boldsymbol{x} \right)^{\frac{1}{p}} \quad \text{for } \ p < \infty \ \text{ and} \\ \|f\|_{\mathrm{L}_\infty(\mathbb{D}^d)} &\coloneqq \operatorname*{ess\,supp}_{\boldsymbol{x} \in \mathbb{D}^d} |f(\boldsymbol{x})| \, . \end{aligned}$$

Additionally, $\mathrm{L}_2(\mathbb{D}^d, \omega)$ is a separable Hilbert space with scalar product

$$\langle f, g \rangle_{\mathrm{L}_2(\mathbb{D}^d, \omega)} = \int_{\mathbb{D}^d} f(\boldsymbol{x}) \, \overline{g(\boldsymbol{x})} \, \omega(\boldsymbol{x}) \, \mathrm{d}\boldsymbol{x}, \ f, g \in \mathrm{L}_2(\mathbb{D}^d, \omega).$$

Under our assumption that we have a probability measure ω in Definition 2.1, we have the embeddings

$$\begin{aligned} \mathrm{L}_p(\mathbb{D}^d, \omega) &\subseteq \mathrm{L}_q(\mathbb{D}^d, \omega), \ 1 \leq q < p < \infty, \quad \text{and} \\ \mathrm{L}_\infty(\mathbb{D}^d) &\subseteq \mathrm{L}_p(\mathbb{D}^d, \omega), \ 1 \leq p \leq \infty, \end{aligned}$$

see e.g. [Vil85, CK04]. Moreover, the continuous functions $C(\mathbb{D}^d)$ with compact domain $\mathbb{D}$ are bounded and therefore elements of $\mathrm{L}_\infty(\mathbb{D}^d)$.

Definition 2.2. *Let $p \in [1, \infty]$. Then we define the **Lebesgue sequence spaces** as*

$$\ell_p := \left\{ \left(x_j\right)_{j \in \mathbb{Z}} \subseteq \mathbb{C} \colon \sum_{j \in \mathbb{Z}} \left|x_j\right|^p < \infty \right\}$$

for $p < \infty$ and

$$\ell_\infty := \left\{ \left(x_j\right)_{j \in \mathbb{Z}} \subseteq \mathbb{C} \colon \sup_{j \in \mathbb{Z}} \left|x_j\right| < \infty \right\}.$$

The norms are given by

$$\left\| \left(x_j\right)_{j \in \mathbb{Z}} \right\|_{\ell_p} := \begin{cases} \left(\sum_{j \in \mathbb{Z}} \left|x_j\right|^p \right)^{\frac{1}{p}} & : p < \infty \\ \sup_{j \in \mathbb{Z}} \left|x_j\right| & : p = \infty. \end{cases}$$

Additionally, ℓ_2 is a separable Hilbert space with scalar product

$$\langle \left(x_j\right)_{j \in \mathbb{Z}}, \left(y_j\right)_{j \in \mathbb{Z}} \rangle_{\ell_2} = \sum_{j \in \mathbb{Z}^d} x_j \, \overline{y_j}, \ \left(x_j\right)_{j \in \mathbb{Z}}, \left(y_j\right)_{j \in \mathbb{Z}} \in \ell_2.$$

We consider the norms $\|\boldsymbol{x}\|_{\ell_p}$ also for finite vectors $\boldsymbol{x} \in \mathbb{R}^d$, $d \in \mathbb{N}$. The Lebesgue sequence spaces are embedded with

$$\ell_p \subseteq \ell_q \quad \text{for} \quad 1 \leq p < q \leq \infty,$$

see e.g. [Tre06].

We consider the separable Hilbert space $L_2(\mathbb{D}^d, \omega)$ which is where we later apply the ANOVA decomposition. Since the space has the property of separability, we know that there exists a countable complete orthonormal system or basis and we have Parseval's identity.

Definition 2.3. *Let $\mathcal{H}$ be a separable Hilbert space with scalar product $\langle \cdot, \cdot \rangle_{\mathcal{H}}$ and induced norm $\|\cdot\|_{\mathcal{H}} = \sqrt{\langle \cdot, \cdot \rangle_{\mathcal{H}}}$. A sequence of elements $(\varphi_k)_{k \in \mathbb{Z}} \subseteq \mathcal{H}$ is called* ***complete orthonormal system*** *or* ***basis*** *in $\mathcal{H}$ if*

$$\langle \varphi_k, \varphi_\ell \rangle = \delta_{k,\ell} \coloneqq \begin{cases} 1 & : k = \ell \\ 0 & : k \neq \ell \end{cases}$$

and

$$f = \sum_{k \in \mathbb{Z}} c_k(f)\, \varphi_k$$

holds for all elements $f \in \mathcal{H}$. We denote with

$$c_k(f) \coloneqq \langle f, \varphi_k \rangle_{\mathcal{H}}, k \in \mathbb{Z},$$

the ***basis coefficients*** *of f with respect to the system $(\varphi_k)_{k=1}^{\infty}$.*

Theorem 2.4 (Parseval's identity)**.** *Let $\mathcal{H}$ be a separable Hilbert space with orthonormal basis $(\varphi_k)_{k \in \mathbb{Z}}$. Then*

$$\|f\|_{\mathcal{H}} = \sqrt{\sum_{k \in \mathbb{Z}} |c_k(f)|^2}$$

holds for all $f \in \mathcal{H}$.

Proof. see e.g. [Wer18, Chapter V] ∎

In the case of product spaces, we are able to construct a basis from the one-dimensional case. To this end, we consider $d = 1$ with probability measure ω, i.e., the space $L_2(\mathbb{D}, \omega)$ for a domain $\mathbb{D} \in$

$\{\mathbb{T}, [-1,1], [0,1], \mathbb{R}\}$ and orthonormal basis $(\varphi_k)_{k\in\mathbb{Z}}$. For $d > 1$ it follows that the product space $\mathrm{L}_2(\mathbb{D}^d, \omega^{(d)})$ with product density

$$\omega^{(d)}(\boldsymbol{x}) \coloneqq \prod_{j=1}^{d} \omega(x_j)$$

has the basis $(\varphi_{\boldsymbol{k}}^{(d)})_{\boldsymbol{k}\in\mathbb{Z}^d}$ with

$$\varphi_{\boldsymbol{k}}^{(d)}(\boldsymbol{x}) \coloneqq \prod_{j=1}^{d} \varphi_{k_j}(x_j), \tag{2.1}$$

see e.g. the product topology in [Hoc88].

2.1.1 Smoothness and Weighted Decay

In this section, we aim to characterize the *smoothness* of a function in relation to the function space by the decay of its basis coefficients. Here, we always consider a product space $\mathrm{L}_2(\mathbb{D}^d, \omega^{(d)})$ for spatial dimension $d \in \mathbb{N}$ with an orthonormal basis $(\varphi_{\boldsymbol{k}}^{(d)})_{\boldsymbol{k}\in\mathbb{Z}^d}$. We assume that $\varphi_{\boldsymbol{k}}^{(d)}$, $\boldsymbol{k} \in \mathbb{Z}^d$, are bounded continuous functions such that we have a **bounded orthonormal system (BOS)** with

$$C_{\mathrm{BOS}} \coloneqq \sup_{\boldsymbol{k}\in\mathbb{Z}^d} \left\| \varphi_{\boldsymbol{k}}^{(d)} \right\|_{\mathrm{L}_\infty(\mathbb{D}^d)} < \infty \tag{2.2}$$

for the **BOS constant**. Note that if our domain $\mathbb{D}$ is compact, then every continuous function is also bounded.

Given a weight function $w\colon \mathbb{Z}^d \to [1,\infty)$, we introduce the **weighted Wiener spaces**

$$\mathcal{A}^w(\mathbb{D}^d, \omega^{(d)}) \coloneqq \left\{ f \in \mathrm{L}_1(\mathbb{D}^d, \omega^{(d)})\colon \sum_{\boldsymbol{k}\in\mathbb{Z}^d} w(\boldsymbol{k})\,|\mathrm{c}_{\boldsymbol{k}}(f)| < \infty \right\} \tag{2.3}$$

$$\|f\|_{\mathcal{A}^w(\mathbb{D}^d,\omega^{(d)})} \coloneqq \sum_{\boldsymbol{k}\in\mathbb{Z}^d} w(\boldsymbol{k})\,|\mathrm{c}_{\boldsymbol{k}}(f)|$$

with $\mathcal{A}^w(\mathbb{D}^d) \coloneqq \mathcal{A}^w(\mathbb{D}^d, 1)$ as well as $\mathcal{A}(\mathbb{D}^d, \omega^{(d)}) \coloneqq \mathcal{A}^1(\mathbb{D}^d, \omega^{(d)})$. Note that $\mathcal{A}(\mathbb{D}^d, \omega^{(d)})$ is called **Wiener Algebra** for $\mathbb{D} = \mathbb{T}$ and $\omega^{(d)} \equiv 1$, cf. [BD73], which motivates the term weighted Wiener spaces, see also [KLT21]. We have the apparent embeddings

$$\mathcal{A}^w(\mathbb{D}^d, \omega^{(d)}) \subseteq \mathcal{A}(\mathbb{D}^d, \omega^{(d)}) \subseteq \mathrm{L}_\infty(\mathbb{D}^d).$$

The embedding into L_∞ follows from the estimate

$$\begin{aligned}\|f\|_{\mathrm{L}_\infty(\mathbb{D}^d)} &= \operatorname*{ess\,supp}_{\boldsymbol{x}\in\mathbb{D}^d} \left| \sum_{\boldsymbol{k}\in\mathbb{Z}^d} \mathrm{c}_{\boldsymbol{k}}(f)\, \varphi_{\boldsymbol{k}}^{(d)}(\boldsymbol{x}) \right| \leq C_{\mathrm{BOS}} \sum_{\boldsymbol{k}\in\mathbb{Z}^d} |\mathrm{c}_{\boldsymbol{k}}(f)| \\ &= C_{\mathrm{BOS}}\, \|f\|_{\mathcal{A}(\mathbb{D}^d, \omega^{(d)})}.\end{aligned}$$

Moreover, we define the space

$$\mathrm{H}^w(\mathbb{D}^d, \omega^{(d)}) \coloneqq \left\{ f \in \mathrm{L}_2(\mathbb{D}^d, \omega^{(d)}) \colon \sum_{\boldsymbol{k}\in\mathbb{Z}^d} w^2(\boldsymbol{k})\, |\mathrm{c}_{\boldsymbol{k}}(f)|^2 < \infty \right\} \tag{2.4}$$

$$\|f\|_{\mathrm{H}^w(\mathbb{D}^d, \omega^{(d)})} \coloneqq \sqrt{\sum_{\boldsymbol{k}\in\mathbb{Z}^d} w^2(\boldsymbol{k})\, |\mathrm{c}_{\boldsymbol{k}}(f)|^2}$$

with $\mathrm{H}^w(\mathbb{D}^d) \coloneqq \mathrm{H}^w(\mathbb{D}^d, 1)$ which may be referred to as **Sobolev type space** or also **weighted Korobov space**, see e.g. [SW01, KMU16, DTU18]. In this setting, we have that the absolute value of the basis coefficients $|\mathrm{c}_{\boldsymbol{k}}(f)|$ decays like the inverse of the weight $w(\boldsymbol{k})$ and specifically $|\mathrm{c}_{\boldsymbol{k}}(f)| \in o(w^{-1}(\boldsymbol{k}))$. In the following lemma, we show that functions in $\mathcal{A}^w(\mathbb{D}^d, \omega^{(d)})$ also have continuous representatives.

Lemma 2.5. *Let $\mathrm{L}_2(\mathbb{D}^d, \omega^{(d)})$ be a weighted Lebesgue product space as in Definition 2.1 with an orthonormal basis $(\varphi_{\boldsymbol{k}}^{(d)})_{\boldsymbol{k}\in\mathbb{Z}^d}$ of bounded continuous functions such that $C_{\mathrm{BOS}} < \infty$. Then every element of the corresponding weighted Wiener space $\mathcal{A}(\mathbb{D}^d, \omega^{(d)})$ has a continuous representative.*

Proof. We prove that for $g \in \mathcal{A}(\mathbb{D}^d, \omega^{(d)})$, the function

$$h(\boldsymbol{x}) \coloneqq \sum_{\boldsymbol{k}\in\mathbb{Z}^d} \mathrm{c}_{\boldsymbol{k}}(g)\, \varphi_{\boldsymbol{k}}^{(d)}(\boldsymbol{x})$$

is this representative. This sum converges absolutely to g since it is an element of the Wiener algebra $\mathcal{A}(\mathbb{D}^d, \omega^{(d)})$. Since the basis functions $\varphi_{\boldsymbol{k}}^{(d)}$ are bounded and continuous, the absolute convergence implies the convergence in the space of bounded continuous functions which proves our statement. ∎

Lemma 2.6. *Let $w\colon \mathbb{Z}^d \to [1,\infty)$ be a weight function with $(w^{-1}(\boldsymbol{k}))_{\boldsymbol{k}\in\mathbb{Z}^d} \in \ell_2$. Then $\mathrm{H}^w(\mathbb{D}^d, \omega^{(d)}) \subseteq \mathcal{A}(\mathbb{D}^d, \omega^{(d)})$.*

Proof. The result follows directly by the Cauchy-Schwarz inequality

$$\sum_{\boldsymbol{k}\in\mathbb{Z}^d} |\mathrm{c}_{\boldsymbol{k}}(f)| = \sum_{\boldsymbol{k}\in\mathbb{Z}^d} w^{-1}(\boldsymbol{k}) \cdot w(\boldsymbol{k})\, |\mathrm{c}_{\boldsymbol{k}}(f)| \leq \|f\|_{\mathrm{H}^w(\mathbb{D}^d,\omega)} \sqrt{\sum_{\boldsymbol{k}\in\mathbb{Z}^d} w^{-2}(\boldsymbol{k})}.$$

∎

Lemma 2.5 and Lemma 2.6 imply that every $f \in \mathrm{H}^w(\mathbb{D}^d, \omega^{(d)})$ with $(w^{-1}(\boldsymbol{k}))_{\boldsymbol{k}\in\mathbb{Z}^d} \in \ell_2$ has a continuous representative.

Lemma 2.7. *Let $w\colon \mathbb{Z}^d \to [1,\infty)$ be a weight function. Then $\mathcal{A}^w(\mathbb{D}^d, \omega^{(d)}) \subseteq \mathrm{H}^w(\mathbb{D}^d, \omega^{(d)})$.*

Proof. This follows directly from embeddings of the Lebesgue sequence spaces, i.e., we have for the norm $\|\cdot\|_{\ell_2} \leq \|\cdot\|_{\ell_1}$. ∎

In the following, we discuss an important type of smoothness weights, **isotropic and dominating-mixed** smoothness. Especially the functions of mixed smoothness are of great importance in many applications and have been studied for a long time. We introduce the related weights

$$w^{\alpha,\beta}(\boldsymbol{k}) \coloneqq \gamma_{\operatorname{supp}\boldsymbol{k}}^{-1} \,(1 + \|\boldsymbol{k}\|_1)^{\alpha} \prod_{s=1}^{d} (1 + |k_s|)^{\beta} \tag{2.5}$$

with $\operatorname{supp}\boldsymbol{k} \coloneqq \{i \in \{1,2,\ldots,d\}\colon k_i \neq 0\}$ as well as parameters $\beta \geq 0$, and $\alpha > -\beta$. The parameters α, β, and the weight $\gamma_{\boldsymbol{u}}$, $\boldsymbol{u} \subseteq \{1,2,\ldots,d\}$, regulate the decay of the basis coefficients. Here, α is the isotropic

smoothness parameter and β the dominating-mixed smoothness parameter, cf. [KMU16, DTU18]. Moreover, $\boldsymbol{\gamma}$ is a weight that controls the influence of dimensions and their interactions. For a general choice of the weights $\boldsymbol{\gamma}$ we refer to [DSWW06]. However, we want to focus on a specific structure for $\boldsymbol{\gamma}$ and choose **product and order-dependent** (POD) weights such that

$$\gamma_{\boldsymbol{u}} = \Gamma_{|\boldsymbol{u}|} \prod_{s \in \boldsymbol{u}} \gamma_s, \tag{2.6}$$

where $\boldsymbol{\Gamma} \in (0,1]^d$ is non-increasing and $\boldsymbol{\gamma} = (\gamma_i)_{i=1}^d \in (0,1]^d$. This POD structure gets its motivation from quasi-Monte Carlo methods for the solution of PDEs with random coefficients, cf. [KSS12, GKN$^+$14, KN16, GKN$^+$18]. Similar weights for isotropic and dominating-mixed smoothness have been considered in [GH14, KPV15, BKUV17]. Different structures for the weights have also been discussed in [CKNS20].

The following theorem shows that a function in a Sobolev type space $\mathrm{H}^{w^{\alpha,\beta+\lambda}}(\mathbb{D}^d, \omega^{(d)})$ with any $\lambda > 1/2$ is an element of the weighted Wiener space $\mathcal{A}^{w^{\alpha,\beta}}(\mathbb{D}^d, \omega^{(d)})$ as well. Consequently, any function contained in a Sobolev type space $\mathrm{H}^{w^{0,\lambda}}(\mathbb{D}^d, \omega^{(d)})$, i.e., any function of dominating-mixed smoothness larger than $1/2$, is an element of the weighted Wiener space $\mathcal{A}(\mathbb{D}^d, \omega^{(d)})$. The theorem is similar to the result [KPV15, Lemma 2.2].

Theorem 2.8. *Let* $\mathrm{H}^{w^{\alpha,\beta+\lambda}}(\mathbb{D}^d, \omega^{(d)})$ *be a Sobolev type space with weight* $w^{\alpha,\beta}$ *as in* (2.5), $\lambda > 1/2$, *and POD weights* $\gamma_{\operatorname{supp} \boldsymbol{k}} \in (0,1]$ *as in* (2.6) *for* $\boldsymbol{k} \in \mathbb{Z}^d$. *Then we have*

$$\|f\|_{\mathcal{A}^{w^{\alpha,\beta}}(\mathbb{D}^d, \omega^{(d)})} \leq \left(\prod_{s=1}^{d} \sqrt{1 + 2\gamma_s^2 \left(\zeta(2\lambda) - 1\right)} \right) \|f\|_{\mathrm{H}^{w^{\alpha,\beta+\lambda}}(\mathbb{D}^d, \omega^{(d)})}$$

for all $f \in \mathrm{H}^{w^{\alpha,\beta+\lambda}}(\mathbb{D}^d, \omega^{(d)})$ *and therefore the embedding* $\mathrm{H}^{w^{\alpha,\beta+\lambda}}(\mathbb{D}^d, \omega^{(d)}) \subseteq \mathcal{A}^{w^{\alpha,\beta}}(\mathbb{D}^d, \omega^{(d)})$.

Proof. We estimate the norm $\|f\|_{\mathcal{A}^{w^{\alpha,\beta}}(\mathbb{D}^d, \omega^{(d)})}$ by applying the Cauchy-

Schwarz inequality to obtain

$$\begin{aligned}\|f\|_{\mathcal{A}^{w^{\alpha,\beta}}(\mathbb{D}^d,\omega^{(d)})} &= \sum_{\boldsymbol{k}\in\mathbb{Z}^d} w^{\alpha,\beta}(\boldsymbol{k})\,|\mathrm{c}_{\boldsymbol{k}}(f)| = \sum_{\boldsymbol{k}\in\mathbb{Z}^d} \frac{w^{0,\lambda}(\boldsymbol{k})}{w^{0,\lambda}(\boldsymbol{k})}\, w^{\alpha,\beta}(\boldsymbol{k})\,|\mathrm{c}_{\boldsymbol{k}}(f)| \\ &\leq \|f\|_{\mathrm{H}^{w^{\alpha,\beta+\lambda}}(\mathbb{D}^d,\omega^{(d)})} \sqrt{\sum_{\boldsymbol{k}\in\mathbb{Z}^d} \frac{1}{w^{0,2\lambda}(\boldsymbol{k})}}.\end{aligned}$$

The remaining sum can be decomposed into a product and expressed as the Riemann zeta function ζ such that we have

$$\begin{aligned}\sum_{\boldsymbol{k}\in\mathbb{Z}^d} \frac{1}{w^{0,2\lambda}(\boldsymbol{k})} &= \sum_{\boldsymbol{k}\in\mathbb{Z}^d} \frac{\Gamma^2_{|\boldsymbol{u}|}\prod_{s\in\mathrm{supp}\,\boldsymbol{k}}\gamma_s^2}{\prod_{s=1}^d (1+|k_s|)^{2\lambda}} \leq \sum_{\boldsymbol{k}\in\mathbb{Z}^d}\prod_{s=1}^d \frac{\gamma_s^{2(1-\delta_{k_s,0})}}{(1+|k_s|)^{2\lambda}} \\ &= \prod_{s=1}^d \sum_{k\in\mathbb{Z}} \frac{\gamma_s^{2(1-\delta_{k,0})}}{(1+|k|)^{2\lambda}} = \prod_{s=1}^d \left(1+2\gamma_s^2 \sum_{k\in\mathbb{N}} \frac{1}{(1+k)^{2\lambda}}\right) \\ &= \prod_{s=1}^d \left(1+2\gamma_s^2\,(\zeta(2\lambda)-1)\right).\end{aligned}$$

This also implies the constraint $\lambda > 1/2$ since the argument in the Riemann zeta function needs to be larger than one. ■

2.1.2 Examples for Complete Orthonormal Systems

While the previous and forthcoming considerations in this section allow for a very general orthonormal system with product structure, we introduce four important examples. These four examples do not only cover a wide range of functions, both periodic and non-periodic, but also important probability measures $\omega^{(d)}$ in the Lebesgue space $\mathrm{L}_2(\mathbb{D}^d, \omega^{(d)})$. This fact will be helpful when dealing with different data distributions in the approximation method in Chapter 4 and the experiments in Chapter 6.

2.1.2.1 The Fourier System

A well-known example for complete orthonormal systems is the Fourier system. We have periodic functions $f\colon \mathbb{T}^d \to \mathbb{C}$ defined over the d-dimensional torus $\mathbb{T}^d$ and a density $\omega \equiv 1$ which yields the space $\mathrm{L}_2(\mathbb{T}^d)$ as in Definition 2.1. It is well-known that the Fourier system given by the functions

$$\varphi_{\boldsymbol{k}}^{(d),\exp}(\boldsymbol{x}) = \mathrm{e}^{2\pi \mathrm{i}\, \boldsymbol{k}\cdot\boldsymbol{x}},\ \boldsymbol{k} \in \mathbb{Z}^d, \tag{2.7}$$

forms a complete orthonormal system in $\mathrm{L}_2(\mathbb{T}^d)$, see e.g. [PPST18, Chapter 1]. Moreover, the basis functions are continuous and bounded with

$$\left|\varphi_{\boldsymbol{k}}^{(d),\exp}(\boldsymbol{x})\right| = 1$$

for all $\boldsymbol{k} \in \mathbb{Z}^d$ and $\boldsymbol{x} \in \mathbb{T}^d$. The BOS constant (2.2) is $C_{\mathrm{BOS}} = 1$.

2.1.2.2 The Chebyshev Polynomials

As a second example, we consider functions $f\colon [-1,1]^d \to \mathbb{R}$ defined over the cube $[-1,1]^d$ and the Chebyshev probability density

$$\omega^{(d),\mathrm{cheb}}(\boldsymbol{x}) = \prod_{s=1}^{d} \frac{1}{\pi\sqrt{1-x_s^2}}.$$

If we consider the weighted Lebesgue space $\mathrm{L}_2([-1,1]^d, \omega^{(d),\mathrm{cheb}})$, the (normed) Chebyshev polynomials of first kind

$$\varphi_{\boldsymbol{k}}^{(d),\mathrm{cheb}}(\boldsymbol{x}) = \sqrt{2}^{|\operatorname{supp}\boldsymbol{k}|} \prod_{s=1}^{d} \cos(k_s \arccos x_s),\ \boldsymbol{k} \in \mathbb{N}_0^d, \tag{2.8}$$

form an orthonormal basis, see e.g. [Tre20]. Moreover, the basis functions are continuous and bounded with

$$\left\|\varphi_{\boldsymbol{k}}^{(d),\mathrm{cheb}}\right\|_{\mathrm{L}_\infty([-1,1]^d)} = \sqrt{2}^{|\operatorname{supp}\boldsymbol{k}|} \tag{2.9}$$

for $\boldsymbol{k} \in \mathbb{N}_0^d$. This implies for the BOS constant (2.2)

$$C_{\mathrm{BOS}} = \sqrt{2}^d$$

which rises exponentially for a growing spatial dimension d.

2.1.2.3 The Cosine Basis

The so-called half-period cosine with basis functions

$$\varphi_{\boldsymbol{k}}^{(d),\cos}(\boldsymbol{x}) = \sqrt{2}^{|\operatorname{supp} \boldsymbol{k}|} \prod_{s=1}^{d} \cos(\pi k_s x_s),\ \boldsymbol{k} \in \mathbb{N}_0^d, \tag{2.10}$$

defined over the cube $[0,1]^d$ is a well-known basis of $\mathrm{L}_2([0,1]^d)$, cf. [Sut18, Chapter 9]. As for the Chebyshev system, we have the norm

$$\left\| \varphi_{\boldsymbol{k}}^{(d),\cos} \right\|_{\mathrm{L}_\infty([0,1]^d)} = \sqrt{2}^{|\operatorname{supp} \boldsymbol{k}|}$$

and therefore the BOS constant (2.2)

$$C_{\mathrm{BOS}} = \sqrt{2}^d$$

which rises exponentially in the spatial dimension.

2.1.2.4 The Transformed Cosine

We consider the space $\mathrm{L}_2(\mathbb{R}^d, \omega^{(d),\mathrm{std}})$ with the density

$$\omega^{(d),\mathrm{std}}(\boldsymbol{x}) := \prod_{s=1}^{d} \frac{1}{\sqrt{2\pi}} \mathrm{e}^{-\frac{x_s^2}{2}} = (2\pi)^{-\frac{d}{2}} \mathrm{e}^{-\frac{1}{2}\|\boldsymbol{x}\|_{\ell_2}^2}. \tag{2.11}$$

This is the probability density function of the standard normal distribution, i.e., the normal distribution with zero mean and variance one. We have $\int_{\mathbb{R}^d} \omega^{(d),\mathrm{std}}(\boldsymbol{x})\,\mathrm{d}\boldsymbol{x} = 1$ as well as $\sup_{\boldsymbol{x}\in\mathbb{R}^d} \omega^{(d),\mathrm{std}}(\boldsymbol{x}) = (2\pi)^{-\frac{d}{2}}$ which

implies $\omega^{(d),\,\mathrm{std}} \in \mathrm{L}_\infty(\mathbb{R}^d)$. The cumulative distribution function of the standard normal distribution is given by

$$\Phi\colon \mathbb{R} \to [0,1], \quad \Phi(x) = \frac{1}{2}\left[1 + \operatorname{erf}\left(\frac{x}{\sqrt{2}}\right)\right] \tag{2.12}$$

with the error function defined as

$$\operatorname{erf}(x) = \frac{2}{\sqrt{\pi}} \int_0^x \mathrm{e}^{-t^2}\,\mathrm{d}t.$$

It is our goal to construct a basis in $\mathrm{L}_2(\mathbb{R}^d, \omega^{(d),\,\mathrm{std}})$ using transformation ideas from [NP20, NK14] and the half-period cosine basis in $\mathrm{L}_2([0,1]^d)$, see (2.10), by using the approach from [PS22b]. As transformation we propose to apply the cumulative distribution function Φ for each variable yielding

$$\psi\colon \mathbb{R}^d \to [0,1]^d,\ \psi(\boldsymbol{x}) = \begin{pmatrix} \Phi(x_1) \\ \Phi(x_2) \\ \vdots \\ \Phi(x_d) \end{pmatrix} \tag{2.13}$$

with the inverse

$$\psi^{-1}\colon [0,1]^d \to \mathbb{R}^d,\ \psi^{-1}(\boldsymbol{x}) = \begin{pmatrix} \Phi^{-1}(x_1) \\ \Phi^{-1}(x_2) \\ \vdots \\ \Phi^{-1}(x_d) \end{pmatrix}. \tag{2.14}$$

If we have a given function $f\colon [0,1]^d \to \mathbb{R}$, $f \in \mathrm{L}_2([0,1]^d)$, we may apply the transformation to obtain $f \circ \psi \in \mathrm{L}_2(\mathbb{R}^d, \omega^{(d),\,\mathrm{std}})$. As a result, we have the commutative diagram in Figure 2.1. This process can also be related to inverse transform sampling, see e.g. [Hö04]. Now, we aim to transform the half-period cosine to a complete orthonormal system on $\mathrm{L}_2(\mathbb{R}^d, \omega^{(d),\,\mathrm{std}})$ using ψ.

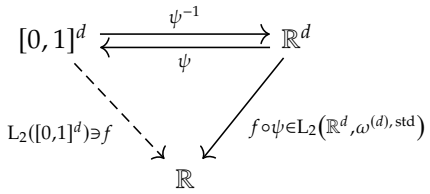

Figure 2.1: Commutative diagram of spaces and the transformations between them.

Lemma 2.9. *Let* $g, h \in \mathrm{L}_2([0,1]^d)$, $u, v \in \mathrm{L}_2(\mathbb{R}^d, \omega^{(d),\,\mathrm{std}})$ *with probability density* $\omega^{(d),\,\mathrm{std}}$ *from* (2.11)*, and transformation* ψ, ψ^{-1} *as in* (2.13) *and* (2.14) *respectively. Then*

$$\begin{aligned} \langle g \circ \psi, h \circ \psi \rangle_{\mathrm{L}_2(\mathbb{R}^d, \omega^{(d),\,\mathrm{std}})} &= \langle g, h \rangle_{\mathrm{L}_2([0,1]^d)} \\ \langle u, v \rangle_{\mathrm{L}_2(\mathbb{R}^d, \omega^{(d),\,\mathrm{std}})} &= \langle u \circ \psi^{-1}, v \circ \psi^{-1} \rangle_{\mathrm{L}_2([0,1]^d)} \end{aligned}$$

and $\|h\|_{\mathrm{L}_2([0,1]^d)} = \big\|h \circ \psi^{-1}\big\|_{\mathrm{L}_2(\mathbb{R}^d, \omega^{(d),\,\mathrm{std}})}$, $\|u \circ \psi\|_{\mathrm{L}_2([0,1]^d)} = \|u\|_{\mathrm{L}_2(\mathbb{R}^d, \omega^{(d),\,\mathrm{std}})}$.

Proof. In order to prove the first equality, we insert the definition and perform a change of variable as follows

$$\begin{aligned} \langle g \circ \psi, h \circ \psi \rangle_{\mathrm{L}_2(\mathbb{R}^d, \omega^{(d),\,\mathrm{std}})} &= \int_{\mathbb{R}^d} g(\psi(\boldsymbol{x}))\, h(\psi(\boldsymbol{x}))\, \omega^{(d),\,\mathrm{std}}(\boldsymbol{x})\, \mathrm{d}\boldsymbol{x} \\ &= \int_{[0,1]^d} g(\boldsymbol{t})\, h(\boldsymbol{t})\, \omega^{(d),\,\mathrm{std}}(\psi^{-1}(\boldsymbol{t}))\, \left|\det(\psi^{-1})'(\boldsymbol{t})\right|\, \mathrm{d}\boldsymbol{t}. \end{aligned}$$

As functional determinant we obtain the product $\left|\det(\psi^{-1})'(\boldsymbol{t})\right| = \prod_{s=1}^{d} \sqrt{2\pi}\, \mathrm{e}^{\mathrm{erf}^{-2}(2x_s - 1)}$ and subsequently

$$\begin{aligned} \omega^{(d),\,\mathrm{std}}(\psi^{-1}(\boldsymbol{t}))\, \left|\det(\psi^{-1})'(\boldsymbol{t})\right| &= \prod_{s=1}^{d} \frac{1}{\sqrt{2\pi}} \mathrm{e}^{-\mathrm{erf}^{-2}(2x_s - 1)} \cdot \sqrt{2\pi}\, \mathrm{e}^{\mathrm{erf}^{-2}(2x_s - 1)} \\ &= 1. \end{aligned}$$

This proves the first equality. The proof for the second equality works analogously. ■

Theorem 2.10. *The functions* $(\varphi_{\boldsymbol{k}}^{(d),\,\mathrm{std}})_{\boldsymbol{k}\in\mathbb{N}_0^d}$ *with*

$$\varphi_{\boldsymbol{k}}^{(d),\,\mathrm{std}}(\boldsymbol{x}) \coloneqq \left(\varphi_{\boldsymbol{k}}^{(d),\,\cos} \circ \psi\right)(\boldsymbol{x}) = \sqrt{2}^{\|\boldsymbol{k}\|_0} \prod_{s=1}^{d} \cos\left(\pi k_i\, \Phi(x_i)\right), \qquad (2.15)$$

the cumulative distribution function Φ *from* (2.12)*, and the transformation* ψ *from* (2.14) *form a complete orthonormal system in* $\mathrm{L}_2(\mathbb{R}^d, \omega^{(d),\,\mathrm{std}})$.

Proof. The cumulative distribution function Φ is bijective and Lemma 2.9 implies that $f \mapsto f \circ \psi$ is an isometric isomorphism between $\mathrm{L}_2([0,1]^d)$ and $\mathrm{L}_2(\mathbb{R}^d, \omega^{(d),\,\mathrm{std}})$. An isometric isomorphism between two spaces maps an orthonormal basis in one space to an orthonormal basis in the other. This directly implies that $(\varphi_{\boldsymbol{k}}^{(d),\,\mathrm{std}})_{\boldsymbol{k}\in\mathbb{N}_0^d}$ is an orthonormal basis in $\mathrm{L}_2(\mathbb{R}^d, \omega^{(d),\,\mathrm{std}})$. ■

In summary, we have constructed a complete orthonormal system $(\varphi_{\boldsymbol{k}}^{(d),\,\mathrm{std}})_{\boldsymbol{k}\in\mathbb{N}_0^d}$ in the weighted space $\mathrm{L}_2(\mathbb{R}^d, \omega^{(d),\,\mathrm{std}})$ using transformation ideas from [NP20, NK14] and the well-known half-period cosine basis $(\varphi_{\boldsymbol{k}}^{(d),\,\cos})_{\boldsymbol{k}\in\mathbb{N}_0^d}$ on $\mathrm{L}_2([0,1]^d)$. The transformation and some basis functions have been visualized in Figure 2.2. The BOS constant (2.2) is then equal to that of the half-period cosine, i.e., $C_{\mathrm{BOS}} = \sqrt{2}^d$.

Remark 2.11. *The same transformation idea can be applied to different distributions and corresponding probability densities. As origin space, we may always use* $\mathrm{L}_2([0,1^d])$ *with the half-period cosine basis. This is the same connection a random variable of any distribution has to the uniform distribution via inverse transform sampling.*

2.1.3 Approximation with Partial Sums

In this subsection, we consider a Lebesgue product space $\mathrm{L}_2(\mathbb{D}^d, \omega^{(d)})$, see Definition 2.1, with an orthonormal basis $(\varphi_{\boldsymbol{k}}^{(d)})_{\boldsymbol{k}\in\mathbb{Z}^d}$ that is a bounded

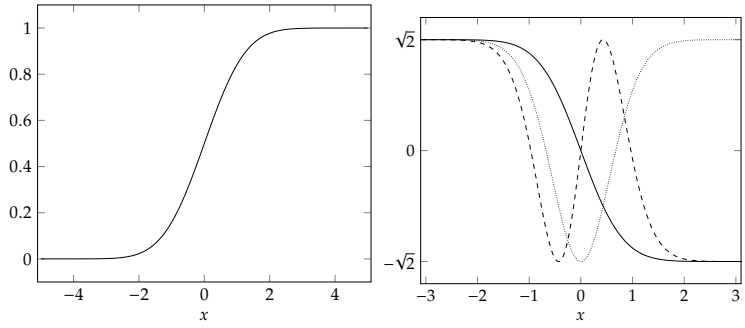

(a) Cumulative distribution function Φ from (2.12).

(b) Basis functions $\varphi_k^{(1),\mathrm{std}}$ from (2.15) for $k = 1$ (solid), $k = 2$ (dotted), and $k = 3$ (dashed).

Figure 2.2: Cumulative distribution function Φ and transformed basis functions $\varphi_k^{\mathrm{trafo}}$ in one dimension.

orthonormal system. Note that our index set may also be the subset $\mathbb{N}_0^d \subseteq \mathbb{Z}^d$, cf. Section 2.1.2. However, this is contained in our statements since we may set $\varphi_{\boldsymbol{k}}^{(d)} \equiv 0$ for $\boldsymbol{k} \in \mathbb{Z}^d \setminus \mathbb{N}_0^d$. The main goal of this work is the approximation of functions. With our methods in Chapter 4, we are always going to consider only a finite part of the basis expansion. This part is given by a finite *frequency* or *index set* which we denote in general by $\mathcal{I} \subseteq \mathbb{Z}^d$. Given such an index set $\mathcal{I}$, we define the corresponding partial sum operator as

$$\mathrm{S}_{\mathcal{I}} f(\boldsymbol{x}) \coloneqq \sum_{\boldsymbol{k} \in \mathcal{I}} \mathrm{c}_{\boldsymbol{k}}(f)\ \varphi_{\boldsymbol{k}}^{(d)}(\boldsymbol{x}) \tag{2.16}$$

for every $f \in \mathrm{L}_2(\mathbb{D}^d, \omega^{(d)})$ and call $\mathrm{S}_{\mathcal{I}} f$ the **partial sum** of f with respect to $\mathcal{I}$. Since our basis functions $\varphi_{\boldsymbol{k}}^{(d)}(\boldsymbol{x})$ are continuous, the function $\mathrm{S}_{\mathcal{I}} f(\boldsymbol{x})$ as a linear combination is a continuous function as well. For a given weight $w \colon \mathbb{Z}^d \to [1, \infty)$, we consider index sets of type

$$\mathcal{I} \coloneqq \{\boldsymbol{k} \in \mathbb{Z}^d \colon w(\boldsymbol{k}) \leq N\} \tag{2.17}$$

with cut-off parameter $N \in \mathbb{N}$. Figure 2.3 shows two possible examples in 3 dimensions, the full grid version with

$$w^{\infty}(\boldsymbol{k}) \coloneqq \|\boldsymbol{k}\|_{\ell_\infty} \tag{2.18}$$

and a version with our weights $w^{\alpha,\beta}$ from (2.5). Figure 2.3a is also called a hyperbolic cross. The approximation with hyperbolic crosses and the related mixed smoothness functions presents an important problem in many applications. For a detailed overview, we refer to [DTU18]. In the following two lemmas, we discuss the errors that arise through this truncation.

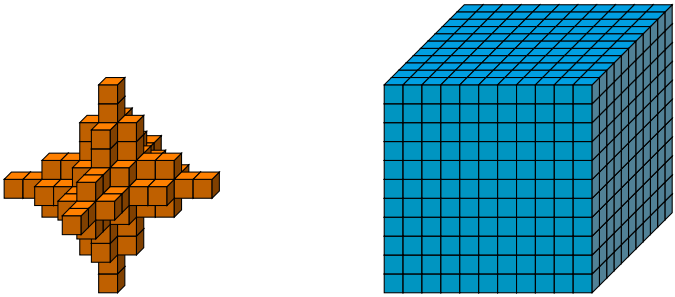

(a) $\mathcal{I}$ with $w^{\alpha,\beta}$, $\alpha = \beta = 1$, and $N = 40$. (b) $\mathcal{I}$ with w^{∞} from (2.18) and $N = 5$.

Figure 2.3: Two possible index sets $\mathcal{I}$ with different weight functions w and cut-off parameter N.

Lemma 2.12. *Let* $\mathrm{H}^{w}(\mathbb{D}^d, \omega^{(d)})$ *be a Sobolev type space with weight function* $w\colon \mathbb{Z}^d \to [1,\infty)$ *and* $\mathcal{I}$ *as in* (2.17) *with cut-off parameter* $N \in \mathbb{N}$*. Then we have the truncation error*

$$\sup_{\|f\|_{\mathrm{H}^{w}(\mathbb{D}^d,\omega^{(d)})}\leq 1} \|f - \mathrm{S}_{\mathcal{I}}\, f\|_{\mathrm{L}_2(\mathbb{D}^d,\omega^{(d)})} \leq \frac{1}{N}.$$

Proof. We employ Parseval's identity and incorporate the weight to

obtain

$$\begin{aligned}\|f - \mathrm{S}_{\mathcal{I}} f\|^2_{\mathrm{L}_2(\mathbb{D}^d,\omega^{(d)})} &= \sum_{\boldsymbol{k}\in\mathbb{Z}^d\setminus\mathcal{I}} |\mathrm{c}_{\boldsymbol{k}}(f)|^2 = \sum_{\boldsymbol{k}\in\mathbb{Z}^d\setminus\mathcal{I}} \frac{w^2(\boldsymbol{k})}{w^2(\boldsymbol{k})} |\mathrm{c}_{\boldsymbol{k}}(f)|^2 \\ &\le \sup_{\boldsymbol{k}\in\mathbb{Z}^d\setminus\mathcal{I}} \frac{1}{w^2(\boldsymbol{k})} \sum_{\boldsymbol{k}\in\mathbb{Z}^d\setminus\mathcal{I}} w^2(\boldsymbol{k}) |\mathrm{c}_{\boldsymbol{k}}(f)|^2 \\ &\le \frac{1}{\inf_{\boldsymbol{k}\in\mathbb{Z}^d\setminus\mathcal{I}} w^2(\boldsymbol{k})} \|f\|^2_{\mathrm{H}^w(\mathbb{D}^d,\omega^{(d)})}.\end{aligned}$$

The result follows since $\inf_{\boldsymbol{k}\in\mathbb{Z}^d\setminus\mathcal{I}} w^2(\boldsymbol{k}) = N^2$, cf. (2.17). ∎

Lemma 2.13. *Let $\mathcal{A}^w(\mathbb{D}^d,\omega^{(d)})$ be a weighted Wiener space with weight function $w\colon\mathbb{Z}^d\to[1,\infty)$ and $\mathcal{I}$ as in* (2.17) *with cut-off parameter $N\in\mathbb{N}$. Then we have the truncation error*

$$\sup_{\|f\|_{\mathcal{A}^w(\mathbb{D}^d,\omega^{(d)})}\le 1} \|f - \mathrm{S}_{\mathcal{I}} f\|_{\mathrm{L}_\infty(\mathbb{D}^d)} \le \frac{C_{\mathrm{BOS}}}{N}$$

with C_{BOS} from (2.2)*.*

Proof. We estimate the L_∞ norm and incorporate the weight in a similar fashion to the proof of Lemma 2.12 to obtain

$$\begin{aligned}\|f - \mathrm{S}_{\mathcal{I}} f\|_{\mathrm{L}_\infty(\mathbb{D}^d)} &= \operatorname*{ess\,supp}_{\boldsymbol{x}\in\mathbb{D}^d} \left| \sum_{\boldsymbol{k}\in\mathbb{Z}^d\setminus\mathcal{I}} \mathrm{c}_{\boldsymbol{k}}(f)\, \varphi^{(d)}_{\boldsymbol{k}}(\boldsymbol{x}) \right| \\ &\le \sum_{\boldsymbol{k}\in\mathbb{Z}^d\setminus\mathcal{I}} |\mathrm{c}_{\boldsymbol{k}}(f)| \operatorname*{ess\,supp}_{\boldsymbol{x}\in\mathbb{D}^d} \left|\varphi^{(d)}_{\boldsymbol{k}}(\boldsymbol{x})\right| \\ &\le \sup_{\boldsymbol{k}\in\mathbb{Z}^d} \left\|\varphi^{(d)}_{\boldsymbol{k}}\right\|_{\mathrm{L}_\infty(\mathbb{D}^d)} \left(\sum_{\boldsymbol{k}\in\mathbb{Z}^d\setminus\mathcal{I}} \frac{w(\boldsymbol{k})}{w(\boldsymbol{k})} |\mathrm{c}_{\boldsymbol{k}}(f)| \right) \\ &\le \frac{C_{\mathrm{BOS}}}{\inf_{\boldsymbol{k}\in\mathbb{Z}^d\setminus\mathcal{I}} w(\boldsymbol{k})} \|f\|_{\mathcal{A}^w(\mathbb{D}^d,\omega^{(d)})}.\end{aligned}$$

The result follows since $\inf_{\boldsymbol{k}\in\mathbb{Z}^d\setminus\mathcal{I}} w(\boldsymbol{k}) = N$, cf. (2.17). ∎

As Lemma 2.12 and Lemma 2.13 show, the relation between the weight function w and the truncation parameter N is the key factor in the truncation error. In all generality, for a fixed $N \in \mathbb{N}$, we observe that with rising smoothness of a function, we need less elements in the corresponding index set $\mathcal{I}$, i.e., less basis functions to achieve the same error. If we do not fix N, we may state that with the same amount of basis functions, we achieve a better error. In Figure 2.4, we have visualized the relationship between N and $|\mathcal{I}|$ for our two weight functions from before in three dimensions.

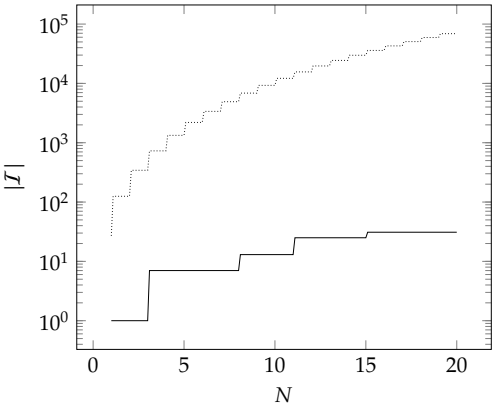

Figure 2.4: Number of elements in $\mathcal{I}$ in relation to the cut-off parameter N for $d = 3$ and w^{∞} from (2.18) (dotted) as well as $w^{\alpha,\beta}$, $\alpha = \beta = 1$, from (2.5) (solid).

2.2 Projection, ANOVA Terms and the ANOVA Decomposition

In this section, we lay the foundation for and subsequently introduce the classical analysis of variance (ANOVA) decomposition, see e.g. [CMO97, RFA99, LO06, KSWW09, Hol11, Gu13]. It is based on and an

extension of results in [PS21a, PS22a]. We specifically want to point out [Owe13, Appendix A] as a detailed reference to ANOVA with many important remarks and connections. We consider Lebesgue space $\mathrm{L}_2(\mathbb{D}^d, \omega^{(d)})$ from Definition 2.1 with functions $f\colon \mathbb{D}^d \to \mathbb{C}$ and a product structure, i.e., we have a complete orthonormal system

$$\varphi_{\boldsymbol{k}}^{(d)}(\boldsymbol{x}) \coloneqq \prod_{j=1}^{d} \varphi_{k_j}(x_j),\, \boldsymbol{k} \in \mathbb{Z}^d,$$

where φ_k, $k \in \mathbb{Z}$, is a orthonormal basis in $\mathrm{L}_2(\mathbb{D}, \omega)$ with

$$\omega^{(d)}(\boldsymbol{x}) \coloneqq \prod_{j=1}^{d} \omega(x_j),$$

cf. (2.1). Moreover, we assume the basis functions are bounded and continuous with BOS constant $\mathrm{C}_{\mathrm{BOS}} < \infty$, cf. (2.2). A final assumption that we can make without the loss of generality is $\varphi_0 \equiv 1$. Now, we may write any $f \in \mathrm{L}_2(\mathbb{D}^d, \omega^{(d)})$ as the basis expansion

$$f(\boldsymbol{x}) = \sum_{\boldsymbol{k} \in \mathbb{Z}^d} \mathrm{c}_{\boldsymbol{k}}(f)\ \varphi_{\boldsymbol{k}}^{(d)}(\boldsymbol{x}). \tag{2.19}$$

In the following, we denote the *set of coordinate indices* as $[d] \coloneqq \{1, 2, \dots, d\}$ and its subsets with bold small letters, e.g., $\boldsymbol{u} \subseteq [d]$. The complement is always considered with respect to $[d]$, e.g., $\boldsymbol{u}^{\mathrm{c}} \coloneqq [d] \setminus \boldsymbol{u}$.

The foundation of a multivariate decomposition is a projection operator, cf. [KSWW09]. For the classical ANOVA decomposition, we use the integral projection

$$\mathrm{P}_{\boldsymbol{u}} f(\boldsymbol{x}) \coloneqq \int_{\mathbb{D}^{d-|\boldsymbol{u}|}} f(\boldsymbol{x})\, \omega^{(d-|\boldsymbol{u}|)}(\boldsymbol{x}_{\boldsymbol{u}^{\mathrm{c}}})\, \mathrm{d}\boldsymbol{x}_{\boldsymbol{u}^{\mathrm{c}}} \tag{2.20}$$

which means integrating over the variables x_i with $i \notin \boldsymbol{u}$. If $\boldsymbol{u} = \emptyset$ we get the constant $\mathrm{P}_{\emptyset} f \in \mathbb{C}$ and for $|\boldsymbol{u}| > 0$ a function $\mathrm{P}_{\boldsymbol{u}} f \in \mathrm{L}_2(\mathbb{D}^{|\boldsymbol{u}|}, \omega^{(|\boldsymbol{u}|)})$. Since $\mathrm{P}_{\boldsymbol{u}} f$ only depends on the variables $\boldsymbol{x}_{\boldsymbol{u}}$, we have $\mathrm{P}_{\boldsymbol{u}} f(\boldsymbol{x}) = \mathrm{P}_{\boldsymbol{u}} f(\boldsymbol{x}_{\boldsymbol{u}})$. The following lemma provides a connection between the projections $\mathrm{P}_{\boldsymbol{u}} f$ and the basis expansion (2.19) of functions.

Lemma 2.14. *Let* $f \in \mathrm{L}_2(\mathbb{D}^d, \omega^{(d)})$ *and* $\mathrm{P}_{\boldsymbol{u}} f$, $\emptyset \neq \boldsymbol{u} \subseteq [d]$, *as in* (2.20). *Then for an index* $\boldsymbol{\ell} \in \mathbb{Z}^{|\boldsymbol{u}|}$ *we have*

$$\mathrm{c}_{\boldsymbol{\ell}}(\mathrm{P}_{\boldsymbol{u}} f) = \mathrm{c}_{\boldsymbol{k}}(f)$$

where $\boldsymbol{k} \in \mathbb{Z}^d$ *is the index with* $\boldsymbol{k}_{\boldsymbol{u}} = \boldsymbol{\ell}$ *and* $\boldsymbol{k}_{\boldsymbol{u}^{\mathrm{c}}} = \mathbf{0}$. *Note that the basis coefficient* $\mathrm{c}_{\boldsymbol{\ell}}(\mathrm{P}_{\boldsymbol{u}} f)$ *is with respect to the basis* $(\varphi_{\boldsymbol{\ell}}^{(|\boldsymbol{u}|)})_{\boldsymbol{\ell} \in \mathbb{Z}^{|\boldsymbol{u}|}}$ *in* $\mathrm{L}_2(\mathbb{D}^{|\boldsymbol{u}|}, \omega^{(|\boldsymbol{u}|)})$. *Moreover, we have*

$$\mathrm{P}_{\emptyset} f = \mathrm{c}_{\mathbf{0}}(f)\,.$$

Proof. The basis coefficient is given by definition as

$$\mathrm{c}_{\boldsymbol{\ell}}(\mathrm{P}_{\boldsymbol{u}} f) = \int_{\mathbb{D}^{|\boldsymbol{u}|}} \int_{\mathbb{D}^{d-|\boldsymbol{u}|}} f(\boldsymbol{x})\, \omega^{(d-|\boldsymbol{u}|)}(\boldsymbol{x}_{\boldsymbol{u}^{\mathrm{c}}})\, \mathrm{d}\boldsymbol{x}_{\boldsymbol{u}^{\mathrm{c}}}\, \overline{\varphi}_{\boldsymbol{\ell}}^{(|\boldsymbol{u}|)}(\boldsymbol{x}_{\boldsymbol{u}})\, \omega^{(|\boldsymbol{u}|)}(\boldsymbol{x}_{\boldsymbol{u}})\, \mathrm{d}\boldsymbol{x}_{\boldsymbol{u}}.$$

We consolidate the two integrals and exploit the product structure of the weight to obtain

$$\mathrm{c}_{\boldsymbol{\ell}}(\mathrm{P}_{\boldsymbol{u}} f) = \int_{\mathbb{D}^d} f(\boldsymbol{x})\, \overline{\varphi}_{\boldsymbol{\ell}}^{(|\boldsymbol{u}|)}(\boldsymbol{x}_{\boldsymbol{u}})\, \omega^{(d)}(\boldsymbol{x})\, \mathrm{d}\boldsymbol{x}.$$

If we take the index $\boldsymbol{k} \in \mathbb{Z}^d$ with $\boldsymbol{k}_{\boldsymbol{u}} = \boldsymbol{\ell}$ and $\operatorname{supp} \boldsymbol{k} \subseteq \boldsymbol{u}$ we have $\varphi_{\boldsymbol{\ell}}^{(|\boldsymbol{u}|)}(\boldsymbol{x}_{\boldsymbol{u}}) = \varphi_{\boldsymbol{k}}^{(d)}(\boldsymbol{x})$ which leads to

$$\mathrm{c}_{\boldsymbol{\ell}}(\mathrm{P}_{\boldsymbol{u}} f) = \int_{\mathbb{D}^d} f(\boldsymbol{x})\, \overline{\varphi}_{\boldsymbol{k}}^{(d)}(\boldsymbol{x})\, \omega^{(d)}(\boldsymbol{x})\, \mathrm{d}\boldsymbol{x} = \mathrm{c}_{\boldsymbol{k}}(f)\,.$$

and yields our statement. ∎

Using the projections (2.20), we recursively define the ANOVA terms of a function $f \in \mathrm{L}_2(\mathbb{D}^d, \omega^{(d)})$ as

$$f_{\boldsymbol{u}}(\boldsymbol{x}) \coloneqq \mathrm{P}_{\boldsymbol{u}} f(\boldsymbol{x}) - \sum_{\boldsymbol{v} \subsetneq \boldsymbol{u}} f_{\boldsymbol{v}}(\boldsymbol{x}). \tag{2.21}$$

This yields the constant $f_{\emptyset} = \mathrm{P}_{\emptyset} f \in \mathbb{C}$ and for $\emptyset \neq \boldsymbol{u} \subseteq [d]$ functions $f_{\boldsymbol{u}} \in \mathrm{L}_2(\mathbb{D}^{|\boldsymbol{u}|}, \omega^{(|\boldsymbol{u}|)})$. There also exists a direct formula for the ANOVA terms $f_{\boldsymbol{u}}$ which has been proven in [KSWW09] using properties of projection operators. We show the same formula in Theorem 2.16 using combinatorial arguments and the following lemma.

Lemma 2.15. *Let $a \in \mathbb{N}_0$ and $b \in \mathbb{N}$ with $b > a$. Then*

$$\sum_{n=a}^{b-1} (-1)^{n-a+1} \binom{b-a}{n-a} = (-1)^{b-a}.$$

Proof. We prove an equivalent form obtained through multiplication with $(-1)^a$ and an index shift

$$\sum_{n=0}^{b-a-1} (-1)^{n+a+1} \binom{b-a}{n} = (-1)^b.$$

Splitting the sum and applying the Binomial theorem yields

$$\begin{aligned}
\sum_{n=0}^{b-a-1} (-1)^{n+a+1} \binom{b-a}{n} &= \sum_{n=0}^{b-a} (-1)^{n+a+1} \binom{b-a}{n} - (-1)^{b+1} \\
&= (-1)^{a+1} \underbrace{\sum_{n=0}^{b-a} (-1)^n \binom{b-a}{n}}_{=(-1+1)^{b-a}=0} + (-1)^b \\
&= (-1)^b.
\end{aligned}$$

■

Theorem 2.16. *Let $f \in \mathrm{L}_2(\mathbb{D}^d, \omega^{(d)})$ with $\boldsymbol{u} \subseteq [d]$. Then*

$$f_{\boldsymbol{u}} = \sum_{\boldsymbol{v} \subseteq \boldsymbol{u}} (-1)^{|\boldsymbol{u}|-|\boldsymbol{v}|} \, \mathrm{P}_{\boldsymbol{v}} f. \tag{2.22}$$

Proof. We prove this statement through structural induction over the cardinality of $\boldsymbol{u}$. For $|\boldsymbol{u}| = 0$, i.e., $\boldsymbol{u} = \emptyset$, we have

$$(-1)^{0-0} \, \mathrm{P}_{\emptyset} f(\boldsymbol{x}) = \mathrm{P}_{\emptyset} f(\boldsymbol{x}) = \mathrm{P}_{\emptyset} f(\boldsymbol{x}) - \sum_{\boldsymbol{v} \subsetneq \emptyset} f_{\boldsymbol{v}}(\boldsymbol{x}).$$

Now, let (2.22) be true for $\boldsymbol{v} \subseteq [d]$, $|\boldsymbol{v}| = 0, 1, \ldots, m-1$, $m \in [d]$, and take a subset $\boldsymbol{u} \subseteq [d]$ with $|\boldsymbol{u}| = m$. We use the notation

$$\delta_{\boldsymbol{w}\subseteq\boldsymbol{v}} = \begin{cases} 1 & : \boldsymbol{w} \subseteq \boldsymbol{v} \\ 0 & : \text{otherwise.} \end{cases}$$

and start from the recursive expression in (2.21) to obtain

$$\begin{aligned} f_{\boldsymbol{u}}(\boldsymbol{x}) &= \mathrm{P}_{\boldsymbol{u}} f(\boldsymbol{x}) - \sum_{\boldsymbol{v}\subsetneq\boldsymbol{u}} f_{\boldsymbol{v}}(\boldsymbol{x}) = \mathrm{P}_{\boldsymbol{u}} f(\boldsymbol{x}) - \sum_{\boldsymbol{v}\subsetneq\boldsymbol{u}} \sum_{\boldsymbol{w}\subseteq\boldsymbol{v}} (-1)^{|\boldsymbol{v}|-|\boldsymbol{w}|} \mathrm{P}_{\boldsymbol{w}} f(\boldsymbol{x}) \\ &= \mathrm{P}_{\boldsymbol{u}} f(\boldsymbol{x}) - \sum_{\boldsymbol{v}\subsetneq\boldsymbol{u}} \sum_{\boldsymbol{w}\subsetneq\boldsymbol{u}} (-1)^{|\boldsymbol{v}|-|\boldsymbol{w}|} \mathrm{P}_{\boldsymbol{w}} f(\boldsymbol{x})\, \delta_{\boldsymbol{w}\subseteq\boldsymbol{v}}. \end{aligned}$$

We exchange the two sums and sum over the order of the ANOVA terms

$$\begin{aligned} \sum_{\boldsymbol{v}\subsetneq\boldsymbol{u}} \sum_{\boldsymbol{w}\subsetneq\boldsymbol{u}} (-1)^{|\boldsymbol{v}|-|\boldsymbol{w}|} \mathrm{P}_{\boldsymbol{w}} f(\boldsymbol{x})\, \delta_{\boldsymbol{w}\subseteq\boldsymbol{v}} &= \sum_{\boldsymbol{w}\subsetneq\boldsymbol{u}} \mathrm{P}_{\boldsymbol{w}} f(\boldsymbol{x}) \sum_{\boldsymbol{v}\subsetneq\boldsymbol{u}} (-1)^{|\boldsymbol{v}|-|\boldsymbol{w}|}\, \delta_{\boldsymbol{w}\subseteq\boldsymbol{v}} \\ &= \sum_{\boldsymbol{w}\subsetneq\boldsymbol{u}} \mathrm{P}_{\boldsymbol{w}} f(\boldsymbol{x}) \sum_{n=|\boldsymbol{w}|}^{m-1} \sum_{\substack{\boldsymbol{v}\subsetneq\boldsymbol{u} \\ |\boldsymbol{v}|=n}} (-1)^{|\boldsymbol{v}|-|\boldsymbol{w}|} \delta_{\boldsymbol{w}\subseteq\boldsymbol{v}} \\ &= \sum_{\boldsymbol{w}\subsetneq\boldsymbol{u}} \mathrm{P}_{\boldsymbol{w}} f(\boldsymbol{x}) \sum_{n=|\boldsymbol{w}|}^{m-1} (-1)^{n-|\boldsymbol{w}|} \sum_{\substack{\boldsymbol{v}\subsetneq\boldsymbol{u} \\ |\boldsymbol{v}|=n}} \delta_{\boldsymbol{w}\subseteq\boldsymbol{v}}. \end{aligned}$$

The application of Lemma 2.15 then yields the direct formula (2.22). ■

As for the projections $\mathrm{P}_{\boldsymbol{u}} f$ in Lemma 2.14, we are able to prove a connection between the ANOVA terms $f_{\boldsymbol{u}}$ and the basis expansion (2.19) of f.

Lemma 2.17. *Let $f \in \mathrm{L}_2(\mathbb{D}^d, \omega^{(d)})$ and $f_{\boldsymbol{u}}$, $\emptyset \neq \boldsymbol{u} \subseteq [d]$, as in* (2.21)*. Then for an index $\boldsymbol{\ell} \in \mathbb{Z}^{|\boldsymbol{u}|}$ we have*

$$\mathrm{c}_{\boldsymbol{\ell}}(f_{\boldsymbol{u}}) = \begin{cases} \mathrm{c}_{\boldsymbol{k}}(f) & : \boldsymbol{\ell} \in (\mathbb{Z} \setminus \{0\})^{|\boldsymbol{u}|} \\ 0 & : \text{otherwise} \end{cases}$$

where $\boldsymbol{k} \in \mathbb{Z}^d$ *is the index with* $\boldsymbol{k}_{\boldsymbol{u}} = \boldsymbol{\ell}$ *and* $\boldsymbol{k}_{\boldsymbol{u}^c} = \mathbf{0}$*. Note that the basis coefficient* $\mathrm{c}_{\boldsymbol{\ell}}(f_{\boldsymbol{u}})$ *is with respect to the basis* $(\varphi_{\boldsymbol{\ell}}^{(|\boldsymbol{u}|)})_{\boldsymbol{\ell} \in \mathbb{Z}^{|\boldsymbol{u}|}}$ *in* $\mathrm{L}_2(\mathbb{D}^{|\boldsymbol{u}|}, \omega^{(|\boldsymbol{u}|)})$*. Moreover, we have*

$$f_{\emptyset} = \mathrm{P}_{\emptyset} f = \mathrm{c}_{\mathbf{0}}(f)\,.$$

Proof. We define $\boldsymbol{k} \in \mathbb{Z}^d$ as the index with $\boldsymbol{k}_{\boldsymbol{u}} = \boldsymbol{\ell}$ and $\boldsymbol{k}_{\boldsymbol{u}^c} = \mathbf{0}$. Employing the direct formula (2.22) yields

$$\begin{aligned}
\mathrm{c}_{\boldsymbol{\ell}}(f_{\boldsymbol{u}}) &= \int_{\mathbb{D}^{|\boldsymbol{u}|}} f_{\boldsymbol{u}}(\boldsymbol{x}_{\boldsymbol{u}})\, \overline{\varphi}_{\boldsymbol{\ell}}^{(|\boldsymbol{u}|)}(\boldsymbol{x}_{\boldsymbol{u}})\, \omega^{(|\boldsymbol{u}|)}(\boldsymbol{x}_{\boldsymbol{u}})\, \mathrm{d}\boldsymbol{x}_{\boldsymbol{u}} \\
&= \int_{\mathbb{D}^{|\boldsymbol{u}|}} \left[\sum_{\boldsymbol{v} \subseteq \boldsymbol{u}} (-1)^{|\boldsymbol{u}|-|\boldsymbol{v}|} \mathrm{P}_{\boldsymbol{v}} f(\boldsymbol{x}_{\boldsymbol{v}}) \right] \overline{\varphi}_{\boldsymbol{\ell}}^{(|\boldsymbol{u}|)}(\boldsymbol{x}_{\boldsymbol{u}})\, \omega^{(|\boldsymbol{u}|)}(\boldsymbol{x}_{\boldsymbol{u}})\, \mathrm{d}\boldsymbol{x}_{\boldsymbol{u}} \\
&= \sum_{\boldsymbol{v} \subseteq \boldsymbol{u}} (-1)^{|\boldsymbol{u}|-|\boldsymbol{v}|} \int_{\mathbb{D}^{|\boldsymbol{u}|}} \mathrm{P}_{\boldsymbol{v}} f(\boldsymbol{x}_{\boldsymbol{v}})\, \overline{\varphi}_{\boldsymbol{\ell}}^{(|\boldsymbol{u}|)}(\boldsymbol{x}_{\boldsymbol{u}})\, \omega^{(|\boldsymbol{u}|)}(\boldsymbol{x}_{\boldsymbol{u}})\, \mathrm{d}\boldsymbol{x}_{\boldsymbol{u}} \\
&= \sum_{\boldsymbol{v} \subseteq \boldsymbol{u}} (-1)^{|\boldsymbol{u}|-|\boldsymbol{v}|}\, \mathrm{c}_{\boldsymbol{k}_{\boldsymbol{v}}}(\mathrm{P}_{\boldsymbol{v}} f) \prod_{h \in \boldsymbol{u} \setminus \boldsymbol{v}} \delta_{h,0}.
\end{aligned}$$

For $\boldsymbol{\ell} \in (\mathbb{Z} \setminus \{0\})^{|\boldsymbol{u}|}$, i.e., $\operatorname{supp} \boldsymbol{k} = \boldsymbol{u}$, we have $\prod_{h \in \boldsymbol{u} \setminus \boldsymbol{v}} \delta_{h,0} = 1 \iff \boldsymbol{v} = \boldsymbol{u}$ and it follows that

$$\mathrm{c}_{\boldsymbol{\ell}}(f_{\boldsymbol{u}}) = (-1)^0\, \mathrm{c}_{\boldsymbol{k}_{\boldsymbol{u}}}(\mathrm{P}_{\boldsymbol{u}} f) = \mathrm{c}_{\boldsymbol{k}}(f)\,.$$

In the case that $\operatorname{supp} \boldsymbol{k} \subsetneq \boldsymbol{u}$, we have $\prod_{h \in \boldsymbol{u} \setminus \boldsymbol{v}} \delta_{h,0} = 1 \iff \operatorname{supp} \boldsymbol{k} \subseteq \boldsymbol{v}$ and therefore

$$\mathrm{c}_{\boldsymbol{\ell}}(f_{\boldsymbol{u}}) = \sum_{\substack{\boldsymbol{v} \subseteq \boldsymbol{u} \\ \operatorname{supp} \boldsymbol{k} \subseteq \boldsymbol{v}}} (-1)^{|\boldsymbol{u}|-|\boldsymbol{v}|}\, \mathrm{c}_{\boldsymbol{k}_{\boldsymbol{v}}}(\mathrm{P}_{\boldsymbol{v}} f) = \mathrm{c}_{\boldsymbol{k}}(f) \sum_{\substack{\boldsymbol{v} \subseteq \boldsymbol{u} \\ \operatorname{supp} \boldsymbol{k} \subseteq \boldsymbol{v}}} (-1)^{|\boldsymbol{u}|-|\boldsymbol{v}|}.$$

We show that the appearing sum is zero by the binomial theorem

$$\sum_{\substack{\boldsymbol{v} \subseteq \boldsymbol{u} \\ \operatorname{supp} \boldsymbol{k} \subseteq \boldsymbol{v}}} (-1)^{|\boldsymbol{u}|-|\boldsymbol{v}|} = \sum_{j=0}^{|\boldsymbol{u}|-|\operatorname{supp} \boldsymbol{k}|} \binom{|\boldsymbol{u}| - |\operatorname{supp} \boldsymbol{k}|}{j} (-1)^{|\boldsymbol{u}|-(|\operatorname{supp} \boldsymbol{k}|+j)} = 0$$

which yields the result. ∎

Lemma 2.14 and Lemma 2.17 tell us the following interesting connection between the projections $\mathrm{P}_{\boldsymbol{u}} f$ and the ANOVA terms $f_{\boldsymbol{u}}$ with the basis expansion of f, i.e.,

$$\mathrm{P}_{\boldsymbol{u}} f(\boldsymbol{x}) = \sum_{\boldsymbol{\ell} \in \mathbb{Z}^{|\boldsymbol{u}|}} \mathrm{c}_{\boldsymbol{\ell}}(\mathrm{P}_{\boldsymbol{u}} f)\, \varphi_{\boldsymbol{\ell}}^{(|\boldsymbol{u}|)}(\boldsymbol{x}) = \sum_{\substack{\boldsymbol{h} \in \mathbb{Z}^d \\ \operatorname{supp} \boldsymbol{h} \subseteq \boldsymbol{u}}} \mathrm{c}_{\boldsymbol{h}}(f)\, \varphi_{\boldsymbol{h}}^{(d)}(\boldsymbol{x}).$$

and

$$f_{\boldsymbol{u}}(\boldsymbol{x}) = \sum_{\boldsymbol{\ell} \in (\mathbb{Z} \setminus \{0\})^{|\boldsymbol{u}|}} \mathrm{c}_{\boldsymbol{\ell}}(f_{\boldsymbol{u}})\, \varphi_{\boldsymbol{\ell}}^{(|\boldsymbol{u}|)}(\boldsymbol{x}) = \sum_{\substack{\boldsymbol{h} \in \mathbb{Z}^d \\ \operatorname{supp} \boldsymbol{h} = \boldsymbol{u}}} \mathrm{c}_{\boldsymbol{h}}(f)\, \varphi_{\boldsymbol{h}}^{(d)}(\boldsymbol{x}).$$

We observe the recursive definition of the ANOVA terms directly here since the difference between the terms and the projections lies only in the support of the respective indices $\boldsymbol{h} \in \mathbb{Z}^d$. This connection to the basis expansion allows us to work with these objects in an elegant manner. An example for this is the proof of the following corollary, showing the orthogonality of ANOVA terms. This is a well-known fact, see e.g. [Gri06, KSWW09].

Corollary 2.18. *Let $f \in \mathrm{L}_2(\mathbb{D}^d, \omega^{(d)})$ and $\boldsymbol{u}, \boldsymbol{v} \subseteq [d]$ with $\boldsymbol{u} \neq \boldsymbol{v}$. Then the ANOVA terms $f_{\boldsymbol{u}}$ and $f_{\boldsymbol{v}}$ are orthogonal, i.e.,*

$$\langle f_{\boldsymbol{u}}, f_{\boldsymbol{v}} \rangle_{\mathrm{L}_2(\mathbb{D}^d, \omega^{(d)})} = 0.$$

Proof. We employ Lemma 2.17 to obtain

$$\begin{aligned} \langle f_{\boldsymbol{u}}, f_{\boldsymbol{v}} \rangle_{\mathrm{L}_2(\mathbb{D}^d, \omega^{(d)})} &= \sum_{\substack{\boldsymbol{k} \in \mathbb{Z}^d \\ \operatorname{supp} \boldsymbol{k} = \boldsymbol{u}}} \sum_{\substack{\boldsymbol{h} \in \mathbb{Z}^d \\ \operatorname{supp} \boldsymbol{h} = \boldsymbol{v}}} \mathrm{c}_{\boldsymbol{k}}(f)\, \overline{\mathrm{c}_{\boldsymbol{h}}(f)}\, \langle \varphi_{\boldsymbol{k}}^{(d)}(\boldsymbol{x}), \varphi_{\boldsymbol{h}}^{(d)}(\boldsymbol{x}) \rangle_{\mathrm{L}_2(\mathbb{D}^d, \omega^{(d)})} \\ &= \sum_{\substack{\boldsymbol{k} \in \mathbb{Z}^d \\ \operatorname{supp} \boldsymbol{k} = \boldsymbol{u}}} \sum_{\substack{\boldsymbol{h} \in \mathbb{Z}^d \\ \operatorname{supp} \boldsymbol{h} = \boldsymbol{v}}} \mathrm{c}_{\boldsymbol{k}}(f)\, \overline{\mathrm{c}_{\boldsymbol{h}}(f)}\, \delta_{\boldsymbol{k},\boldsymbol{h}} = 0. \end{aligned}$$

■

We have collected all ingredients and are now prepared to introduce the classical ANOVA decomposition in our setting, cf. [KSWW09].

Theorem 2.19. *Let $f \in \mathrm{L}_2(\mathbb{D}^d, \omega^{(d)})$, the ANOVA terms $f_{\boldsymbol{u}}$ as in* (2.21) *and the set of coordinate indices $[d] = \{1, 2, \dots, d\}$. Then f can be uniquely decomposed as*

$$f(\boldsymbol{x}) = f_\emptyset + \sum_{i=1}^{d} f_{\{i\}}(x_i) + \sum_{i=1}^{d-1} \sum_{j=i+1}^{d} f_{\{i,j\}}(\boldsymbol{x}_{\{i,j\}}) + \cdots + f_{[d]}(\boldsymbol{x}) = \sum_{\boldsymbol{u} \subseteq [d]} f_{\boldsymbol{u}}(\boldsymbol{x}_{\boldsymbol{u}}) \tag{2.23}$$

which we call ***analysis of variance (ANOVA) decomposition****.*

Proof. The statement is well-known and can be proven straightforward by summation

$$\sum_{\boldsymbol{u} \subseteq [d]} f_{\boldsymbol{u}}(\boldsymbol{x}_{\boldsymbol{u}}) = \sum_{\boldsymbol{u} \subseteq [d]} \sum_{\substack{\boldsymbol{k} \in \mathbb{Z}^d \\ \operatorname{supp} \boldsymbol{k} = \boldsymbol{u}}} \mathrm{c}_{\boldsymbol{k}}(f)\, \varphi_{\boldsymbol{k}}^{(d)}(\boldsymbol{x}) = \sum_{\boldsymbol{k} \in \mathbb{Z}^d} \mathrm{c}_{\boldsymbol{k}}(f)\, \varphi_{\boldsymbol{k}}^{(d)}(\boldsymbol{x}) = f(\boldsymbol{x}).$$

The uniqueness of the decomposition follows from the fact that every basis coefficient $\mathrm{c}_{\boldsymbol{k}}(f)$, $\boldsymbol{k} \in \mathbb{Z}^d$, appears only once in the ANOVA term $f_{\operatorname{supp} \boldsymbol{k}}$. ∎

Multivariate decompositions in general and the ANOVA decomposition in particular can of course be considered in a much more general setting. For this, we refer to the article [KSWW09]. In our setting, we not only have uniqueness of the decomposition, but also our one to one connection of every basis coefficient $\mathrm{c}_{\boldsymbol{k}}(f)$, $\boldsymbol{k} \in \mathbb{Z}^d$, and ANOVA term $f_{\operatorname{supp} \boldsymbol{k}}$. This view of the decomposition in the *frequency* domain, which we visualized in Figure 2.5, will be an essential tool in our approximation method of Chapter 4. It also an interesting observation how the decomposition reflects the curse of dimensionality trough the number of terms $|\mathcal{P}([d])| = 2^d$ rising exponentially in the spatial dimension.

Remark 2.20. *The ANOVA decomposition* (2.23) *depends strongly on the projection operator $\mathrm{P}_{\boldsymbol{u}} f$ from* (2.20)*. The integral operator considered in this thesis leads to the so called classical ANOVA decomposition. Another*

important variant is the anchored decomposition where one chooses an anchor point $\boldsymbol{p} \in \mathbb{D}^d$ *and the projection operator is then defined as*

$$\mathrm{P}_{\boldsymbol{u}} f(\boldsymbol{x}_{\boldsymbol{u}}) = f(\boldsymbol{y}),\ \boldsymbol{y}_{\boldsymbol{u}} = \boldsymbol{x}_{\boldsymbol{u}}, \boldsymbol{y}_{\boldsymbol{u}^{\mathrm{c}}} = \boldsymbol{p}_{\boldsymbol{u}^{\mathrm{c}}}.$$

This decomposition can for example be used for the integration of high-dimensional functions, see e.g. [DG14, KNP+17, GKNW18]. However, the error analysis may again be based on the classical ANOVA decomposition, see e.g. [GHHR17]. In our scattered data setting, we always focus on the classical version of the decomposition.

In the end of this section, we discuss how the smoothness of a function $f \in \mathrm{L}_2(\mathbb{D}^d, \omega^{(d)})$ defined by the decay of the basis coefficients translates to its projections $\mathrm{P}_{\boldsymbol{u}} f$ and ANOVA terms $f_{\boldsymbol{u}}$. This has also been discussed for a different setting in [LO06, GKS10, GKS16] and therein called **inheritance of smoothness**. In our setting, we consider smoothness trough the Sobolev type spaces $\mathrm{H}^w(\mathbb{D}^d, \omega^{(d)})$ and weighted Wiener spaces $\mathcal{A}^w(\mathbb{D}^d, \omega^{(d)})$ with weight function $w\colon \mathbb{Z}^d \to [1, \infty)$, see (2.4) and (2.3).

Theorem 2.21 (Inheritance of smoothness for Sobolev type spaces)**.** *Let* $f \in \mathrm{H}^w(\mathbb{D}^d, \omega^{(d)})$ *with weight function* $w\colon \mathbb{Z}^d \to [1, \infty)$*. Then for any weight* $w_{\boldsymbol{u}}\colon \mathbb{Z}^{|\boldsymbol{u}|} \to [1, \infty)$ *with*

$$w_{\boldsymbol{u}}(\boldsymbol{k}_{\boldsymbol{u}}) \le w(\boldsymbol{k})\ \forall \boldsymbol{k} \in \mathbb{Z}^d, \operatorname{supp} \boldsymbol{k} \subseteq \boldsymbol{u},$$

we have $\mathrm{P}_{\boldsymbol{u}} f \in \mathrm{H}^{w_{\boldsymbol{u}}}(\mathbb{D}^{|\boldsymbol{u}|}, \omega^{(|\boldsymbol{u}|)})$ *and* $f_{\boldsymbol{u}} \in \mathrm{H}^{w_{\boldsymbol{u}}}(\mathbb{D}^{|\boldsymbol{u}|}, \omega^{(|\boldsymbol{u}|)})$*. This holds true in particular for a weight defined by* $w_{\boldsymbol{u}}(\boldsymbol{\ell}) \coloneqq w(\boldsymbol{h})$ *with* $\boldsymbol{h}_{\boldsymbol{u}} = \boldsymbol{\ell}$ *and* $\boldsymbol{h}_{\boldsymbol{u}^{\mathrm{c}}} = \boldsymbol{0}$*.*

Proof. We show that the norm $\|\mathrm{P}_{\boldsymbol{u}} f\|_{\mathrm{H}^{w_{\boldsymbol{u}}}(\mathbb{D}^{|\boldsymbol{u}|}, \omega^{(|\boldsymbol{u}|)})}$ is finite by using Lemma 2.14

$$\begin{aligned}\sum_{\boldsymbol{\ell} \in \mathbb{Z}^{|\boldsymbol{u}|}} w_{\boldsymbol{u}}^2(\boldsymbol{\ell}) \, |\mathrm{c}_{\boldsymbol{\ell}}(\mathrm{P}_{\boldsymbol{u}} f)|^2 &= \sum_{\substack{\boldsymbol{k} \in \mathbb{Z}^d \\ \operatorname{supp} \boldsymbol{k} \subseteq \boldsymbol{u}}} w_{\boldsymbol{u}}^2(\boldsymbol{k}_{\boldsymbol{u}}) \, |\mathrm{c}_{\boldsymbol{k}}(f)|^2 \le \sum_{\substack{\boldsymbol{k} \in \mathbb{Z}^d \\ \operatorname{supp} \boldsymbol{k} \subseteq \boldsymbol{u}}} w^2(\boldsymbol{k}) \, |\mathrm{c}_{\boldsymbol{k}}(f)|^2 \\ &\le \sum_{\boldsymbol{k} \in \mathbb{Z}^d} w^2(\boldsymbol{k}) \, |\mathrm{c}_{\boldsymbol{k}}(f)|^2 = \|f\|^2_{\mathrm{H}^w(\mathbb{D}^d, \omega^{(d)})} < \infty.\end{aligned}$$

(a) The origin as the index $\boldsymbol{k} \in \mathbb{Z}^3$ with $|\operatorname{supp} \boldsymbol{k}| = 0$.

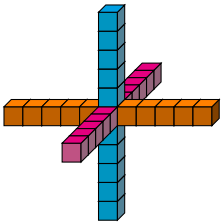

(b) The indices $\boldsymbol{k} \in \mathbb{Z}^3$ with $|\operatorname{supp} \boldsymbol{k}| = 1$ belonging to $f_{\{1\}}$ in orange, $f_{\{2\}}$ in magenta, and $f_{\{3\}}$ in cyan.

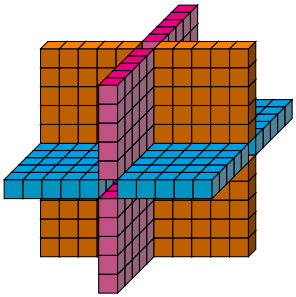

(c) The indices $\boldsymbol{k} \in \mathbb{Z}^3$ with $|\operatorname{supp} \boldsymbol{k}| = 2$ belonging to $f_{\{1,2\}}$ in orange, $f_{\{1,3\}}$ in magenta, and $f_{\{2,3\}}$ in cyan.

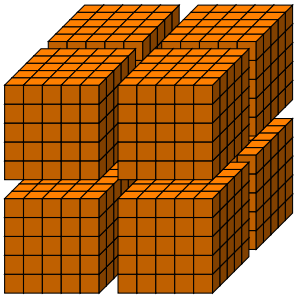

(d) The indices $\boldsymbol{k} \in \mathbb{Z}^3$ with $|\operatorname{supp} \boldsymbol{k}| = 3$ belonging to $f_{\{1,2,3\}}$ in orange.

Figure 2.5: The ANOVA decomposition in the frequency domain visualized within the cube $[-5, 5]^3 \cap \mathbb{Z}^3$.

Analogously, we employ Lemma 2.17 to prove $f_{\boldsymbol{u}} \in \mathrm{H}^{w_{\boldsymbol{u}}}(\mathbb{D}^{|\boldsymbol{u}|}, \omega^{(|\boldsymbol{u}|)})$

$$\sum_{\boldsymbol{\ell} \in \mathbb{Z}^{|\boldsymbol{u}|}} w_{\boldsymbol{u}}^2(\boldsymbol{\ell}) \, |\mathrm{c}_{\boldsymbol{\ell}}(f_{\boldsymbol{u}})|^2 = \sum_{\substack{\boldsymbol{k} \in \mathbb{Z}^d \\ \operatorname{supp} \boldsymbol{k} = \boldsymbol{u}}} w_{\boldsymbol{u}}^2(\boldsymbol{k}_{\boldsymbol{u}}) \, |\mathrm{c}_{\boldsymbol{k}}(f)|^2 \leq \sum_{\substack{\boldsymbol{k} \in \mathbb{Z}^d \\ \operatorname{supp} \boldsymbol{k} = \boldsymbol{u}}} w^2(\boldsymbol{k}) \, |\mathrm{c}_{\boldsymbol{k}}(f)|^2$$
$$\leq \sum_{\boldsymbol{k} \in \mathbb{Z}^d} w^2(\boldsymbol{k}) \, |\mathrm{c}_{\boldsymbol{k}}(f)|^2 = \|f\|^2_{\mathrm{H}^w(\mathbb{D}^d, \omega^{(d)})} < \infty.$$

■

Theorem 2.22 (Inheritance of smoothness for the weighted algebra)**.** *Let f be an element of $\mathcal{A}^w(\mathbb{D}^d, \omega^{(d)})$ with weight function $w \colon \mathbb{Z}^d \to [1, \infty)$. Then for any weight $w_{\boldsymbol{u}} \colon \mathbb{Z}^{|\boldsymbol{u}|} \to [1, \infty)$ with*

$$w_{\boldsymbol{u}}(\boldsymbol{k}_{\boldsymbol{u}}) \leq w(\boldsymbol{k}) \; \forall \boldsymbol{k} \in \mathbb{Z}^d, \operatorname{supp} \boldsymbol{k} \subseteq \boldsymbol{u},$$

we have $\mathrm{P}_{\boldsymbol{u}} f \in \mathcal{A}^{w_{\boldsymbol{u}}}(\mathbb{D}^{|\boldsymbol{u}|}, \omega^{(|\boldsymbol{u}|)})$ and $f_{\boldsymbol{u}} \in \mathcal{A}^{w_{\boldsymbol{u}}}(\mathbb{D}^{|\boldsymbol{u}|}, \omega^{(|\boldsymbol{u}|)})$. This holds true in particular for a weight defined by $w_{\boldsymbol{u}}(\boldsymbol{\ell}) := w(\boldsymbol{h})$ with $\boldsymbol{h}_{\boldsymbol{u}} = \boldsymbol{\ell}$ and $\boldsymbol{h}_{\boldsymbol{u}^{\mathrm{c}}} = \mathbf{0}$.

Proof. First, we prove that $\|\mathrm{P}_{\boldsymbol{u}} f\|_{\mathcal{A}^{w_{\boldsymbol{u}}}(\mathbb{D}^{|\boldsymbol{u}|}, \omega^{(|\boldsymbol{u}|)})}$ is finite with the help of Lemma 2.14

$$\sum_{\boldsymbol{\ell} \in \mathbb{Z}^{|\boldsymbol{u}|}} w_{\boldsymbol{u}}(\boldsymbol{\ell}) \, |\mathrm{c}_{\boldsymbol{\ell}}(\mathrm{P}_{\boldsymbol{u}} f)| = \sum_{\substack{\boldsymbol{k} \in \mathbb{Z}^d \\ \operatorname{supp} \boldsymbol{k} \subseteq \boldsymbol{u}}} w_{\boldsymbol{u}}(\boldsymbol{k}_{\boldsymbol{u}}) \, |\mathrm{c}_{\boldsymbol{k}}(f)| \leq \sum_{\substack{\boldsymbol{k} \in \mathbb{Z}^d \\ \operatorname{supp} \boldsymbol{k} \subseteq \boldsymbol{u}}} w(\boldsymbol{k}) \, |\mathrm{c}_{\boldsymbol{k}}(f)|$$
$$\leq \sum_{\boldsymbol{k} \in \mathbb{Z}^d} w(\boldsymbol{k}) \, |\mathrm{c}_{\boldsymbol{k}}(f)| = \|f\|_{\mathcal{A}^w(\mathbb{D}^d, \omega^{(d)})} < \infty.$$

In a similar fashion, we use Lemma 2.17 and prove $f_{\boldsymbol{u}} \in \mathcal{A}^{w_{\boldsymbol{u}}}(\mathbb{D}^{|\boldsymbol{u}|}, \omega^{(|\boldsymbol{u}|)})$

$$\sum_{\boldsymbol{\ell} \in \mathbb{Z}^{|\boldsymbol{u}|}} w_{\boldsymbol{u}}(\boldsymbol{\ell}) \, |\mathrm{c}_{\boldsymbol{\ell}}(f_{\boldsymbol{u}})| = \sum_{\substack{\boldsymbol{k} \in \mathbb{Z}^d \\ \operatorname{supp} \boldsymbol{k} = \boldsymbol{u}}} w_{\boldsymbol{u}}(\boldsymbol{k}_{\boldsymbol{u}}) \, |\mathrm{c}_{\boldsymbol{k}}(f)| \leq \sum_{\substack{\boldsymbol{k} \in \mathbb{Z}^d \\ \operatorname{supp} \boldsymbol{k} = \boldsymbol{u}}} w(\boldsymbol{k}) \, |\mathrm{c}_{\boldsymbol{k}}(f)|$$
$$\leq \sum_{\boldsymbol{k} \in \mathbb{Z}^d} w(\boldsymbol{k}) \, |\mathrm{c}_{\boldsymbol{k}}(f)| = \|f\|_{\mathcal{A}^w(\mathbb{D}^d, \omega^{(d)})} < \infty.$$

■

Theorem 2.21 and Theorem 2.22 show that the projections $\mathrm{P}_{\boldsymbol{u}} f$ and the ANOVA terms $f_{\boldsymbol{u}}$ are at least as smooth as f itself. In certain cases, e.g., for kink functions, it has been observed that some ANOVA terms are indeed smoother than the function itself. Those kink functions arise, e.g., in financial applications, see [GKS10].

2.3 Effective Dimensions and the Truncated ANOVA Decomposition

In this section, we discuss the interpretability of the ANOVA decomposition based on the well-known Sobol indices or global sensitivity indices, cf. [Sob90, Sob01, LO06]. We introduce notions of effective dimensions and the truncated ANOVA decomposition. This helps us achieve two purposes: We lay the foundation for our interpretable approximation method from Chapter 4 where the sensitivity indices play a major role and moreover it helps us discover a way to circumvent the curse of dimensionality in terms of our decomposition.

We aim to understand the importance of ANOVA terms $f_{\boldsymbol{u}}$, $\emptyset \neq \boldsymbol{u} \subseteq [d]$, by considering variances. The **variance of a function** is defined as the integral

$$\sigma^2(f) \coloneqq \int_{\mathbb{D}^d} (f(\boldsymbol{x}) - \mathrm{c}_{\mathbf{0}}(f))^2 \ \omega^{(d)}(\boldsymbol{x}) \ \mathrm{d}\boldsymbol{x}$$

for a real-valued function $f \in \mathrm{L}_2(\mathbb{D}^d, \omega^{(d)})$. In this case, we have the equivalent formulation

$$\sigma^2(f) = \|f\|^2_{\mathrm{L}_2(\mathbb{D}^d, \omega^{(d)})} - |\mathrm{c}_{\mathbf{0}}(f)|^2$$

which yields a sensible definition for complex-valued functions as well. Subsequently, we obtain that for the ANOVA terms $f_{\boldsymbol{u}}$ with $\emptyset \neq \boldsymbol{u} \subseteq [d]$ we have $\mathrm{c}_{\mathbf{0}}(f_{\boldsymbol{u}}) = 0$ by Lemma 2.17 and therefore

$$\sigma^2(f_{\boldsymbol{u}}) = \|f_{\boldsymbol{u}}\|^2_{\mathrm{L}_2(\mathbb{D}^{|\boldsymbol{u}|}, \omega^{(|\boldsymbol{u}|)})}. \tag{2.24}$$

The following lemma shows how the ANOVA decomposition works with regard to the variances of our terms.

Lemma 2.23. *Let $f \in \mathrm{L}_2(\mathbb{D}^d, \omega^{(d)})$. Then we have*

$$\sigma^2(f) = \sum_{\emptyset \neq \boldsymbol{u} \subseteq [d]} \sigma^2(f_{\boldsymbol{u}}).$$

Proof. We show that the right-hand side equals the left-hand side by applying Lemma 2.14 as follows

$$\begin{aligned}\sum_{\emptyset\neq\boldsymbol{u}\subseteq[d]}\sigma^2(f_{\boldsymbol{u}}) &= \sum_{\emptyset\neq\boldsymbol{u}\subseteq[d]}\sum_{\substack{\boldsymbol{k}\in\mathbb{Z}^d\\ \operatorname{supp}\boldsymbol{k}=\boldsymbol{u}}}|c_{\boldsymbol{k}}(f)|^2\\ &= \sum_{\boldsymbol{k}\in\mathbb{Z}^d}|c_{\boldsymbol{k}}(f)|^2 - |c_{\boldsymbol{0}}(f)|^2 = \|f\|^2_{L_2(\mathbb{D}^d,\omega^{(d)})} - |c_{\boldsymbol{0}}(f)|^2\,.\end{aligned}$$

■

In order to find a comparable score to rank the importance of ANOVA terms against each other, we introduce the **Sobol indices** or **global sensitivity indices** (gsi)

$$\varrho(\boldsymbol{u},f) := \frac{\sigma^2(f_{\boldsymbol{u}})}{\sigma^2(f)} \in [0,1] \tag{2.25}$$

for a subset of coordinate indices $\emptyset \neq \boldsymbol{u} \subseteq [d]$, see e.g. [Sob90, Sob01, LO06]. The global sensitivity index $\varrho(\boldsymbol{u},f)$ for a term $f_{\boldsymbol{u}}$ tells us how much of the variance $\sigma^2(f)$ is explained by $f_{\boldsymbol{u}}$. We have $\sum_{\emptyset\neq\boldsymbol{u}\subseteq[d]}\varrho(\boldsymbol{u},f) = 1$ by Lemma 2.23. The sensitivity indices will be an important tool in the detection of sparsity in the ANOVA decomposition in Section 4.2.1.

Based on the concept of global sensitivity indices, we introduce the notions of **effective dimensions** as proposed, e.g., in [CMO97, Hol11]. Given a fixed $\delta \in (0,1]$, the notion of **superposition dimension** is defined as the minimum

$$d^{(\mathrm{sp})}(\delta) := \min\left\{ s\in[d]\colon \sum_{\substack{\emptyset\neq\boldsymbol{u}\subseteq[d]\\ |\boldsymbol{u}|\leq s}}\sigma^2(f_{\boldsymbol{u}}) \geq \delta\sigma^2(f)\right\}. \tag{2.26}$$

We observe the equivalence

$$\sum_{\substack{\emptyset\neq\boldsymbol{u}\subseteq[d]\\ |\boldsymbol{u}|\leq s}}\sigma^2(f_{\boldsymbol{u}}) \geq \delta\sigma^2(f) \quad\Longleftrightarrow\quad \sum_{\substack{\emptyset\neq\boldsymbol{u}\subseteq[d]\\ |\boldsymbol{u}|\leq s}}\varrho(\boldsymbol{u},f) \geq \delta.$$

In other words, δ percentage of the variance $\sigma^2(f)$ of our function f is explained by the ANOVA terms $f_{\boldsymbol{u}}$ with $|\boldsymbol{u}| \leq d^{(\mathrm{sp})}(\delta)$. In general, if we have a small $d^{(\mathrm{sp})}(\delta)$ for a δ close to one, we call the function of *low-dimensional structure*.

The effective dimension in the **truncation sense** for a $\delta \in (0, 1]$ is defined as

$$d^{(\mathrm{t})}(\delta) = \min \left\{ s \in [d] \colon \sum_{\emptyset \neq \boldsymbol{u} \subseteq [s]} \sigma^2(f_{\boldsymbol{u}}) \geq \delta \sigma^2(f) \right\}. \tag{2.27}$$

In this case, δ percentage of the variance $\sigma^2(f)$ can be explained by a part of the variables, i.e., the subset $\{1, 2, \ldots, d^{(\mathrm{t})}(\delta)\}$. In other words, if $d^{(\mathrm{t})}(\delta)$ is small for a δ close to one, only a few variables contribute to a significant amount of the variance of f. In this work, we focus on the superposition dimension $d^{(\mathrm{sp})}(\delta)$.

The concept of effective dimensions motivates the idea of considering only a part of the ANOVA decomposition of a function which may yield some interesting benefits. We say that $U \subseteq \mathcal{P}([d])$ is a **subset of ANOVA terms** if it is downward closed with regard to set inclusion, i.e., for $\boldsymbol{u}, \boldsymbol{v} \subseteq [d]$ it holds that

$$(\boldsymbol{v} \subseteq \boldsymbol{u} \text{ and } \boldsymbol{u} \in U) \Longrightarrow \boldsymbol{v} \in U.$$

This condition is necessary because of the recursive definition of the ANOVA terms (2.21). However, it can be relaxed if one assumes $f_{\boldsymbol{v}} \equiv 0$ for all $\boldsymbol{v} \subseteq [d]$, $\boldsymbol{v} \notin U$, where there exists a $\boldsymbol{u} \in U$ with $\boldsymbol{v} \subseteq \boldsymbol{u}$.

For any subset of ANOVA terms $U \subseteq \mathcal{P}([d])$, we define the truncated ANOVA decomposition as

$$\mathrm{T}_U f \coloneqq \sum_{\boldsymbol{u} \in U} f_{\boldsymbol{u}}.$$

A specific truncation idea can be obtained by relating to the superposition dimension $d^{(\mathrm{sp})}(\delta)$, see (2.26). For a chosen superposition threshold $d_s \in [d]$, we define

$$U^{(d,d_s)} \coloneqq \{\boldsymbol{u} \subseteq [d] \colon |\boldsymbol{u}| \leq d_s\} \tag{2.28}$$

and subsequently

$$\mathrm{T}_{d_s} f \coloneqq \mathrm{T}_{U^{(d,d_s)}} f = \sum_{\substack{\boldsymbol{u}\subseteq[d]\\ |\boldsymbol{u}|\le d_s}} f_{\boldsymbol{u}}.$$

As before, we are interested in how this truncation works in the frequency domain and show the relationship between the basis coefficients of T_U and f.

Lemma 2.24. *Let $f \in \mathrm{L}_2(\mathbb{D}^d, \omega^{(d)})$ and $U \subseteq \mathcal{P}([d])$ a subset of ANOVA terms. Then $\mathrm{T}_U f \in \mathrm{L}_2(\mathbb{D}^d, \omega^{(d)})$ and for any index $\boldsymbol{k} \in \mathbb{Z}^d$, the basis coefficient is given by*

$$\mathrm{c}_{\boldsymbol{k}}(\mathrm{T}_U f) = \begin{cases} \mathrm{c}_{\boldsymbol{k}}(f) & : \operatorname{supp} \boldsymbol{k} \in U \\ 0 & : \text{otherwise.} \end{cases}$$

In particular, for $U = U^{(d,d_s)}$ with $d_s \in [d]$, we have

$$\mathrm{c}_{\boldsymbol{k}}(\mathrm{T}_{d_s} f) = \begin{cases} \mathrm{c}_{\boldsymbol{k}}(f) & : |\operatorname{supp} \boldsymbol{k}| \le d_s \\ 0 & : \text{otherwise.} \end{cases}$$

Proof. Let $\boldsymbol{k} \in \mathbb{Z}^d$. Employing linearity and Lemma 2.17 yields

$$\mathrm{c}_{\boldsymbol{k}}(\mathrm{T}_U f) = \sum_{u\in U} \sum_{\substack{\boldsymbol{h}\in\mathbb{Z}^d\\ \operatorname{supp}\boldsymbol{h}=\boldsymbol{u}}} \mathrm{c}_{\boldsymbol{h}}(f)\, \delta_{\boldsymbol{k},\boldsymbol{h}} = \begin{cases} \mathrm{c}_{\boldsymbol{k}}(f) & : \operatorname{supp} \boldsymbol{k} \in U \\ 0 & : \text{otherwise.} \end{cases}$$

The statement for $\mathrm{T}_{d_s} f$ follows since $\operatorname{supp} \boldsymbol{k} \in U^{(d,d_s)} \iff |\operatorname{supp} \boldsymbol{k}| \le d_s$. ∎

Since there exists a direct formula for the ANOVA terms themselves, see (2.22), the existence of such formulas for the truncated decomposition can be assumed. The following theorem and its subsequent corollary show such a formula for the general case and the superposition case.

Theorem 2.25. *Let $f \in \mathrm{L}_2(\mathbb{D}^d, \omega^{(d)})$ and $U \subseteq \mathcal{P}([d])$ a subset of ANOVA terms. Then we have the direct formula*

$$\mathrm{T}_U f = \sum_{\boldsymbol{u} \in U} \sum_{\substack{\boldsymbol{v} \in U \\ \boldsymbol{u} \subseteq \boldsymbol{v}}} (-1)^{|\boldsymbol{v}|-|\boldsymbol{u}|} \mathrm{P}_{\boldsymbol{u}} f.$$

Proof. We apply (2.22) and obtain immediately

$$\begin{aligned} \mathrm{T}_U f &= \sum_{\boldsymbol{u} \in U} f_{\boldsymbol{u}} = \sum_{\boldsymbol{u} \in U} \sum_{\boldsymbol{v} \subseteq \boldsymbol{u}} (-1)^{|\boldsymbol{u}|-|\boldsymbol{v}|} \mathrm{P}_{\boldsymbol{v}} f = \sum_{\boldsymbol{u} \in U} \sum_{\boldsymbol{v} \in U} (-1)^{|\boldsymbol{u}|-|\boldsymbol{v}|} \mathrm{P}_{\boldsymbol{v}} f \, \delta_{\boldsymbol{v} \subseteq \boldsymbol{u}} \\ &= \sum_{\boldsymbol{v} \in U} \sum_{\substack{\boldsymbol{u} \in U \\ \boldsymbol{v} \subseteq \boldsymbol{u}}} (-1)^{|\boldsymbol{u}|-|\boldsymbol{v}|} \mathrm{P}_{\boldsymbol{v}} f. \end{aligned}$$

■

Corollary 2.26. *Let $f \in \mathrm{L}_2(\mathbb{D}^d, \omega^{(d)})$ and $d_s \in [d]$ a superposition threshold. Then we have the direct formula*

$$\mathrm{T}_{d_s} f = \sum_{\substack{\boldsymbol{u} \subseteq [d] \\ |\boldsymbol{u}| \le d_s}} \left[\sum_{n=|\boldsymbol{u}|}^{d_s} (-1)^{n-|\boldsymbol{u}|} \binom{d-|\boldsymbol{u}|}{n-|\boldsymbol{u}|} \right] \mathrm{P}_{\boldsymbol{u}} f.$$

Proof. Let $\boldsymbol{u} \in U^{(d,d_s)}$. The statement follows from the equality

$$\begin{aligned} \sum_{\substack{\boldsymbol{v} \in U^{(d,d_s)} \\ \boldsymbol{u} \subseteq \boldsymbol{v}}} (-1)^{|\boldsymbol{v}|-|\boldsymbol{u}|} &= \sum_{n=|\boldsymbol{u}|}^{d_s} (-1)^{n-|\boldsymbol{u}|} \left| \{ \boldsymbol{v} \in U^{(d,d_s)} \colon \boldsymbol{u} \subseteq \boldsymbol{v}, |\boldsymbol{v}| = n \} \right| \\ &= \sum_{n=|\boldsymbol{u}|}^{d_s} (-1)^{n-|\boldsymbol{u}|} \binom{d-|\boldsymbol{u}|}{n-|\boldsymbol{u}|}, \end{aligned}$$

and Theorem 2.25. ■

As mentioned before, the number of terms in the ANOVA decomposition is 2^d and therefore grows exponentially in the dimension which

reflects the curse of dimensionality in the sense of our multivariate decomposition. Now, we consider how the truncation may impact this exponential growth. The following well-known lemma from learning theory shows us that the number of terms in $U^{(d,d_s)}$ grows polynomially in the spatial dimension d for a fixed superposition dimension d_s which represents an important observation we exploit in our approximation approach in Chapter 4. In other words, it provides a way around the curse of dimensionality.

Lemma 2.27. *Let $d_s \in \mathbb{N}$. Then for any $d \in \mathbb{N}$, $d > d_s$, we estimate the cardinality of $U^{(d,d_s)}$ by*

$$\left|U^{(d,d_s)}\right| < \left(\frac{\mathrm{e} \cdot d}{d_s}\right)^{d_s},$$

i.e., the number of terms in $U^{(d,d_s)}$ has polynomial growth in d for fixed d_s.

Proof. We estimate the sum as follows

$$\left|U^{(d,d_s)}\right| = \sum_{n=0}^{d_s} \binom{d}{n} \leq \sum_{n=0}^{d_s} \frac{d^n d_s^n}{n!\, d_s^n} = \sum_{n=0}^{d_s} \left(\frac{d}{d_s}\right)^n \frac{d_s^n}{n!} \leq \left(\frac{d}{d_s}\right)^{d_s} \sum_{n=0}^{d_s} \frac{d_s^n}{n!}.$$

The statement follows from estimating the sum by the Taylor series for e^{d_s}. ∎

The truncated ANOVA decomposition will play a major role in our approximation approach since truncating to a subset of ANOVA terms may maintain a large part of the variance of the function while simultaneously simplifying a possible approximation model. Therefore, we are interested in functions that can be approximated well by such a truncated ANOVA decomposition, i.e., $\mathrm{T}_U f \approx f$. We are considering relative truncation errors of the form

$$\frac{\|f - \mathrm{T}_U f\|_{H_1}}{\|f\|_{H_2}} \tag{2.29}$$

with $H_1 \in \{\mathrm{L}_2(\mathbb{D}^d, \omega^{(d)}), \mathrm{L}_\infty(\mathbb{D}^d)\}$, $H_2 \in \{\mathrm{H}^w(\mathbb{D}^d, \omega^{(d)}), \mathcal{A}^w(\mathbb{D}^d, \omega^{(d)})\}$ for a weight $w\colon \mathbb{Z}^d \to [1, \infty)$. In other words, we try to relate the truncation of the ANOVA decomposition to the smoothness of the function characterized by the decay of the basis coefficients. If this relative error is small, the truncation will be sensible since we have sparsity in the ANOVA decomposition.

Specifically, we are interested in relating the concept of superposition dimension to the smoothness of the function. To this end, we modify the superposition dimension in the sense of this space, cf. in [Owe19]. For $\mathrm{H}^w(\mathbb{D}^d, \omega^{(d)})$ and accuracy $\delta \in (0, 1]$ we define the **worst-case superposition dimension** as

$$d^{(\mathrm{wcsp})}(\delta) \coloneqq \min\left\{ s \in [d] \colon \sup_{\|f\|_{\mathrm{H}^w(\mathbb{D}^d, \omega^{(d)})} \le 1} \sum_{\substack{\boldsymbol{u} \subseteq [d] \\ |\boldsymbol{u}| > s}} \sigma^2(f_{\boldsymbol{u}}) \le 1 - \delta \right\}. \quad (2.30)$$

In contrast to the superposition dimension $d^{(\mathrm{sp})}(\delta)$ itself, it is not a statement for a single function, but for the space $\mathrm{H}^w(\mathbb{D}^d, \omega^{(d)})$. The following lemma shows the connection between the worst-case superposition dimension and the truncation error (2.29) for $U = U^{(d,d_s)}$.

Lemma 2.28. *Let $\mathrm{H}^w(\mathbb{D}^d, \omega^{(d)})$ be a Sobolev type space with weight function $w\colon \mathbb{Z}^d \to [1, \infty)$. Then for a superposition threshold $d_s \in [d]$, and $\varepsilon \in [0, 1]$ we have the equivalence*

$$\sup_{\|f\|_{\mathrm{H}^w(\mathbb{D}^d, \omega^{(d)})} \le 1} \|f - \mathrm{T}_{d_s} f\|_{\mathrm{L}_2(\mathbb{D}^d, \omega^{(d)})} \le \varepsilon \iff d^{(\mathrm{wcsp})}(1 - \varepsilon^2) \le d_s.$$

Proof. We use (2.24) in (2.30) to obtain the equivalent formulation

$$\sup_{\|f\|_{\mathrm{H}^w(\mathbb{D}^d, \omega^{(d)})} \le 1} \sum_{\substack{\boldsymbol{u} \subseteq [d] \\ |\boldsymbol{u}| > s}} \sigma^2(f_{\boldsymbol{u}}) = \sup_{\|f\|_{\mathrm{H}^w(\mathbb{D}^d, \omega^{(d)})} \le 1} \|f - \mathrm{T}_{d_s} f\|^2_{\mathrm{L}_2(\mathbb{D}^d, \omega^{(d)})}.$$

Defining $\delta \coloneqq 1 - \varepsilon^2$ yields our desired result. ∎

Lemma 2.28 tells us that if we are able to bound the corresponding truncation error, we immediately obtain a bound on the worst-case superposition dimension $d^{(\mathrm{wcsp})}(\delta)$.

Theorem 2.29. *Let $\mathrm{H}^w(\mathbb{D}^d, \omega^{(d)})$ be a Sobolev type space with weight function $w\colon \mathbb{Z}^d \to [1,\infty)$ and $U \subseteq \mathcal{P}([d])$ a subset of ANOVA terms. Then*

$$\sup_{\|f\|_{\mathrm{H}^w(\mathbb{D}^d,\omega^{(d)})}\leq 1} \|f - \mathrm{T}_U f\|_{\mathrm{L}_2(\mathbb{D}^d,\omega^{(d)})} \leq \frac{1}{\min\limits_{\substack{\boldsymbol{k}\in\mathbb{Z}^d \\ \operatorname{supp}\boldsymbol{k}\notin U}} w(\boldsymbol{k})}.$$

Proof. We employ Parseval's identity and Lemma 2.24 to derive

$$\begin{aligned}
\|f - \mathrm{T}_U f\|^2_{\mathrm{L}_2(\mathbb{D}^d,\omega^{(d)})} &= \sum_{\boldsymbol{k}\in\mathbb{Z}^d} |\mathrm{c}_{\boldsymbol{k}}(f) - \mathrm{c}_{\boldsymbol{k}}(\mathrm{T}_U f)|^2 = \sum_{\substack{\boldsymbol{k}\in\mathbb{Z}^d \\ \operatorname{supp}\boldsymbol{k}\notin U}} |\mathrm{c}_{\boldsymbol{k}}(f)|^2 \\
&= \sum_{\substack{\boldsymbol{k}\in\mathbb{Z}^d \\ \operatorname{supp}\boldsymbol{k}\notin U}} \frac{w^2(\boldsymbol{k})}{w^2(\boldsymbol{k})} |\mathrm{c}_{\boldsymbol{k}}(f)|^2 \\
&\leq \frac{1}{\min\limits_{\substack{\boldsymbol{k}\in\mathbb{Z}^d \\ \operatorname{supp}\boldsymbol{k}\notin U}} w^2(\boldsymbol{k})} \|f\|^2_{\mathrm{H}^w(\mathbb{D}^d,\omega^{(d)})}.
\end{aligned}$$

Applying the square root on both sides yields the result. ∎

Theorem 2.30. *Let $\mathcal{A}^w(\mathbb{D}^d, \omega^{(d)})$ be a weighted Wiener space with weight function $w\colon \mathbb{Z}^d \to [1,\infty)$ and $U \subseteq \mathcal{P}([d])$ a subset of ANOVA terms. Then*

$$\sup_{\|f\|_{\mathcal{A}^w(\mathbb{D}^d,\omega^{(d)})}\leq 1} \|f - \mathrm{T}_U f\|_{\mathrm{L}_\infty(\mathbb{D}^d)} \leq \frac{C_{\mathrm{BOS}}}{\min\limits_{\substack{\boldsymbol{k}\in\mathbb{Z}^d \\ \operatorname{supp}\boldsymbol{k}\notin U}} w(\boldsymbol{k})}.$$

with C_{BOS} the constant (2.2)*. Additionally, for $\mathrm{H}^w(\mathbb{D}^d, \omega^{(d)})$ with weight function $w\colon \mathbb{Z}^d \to [1,\infty)$ such that $\{w^{-1}(\boldsymbol{k})\}_{\boldsymbol{k}\in\mathbb{Z}^d} \in \ell_2$, we have*

$$\sup_{\|f\|_{\mathrm{H}^w(\mathbb{D}^d,\omega^{(d)})}\leq 1} \|f - \mathrm{T}_U f\|_{\mathrm{L}_\infty(\mathbb{D}^d)} \leq C_{\mathrm{BOS}} \sqrt{\sum_{\substack{\boldsymbol{k}\in\mathbb{Z}^d \\ \operatorname{supp}\boldsymbol{k}\notin U}} \frac{1}{w^2(\boldsymbol{k})}}.$$

Proof. We estimate the L_∞-norm by the sum of the absolute values of the basis coefficients and then use Lemma 2.24 to obtain

$$\begin{aligned}
\|f - \mathrm{T}_U f\|_{\mathrm{L}_\infty(\mathbb{D}^d)} &= \operatorname*{ess\,supp}_{\boldsymbol{x}\in\mathbb{D}^d} \left| \sum_{\boldsymbol{k}\in\mathbb{Z}^d} (\mathrm{c}_{\boldsymbol{k}}(f) - \mathrm{c}_{\boldsymbol{k}}(\mathrm{T}_U f))\, \varphi_{\boldsymbol{k}}^{(d)}(\boldsymbol{x}) \right| \\
&\leq \operatorname*{ess\,supp}_{\boldsymbol{x}\in\mathbb{D}^d} \sum_{\substack{\boldsymbol{k}\in\mathbb{Z}^d \\ \operatorname{supp}\boldsymbol{k}\notin U}} |\mathrm{c}_{\boldsymbol{k}}(f)| \left|\varphi_{\boldsymbol{k}}^{(d)}(\boldsymbol{x})\right| \\
&\leq \sup_{\boldsymbol{k}\in\mathbb{Z}^d} \left\|\varphi_{\boldsymbol{k}}^{(d)}\right\|_{\mathrm{L}_\infty(\mathbb{D}^d)} \sum_{\substack{\boldsymbol{k}\in\mathbb{Z}^d \\ \operatorname{supp}\boldsymbol{k}\notin U}} \frac{w(\boldsymbol{k})}{w(\boldsymbol{k})} |\mathrm{c}_{\boldsymbol{k}}(f)| \qquad (2.31) \\
&\leq \frac{C_{\mathrm{BOS}}}{\min\limits_{\substack{\boldsymbol{k}\in\mathbb{Z}^d \\ \operatorname{supp}\boldsymbol{k}\notin U}} w(\boldsymbol{k})} \|f\|_{\mathcal{A}^w(\mathbb{D}^d,\omega^{(d)})}.
\end{aligned}$$

Employing the Cauchy-Schwarz inequality in (2.31) instead of extracting the minimum yields

$$\|f - \mathrm{T}_U f\|_{\mathrm{L}_\infty(\mathbb{D}^d,\omega^{(d)})} \leq C_{\mathrm{BOS}} \sqrt{\sum_{\substack{\boldsymbol{k}\in\mathbb{Z}^d \\ \operatorname{supp}\boldsymbol{k}\notin U}} \frac{1}{w^2(\boldsymbol{k})}}\ \|f\|_{\mathrm{H}^w(\mathbb{D}^d,\omega^{(d)})}.$$

The condition $\{w^{-1}(\boldsymbol{k})\}_{\boldsymbol{k}\in\mathbb{Z}^d} \in \ell_2$ assures that the sum appearing in the bound is finite. ∎

In the following, we consider the bounds for our special isotropic and dominating-mixed smoothness weights

$$w^{\alpha,\beta}(\boldsymbol{k}) = \gamma_{\operatorname{supp}\boldsymbol{k}}^{-1} (1 + \|\boldsymbol{k}\|_1)^\alpha \prod_{s=1}^{d} (1 + |k_s|)^\beta$$

from (2.5). Specifically, we aim to show that a cut-off based on a superposition threshold d_s is sensible for Sobolev type spaces and weighted Wiener spaces with this weight. We consider the worst-case truncation as corollaries of the previous results in Theorem 2.29 and Theorem 2.30.

Lemma 2.31. *Let $n \in [d]$ and $\boldsymbol{\gamma} \in (0,1]^d$. Then*

$$\sum_{\substack{\boldsymbol{u} \subseteq [d] \\ |\boldsymbol{u}|=n}} \prod_{s \in \boldsymbol{u}} \gamma_s^2 \leq \|\boldsymbol{\gamma}\|_2^{2n}.$$

Proof. We rewrite the sum as follows

$$\sum_{\substack{\boldsymbol{u} \subseteq [d] \\ |\boldsymbol{u}|=n}} \prod_{s \in \boldsymbol{u}} \gamma_s^2 = \sum_{i_1=1}^{d} \gamma_{i_1}^2 \sum_{i_2=i_1+1}^{d} \gamma_{i_2}^2 \cdots \sum_{i_n=i_{n-1}+1}^{d} \gamma_{i_n}^2.$$

Then every single sum can be estimated by $\|\boldsymbol{\gamma}\|_2^2$, i.e.,

$$\sum_{i_j=i_{j-1}+1}^{d} \gamma_{i_j}^2 \leq \sum_{i_j=1}^{d} \gamma_{i_j}^2 = \|\boldsymbol{\gamma}\|_2^2$$

for $j \in \{2, 3, \ldots, d\}$ with equality for $j = 1$. ∎

Corollary 2.32. *Let $\mathrm{H}^{w^{\alpha,\beta}}(\mathbb{D}^d, \omega^{(d)})$ be a Sobolev type space with weight function $w^{\alpha,\beta}$ from (2.5) with POD structure (2.6), $\beta \geq 0$, $\alpha > -\beta$, $\boldsymbol{\Gamma} \in (0,1]^d$, and $\boldsymbol{\gamma} \in (0,1]^d$. Then*

$$\sup_{\|f\|_{\mathrm{H}^{w^{\alpha,\beta}}(\mathbb{D}^d,\omega^{(d)})} \leq 1} \|f - \mathrm{T}_{d_s} f\|_{\mathrm{L}_2(\mathbb{D}^d,\omega^{(d)})} \leq \Gamma_{d_s+1} (2+d_s)^{-\alpha} 2^{-\beta(d_s+1)} \prod_{s=1}^{d_s+1} \gamma_s^* \tag{2.32}$$

for a superposition threshold $d_s \in [d]$ where $\boldsymbol{\gamma}^* = (\gamma_s^*)_{s=1}^d$ is the non-increasing rearrangement of $\boldsymbol{\gamma}$. For functions with isotropic smoothness $\alpha = 0$ and dominating mixed smoothness $\beta > 1/2$, we have

$$\sup_{\|f\|_{\mathrm{H}^{w^{\alpha,\beta}}(\mathbb{D}^d,\omega^{(d)})} \leq 1} \|f - \mathrm{T}_{d_s} f\|_{\mathrm{L}_\infty(\mathbb{D}^d)} \tag{2.33}$$

$$\leq C_{\mathrm{BOS}} \sqrt{\sum_{n=d_s+1}^{d} 2^n \Gamma_n^2 \left(\zeta(2\beta)-1\right)^n \|\boldsymbol{\gamma}\|_2^{2n}}$$

where ζ is the Riemann zeta function and C_{BOS} the BOS constant (2.2). *Assuming exponential decay for Γ_s, i.e., $\Gamma_s = c^s$ with $0 < c \leq 1$, such that*

$$c \left\|\boldsymbol{\gamma}\right\|_2 \sqrt{2\zeta(2\beta) - 2} < 1 \tag{2.34}$$

yields the bound

$$\begin{aligned} \sup_{\|f\|_{\mathrm{H}^{w^{\alpha,\beta}}(\mathbb{D}^d,\omega(d))} \leq 1} & \|f - \mathrm{T}_{d_s} f\|_{\mathrm{L}_\infty(\mathbb{D}^d)} \\ & \leq \frac{C_{\mathrm{BOS}} \left(c \left\|\boldsymbol{\gamma}\right\|_2 \sqrt{2\zeta(2\beta) - 2}\right)^{d_s+1}}{\sqrt{1 - 2c^2 \left\|\boldsymbol{\gamma}\right\|_2^2 (\zeta(2\beta) - 1)}}. \end{aligned} \tag{2.35}$$

Proof. We apply Theorem 2.29 and solve the appearing minimization as follows

$$\begin{aligned} & \min_{\substack{\boldsymbol{k} \in \mathbb{Z}^d \\ |\operatorname{supp} \boldsymbol{k}| > d_s}} w^{\alpha,\beta}(\boldsymbol{k}) \\ & \quad = \min_{\substack{\boldsymbol{k} \in \mathbb{Z}^d \\ |\operatorname{supp} \boldsymbol{k}| > d_s}} \Gamma^{-1}_{|\operatorname{supp} \boldsymbol{k}|} (1 + \|\boldsymbol{k}\|_1)^\alpha \prod_{s=1}^{d} (1 + |k_s|)^\beta \prod_{s \in \operatorname{supp} \boldsymbol{k}} \gamma_s^{-1} \\ & \quad = (2 + d_s)^\alpha \cdot 2^{\beta(d_s+1)} \cdot \min_{\substack{\boldsymbol{k} \in \mathbb{Z}^d \\ |\operatorname{supp} \boldsymbol{k}| > d_s}} \Gamma^{-1}_{|\operatorname{supp} \boldsymbol{k}|} \prod_{s \in \operatorname{supp} \boldsymbol{k}} \gamma_s^{-1} \\ & \quad = (2 + d_s)^\alpha \cdot 2^{\beta(d_s+1)} \cdot \Gamma^{-1}_{d_s+1} \cdot \prod_{s=1}^{d_s+1} (\gamma_s^*)^{-1} \end{aligned}$$

to obtain (2.32). In order to prove (2.33), we calculate the bound from

Theorem 2.30 by rearranging the terms

$$\begin{aligned}
\sum_{\substack{\boldsymbol{k}\in\mathbb{Z}^d\\ |\operatorname{supp}\boldsymbol{k}|>d_s}} \frac{1}{w^2(\boldsymbol{k})} &= \sum_{\substack{\boldsymbol{u}\subseteq[d]\\ |\boldsymbol{u}|>d_s}} \sum_{\substack{\boldsymbol{k}\in\mathbb{Z}^d\\ \operatorname{supp}\boldsymbol{k}=\boldsymbol{u}}} \frac{1}{\Gamma_{|\boldsymbol{u}|}^{-2}\prod_{s\in\boldsymbol{u}}\gamma_s^{-2}\,(1+|k_s|)^{2\beta}} \\
&= \sum_{\substack{\boldsymbol{u}\subseteq[d]\\ |\boldsymbol{u}|>d_s}} \Gamma_{|\boldsymbol{u}|}^2 \sum_{\boldsymbol{h}\in(\mathbb{Z}\setminus\{0\})^{|\boldsymbol{u}|}} \frac{1}{\left(\prod_{s\in\boldsymbol{u}}\gamma_s^{-2}\right)\left(\prod_{s=1}^{|\boldsymbol{u}|}(1+|h_s|)^{2\beta}\right)} \\
&= \sum_{\substack{\boldsymbol{u}\subseteq[d]\\ |\boldsymbol{u}|>d_s}} \Gamma_{|\boldsymbol{u}|}^2 \left(\prod_{s\in\boldsymbol{u}}\gamma_s^2\right) \sum_{\boldsymbol{h}\in(\mathbb{Z}\setminus\{0\})^{|\boldsymbol{u}|}} \frac{1}{\prod_{s=1}^{|\boldsymbol{u}|}(1+|h_s|)^{2\beta}} \\
&= \sum_{\substack{\boldsymbol{u}\subseteq[d]\\ |\boldsymbol{u}|>d_s}} \Gamma_{|\boldsymbol{u}|}^2 \left(\prod_{s\in\boldsymbol{u}}\gamma_s^2\right)\left(\sum_{k\in\mathbb{Z}\setminus\{0\}} \frac{1}{(1+|k|)^{2\beta}}\right)^{|\boldsymbol{u}|}.
\end{aligned}$$

Replacing the resulting sum by the Riemann zeta function and applying Lemma 2.31 yields

$$\begin{aligned}
\sum_{\substack{\boldsymbol{k}\in\mathbb{Z}^d\\ |\operatorname{supp}\boldsymbol{k}|>d_s}} \frac{1}{w^2(\boldsymbol{k})} &= \sum_{\substack{\boldsymbol{u}\subseteq[d]\\ |\boldsymbol{u}|>d_s}} \Gamma_{|\boldsymbol{u}|}^2 \left(\prod_{s\in\boldsymbol{u}}\gamma_s^2\right) 2^{|\boldsymbol{u}|}\,(\zeta(2\beta)-1)^{|\boldsymbol{u}|} \\
&= \sum_{n=d_s+1}^{d} \Gamma_n^2 2^n\,(\zeta(2\beta)-1)^n \sum_{\substack{\boldsymbol{u}\subseteq[d]\\ |\boldsymbol{u}|=n}} \left(\prod_{s\in\boldsymbol{u}}\gamma_s^2\right) \\
&\le \sum_{n=d_s+1}^{d} \Gamma_n^2 2^n\,(\zeta(2\beta)-1)^n \left\|\boldsymbol{\gamma}\right\|_2^{2n}
\end{aligned}$$

■

Corollary 2.33. *Let $\mathcal{A}^{w^{\alpha,\beta}}(\mathbb{D}^d, \omega^{(d)})$ be a weighted Wiener space with weight function $w^{\alpha,\beta}$ from* (2.5) *with POD structure* (2.6), $\beta \ge 0$, $\alpha > -\beta$, $\boldsymbol{\Gamma} \in (0,1]^d$,

and $\boldsymbol{\gamma} \in (0,1]^d$. *Then*

$$\sup_{\|f\|_{\mathcal{A}^{w^{\alpha,\beta}}(\mathbb{D}^d,\omega(d))} \leq 1} \|f - \mathrm{T}_{d_s} f\|_{\mathrm{L}_\infty(\mathbb{D}^d)} \leq C_{\mathrm{BOS}}\, \Gamma_{d_s+1}\, (2+d_s)^{-\alpha}\, 2^{-\beta(d_s+1)} \prod_{s=1}^{d_s+1} \gamma_s^* \tag{2.36}$$

for a superposition threshold $d_s \in [d]$ *where* $\boldsymbol{\gamma}^*$ *is the non-increasing rearrangement of* $\boldsymbol{\gamma}$ *and* C_{BOS} *the BOS constant* (2.2).

Proof. We use Theorem 2.30 and calculate the bound for the weight function $w^{\alpha,\beta}$ by computing the minimum as in the proof of Corollary 2.32. ∎

The previous results deliver us a wide range of error estimates for the truncation of the ANOVA decomposition in different norms. We specifically point out that for our weights, the bounds (2.32) and (2.36) are independent of the spatial dimension d. Similarly, if $\|\boldsymbol{\gamma}\|_2$ is bounded then also (2.35) can be considered independently of d.

Moreover, (2.32) gives us information about the worst-case superposition dimension $d^{(\mathrm{wcsp})}$. We fix the weights $\boldsymbol{\Gamma}$, $\boldsymbol{\gamma}$, and a superposition threshold $d_s \in \mathbb{N}$. Then Lemma 2.28 implies for the worst-case superposition dimension

$$d^{(\mathrm{wcsp})}(1 - \varepsilon^2(\alpha,\beta)) \leq d_s.$$

with

$$\varepsilon(\alpha,\beta) \coloneqq \Gamma_{d_s+1}\, (2+d_s)^{-\alpha}\, 2^{-\beta(d_s+1)} \prod_{s=1}^{d_s+1} \gamma_s^*.$$

In other words, the worst-case superposition dimension is at most d_s for accuracy $1 - \varepsilon^2(\alpha,\beta)$. In Figure 2.6, we have visualized truncation with $d_s = 3$. The figure shows $\varepsilon^2(\alpha,\beta)$ depending on the isotropic smoothness α and the dominating-mixed smoothness β from the weights $w^{\alpha,\beta}$, see (2.5). We observe that a high accuracy is obtainable in our setting even for small smoothness parameters α, and β.

In summary, we find that smoothness of this type relates to sparsity in the ANOVA decomposition in the superposition sense.

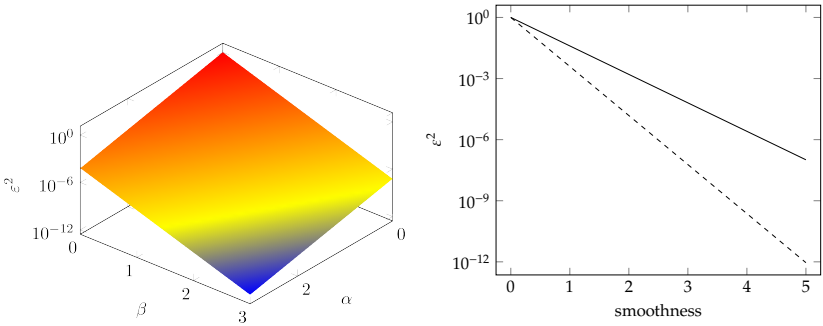

(a) Isotropic smoothness $\alpha \geq 0$ and dominating-mixed $\beta \geq 0$.

(b) Isotropic smoothness $\alpha \geq 0$ with $\beta = 0$ (solid) and dominating-mixed smoothness $\beta \geq 0$ with $\alpha = 0$ (dashed).

Figure 2.6: Bound from (2.32) with $\alpha \geq 0$ and $\beta \geq 0$ as well as parameters $\Gamma = \mathbf{1}$ and $\gamma = \mathbf{1}$.

3

Fast Multiplication with Grouped Transformations

The fast realization of discrete transformations like the fast Fourier transform (FFT), see e.g. [Bri88], play an important role in many applications. In fact, the FFT is one of the most important algorithms of our time. The non-equispaced fast Fourier transform (NFFT) and the non-equispaced fast cosine transform (NFCT), cf. [KKP09, PPST18, KKP], provide the fast realization of the discrete Fourier transform and the discrete cosine transform, respectively, if the spatial nodes are non-equispaced. However, as an index set, we still need to use full grids that grow exponentially in the spatial dimension. This can be remedied, e.g., with the lattice fast Fourier transform, see [Käm13], but then the nodes have to be chosen as a rank-1 lattice. With grouped transformations, we propose a fast realization of a transformation with non-equispaced scattered nodes and a new form of index set motivated by the ANOVA decomposition from Chapter 2.

The goal of this chapter is to combine the ideas of the ANOVA decomposition and specifically its truncation from Section 2.3 with the concept of fast transformations. This process is always in combination

with a transformation that fits to the chosen basis, e.g., the systems from Section 2.1.2. We reiterate on the NFFT and the NFCT in Section 3.1. The core ideas for the grouped transformations from [BPS22] are presented in Section 3.2 which we simultaneously generalize to new systems. Section 3.2.1 introduces grouped index sets as a combination of the index sets we have used to truncate basis expansions in Section 2.1.3 and the truncated ANOVA decomposition from Section 2.3. Section 3.2.2 is concerned with the fast transformations for non-equispaced data and matrices that are based on the grouped index sets. Moreover, we described in detail how the transformations are realized for every one of the system presented in Section 2.1.2. The grouped transformations are going to be used as a main part of the ANOVA approximation method in Chapter 4.

The core concept for grouped transformations was developed by the author in [PS21a] and later formalized in [BPS22]. The contributions by F. Bartel were focus on the group lasso regularization and the fast iterative shrinkage-thresholding algorithm.

3.1 Non-Equispaced Transformations

In this section, we consider two systems of functions, the Fourier system

$$\xi_{\boldsymbol{k}}^{(\exp)}(\boldsymbol{x}) = \mathrm{e}^{2\pi \mathrm{i}\, \boldsymbol{k}\cdot\boldsymbol{x}},\ \boldsymbol{k} \in \mathbb{Z}^d, \tag{3.1}$$

and the cosine system

$$\xi_{\boldsymbol{k}}^{(\cos)}(\boldsymbol{x}) = \prod_{s=1}^{d} \cos(2\pi\, k_s x_s),\ \boldsymbol{k} \in \mathbb{N}_0^d, \tag{3.2}$$

for a spatial dimension $d \in \mathbb{N}$. Subsequently, we take polynomials

$$p\colon \mathbb{D}^d \to \mathbb{C}, \quad p(\boldsymbol{x}) \coloneqq \sum_{\boldsymbol{k}\in\mathcal{I}} \hat{p}_{\boldsymbol{k}}\, \xi_{\boldsymbol{k}}(\boldsymbol{x}) \tag{3.3}$$

with coefficients $\hat{p}_{\boldsymbol{k}} \in \mathbb{C}$, $\boldsymbol{k} \in \mathcal{I}$ and a finite index set $\mathcal{I} \subseteq \mathbb{Z}^d$ for the Fourier system $(\xi_{\boldsymbol{k}}^{(\exp)})_{\boldsymbol{k}\in\mathcal{I}}$ and $\mathcal{I} \subseteq \mathbb{N}_0^d$ for the cosine system $(\xi_{\boldsymbol{k}}^{(\cos)})_{\boldsymbol{k}\in\mathcal{I}}$. Here, our domain is the torus, i.e., $\mathbb{D} = \mathbb{T}$, which we identify with the interval $\mathbb{T} \cong [-1/2, 1/2)$ for the Fourier system $\xi_{\boldsymbol{k}}^{(\exp)}$. For the cosine system $\xi_{\boldsymbol{k}}^{(\cos)}$, we have the domain $\mathbb{D} = [0, 1/2]^d$. Our main topic of interest is the *fast evaluation* of p on a set of nodes $\mathcal{X} \coloneqq \{\boldsymbol{x}_1, \boldsymbol{x}_2, \ldots, \boldsymbol{x}_M\} \subseteq \mathbb{D}^d$, $M \in \mathbb{N}$. For index sets of a full-grid type, cf. Section 2.1.3, this is referred to as a non-equispaced discrete transformation. Here, *non-equispaced* refers to the nodes $\mathcal{X}$ since they may lie in our domain in an arbitrary way. If the nodes are equidistant, we would have a discrete Fourier transform (DFT) or discrete cosine transform (DCT), see e.g. [BH95].

Definition 3.1 (Non-equispaced discrete Fourier transform)**.** *Let* $\mathcal{X} \coloneqq \{\boldsymbol{x}_1, \boldsymbol{x}_2, \ldots, \boldsymbol{x}_M\}$ *with* $\mathcal{X} \subseteq [-1/2, 1/2)^d$, $M \in \mathbb{N}$ *a set of nodes and*

$$\mathcal{I}_{\boldsymbol{N}}^{(\exp)} \coloneqq \left\{ \boldsymbol{k} \in \mathbb{Z}^d \colon k_s \in \left[-\frac{N_s}{2}, \frac{N_s}{2} - 1 \right], s \in [d] \right\} \tag{3.4}$$

an equispaced full-grid index set with parameter vector $\boldsymbol{N} \in (2\mathbb{N})^d$. *Given coefficients* $\hat{p}_{\boldsymbol{k}} \in \mathbb{C}$, $\boldsymbol{k} \in \mathcal{I}_{\boldsymbol{N}}^{(\exp)}$, *the evaluation of*

$$p(\boldsymbol{x}) = \sum_{\boldsymbol{k} \in \mathcal{I}_{\boldsymbol{N}}^{(\exp)}} \hat{p}_{\boldsymbol{k}} \, \xi_{\boldsymbol{k}}^{(\exp)}(\boldsymbol{x}),$$

at the nodes $\mathcal{X}$, *i.e.,* $p(\boldsymbol{x}_1), p(\boldsymbol{x}_2), \ldots, p(\boldsymbol{x}_M)$, *is called* non-equispaced discrete Fourier transform *or* NDFT. *For given coefficients* $h_{\boldsymbol{x}} \in \mathbb{C}$, $\boldsymbol{x} \in \mathcal{X}$, *we refer to the evaluation of*

$$\hat{h}(\boldsymbol{k}) = \sum_{\boldsymbol{x} \in \mathcal{X}} h_{\boldsymbol{x}} \, \overline{\xi}_{\boldsymbol{k}}^{(\exp)}(\boldsymbol{x}),$$

at the frequencies $\boldsymbol{k} \in \mathcal{I}_{\boldsymbol{N}}^{(\exp)}$ *as* adjoint non-equispaced discrete Fourier transform *or* adjoint NDFT.

Definition 3.2 (Non-equispaced discrete cosine transform)**.** *Let* $\mathcal{X} \coloneqq \{\boldsymbol{x}_1, \boldsymbol{x}_2, \ldots, \boldsymbol{x}_M\}$, $\mathcal{X} \subseteq [0, 1/2]^d$, *with* $M \in \mathbb{N}$ *a set of nodes and*

$$\mathcal{I}_{\boldsymbol{N}}^{(\cos)} \coloneqq \left\{ \boldsymbol{k} \in \mathbb{Z}^d \colon k_s \in [0, N_s - 1], s \in [d] \right\} \tag{3.5}$$

an equispaced full-grid index set with parameter vector $\boldsymbol{N} \in \mathbb{N}^d$. *Given coefficients* $\hat{p}_{\boldsymbol{k}} \in \mathbb{R}$, $\boldsymbol{k} \in \mathcal{I}_{\boldsymbol{N}}^{(\cos)}$, *the evaluation of*

$$p(\boldsymbol{x}) = \sum_{\boldsymbol{k} \in \mathcal{I}_{\boldsymbol{N}}^{(\cos)}} \hat{p}_{\boldsymbol{k}} \, \xi_{\boldsymbol{k}}^{(\cos)}(\boldsymbol{x}),$$

at the nodes $\mathcal{X}$, *i.e.,* $p(\boldsymbol{x}_1), p(\boldsymbol{x}_2), \ldots, p(\boldsymbol{x}_M)$, *is called* non-equispaced discrete cosine transform *or* NDCT. *For given coefficients* $h_{\boldsymbol{x}} \in \mathbb{R}$, $\boldsymbol{x} \in \mathcal{X}$, *we refer to the evaluation of*

$$\hat{h}(\boldsymbol{k}) = \sum_{\boldsymbol{x} \in \mathcal{X}} h_{\boldsymbol{x}} \, \xi_{\boldsymbol{k}}^{(\cos)}(\boldsymbol{x}),$$

at the frequencies $\boldsymbol{k} \in \mathcal{I}_{\boldsymbol{N}}^{(\cos)}$ *as* transposed non-equispaced discrete cosine transform *or* transposed NDCT.

We understand the NDFT and the NDCT as a matrix-vector multiplication. In general, we denote with $\xi_{\boldsymbol{k}}$ the functions which can be the Fourier system $\xi_{\boldsymbol{k}}^{(\exp)}$ or the cosine system $\xi_{\boldsymbol{k}}^{(\cos)}$ together with the respective index set $\mathcal{I}$ which is of type $\mathcal{I}_N^{(\exp)}$ in the former case and $\mathcal{I}_N^{(\cos)}$ in the latter. We write the evaluation of p from (3.3) at nodes $\mathcal{X} := \{\boldsymbol{x}_1, \boldsymbol{x}_2, \ldots, \boldsymbol{x}_M\} \subseteq \mathbb{D}^d$ as

$$\boldsymbol{p} := \begin{pmatrix} p(\boldsymbol{x}_1) \\ p(\boldsymbol{x}_2) \\ \vdots \\ p(\boldsymbol{x}_M) \end{pmatrix} = \begin{pmatrix} \xi_{\boldsymbol{k}_1}(\boldsymbol{x}_1) & \xi_{\boldsymbol{k}_2}(\boldsymbol{x}_1) & \cdots & \xi_{\boldsymbol{k}_n}(\boldsymbol{x}_1) \\ \xi_{\boldsymbol{k}_1}(\boldsymbol{x}_2) & \xi_{\boldsymbol{k}_2}(\boldsymbol{x}_2) & \cdots & \xi_{\boldsymbol{k}_n}(\boldsymbol{x}_2) \\ \vdots & \vdots & \vdots & \vdots \\ \xi_{\boldsymbol{k}_1}(\boldsymbol{x}_M) & \xi_{\boldsymbol{k}_2}(\boldsymbol{x}_M) & \cdots & \xi_{\boldsymbol{k}_n}(\boldsymbol{x}_M) \end{pmatrix} \begin{pmatrix} \hat{p}_{\boldsymbol{k}_1} \\ \hat{p}_{\boldsymbol{k}_2} \\ \vdots \\ \hat{p}_{\boldsymbol{k}_n} \end{pmatrix} =: \boldsymbol{F}_{\mathcal{I}}^{\mathcal{X}}\, \hat{\boldsymbol{f}}$$

with $\boldsymbol{k}_i$, $i = 1, 2, \ldots, n$, $n := |\mathcal{I}|$, a chosen order of the indices in $\mathcal{I}$. Since this order can be arbitrary, we omit denoting it explicitly, e.g., when we write $\boldsymbol{F}_{\mathcal{I}}^{\mathcal{X}} = (\xi_{\boldsymbol{k}}(\boldsymbol{x}))_{\boldsymbol{x}\in\mathcal{X}, \boldsymbol{k}\in\mathcal{I}}$ and $\hat{\boldsymbol{p}} = (\hat{p}_{\boldsymbol{k}})_{\boldsymbol{k}\in\mathcal{I}}$. In a similar way, we consider the 'adjoint' or 'transposed' problem, i.e., the evaluation of

$$\hat{h}(\boldsymbol{k}) = \sum_{\boldsymbol{x}\in\mathcal{X}} h_{\boldsymbol{x}}\, \overline{\xi}_{\boldsymbol{k}}(\boldsymbol{x})$$

with coefficients $h_{\boldsymbol{x}} \in \mathbb{C}$, $\boldsymbol{x} \in \mathcal{X}$ on the index set $\mathcal{I}$. This translates to a matrix-vector multiplication with the adjoint (or transposed in the real-valued cosine case) of $\boldsymbol{F}_{\mathcal{I}}^{\mathcal{X}}$, i.e.,

$$\hat{\boldsymbol{h}} := \begin{pmatrix} \hat{h}(\boldsymbol{k}_1) \\ \hat{h}(\boldsymbol{k}_2) \\ \vdots \\ \hat{h}(\boldsymbol{k}_n) \end{pmatrix} = \begin{pmatrix} \overline{\xi}_{\boldsymbol{k}_1}(\boldsymbol{x}_1) & \overline{\xi}_{\boldsymbol{k}_1}(\boldsymbol{x}_2) & \cdots & \overline{\xi}_{\boldsymbol{k}_1}(\boldsymbol{x}_M) \\ \overline{\xi}_{\boldsymbol{k}_2}(\boldsymbol{x}_1) & \overline{\xi}_{\boldsymbol{k}_2}(\boldsymbol{x}_2) & \cdots & \overline{\xi}_{\boldsymbol{k}_2}(\boldsymbol{x}_M) \\ \vdots & \vdots & \vdots & \vdots \\ \overline{\xi}_{\boldsymbol{k}_n}(\boldsymbol{x}_1) & \overline{\xi}_{\boldsymbol{k}_n}(\boldsymbol{x}_2) & \cdots & \overline{\xi}_{\boldsymbol{k}_n}(\boldsymbol{x}_M) \end{pmatrix} \begin{pmatrix} h_{\boldsymbol{x}_1} \\ h_{\boldsymbol{x}_2} \\ \vdots \\ h_{\boldsymbol{x}_M} \end{pmatrix} =: \left(\boldsymbol{F}_{\mathcal{I}}^{\mathcal{X}}\right)^{\mathsf{H}} \boldsymbol{h}.$$

The NDFT and the NDCT are therefore naive multiplications of the matrix $\boldsymbol{F}_{\mathcal{I}}^{\mathcal{X}}$ with a vector. These multiplications are in the complexity class $O(n \cdot M)$ with $n = |\mathcal{I}_N| = \prod_{s=1}^{d} N_s$. Since the cardinalities rise exponentially in the spatial dimension d, we observe that the curse of dimensionality is present.

The *non-equispaced fast Fourier transform* or *NFFT* is a fast algorithm for the realization of the NDFT. The algorithm approximates the result of the matrix-vector multiplication $\boldsymbol{F}_I^{\mathcal{X}} \hat{\boldsymbol{f}}$ for the Fourier system $\xi_{\boldsymbol{k}}^{(\exp)}$. It is based on the approximation of d-variate trigonometric polynomials by linear combinations of translates of a periodic window function. The NFFT is in the complexity class

$$O\left(\prod_{s=1}^{d} N_s \log N_s + \left|\log \varepsilon\right|^d |\mathcal{X}|\right) \tag{3.6}$$

with $\varepsilon > 0$ being the desired accuracy. This represents a significant improvement to the naive multiplication. For a detailed description of the algorithm we refer to [PPST18, Chapter 7] as well as [KKP09]. Similarly, there exists the non-equispaced fast cosine transform or NFCT which is a fast algorithm for the computation of a NDCT. It approximates the result of $\boldsymbol{F}_I^{\mathcal{X}} \hat{\boldsymbol{f}}$ for the cosine system $\xi_{\boldsymbol{k}}^{(\cos)}$. The algorithm can be derived from the NFFT as described in [PPST18, Section 7.4] and it is in the complexity class (3.6) as well.

The software package NFFT3, cf. [KKP], combines a number of algorithms including the NFFT and the NFCT as a C library. It can be included in many different programming languages including Python, Matlab, and Julia, see [Sch18, Schb].

3.2 Grouped Transformations

In Chapter 2, we have seen a connection between the support supp $\boldsymbol{k}$ of an index $\boldsymbol{k} \in \mathbb{Z}^d$ and the ANOVA term $f_{\boldsymbol{u}}$, $\boldsymbol{u} \subseteq [d]$, of a function $f\colon \mathbb{D}^d \to \mathbb{C}$ in a space $\mathrm{L}_2(\mathbb{D}^d, \omega^{(d)})$ with product basis $(\varphi_{\boldsymbol{k}}^{(d)})_{\boldsymbol{k}\in\mathbb{Z}^d}$ from Section 2.1.2. Moreover, we have considered the truncation of the ANOVA decomposition in Section 2.3 to subsets $U \subseteq \mathcal{P}([d])$ of ANOVA terms. Grouped index sets bring together the concepts of subsets of ANOVA terms and the partial sums from Section 2.1.3 with the goal of a unified approach in truncating both the ANOVA decomposition and the basis expansion.

The grouped transformations were first introduced in [BPS22] and have the aim to provide transformations as in Section 3.1 for non-equispaced data when using grouped index sets which will be introduced in Section 3.2.1. The major idea is to reduce the d-dimensional problem to a number of low-dimensional problems trough exploitation of the grouped ANOVA structure. The algorithms have been applied successfully in [PS21a, PS21b, PS22a].

3.2.1 Grouped Index Sets

We distinguish between the periodic case with the Fourier system (2.7) and the non-periodic case with the cosine based systems (2.8), (2.10), and (2.15). The index sets

$$\mathcal{I}_N^{(\mathrm{per})} \coloneqq \{-N/2, -N/2+1, \dots, -1, 1, 2, \dots, N/2-1\} \subseteq \mathbb{Z} \tag{3.7}$$

for bandwidth parameter $N \in 2\mathbb{N}$ and

$$\mathcal{I}_N^{(\mathrm{nper})} \coloneqq \{1, 2, \dots, N-1\} \subseteq \mathbb{N}_0 \tag{3.8}$$

provide the one-dimensional foundation. Note that both sets do not contain the 0 index. Subsequently, for a given subset of coordinate indices $\emptyset \neq \boldsymbol{u} \subseteq [d]$, we define

$$\mathcal{I}_{\boldsymbol{u},N}^{(\mathrm{per})} \coloneqq \left\{ \boldsymbol{k} \in \mathbb{Z}^d \colon \operatorname{supp} \boldsymbol{k} = \boldsymbol{u} \text{ and } \boldsymbol{k}_{\boldsymbol{u}} \in \left(\mathcal{I}_N^{(\mathrm{per})}\right)^{|\boldsymbol{u}|} \right\} \tag{3.9}$$

for the periodic case and

$$\mathcal{I}_{\boldsymbol{u},N}^{(\mathrm{nper})} := \left\{ \boldsymbol{k} \in \mathbb{N}_0^d \colon \operatorname{supp} \boldsymbol{k} = \boldsymbol{u} \text{ and } \boldsymbol{k}_{\boldsymbol{u}} \in \left(\mathcal{I}_N^{(\mathrm{nper})} \right)^{|\boldsymbol{u}|} \right\}$$

for the non-periodic case. The empty set always belongs to the zero index, i.e., $\mathcal{I}_{\emptyset} = \mathcal{I}_{\emptyset}^{(\mathrm{per})} = \mathcal{I}_{\emptyset}^{(\mathrm{nper})} = \{\mathbf{0}\}$. We observe that these index sets provide a disjoint decomposition of a cube in their respective domains, i.e., we have

$$\left(\mathcal{I}_N^{(\mathrm{per})} \right)^d = \mathcal{I}_{\emptyset} \cup \bigcup_{\substack{\boldsymbol{u} \subseteq [d] \\ \boldsymbol{u} \neq \emptyset}} \mathcal{I}_{\boldsymbol{u},N}^{(\mathrm{per})} \qquad \text{and} \qquad \left(\mathcal{I}_N^{(\mathrm{nper})} \right)^d = \mathcal{I}_{\emptyset} \cup \bigcup_{\substack{\boldsymbol{u} \subseteq [d] \\ \boldsymbol{u} \neq \emptyset}} \mathcal{I}_{\boldsymbol{u},N}^{(\mathrm{nper})}.$$

It remains to show the connection to the ANOVA terms $f_{\boldsymbol{u}}$. To this end, we recall Lemma 2.14, i.e., the fact that all indices $\boldsymbol{k}$ with $\operatorname{supp} \boldsymbol{k} = \boldsymbol{u}$ belong to the ANOVA term $f_{\boldsymbol{u}}$. For our index sets, we observe that $\mathcal{I}_{\boldsymbol{u},N}^{(\mathrm{per})} \subseteq \{\boldsymbol{k} \in \mathbb{Z}^d \colon \operatorname{supp} \boldsymbol{k} = \boldsymbol{u}\}$ and $\mathcal{I}_{\boldsymbol{u},N}^{(\mathrm{nper})} \subseteq \{\boldsymbol{k} \in \mathbb{N}_0^d \colon \operatorname{supp} \boldsymbol{k} = \boldsymbol{u}\}$. In terms of partial sums, cf. Section 2.1.3, our index sets therefore provide a way to truncate the basis expansion of the corresponding ANOVA term. Therefore, we have

$$f_{\boldsymbol{u}} = \sum_{\substack{\boldsymbol{k} \in \mathbb{Z}^d \\ \operatorname{supp} \boldsymbol{k} = \boldsymbol{u}}} \mathrm{c}_{\boldsymbol{k}}(f)\ \varphi_{\boldsymbol{k}}^{(d)} \approx \mathrm{S}_{\mathcal{I}_{\boldsymbol{u},N}^{(\mathrm{per})}} f = \sum_{\boldsymbol{k} \in \mathcal{I}_{\boldsymbol{u},N}^{(\mathrm{per})}} \mathrm{c}_{\boldsymbol{k}}(f)\ \varphi_{\boldsymbol{k}}^{(d)} \tag{3.10}$$

$$f_{\boldsymbol{u}} = \sum_{\substack{\boldsymbol{k} \in \mathbb{N}_0^d \\ \operatorname{supp} \boldsymbol{k} = \boldsymbol{u}}} \mathrm{c}_{\boldsymbol{k}}(f)\ \varphi_{\boldsymbol{k}}^{(d)} \approx \mathrm{S}_{\mathcal{I}_{\boldsymbol{u},N}^{(\mathrm{nper})}} f = \sum_{\boldsymbol{k} \in \mathcal{I}_{\boldsymbol{u},N}^{(\mathrm{nper})}} \mathrm{c}_{\boldsymbol{k}}(f)\ \varphi_{\boldsymbol{k}}^{(d)}. \tag{3.11}$$

In summary, index sets of this type allow for truncation of the basis expansion for a single ANOVA term.

Finally, bringing together the truncated ANOVA decomposition of the function with our index, we observe

$$\sum_{\boldsymbol{u} \in \mathcal{U}} f_{\boldsymbol{u}} \approx \sum_{\boldsymbol{u} \in \mathcal{U}} \sum_{\boldsymbol{k} \in \mathcal{I}_{\boldsymbol{u},N}} \mathrm{c}_{\boldsymbol{k}}(f)\ \varphi_{\boldsymbol{k}}^{(d)}$$

for a subset of ANOVA terms $U \subseteq \mathcal{P}([d])$ with $\mathcal{I}_{\boldsymbol{u},N} = \mathcal{I}_{\boldsymbol{u},N}^{(\mathrm{per})}$ in the periodic case and $\mathcal{I}_{\boldsymbol{u},N} = \mathcal{I}_{\boldsymbol{u},N}^{(\mathrm{nper})}$ in the non-periodic case. We formalize this concept as *grouped index sets* in the sense of 'grouping' indices with the same support for the corresponding ANOVA term. In other words, we construct index sets that fit the chosen ANOVA truncation.

Definition 3.3 (Grouped index set)**.** *Let $d \in \mathbb{N}$ be the spatial dimension and $U \subseteq \mathcal{P}([d])$ a subset of ANOVA terms, cf. Section 2.3. Moreover, we have a bandwidth parameter $N_{\boldsymbol{u}} \in \mathbb{N}$ for every set of coordinate indices $\emptyset \neq \boldsymbol{u} \in U$. In the periodic case, $N_{\boldsymbol{u}}$ must be an even number. We define the index sets*

$$\mathcal{I}_{\boldsymbol{N}}^{(\mathrm{per})}(U) \coloneqq \mathcal{I}_{\emptyset} \cup \bigcup_{\boldsymbol{u} \in U \setminus \{\emptyset\}} \mathcal{I}_{\boldsymbol{u},N_{\boldsymbol{u}}}^{(\mathrm{per})} \tag{3.12}$$

$$\mathcal{I}_{\boldsymbol{N}}^{(\mathrm{nper})}(U) \coloneqq \mathcal{I}_{\emptyset} \cup \bigcup_{\boldsymbol{u} \in U \setminus \{\emptyset\}} \mathcal{I}_{\boldsymbol{u},N_{\boldsymbol{u}}}^{(\mathrm{nper})} \tag{3.13}$$

and call them grouped index sets*. Here, $\boldsymbol{N} = (N_{\boldsymbol{u}})_{\boldsymbol{u} \in U \setminus \{\emptyset\}}$ collects bandwidth parameters. In the case of superposition cut-off, i.e., $U = U^{(d,d_s)}$ with superposition threshold $d_s \in [d]$, cf.* (2.28)*, we define the grouped index sets order-dependent, i.e., $N_{\boldsymbol{u}} = N_{\boldsymbol{v}}$ for $\boldsymbol{u}, \boldsymbol{v} \in U^{(d,d_s)}$ with $|\boldsymbol{u}| = |\boldsymbol{v}|$. Therefore, the grouped index set $\mathcal{I}_{\boldsymbol{N}}^{(\mathrm{per})}(U^{(d,d_s)})$ or $\mathcal{I}_{\boldsymbol{N}}^{(\mathrm{nper})}(U^{(d,d_s)})$ is well-defined for $\boldsymbol{N} = (N_s)_{s=1}^{d_s}$.*

The cardinalities of the grouped index are considered in the following lemma.

Lemma 3.4. *Let $d \in \mathbb{N}$ be the spatial dimension, $U \subseteq \mathcal{P}([d])$ a subset of ANOVA terms, and $N_{\boldsymbol{u}} \in \mathbb{N}$, $\boldsymbol{u} \in U$, the bandwidth parameters. The cardinality of the respective grouped index set is*

$$\left|\mathcal{I}_{\boldsymbol{N}}^{(\mathrm{per})}(U)\right| = \left|\mathcal{I}_{\boldsymbol{N}}^{(\mathrm{nper})}(U)\right| = 1 + \sum_{\emptyset \neq \boldsymbol{u} \in U} (N_{\boldsymbol{u}} - 1)^{|\boldsymbol{u}|}\,.$$

For $U = U^{(d,d_s)}$ with superposition threshold $1 \leq d_s < d$ and order-dependent

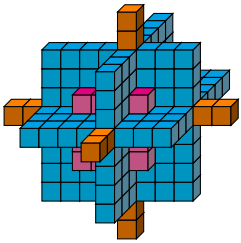

(a) Index set $\mathcal{I}_{\boldsymbol{N}}^{(\mathrm{per})}(U^{(3,3)})$ with $N_1 = 12$, $N_2 = 8$, $N_3 = 4$ ($\mathcal{I}_{\boldsymbol{u},N_{|\boldsymbol{u}|}}^{(\mathrm{per})}$ in orange for $|\boldsymbol{u}| = 1$, in cyan for $|\boldsymbol{u}| = 2$, and in magenta for $|\boldsymbol{u}| = 3$).

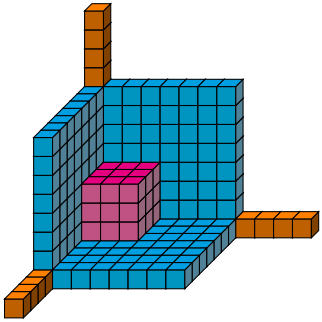

(b) Index set $\mathcal{I}_{\boldsymbol{N}}^{(\mathrm{nper})}(U^{(3,3)})$ with $N_1 = 12$, $N_2 = 8$, $N_3 = 4$ ($\mathcal{I}_{\boldsymbol{u},N_{|\boldsymbol{u}|}}^{(\mathrm{nper})}$ in orange for $|\boldsymbol{u}| = 1$, in cyan for $|\boldsymbol{u}| = 2$, and in magenta for $|\boldsymbol{u}| = 3$).

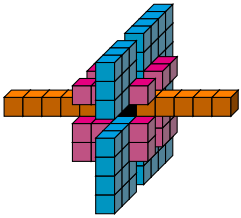

(c) Index set $\mathcal{I}_{\boldsymbol{N}}^{(\mathrm{per})}(U)$ with $U = \{\emptyset, \{1\}, \{2,3\}, \{1,2,3\}\}$, $N_{\{1\}} = 12$, $N_{\{2,3\}} = 8$, $N_{\{1,2,3\}} = 4$ ($\mathcal{I}_{\boldsymbol{u},N_{\boldsymbol{u}}}^{(\mathrm{per})}$ in black for $\boldsymbol{u} = \emptyset$, in orange for $\boldsymbol{u} = \{1\}$, in cyan for $\boldsymbol{u} = \{2,3\}$, and in magenta for $\boldsymbol{u} = \{1,2,3\}$).

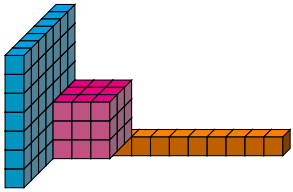

(d) Index set $\mathcal{I}_{\boldsymbol{N}}^{(\mathrm{nper})}(U)$ with $U = \{\emptyset, \{1\}, \{2,3\}, \{1,2,3\}\}$, $N_{\{1\}} = 12$, $N_{\{2,3\}} = 8$, $N_{\{1,2,3\}} = 4$ ($\mathcal{I}_{\boldsymbol{u},N_{\boldsymbol{u}}}^{(\mathrm{nper})}$ in orange for $\boldsymbol{u} = \{1\}$, in cyan for $\boldsymbol{u} = \{2,3\}$, and in magenta for $\boldsymbol{u} = \{1,2,3\}$).

Figure 3.1: Visualization of grouped index sets $\mathcal{I}_{\boldsymbol{N}}^{(\mathrm{per})}(U)$ and $\mathcal{I}_{\boldsymbol{N}}^{(\mathrm{nper})}(U)$ from Definition 3.3.

bandwidth parameters N_s, $s = 1, 2, \ldots, d_s$, *we have*

$$\left|\mathcal{I}_{\boldsymbol{N}}^{(\mathrm{per})}(U^{(d,d_s)})\right| = \left|\mathcal{I}_{\boldsymbol{N}}^{(\mathrm{nper})}(U^{(d,d_s)})\right| = 1 + \sum_{s=1}^{d_s} \binom{d}{s} (N_s - 1)^s \,.$$

Proof. Clearly, we have

$$\left|\mathcal{I}_{\boldsymbol{u},N_{\boldsymbol{u}}}^{(\mathrm{per})}\right| = \left|\mathcal{I}_{\boldsymbol{u},N_{\boldsymbol{u}}}^{(\mathrm{nper})}\right| = (N_{\boldsymbol{u}} - 1)^{|\boldsymbol{u}|} \,.$$

The statement follows from the disjointness of the index sets. ∎

Similar to the projection operator $\mathrm{P}_{\boldsymbol{u}} f$ from (2.20), for an index set $\mathcal{I} \subseteq \mathbb{Z}^d$ and a subset of coordinate indices $\emptyset \neq \boldsymbol{u} \subseteq [d]$, we define the discrete projection

$$\mathrm{P}_{\boldsymbol{u}}\mathcal{I} := \{\boldsymbol{\ell} \in \mathbb{Z}^{|\boldsymbol{u}|} \colon \exists \boldsymbol{k} \in \mathcal{I} \quad \text{with} \quad \boldsymbol{k}_{\boldsymbol{u}} = \boldsymbol{\ell}\}. \tag{3.14}$$

with $\mathrm{P}_{\emptyset}\mathcal{I} := \{\mathbf{0}\}$. This projection filters the relevant information about indices with a support of $\boldsymbol{u}$, i.e., we have for the grouped index sets $\mathrm{P}_{\boldsymbol{u}}\mathcal{I}_{\boldsymbol{N}}^{(\mathrm{per})}(U) = \mathrm{P}_{\boldsymbol{u}}\mathcal{I}_{\boldsymbol{u},N_{\boldsymbol{u}}}^{(\mathrm{per})}$ and $\mathrm{P}_{\boldsymbol{u}}\mathcal{I}_{\boldsymbol{N}}^{(\mathrm{nper})}(U) = \mathrm{P}_{\boldsymbol{u}}\mathcal{I}_{\boldsymbol{u},N_{\boldsymbol{u}}}^{(\mathrm{nper})}$.

3.2.2 Fast Multiplication

In Section 3.1 we have introduced the NDFT and the NDCT and their fast counterparts, the NFFT and the NFCT. Although the fast transformations provide a significant improvement in complexity, we still suffer from the curse of dimensionality. However, the transformations are coupled to the use of full-grid index sets as in (3.4) and (3.5). Here, we modify the approach to grouped transformations which will be coupled to the grouped index sets from Section 3.2.1.

We consider a space $\mathrm{L}_2(\mathbb{D}^d, \omega^{(d)})$ as in Definition 2.1 with product basis $(\varphi_{\boldsymbol{k}}^{(d)})_{\boldsymbol{k}\in\mathbb{Z}^d}$ of bounded continuous functions $\varphi_{\boldsymbol{k}}^{(d)}$. Then we take functions

$$p \colon \mathbb{D}^d \to \mathbb{C}, \quad p(\boldsymbol{x}) = \sum_{\boldsymbol{k}\in I_{\boldsymbol{N}}(U)} \hat{p}_{\boldsymbol{k}}\, \varphi_{\boldsymbol{k}}^{(d)}(\boldsymbol{x})$$

supported on a grouped index set $\mathcal{I}_{\boldsymbol{N}}(U)$ from Definition 3.3 with $U \subseteq \mathcal{P}([d])$ a subset of ANOVA terms and bandwidth parameters $\boldsymbol{N} \in \mathbb{N}^{|U|-1}$. We have $\mathcal{I}_{\boldsymbol{N}}(U) = \mathcal{I}_{\boldsymbol{N}}^{(\mathrm{per})}(U)$ for the periodic Fourier system or $\mathcal{I}_{\boldsymbol{N}}(U) = \mathcal{I}_{\boldsymbol{N}}^{(\mathrm{nper})}(U)$ otherwise. The values $\hat{p}_{\boldsymbol{k}} \in \mathbb{C}$, $\boldsymbol{k} \in \mathcal{I}_{\boldsymbol{N}}(U)$, are coefficients. We are again interested in the evaluation of p at $M \in \mathbb{N}$ arbitrary nodes $\mathcal{X} \coloneqq \{\boldsymbol{x}_1, \boldsymbol{x}_2, \dots, \boldsymbol{x}_M\} \subseteq \mathbb{D}^d$.

As in Section 3.1, this evaluation can be understood as a matrix-vector multiplication as follows

$$\begin{aligned}\boldsymbol{p} \coloneqq \begin{pmatrix} p(\boldsymbol{x}_1) \\ p(\boldsymbol{x}_2) \\ \vdots \\ p(\boldsymbol{x}_M) \end{pmatrix} &= \begin{pmatrix} \varphi^{(d)}_{\boldsymbol{k}_1}(\boldsymbol{x}_1) & \varphi^{(d)}_{\boldsymbol{k}_2}(\boldsymbol{x}_1) & \cdots & \varphi^{(d)}_{\boldsymbol{k}_n}(\boldsymbol{x}_1) \\ \varphi^{(d)}_{\boldsymbol{k}_1}(\boldsymbol{x}_2) & \varphi^{(d)}_{\boldsymbol{k}_2}(\boldsymbol{x}_2) & \cdots & \varphi^{(d)}_{\boldsymbol{k}_n}(\boldsymbol{x}_2) \\ \vdots & \vdots & \vdots & \vdots \\ \varphi^{(d)}_{\boldsymbol{k}_1}(\boldsymbol{x}_M) & \varphi^{(d)}_{\boldsymbol{k}_2}(\boldsymbol{x}_M) & \cdots & \varphi^{(d)}_{\boldsymbol{k}_n}(\boldsymbol{x}_M) \end{pmatrix} \begin{pmatrix} \hat{p}_{\boldsymbol{k}_1} \\ \hat{p}_{\boldsymbol{k}_2} \\ \vdots \\ \hat{p}_{\boldsymbol{k}_n} \end{pmatrix} \\ &=: \boldsymbol{F}^{\mathcal{X}}_{\mathcal{I}_{\boldsymbol{N}}(U)} \hat{\boldsymbol{p}} \end{aligned} \tag{3.15}$$

with $\boldsymbol{k}_i$, $i = 1, 2, \dots, n$, $n \coloneqq 1 + \sum_{\emptyset \neq \boldsymbol{u} \in U} (N_{\boldsymbol{u}} - 1)^{|\boldsymbol{u}|}$, a chosen order of the indices in $\mathcal{I}_{\boldsymbol{N}}(U)$. Now, we recognize a structure in the matrix $\boldsymbol{F}^{\mathcal{X}}_{\mathcal{I}_{\boldsymbol{N}}(U)}$ which fits our groups, the subsets of coordinate indices $\boldsymbol{u} \in U \coloneqq \{\emptyset, \boldsymbol{u}_1, \boldsymbol{u}_2, \dots, \boldsymbol{u}_m\}$, $m \coloneqq |U| - 1$, since

$$\boldsymbol{F}^{\mathcal{X}}_{\mathcal{I}_{\boldsymbol{N}}(U)} \hat{\boldsymbol{p}} = \left(\boldsymbol{F}_{\mathcal{I}_\emptyset}, \boldsymbol{F}^{\mathcal{X}}_{\mathcal{I}_{\boldsymbol{u}_1, N_{\boldsymbol{u}_1}}}, \cdots, \boldsymbol{F}^{\mathcal{X}}_{\mathcal{I}_{\boldsymbol{u}_m, N_{\boldsymbol{u}_m}}} \right) \begin{pmatrix} \hat{\boldsymbol{p}}_\emptyset \\ \hat{\boldsymbol{p}}_{\boldsymbol{u}_1} \\ \vdots \\ \hat{\boldsymbol{p}}_{\boldsymbol{u}_m} \end{pmatrix} = \sum_{\boldsymbol{u} \in U} \boldsymbol{F}^{\mathcal{X}}_{\mathcal{I}_{\boldsymbol{u}, N_{\boldsymbol{u}}}} \hat{\boldsymbol{p}}_{\boldsymbol{u}}. \tag{3.16}$$

Here, we have grouped the indices belonging to the same set $\boldsymbol{u}$ together yielding the matrices

$$\boldsymbol{F}_{\mathcal{I}_\emptyset} \coloneqq \begin{pmatrix} 1 \\ 1 \\ \vdots \\ 1 \end{pmatrix}, \quad \text{and} \quad \boldsymbol{F}^{\mathcal{X}}_{\mathcal{I}_{\boldsymbol{u}, N_{\boldsymbol{u}}}} = \left(\varphi^{(d)}_{\boldsymbol{k}}(\boldsymbol{x}) \right)_{\boldsymbol{x} \in \mathcal{X}, \boldsymbol{k} \in \mathcal{I}_{\boldsymbol{u}, N_{\boldsymbol{u}}}}$$

as well as the coefficient vectors

$$\hat{\boldsymbol{p}}_{\emptyset} = \hat{p}_{\boldsymbol{0}}, \quad \text{and} \quad \hat{\boldsymbol{p}}_{\boldsymbol{u}} = (\hat{p}_{\boldsymbol{k}})_{\boldsymbol{k} \in \mathcal{I}_{\boldsymbol{u},N_{\boldsymbol{u}}}} .$$

Note that the order of the indices $\boldsymbol{k} \in \mathcal{I}_{\boldsymbol{u},N_{\boldsymbol{u}}}$, $\boldsymbol{u} \in U$, has to be consistent across the matrices $\boldsymbol{F}^{\mathcal{X}}_{\mathcal{I}_{\boldsymbol{u},N_{\boldsymbol{u}}}}$ and the coefficient vectors $\hat{\boldsymbol{p}}_{\boldsymbol{u}}$.

In (3.16) we observe that the multiplication of our main matrix $\boldsymbol{F}^{\mathcal{X}}_{\mathcal{I}_N(U)}$ with the coefficient vector $\hat{\boldsymbol{p}}$ can be written as sum of the matrix-vector multiplications $\boldsymbol{F}^{\mathcal{X}}_{\mathcal{I}_{\boldsymbol{u},N_{\boldsymbol{u}}}} \hat{\boldsymbol{p}}_{\boldsymbol{u}}$. Moreover, every single multiplication in this sum is independent, i.e., we are able to parallelize its evaluation which will be a key factor. For now, we still have matrices $\boldsymbol{F}^{\mathcal{X}}_{\mathcal{I}_{\boldsymbol{u},N_{\boldsymbol{u}}}}$ with d-dimensional basis functions $\varphi^{(d)}_{\boldsymbol{k}}$, d-dimensional nodes $\boldsymbol{x}$, and d-dimensional indices $\boldsymbol{k}$. Using the ideas of projections and the product structure of our space, we can reduce the dimensionality of this problem.

The first key observation is that under our assumptions on the space and the basis, we have

$$\varphi^{(d)}_{\boldsymbol{k}}(\boldsymbol{x}) = \varphi^{(|\boldsymbol{u}|)}_{\boldsymbol{k}_{\boldsymbol{u}}}(\boldsymbol{x}_{\boldsymbol{u}}) \quad \text{for every} \quad \boldsymbol{k} \in \mathcal{I}_{\boldsymbol{u},N_{\boldsymbol{u}}} \quad \text{and} \quad \boldsymbol{x} \in \mathcal{X}$$

since $\operatorname{supp} \boldsymbol{k} = \boldsymbol{u}$ and $\varphi_0 \equiv 1$. In the multi-set

$$\mathcal{X}_{\boldsymbol{u}} \coloneqq \{(\boldsymbol{x}_1)_{\boldsymbol{u}}, (\boldsymbol{x}_2)_{\boldsymbol{u}}, \dots, (\boldsymbol{x}_M)_{\boldsymbol{u}}\}$$

we collect the $\boldsymbol{u}$ part of every node $\boldsymbol{x}_j \in \mathcal{X}$, $j = 1, 2, \dots, M$. Note that $\mathcal{X}_{\boldsymbol{u}}$ may contain duplicates therefore we defined it as a multi-set. Using the projection from (3.14), we are also able to collect the relevant part of the indices with $\mathrm{P}_{\boldsymbol{u}}\mathcal{I}_{\boldsymbol{u},N_{\boldsymbol{u}}} \subseteq \mathbb{Z}^{|\boldsymbol{u}|}$. Bringing these concepts together, we have the equivalent formulation

$$\boldsymbol{F}^{\mathcal{X}}_{\mathcal{I}_{\boldsymbol{u},N_{\boldsymbol{u}}}} \hat{\boldsymbol{p}}_{\boldsymbol{u}} = \boldsymbol{F}^{\mathcal{X}_{\boldsymbol{u}}}_{\mathrm{P}_{\boldsymbol{u}}\mathcal{I}_{\boldsymbol{u},N_{\boldsymbol{u}}}} \hat{\boldsymbol{p}}_{\boldsymbol{u}} \quad \text{with} \quad \boldsymbol{F}^{\mathcal{X}_{\boldsymbol{u}}}_{\mathrm{P}_{\boldsymbol{u}}\mathcal{I}_{\boldsymbol{u},N_{\boldsymbol{u}}}} = \left(\varphi^{(|\boldsymbol{u}|)}_{\boldsymbol{\ell}}(\boldsymbol{x})\right)_{\boldsymbol{x} \in \mathcal{X}_{\boldsymbol{u}}, \boldsymbol{\ell} \in \mathrm{P}_{\boldsymbol{u}}\mathcal{I}_{\boldsymbol{u},N_{\boldsymbol{u}}}} .$$

In summary, we have obtained matrices $\boldsymbol{F}^{\mathcal{X}_{\boldsymbol{u}}}_{\mathrm{P}_{\boldsymbol{u}}\mathcal{I}_{\boldsymbol{u},N_{\boldsymbol{u}}}}$ with $|\boldsymbol{u}|$-dimensional basis functions $\varphi^{(|\boldsymbol{u}|)}_{\boldsymbol{\ell}}$, $|\boldsymbol{u}|$-dimensional nodes $\boldsymbol{x}_{\boldsymbol{u}}$, and $|\boldsymbol{u}|$-dimensional indices $\boldsymbol{\ell}$. So, our d-dimensional transformation is reduced to $|U|$ many low-dimensional transformations.

The ideas can be translated to the 'adjoint' or 'transposed' problem as well. We consider the function

$$h\colon \mathcal{I}_N(U) \to \mathbb{C}, \quad h(\boldsymbol{k}) = \sum_{\boldsymbol{x}\in\mathcal{X}} h_{\boldsymbol{x}}\, \overline{\varphi}^{(d)}_{\boldsymbol{k}}(\boldsymbol{x}).$$

with coefficients $\boldsymbol{h}_{\boldsymbol{x}} \in \mathbb{C}$, $\boldsymbol{x} \in \mathcal{X}$. The evaluation of h on the index set $\mathcal{I}_N(U)$ can be understood as the matrix-vector multiplication

$$\begin{aligned}\hat{\boldsymbol{h}} &:= \begin{pmatrix} \hat{h}(\boldsymbol{k}_1) \\ \hat{h}(\boldsymbol{k}_2) \\ \vdots \\ \hat{h}(\boldsymbol{k}_n) \end{pmatrix} = \begin{pmatrix} \overline{\varphi}^{(d)}_{\boldsymbol{k}_1}(\boldsymbol{x}_1) & \overline{\varphi}^{(d)}_{\boldsymbol{k}_1}(\boldsymbol{x}_2) & \cdots & \overline{\varphi}^{(d)}_{\boldsymbol{k}_1}(\boldsymbol{x}_M) \\ \overline{\varphi}^{(d)}_{\boldsymbol{k}_2}(\boldsymbol{x}_1) & \overline{\varphi}^{(d)}_{\boldsymbol{k}_2}(\boldsymbol{x}_2) & \cdots & \overline{\varphi}^{(d)}_{\boldsymbol{k}_2}(\boldsymbol{x}_M) \\ \vdots & \vdots & \vdots & \vdots \\ \overline{\varphi}^{(d)}_{\boldsymbol{k}_n}(\boldsymbol{x}_1) & \overline{\varphi}^{(d)}_{\boldsymbol{k}_n}(\boldsymbol{x}_2) & \cdots & \overline{\varphi}^{(d)}_{\boldsymbol{k}_n}(\boldsymbol{x}_M) \end{pmatrix} \begin{pmatrix} h_{\boldsymbol{x}_1} \\ h_{\boldsymbol{x}_2} \\ \vdots \\ h_{\boldsymbol{x}_M} \end{pmatrix} \\ &=: \left(\boldsymbol{F}^{\mathcal{X}}_{\mathcal{I}_N(U)}\right)^{\mathsf{H}} \boldsymbol{h}\end{aligned}$$

with $n := \mathcal{I}_N(U)$. Using the ideas and notation from before, we may write

$$\left(\boldsymbol{F}^{\mathcal{X}}_{\mathcal{I}_N(U)}\right)^{\mathsf{H}} \boldsymbol{h} = \begin{pmatrix} \left(\boldsymbol{F}_{\mathcal{I}_\emptyset}\right)^{\mathsf{H}} \boldsymbol{h} \\ \left(\boldsymbol{F}^{\mathcal{X}}_{\mathcal{I}_{u_1,N_{u_1}}}\right)^{\mathsf{H}} \boldsymbol{h} \\ \vdots \\ \left(\boldsymbol{F}^{\mathcal{X}}_{\mathcal{I}_{u_m,N_{u_m}}}\right)^{\mathsf{H}} \boldsymbol{h} \end{pmatrix} = \begin{pmatrix} \left(\boldsymbol{F}_{\mathrm{P}_\emptyset \mathcal{I}_{\emptyset,N_\emptyset}}\right)^{\mathsf{H}} \boldsymbol{h} \\ \left(\boldsymbol{F}^{\mathcal{X}_{u_1}}_{\mathrm{P}_{u_1}\mathcal{I}_{u_1,N_{u_1}}}\right)^{\mathsf{H}} \boldsymbol{h} \\ \vdots \\ \left(\boldsymbol{F}^{\mathcal{X}_{u_m}}_{\mathrm{P}_{u_m}\mathcal{I}_{u_m,N_{u_m}}}\right)^{\mathsf{H}} \boldsymbol{h} \end{pmatrix} = \begin{pmatrix} \hat{\boldsymbol{h}}_\emptyset \\ \hat{\boldsymbol{h}}_{\boldsymbol{u}_1} \\ \vdots \\ \hat{\boldsymbol{h}}_{\boldsymbol{u}_m} \end{pmatrix} = \hat{\boldsymbol{h}},$$

$m = |U| - 1$, and therefore reduced the d-dimensional transformation to $|U|$ lower-dimensional transformations which are independent and can be computed in parallel.

We present a general version of the grouped transformations as Algorithm 3.1 and its adjoint counterpart as Algorithm 3.2. However, this algorithm lacks one crucial part which is the fast realization of the multiplications $\boldsymbol{F}^{\mathcal{X}_u}_{\mathrm{P}_u\mathcal{I}_{u,N_u}} \hat{\boldsymbol{p}}_{\boldsymbol{u}}$ and $(\boldsymbol{F}^{\mathcal{X}_u}_{\mathrm{P}_u\mathcal{I}_{u,N_u}})^{\mathsf{H}}\boldsymbol{h}$. This depends on the chosen basis and will be considered for each of the systems from Section 2.1.2 afterwards.

Remark 3.5. *The error of one NFFT with $\xi_{\boldsymbol{k}}^{(\exp)}$, cf. Definition 3.1, can be estimated as follows*

$$\left| \sum_{\boldsymbol{k} \in \mathcal{I}_{\boldsymbol{u},N_{\boldsymbol{u}}}} \hat{p}_{\boldsymbol{k}}\, \xi_{\boldsymbol{k}}^{(\exp)}(\boldsymbol{x}) - \mathrm{NFFT}(\hat{\boldsymbol{p}}_{\boldsymbol{u}}) \right| \leq C(N_{\boldsymbol{u}})\, \|\hat{\boldsymbol{p}}_{\boldsymbol{u}}\|_{\ell_1} .$$

Here, $C(N_{\boldsymbol{u}})$ decays exponentially in $N_{\boldsymbol{u}}$, cf. [PPST18, Theorem 7.8] and references therein. Since the grouped transformation is a sum of the above, we can bound the overall error by

$$\left(\max_{\boldsymbol{u} \in \mathcal{U}} C(N_{\boldsymbol{u}}) \right) \|\hat{\boldsymbol{p}}\|_{\ell_1} .$$

The same statement holds for the NFCT with functions $\xi_{\boldsymbol{k}}^{(\cos)}$, see Definition 3.2.

3.2.2.1 Grouped Transformations with the Fourier System

We consider the periodic functions $f : \mathbb{T}^d \to \mathbb{C}$ in the space $\mathrm{L}_2(\mathbb{T}^d)$ with the Fourier system $\varphi_{\boldsymbol{k}}^{(d),\exp}(\boldsymbol{x})$ as complete orthonormal system, see (2.7). For this system, we propose a fast algorithm for the multiplication

$$\boldsymbol{F}^{\mathcal{X}_{\boldsymbol{u}}}_{\mathrm{P}_{\boldsymbol{u}}\mathcal{I}^{(\mathrm{per})}_{\boldsymbol{u},N}} \hat{\boldsymbol{p}} \quad \text{with} \quad N \in 2\mathbb{N}, \boldsymbol{u} \subseteq [d], \mathcal{X} \subseteq \mathbb{C}^d, \quad \text{and}$$
$$\hat{\boldsymbol{p}} = (\hat{p}_{\boldsymbol{k}})_{\boldsymbol{k} \in \mathcal{I}^{(\mathrm{per})}_{\boldsymbol{u},N}} \in \mathbb{C}^{(N-1)^{|\boldsymbol{u}|}}.$$

The index set $\mathcal{I}^{(\mathrm{per})}_{\boldsymbol{u},N}$ has been defined in (3.9). In the end, it is our goal to apply a $|\boldsymbol{u}|$-variate NFFT from Section 3.1. We observe the connection

$$\mathrm{P}_{\boldsymbol{u}}\mathcal{I}^{(\mathrm{per})}_{\boldsymbol{u},N} = \left\{ \boldsymbol{k} \in \mathbb{Z}^{|\boldsymbol{u}|} \colon \boldsymbol{k} \in \mathcal{I}^{(\exp)}_{\boldsymbol{N}} \text{ and } \operatorname{supp} \boldsymbol{k} = [|\boldsymbol{u}|] \right\}$$

with $[|\boldsymbol{u}|] = \{1, 2, \ldots, |\boldsymbol{u}|\}$ to the index set $\mathcal{I}^{(\exp)}_{\boldsymbol{N}}$ from (3.4) with $\boldsymbol{N} = (N, N, \ldots, N) \in \mathbb{N}^{|\boldsymbol{u}|}$. Since $\mathrm{P}_{\boldsymbol{u}}\mathcal{I}^{(\mathrm{per})}_{\boldsymbol{u},N}$ is a subset of $\mathcal{I}^{(\exp)}_{\boldsymbol{N}}$, we require

Algorithm 3.1 Grouped Transformation

Input:	$d \in \mathbb{N}$	spatial dimension
	$(\varphi_k) \subseteq \mathrm{L}_2(\mathbb{D}, \omega)$	basis of $\mathrm{L}_2(\mathbb{D}, \omega)$
	$U \subseteq \mathcal{P}([d])$	subset of ANOVA terms
	$\boldsymbol{N} = (N_{\boldsymbol{u}})_{\boldsymbol{u} \in U \setminus \{\emptyset\}} \in \mathbb{N}^{\lvert U \rvert - 1}$	bandwidth vector, cf. Def. 3.3
	$\mathcal{X} = \{\boldsymbol{x}_1, \boldsymbol{x}_2, \ldots, \boldsymbol{x}_M\} \subseteq \mathbb{D}^d$	M nodes in the domain
	$\hat{p}_{\boldsymbol{k}} \in \mathbb{C}, \boldsymbol{k} \in \mathcal{I}_{\boldsymbol{N}}(U)$	coefficients

1: **for** $\boldsymbol{u} \in U \setminus \{\emptyset\}$ **do**
2: $\quad \hat{\boldsymbol{p}}_{\boldsymbol{u}} \longleftarrow (\hat{p}_{\boldsymbol{k}})_{\boldsymbol{k} \in \mathcal{I}_{\boldsymbol{u}, N_{\boldsymbol{u}}}}$
3: $\quad \boldsymbol{F}^{\mathcal{X}_{\boldsymbol{u}}}_{\mathrm{P}_{\boldsymbol{u}} \mathcal{I}_{\boldsymbol{u}, N_{\boldsymbol{u}}}} \longleftarrow \left(\varphi^{(\lvert \boldsymbol{u} \rvert)}_{\boldsymbol{\ell}}(\boldsymbol{x}) \right)_{\boldsymbol{x} \in \mathcal{X}_{\boldsymbol{u}}, \boldsymbol{\ell} \in \mathrm{P}_{\boldsymbol{u}} \mathcal{I}_{\boldsymbol{u}, N_{\boldsymbol{u}}}}$
4: **end for**
5: $\boldsymbol{p} \longleftarrow (\hat{p}_{\boldsymbol{0}})_{j=1}^{M}$
6: **for** $\boldsymbol{u} \in U \setminus \{\emptyset\}$ **do**
7: $\quad \boldsymbol{p} \longleftarrow \boldsymbol{p} + \boldsymbol{F}^{\mathcal{X}_{\boldsymbol{u}}}_{\mathrm{P}_{\boldsymbol{u}} \mathcal{I}_{\boldsymbol{u}, N_{\boldsymbol{u}}}} \hat{\boldsymbol{p}}_{\boldsymbol{u}}$ $\quad \triangleleft$ parallelization
8: **end for**

Output: $\boldsymbol{p} \in \mathbb{C}^M$ result of the multiplication $\boldsymbol{F}^{\mathcal{X}}_{\mathcal{I}_{\boldsymbol{N}}(U)} \hat{\boldsymbol{p}}_{\boldsymbol{u}}$

Complexity: $\sum_{\boldsymbol{u} \in U}$ cost of $\boldsymbol{F}^{\mathcal{X}_{\boldsymbol{u}}}_{\mathrm{P}_{\boldsymbol{u}} \mathcal{I}_{\boldsymbol{u}, N_{\boldsymbol{u}}}} \hat{\boldsymbol{p}}_{\boldsymbol{u}}$

Algorithm 3.2 Adjoint Grouped Transformation

Input:

$d \in \mathbb{N}$	spatial dimension
$(\varphi_k) \subseteq \mathrm{L}_2(\mathbb{D}, \omega)$	basis of $\mathrm{L}_2(\mathbb{D}, \omega)$
$U \subseteq \mathcal{P}([d])$	subset of ANOVA terms
$\boldsymbol{N} = (N_{\boldsymbol{u}})_{\boldsymbol{u} \in U \setminus \{\emptyset\}} \in \mathbb{N}^{\lvert U \rvert - 1}$	bandwidth vector, cf. Def. 3.3
$\mathcal{X} = \{\boldsymbol{x}_1, \boldsymbol{x}_2, \ldots, \boldsymbol{x}_M\} \subseteq \mathbb{D}^d$	M nodes in the domain
$h_{\boldsymbol{x}} \in \mathbb{C}, \boldsymbol{x} \in \mathcal{X}$	coefficients

1: **for** $\boldsymbol{u} \in U \setminus \{\emptyset\}$ **do**

2: $\quad \left(\boldsymbol{F}^{\mathcal{X}_{\boldsymbol{u}}}_{\mathrm{P}_{\boldsymbol{u}} \mathcal{I}_{\boldsymbol{u}, N_{\boldsymbol{u}}}}\right)^{\mathsf{H}} \longleftarrow \left(\overline{\varphi}^{(\lvert \boldsymbol{u} \rvert)}_{\boldsymbol{\ell}}(\boldsymbol{x})\right)_{\boldsymbol{\ell} \in \mathrm{P}_{\boldsymbol{u}} \mathcal{I}_{\boldsymbol{u}, N_{\boldsymbol{u}}}, \boldsymbol{x} \in \mathcal{X}_{\boldsymbol{u}}}$

3: **end for**

4: $\hat{\boldsymbol{h}}_{\emptyset} \longleftarrow \sum_{\boldsymbol{x} \in \mathcal{X}} h_{\boldsymbol{x}}$

5: **for** $\boldsymbol{u} \in U \setminus \{\emptyset\}$ **do**

6: $\quad \hat{\boldsymbol{h}}_{\boldsymbol{u}} \longleftarrow \left(\boldsymbol{F}^{\mathcal{X}_{\boldsymbol{u}}}_{\mathrm{P}_{\boldsymbol{u}} \mathcal{I}_{\boldsymbol{u}, N_{\boldsymbol{u}}}}\right)^{\mathsf{H}} \hat{\boldsymbol{p}}_{\boldsymbol{u}}$ ◁ parallelization

7: **end for**

8: $\hat{\boldsymbol{h}} \longleftarrow (\hat{\boldsymbol{h}}_{\boldsymbol{u}})_{\boldsymbol{u} \in U}$

Output: $\hat{\boldsymbol{h}} \in \mathbb{C}^{1 + \sum_{\emptyset \neq \boldsymbol{u} \in U} (N_{\boldsymbol{u}} - 1)^{\lvert \boldsymbol{u} \rvert}}$ result of multiplication $(\boldsymbol{F}^{\mathcal{X}}_{\mathcal{I}_{\boldsymbol{N}}(U)})^{\mathsf{H}} \boldsymbol{h}$

Complexity: $\sum_{\boldsymbol{u} \in U}$ cost of $\left(\boldsymbol{F}^{\mathcal{X}_{\boldsymbol{u}}}_{\mathrm{P}_{\boldsymbol{u}} \mathcal{I}_{\boldsymbol{u}, N_{\boldsymbol{u}}}}\right)^{\mathsf{H}} \hat{\boldsymbol{p}}_{\boldsymbol{u}}$

zero-padding in order to apply the NFFT for this special index set. We define

$$\hat{g} := (\hat{g}_{\ell})_{\ell \in I_N^{(\exp)}} \quad \text{with} \quad \hat{g}_{\ell} := \begin{cases} \hat{p}_k(\ell) & : \operatorname{supp} \ell = [|u|] \\ 0 & : \text{otherwise} \end{cases} \tag{3.17}$$

with $\hat{p}_k(\ell) = \hat{p}_k$ for the index $k \in \mathbb{Z}^d$ with $\operatorname{supp} k = u$ and $k_u = \ell$. The process of projection and subsequent zero-padding has been visualized in Figure 3.2.

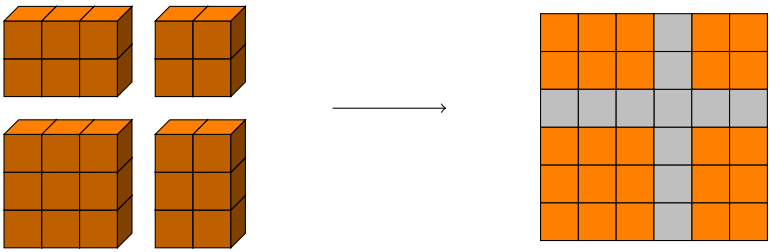

Figure 3.2: Visualization of the projection and zero-padding from $I^{(\mathrm{per})}_{\{1,2\},3}$ to $I^{(\exp)}_{(3,3)}$.

We also notice that our basis functions $\varphi_k^{(d),\exp}$ coincide with $\xi_k^{(\exp)}$ from (3.1). If we denote with $F^{\mathcal{X}}_{I_N^{(\exp)}} = (\xi_{\ell}^{(\exp)}(x))_{x \in \tilde{\mathcal{X}}, \ell \in I_N^{(\exp)}}$ the NDFT matrix for $\tilde{\mathcal{X}} = \mathcal{X}_u$, we have that

$$F^{\mathcal{X}_u}_{\mathrm{P}_u I^{(\mathrm{per})}_{u,N}} \hat{p} = F^{\tilde{\mathcal{X}}}_{I_N^{(\exp)}} \hat{g}.$$

The right-hand side can be computed via a $|u|$-variate NFFT which leads to Algorithm 3.3.

It remains to consider the adjoint multiplication, i.e., the multiplication of $(F^{\mathcal{X}_u}_{\mathrm{P}_u I^{(\mathrm{per})}_{u,N}})^{\mathsf{H}}$ with a vector $h \in \mathbb{C}^M$. We can compute the adjoint

$|\boldsymbol{u}|$-variate NFFT and denote the result as

$$\hat{\boldsymbol{h}} = \left(\hat{h}_{\boldsymbol{\ell}}\right)_{\boldsymbol{\ell}\in\mathcal{I}_{\boldsymbol{N}}^{(\exp)}} = \left(\boldsymbol{F}^{\tilde{\mathcal{X}}}_{\mathcal{I}_{\boldsymbol{N}}^{(\exp)}}\right)^{\mathsf{H}} \boldsymbol{h}.$$

This simultaneously provides the result to our original question since

$$(\boldsymbol{F}^{\mathcal{X}_{\boldsymbol{u}}}_{\mathrm{P}_{\boldsymbol{u}}\mathcal{I}_{\boldsymbol{u},N}^{(\mathrm{per})}})^{\mathsf{H}}\boldsymbol{h} = \left(\hat{h}_{\boldsymbol{\ell}}\right)_{\boldsymbol{\ell}\in\mathrm{P}_{\boldsymbol{u}}\mathcal{I}_{\boldsymbol{u},N}^{(\mathrm{per})}}.$$

In other words, we have computed more coefficients than necessary by using an adjoint NFFT. We present the method as Algorithm 3.4.

3.2.2.2 Grouped Transformations with the Chebyshev System

Now, we consider the Chebyshev system $\varphi_{\boldsymbol{k}}^{(d),\,\mathrm{cheb}}(\boldsymbol{x})$ from (2.8) as a basis in the space $\mathrm{L}_2([-1,1]^d, \omega^{(d),\,\mathrm{cheb}})$ with non-periodic functions $f\colon [-1,1]^d \to \mathbb{R}$. For this system, we propose a fast algorithm for the multiplication

$$\boldsymbol{F}^{\mathcal{X}_{\boldsymbol{u}}}_{\mathrm{P}_{\boldsymbol{u}}\mathcal{I}_{\boldsymbol{u},N}^{(\mathrm{nper})}}\hat{\boldsymbol{p}} \quad \text{with} \quad N \in 2\mathbb{N}, \boldsymbol{u} \subseteq [d], \mathcal{X} \subseteq [-1,1]^d, \quad \text{and}$$
$$\hat{\boldsymbol{p}} = (\hat{p}_{\boldsymbol{k}})_{\boldsymbol{k}\in\mathcal{I}_{\boldsymbol{u},N}^{(\mathrm{nper})}} \in \mathbb{C}^{(N-1)^{|\boldsymbol{u}|}}.$$

While we may reuse some ideas from the Fourier system, the details differ in some aspects. Similar as for the periodic case, we have

$$\mathrm{P}_{\boldsymbol{u}}\mathcal{I}_{\boldsymbol{u},N}^{(\mathrm{nper})} = \left\{\boldsymbol{k} \in \mathbb{N}_0^{|\boldsymbol{u}|} \colon \boldsymbol{k} \in \mathcal{I}_{\boldsymbol{N}}^{(\cos)} \text{ and } \operatorname{supp}\boldsymbol{k} = [|\boldsymbol{u}|]\right\}$$

with the index set $\mathcal{I}_{\boldsymbol{N}}^{(\cos)}$ from (3.5), and $\boldsymbol{N} = (N, N, \ldots, N) \in \mathbb{N}^{|\boldsymbol{u}|}$. The zero-padding also works in the same manner as before in (3.17) and we obtain

$$\hat{\boldsymbol{g}} \coloneqq (\hat{g}_{\boldsymbol{\ell}})_{\boldsymbol{\ell}\in\mathcal{I}_{\boldsymbol{N}}^{(\cos)}} \quad \text{with} \quad \hat{g}_{\boldsymbol{\ell}} \coloneqq \begin{cases} \hat{p}_{\boldsymbol{k}}(\boldsymbol{\ell}) & : \operatorname{supp}\boldsymbol{\ell} = [|\boldsymbol{u}|] \\ 0 & : \text{otheriwse} \end{cases}$$

Algorithm 3.3 Multiplication of $\boldsymbol{F}^{\mathcal{X}_{\boldsymbol{u}}}_{\mathrm{P}_{\boldsymbol{u}}\mathcal{I}^{(\mathrm{per})}_{\boldsymbol{u},N}}$ with a coefficient vector $\hat{\boldsymbol{p}}$ (Fourier system)

Input: $d \in \mathbb{N}$ spatial dimension
$\boldsymbol{u} \subseteq [d]$ subset of coordinate indices
$N \in 2\mathbb{N}$ even bandwidth parameter
$\mathcal{X} = \{\boldsymbol{x}_1, \boldsymbol{x}_2, \ldots, \boldsymbol{x}_M\} \subseteq \mathbb{T}^d$ M nodes in the domain
$\hat{\boldsymbol{p}} = (\hat{p}_{\boldsymbol{k}})_{\boldsymbol{k} \in \mathcal{I}^{(\mathrm{per})}_{\boldsymbol{u},N}} \in \mathbb{C}^{(N-1)^{|\boldsymbol{u}|}}$ coefficients

$\boldsymbol{N} \longleftarrow (N, N, \ldots, N) \in (2\mathbb{N})^{|\boldsymbol{u}|}$
$\tilde{\mathcal{X}} \longleftarrow \mathcal{X}_{\boldsymbol{u}} = \{(\boldsymbol{x}_1)_{\boldsymbol{u}}, (\boldsymbol{x}_2)_{\boldsymbol{u}}, \ldots, (\boldsymbol{x}_M)_{\boldsymbol{u}}\}$
for $\boldsymbol{\ell} \in \mathcal{I}^{(\mathrm{exp})}_{\boldsymbol{N}}$ **do**
  if $\operatorname{supp} \boldsymbol{\ell} = [|\boldsymbol{u}|]$ **then**
    $\boldsymbol{k} \longleftarrow (0)_{s=1}^{d}$
    $\boldsymbol{k}_{\boldsymbol{u}} \longleftarrow \boldsymbol{\ell}$
    $\hat{g}_{\boldsymbol{\ell}} \longleftarrow \hat{p}_{\boldsymbol{k}}$
  else
    $\hat{g}_{\boldsymbol{\ell}} \longleftarrow 0$
  end if
end for
$\hat{\boldsymbol{g}} \longleftarrow (\hat{g}_{\boldsymbol{\ell}})_{\boldsymbol{\ell} \in \mathcal{I}^{(\mathrm{exp})}_{\boldsymbol{N}}}$
$\boldsymbol{p} \longleftarrow \boldsymbol{F}^{\tilde{\mathcal{X}}}_{\mathcal{I}^{(\mathrm{exp})}_{\boldsymbol{N}}} \hat{\boldsymbol{g}}$ ◁ compute via $|\boldsymbol{u}|$-variate NFFT

Output: $\boldsymbol{p} \in \mathbb{C}^M$ result of the multiplication $\boldsymbol{F}^{\mathcal{X}_{\boldsymbol{u}}}_{\mathrm{P}_{\boldsymbol{u}}\mathcal{I}^{(\mathrm{per})}_{\boldsymbol{u},N}} \hat{\boldsymbol{p}}$

Arithmetic cost: $N^{|\boldsymbol{u}|} \log N$

Algorithm 3.4 Multiplication of $(\boldsymbol{F}^{\mathcal{X}_{\boldsymbol{u}}}_{\mathrm{P}_{\boldsymbol{u}}\mathcal{I}^{(\mathrm{per})}_{\boldsymbol{u},N}})^{\mathsf{H}}$ with a coefficient vector $\boldsymbol{h}$ (Fourier system)

Input:	$d \in \mathbb{N}$	spatial dimension
	$\boldsymbol{u} \subseteq [d]$	subset of coordinate indices
	$N \in 2\mathbb{N}$	even bandwidth parameter
	$\mathcal{X} = \{\boldsymbol{x}_1, \boldsymbol{x}_2, \ldots, \boldsymbol{x}_M\} \subseteq \mathbb{T}^d$	M nodes in the domain
	$\boldsymbol{h} = (h_{\boldsymbol{x}})_{\boldsymbol{x}\in\mathcal{X}} \in \mathbb{C}^M$	coefficients

1: $\boldsymbol{N} \longleftarrow (N, N, \ldots, N) \in (2\mathbb{N})^{|\boldsymbol{u}|}$

2: $\tilde{\mathcal{X}} \longleftarrow \mathcal{X}_{\boldsymbol{u}} = \{(\boldsymbol{x}_1)_{\boldsymbol{u}}, (\boldsymbol{x}_2)_{\boldsymbol{u}}, \ldots, (\boldsymbol{x}_M)_{\boldsymbol{u}}\}$

3: $\hat{\boldsymbol{h}} = \left(\hat{h}_{\boldsymbol{k}}\right)_{\boldsymbol{k}\in\mathcal{I}^{(\mathrm{exp})}_{\boldsymbol{N}}} \longleftarrow \left(\boldsymbol{F}^{\tilde{\mathcal{X}}}_{\mathcal{I}^{(\mathrm{exp})}_{\boldsymbol{N}}}\right)^{\mathsf{H}} \boldsymbol{h}$ ◁ compute via $|\boldsymbol{u}|$-variate adjoint NFFT

Output:	$\left(\hat{h}_{\boldsymbol{\ell}}\right)_{\boldsymbol{\ell}\in\mathrm{P}_{\boldsymbol{u}}\mathcal{I}^{(\mathrm{per})}_{\boldsymbol{u},N}} \in \mathbb{C}^M$	result of multiplication $(\boldsymbol{F}^{\mathcal{X}_{\boldsymbol{u}}}_{\mathrm{P}_{\boldsymbol{u}}\mathcal{I}^{(\mathrm{per})}_{\boldsymbol{u},N}})^{\mathsf{H}}\boldsymbol{h}$
Arithmetic cost:	$N^{|\boldsymbol{u}|}\log N$	

with $\hat{p}_k(\boldsymbol{\ell}) = \hat{p}_k$ for the index $\boldsymbol{k} \in \mathbb{N}_0^d$ with $\operatorname{supp} \boldsymbol{k} = \boldsymbol{u}$ and $\boldsymbol{k}_{\boldsymbol{u}} = \boldsymbol{\ell}$.

However, the basis functions $\varphi_{\boldsymbol{k}}^{(d),\,\mathrm{cheb}}$ do not coincide with the cosine system $\xi_{\boldsymbol{k}}^{(\cos)}$ from (3.2), but we have

$$\varphi_{\boldsymbol{k}}^{(d),\,\mathrm{cheb}}(\boldsymbol{x}) = \sqrt{2}^{|\operatorname{supp} \boldsymbol{k}|}\, \xi_{\boldsymbol{k}}^{(\cos)}\left(\frac{\arccos \boldsymbol{x}}{2\pi}\right)$$

where the arccos is applied elementwise to $\boldsymbol{x}$. We denote the transformed nodes with

$$\tilde{\mathcal{X}} = \left\{ \frac{1}{2\pi} \arccos\left(\boldsymbol{x}_1\right)_{\boldsymbol{u}}, \frac{1}{2\pi} \arccos\left(\boldsymbol{x}_2\right)_{\boldsymbol{u}}, \ldots, \frac{1}{2\pi} \arccos\left(\boldsymbol{x}_M\right)_{\boldsymbol{u}} \right\}.$$

As a result we have the identity

$$\boldsymbol{F}^{\mathcal{X}_{\boldsymbol{u}}}_{\mathrm{P}_{\boldsymbol{u}} \mathcal{I}^{(\mathrm{nper})}_{\boldsymbol{u},N}} \hat{\boldsymbol{p}} = \left(\boldsymbol{F}^{\tilde{\mathcal{X}}}_{\mathcal{I}_N^{(\cos)}} \cdot \operatorname{diag}\left(\sqrt{2}^{|\operatorname{supp} \boldsymbol{\ell}|} \right)_{\boldsymbol{\ell} \in \mathcal{I}_N^{(\cos)}} \right) \hat{\boldsymbol{g}}.$$

Algorithm 3.5 summarizes our method with the most notable change that the nodes $\mathcal{X}$ have to be transformed and we require a multiplication with a diagonal matrix. However, both operations are possible in linear time which is why the complexity of the algorithm is still dominated by the $|\boldsymbol{u}|$-variate NFCT.

For the transposed case, i.e., the multiplication of $(\boldsymbol{F}^{\mathcal{X}_{\boldsymbol{u}}}_{\mathrm{P}_{\boldsymbol{u}} \mathcal{I}^{(\mathrm{nper})}_{\boldsymbol{u},N}})^{\mathsf{T}}$ with a vector $\boldsymbol{h} \in \mathbb{R}^M$, we compute the transposed $|\boldsymbol{u}|$-variate NFCT and denote the result as

$$\hat{\boldsymbol{h}} = \left(\hat{h}_{\boldsymbol{\ell}} \right)_{\boldsymbol{\ell} \in \mathcal{I}_N^{(\cos)}} = \operatorname{diag}\left(\sqrt{2}^{|\operatorname{supp} \boldsymbol{\ell}|} \right)_{\boldsymbol{\ell} \in \mathcal{I}_N^{(\cos)}} \left(\boldsymbol{F}^{\tilde{\mathcal{X}}}_{\mathcal{I}_N^{(\cos)}} \right)^{\mathsf{T}} \boldsymbol{h}.$$

As in the periodic case, this provides us with the result of the original matrix-vector multiplication since

$$(\boldsymbol{F}^{\mathcal{X}_{\boldsymbol{u}}}_{\mathrm{P}_{\boldsymbol{u}} \mathcal{I}^{(\mathrm{nper})}_{\boldsymbol{u},N}})^{\mathsf{T}} \boldsymbol{h} = \left(\hat{h}_{\boldsymbol{\ell}} \right)_{\boldsymbol{\ell} \in \mathrm{P}_{\boldsymbol{u}} \mathcal{I}^{(\mathrm{nper})}_{\boldsymbol{u},N}}.$$

The method is summarized in Algorithm 3.6.

Algorithm 3.5 Multiplication of $F^{\mathcal{X}_u}_{\mathrm{P}_u \mathcal{I}^{(\mathrm{nper})}_{u,N}}$ with a coefficient vector $\hat{p}$ (Chebyshev system)

Input:
- $d \in \mathbb{N}$ — spatial dimension
- $u \subseteq [d]$ — subset coordinate indices
- $N \in \mathbb{N}$ — bandwidth parameter
- $\mathcal{X} = \{x_1, x_2, \ldots, x_M\} \subseteq [-1,1]^d$ — M nodes in the domain
- $\hat{p} = (\hat{p}_k)_{k \in \mathcal{I}^{(\mathrm{nper})}_{u,N}} \in \mathbb{R}^{(N-1)^{|u|}}$ — coefficients

1: $N \longleftarrow (N, N, \ldots, N) \in \mathbb{N}^{|u|}$
2: $\tilde{\mathcal{X}} \longleftarrow \mathcal{X}_u = \left\{ \frac{1}{2\pi} \arccos(x_1)_u \,,\, \frac{1}{2\pi} \arccos(x_2)_u \,,\, \ldots \,,\, \frac{1}{2\pi} \arccos(x_M)_u \right\}$
3: **for** $\ell \in \mathcal{I}^{(\cos)}_N$ **do**
4: **if** $\operatorname{supp} \ell = [|u|]$ **then**
5: $k \longleftarrow (0)_{s=1}^{d}$
6: $k_u \longleftarrow \ell$
7: $\hat{g}_\ell \longleftarrow \sqrt{2}^{|u|} \cdot \hat{p}_k$
8: **else**
9: $\hat{g}_\ell \longleftarrow 0$
10: **end if**
11: **end for**
12: $\hat{g} \longleftarrow (\hat{g}_\ell)_{\ell \in \mathcal{I}^{(\cos)}_N}$
13: $\tilde{p} \longleftarrow F^{\tilde{\mathcal{X}}}_{\mathcal{I}^{(\cos)}_N} \hat{g}$ ◁ compute via $|u|$-variate NFCT

Output: $p \in \mathbb{R}^M$ result of the multiplication $F^{\mathcal{X}_u}_{\mathrm{P}_u \mathcal{I}^{(\mathrm{nper})}_{u,N}} \hat{p}$

Arithmetic cost: $N^{|u|} \log N$

Algorithm 3.6 Multiplication of $(\boldsymbol{F}^{\mathcal{X}_{\boldsymbol{u}}}_{\mathrm{P}_{\boldsymbol{u}}\mathcal{I}^{(\mathrm{nper})}_{\boldsymbol{u},N}})^{\mathsf{T}}$ with a coefficient vector $\boldsymbol{h}$ (Chebyshev system)

Input:
- $d \in \mathbb{N}$ — spatial dimension
- $\boldsymbol{u} \subseteq [d]$ — subset coordinate indices
- $N \in \mathbb{N}$ — bandwidth parameter
- $\mathcal{X} = \{\boldsymbol{x}_1, \boldsymbol{x}_2, \ldots, \boldsymbol{x}_M\} \subseteq [-1,1]^d$ — M nodes in the domain
- $\boldsymbol{h} = (h_{\boldsymbol{x}})_{\boldsymbol{x}\in\mathcal{X}} \in \mathbb{R}^M$ — coefficients

1: $\boldsymbol{N} \longleftarrow (N, N, \ldots, N) \in \mathbb{N}^{|\boldsymbol{u}|}$

2: $\tilde{\mathcal{X}} \longleftarrow \mathcal{X}_{\boldsymbol{u}} = \left\{ \frac{1}{2\pi} \arccos(\boldsymbol{x}_1)_{\boldsymbol{u}}, \frac{1}{2\pi} \arccos(\boldsymbol{x}_2)_{\boldsymbol{u}}, \ldots, \frac{1}{2\pi} \arccos(\boldsymbol{x}_M)_{\boldsymbol{u}} \right\}$

3: $\hat{\boldsymbol{h}} = \left(\hat{h}_{\boldsymbol{k}}\right)_{\boldsymbol{k}\in\mathcal{I}^{(\cos)}_{\boldsymbol{N}}} \longleftarrow \left(\boldsymbol{F}^{\tilde{\mathcal{X}}}_{\mathcal{I}^{(\cos)}_{\boldsymbol{N}}}\right)^{\mathsf{T}} \boldsymbol{h}$ ◁ compute via $|\boldsymbol{u}|$-variate transposed NFCT

4: $\hat{\boldsymbol{h}} \leftarrow \operatorname{diag}\left(\sqrt{2}^{|\operatorname{supp}\boldsymbol{\ell}|}\right)_{\boldsymbol{\ell}\in\mathcal{I}^{(\cos)}_{\boldsymbol{N}}} \hat{\boldsymbol{h}}$ ◁ in linear time

Output: $\left(\hat{h}_{\boldsymbol{\ell}}\right)_{\boldsymbol{\ell}\in\mathrm{P}_{\boldsymbol{u}}\mathcal{I}^{(\mathrm{per})}_{\boldsymbol{u},N}} \in \mathbb{R}^M$ result of multiplication $(\boldsymbol{F}^{\mathcal{X}_{\boldsymbol{u}}}_{\mathrm{P}_{\boldsymbol{u}}\mathcal{I}^{(\mathrm{nper})}_{\boldsymbol{u},N}})^{\mathsf{T}}\boldsymbol{h}$

Arithmetic cost: $N^{|\boldsymbol{u}|} \log N$

3.2.2.3 Grouped Transformations with the Half-Period Cosine System

The half-period cosine system $\varphi_{\boldsymbol{k}}^{(d),\cos}(\boldsymbol{x})$ from (2.10) is a basis in $\mathrm{L}_2([0,1]^d)$ with non-periodic functions $f\colon [0,1]^d \to \mathbb{R}$. As for the other systems, we propose a fast algorithm for the multiplication

$$\boldsymbol{F}^{\mathcal{X}_{\boldsymbol{u}}}_{\mathrm{P}_{\boldsymbol{u}}\mathcal{I}^{(\mathrm{nper})}_{\boldsymbol{u},N}}\hat{\boldsymbol{p}} \quad \text{with} \quad N \in 2\mathbb{N}, \boldsymbol{u} \subseteq [d], \mathcal{X} \subseteq [0,1]^d, \quad \text{and}$$
$$\hat{\boldsymbol{p}} = (\hat{p}_{\boldsymbol{k}})_{\boldsymbol{k}\in\mathcal{I}^{(\mathrm{nper})}_{\boldsymbol{u},N}} \in \mathbb{R}^{(N-1)^{|\boldsymbol{u}|}}.$$

Here, there is only one difference to the Chebyshev system from before: We have a different relationship between the basis functions $\varphi_{\boldsymbol{k}}^{(d),\cos}$ and the cosine system $\xi_{\boldsymbol{k}}^{(\cos)}$, i.e.,

$$\varphi_{\boldsymbol{k}}^{(d),\cos}(\boldsymbol{x}) = \sqrt{2}^{|\operatorname{supp}\boldsymbol{k}|}\,\xi_{\boldsymbol{k}}^{(\cos)}\left(\frac{1}{2}\boldsymbol{x}\right).$$

As a result, we use Algorithm 3.5 for the multiplication $\boldsymbol{F}^{\mathcal{X}_{\boldsymbol{u}}}_{\mathrm{P}_{\boldsymbol{u}}\mathcal{I}^{(\mathrm{nper})}_{\boldsymbol{u},N}}\hat{\boldsymbol{p}}$ and modify line 2 to

$$\tilde{\mathcal{X}} \longleftarrow \mathcal{X}_{\boldsymbol{u}} = \left\{\frac{1}{2}(\boldsymbol{x}_1)_{\boldsymbol{u}}, \frac{1}{2}(\boldsymbol{x}_2)_{\boldsymbol{u}}, \ldots, \frac{1}{2}(\boldsymbol{x}_M)_{\boldsymbol{u}}\right\}. \tag{3.18}$$

Similarly, for the transposed multiplication $(\boldsymbol{F}^{\mathcal{X}_{\boldsymbol{u}}}_{\mathrm{P}_{\boldsymbol{u}}\mathcal{I}^{(\mathrm{nper})}_{\boldsymbol{u},N}})^{\mathsf{T}}\boldsymbol{h}$ we use Algorithm 3.6 and again modify line 2 to (3.18).

3.2.2.4 Grouped Transformations with the Transformed Cosine System

The transformed cosine system $\varphi_{\boldsymbol{k}}^{(d),\mathrm{std}}(\boldsymbol{x})$ from (2.15) is a basis in $\mathrm{L}_2(\mathbb{R}^d, \omega^{(d),\mathrm{std}})$ with non-periodic functions $f\colon \mathbb{R}^d \to \mathbb{R}$. Here, we also

propose a fast algorithm for the multiplication

$$\boldsymbol{F}^{\mathcal{X}_{\boldsymbol{u}}}_{\mathrm{P}_{\boldsymbol{u}}\mathcal{I}^{(\mathrm{nper})}_{\boldsymbol{u},N}}\hat{\boldsymbol{p}} \quad \text{with} \quad N \in 2\mathbb{N}, \boldsymbol{u} \subseteq [d], \mathcal{X} \subseteq \mathbb{R}^d, \quad \text{and}$$
$$\hat{\boldsymbol{p}} = (\hat{p}_{\boldsymbol{k}})_{\boldsymbol{k}\in\mathcal{I}^{(\mathrm{nper})}_{\boldsymbol{u},N}} \in \mathbb{R}^{(N-1)^{|\boldsymbol{u}|}}.$$

For the relationship between the basis functions $\varphi^{(d),\,\mathrm{std}}_{\boldsymbol{k}}(\boldsymbol{x})$ and the cosine system $\xi^{(\cos)}_{\boldsymbol{k}}$ we have

$$\varphi^{(d),\,\mathrm{std}}_{\boldsymbol{k}}(\boldsymbol{x}) = \sqrt{2}^{|\mathrm{supp}\,\boldsymbol{k}|}\,\xi^{(\cos)}_{\boldsymbol{k}}\left(\frac{1}{2}\psi^{-1}(\boldsymbol{x})\right)$$

with the transformation function ψ^{-1} from (2.14). We again use Algorithm 3.5 for the multiplication $\boldsymbol{F}^{\mathcal{X}_{\boldsymbol{u}}}_{\mathrm{P}_{\boldsymbol{u}}\mathcal{I}^{(\mathrm{nper})}_{\boldsymbol{u},N}}\hat{\boldsymbol{p}}$ and modify line 2 to

$$\tilde{\mathcal{X}} \longleftarrow \mathcal{X}_{\boldsymbol{u}} = \left\{\frac{1}{2}\left(\psi^{-1}(\boldsymbol{x}_1)\right)_{\boldsymbol{u}}, \frac{1}{2}\left(\psi^{-1}(\boldsymbol{x}_2)\right)_{\boldsymbol{u}}, \ldots, \frac{1}{2}\left(\psi^{-1}(\boldsymbol{x}_M)\right)_{\boldsymbol{u}}\right\}. \tag{3.19}$$

The transposed multiplication $(\boldsymbol{F}^{\mathcal{X}_{\boldsymbol{u}}}_{\mathrm{P}_{\boldsymbol{u}}\mathcal{I}^{(\mathrm{nper})}_{\boldsymbol{u},N}})^{\mathsf{T}}\boldsymbol{h}$ can be realized with Algorithm 3.6 where line 2 is again modified as in (3.19).

3.2.3 Implementation

The grouped transformations have been implemented in the publicly available package *GroupedTransforms.jl* for the programming language Julia, see [SB]. The package uses *NFFT3.jl*, see [Schb], for the computation of the low-dimensional transformation and utilizes parallelization to distribute their computation to different Julia workers depending on the core count of the machine.

In the following, we show code examples for the usage of the package on the examples from Figure 3.1. We begin with the subset of ANOVA terms $U^{(3,3)}$ and the bandwidth vector $N = [12, 8, 4]$. The transformation objects `F_exp` and `F_cos` can be used just like matrices although there is never a matrix constructed explicitly.

```
using Distributed
addprocs(3) # parallelization with 3 workers

@everywhere using GroupedTransforms
using LinearAlgebra

d = 4
ds = 3

M = 1_000 # number of nodes
X = rand(d, M) .- 0.5 # draw nodes at random
N = [12, 8, 4]

# initalize GroupedTransform with exponential functions
F_exp = GroupedTransform("exp", d, ds, N, X)

# generate coefficient vector (initalized with zeros)
fhat = GroupedCoefficients(F_exp.setting)

for i = 1:length(F_exp.setting)
    u = F_exp.setting[i][:u]
    fhat[u] = rand(ComplexF64, size(fhat[u])) # generate coefficients
        ↪ at random
end

f = F_exp * fhat # apply grouped transform to coefficient vector

h = rand(ComplexF64, length(f))
h_hat = F_exp' * h # adjoint transform

# initalize GroupedTransform with cosine functions
```

```
F_cos = GroupedTransform("cos", d, ds, N, X)

# generate coefficient vector (initalized with zeros)
fhat = GroupedCoefficients(F_cos.setting)

for i = 1:length(F_cos.setting)
    u = F_cos.setting[i][:u]
    fhat[u] = rand(Float64, size(fhat[u])) # generate coefficients at
        ↪ random
end

f = F_cos * fhat # apply grouped transform to coefficient vector

h = rand(Float64, length(f))
h_hat = F_cos' * h # adjoint transform
```

Now, we show how to apply a grouped transformation with the subset of ANOVA terms $U = \{\emptyset, \{1\}, \{2,3\}, \{1,2,3\}\}$ and the same bandwidth vector $N = [12, 8, 4]$ as before.

```
using Distributed
addprocs(3) # parallelization with 3 workers

@everywhere using GroupedTransforms
using LinearAlgebra

d = 4
ds = 3

M = 1_000 # number of nodes
X = rand(d, M) .- 0.5 # draw nodes at random

U = Vector{Vector{Int64}}(undef, 3)
U[1] = []
U[2] = [1]
U[3] = [2, 3]
U[4] = [1,2,3]

N = [12, 8, 4]

# initalize GroupedTransform with exponential functions
F_exp = GroupedTransform("exp", U, N, X)

# generate coefficient vector (initalized with zeros)
fhat = GroupedCoefficients(F_exp.setting)

for i = 1:length(F_exp.setting)
    u = F_exp.setting[i][:u]
```

```
    fhat[u] = rand(ComplexF64, size(fhat[u])) # generate coefficients
        ↪ at random
end

f = F_exp * fhat # apply grouped transform to coefficient vector

h = rand(ComplexF64, length(f))
h_hat = F_exp' * h # adjoint transform

# initalize GroupedTransform with cosine functions
F_cos = GroupedTransform("cos", U, N, X)

# generate coefficient vector (initalized with zeros)
fhat = GroupedCoefficients(F_cos.setting)

for i = 1:length(F_cos.setting)
    u = F_cos.setting[i][:u]
    fhat[u] = rand(Float64, size(fhat[u])) # generate coefficients at
        ↪ random
end

f = F_cos * fhat # apply grouped transform to coefficient vector

h = rand(Float64, length(f))
h_hat = F_cos' * h # adjoint transform
```

4

High-Dimensional Explainable ANOVA Approximation

We have collected the main ingredients and are now ready to introduce our method for the explainable approximation of high-dimensional functions from scattered data that has been presented in [PS21a, PS21b, PS22a, PS22b]. The ANOVA decomposition introduced in Chapter 2 represents a crucial building part of the method and the related global sensitivity indices or Sobol indices will be our main tool for interpretability. On the other hand, the grouped transformations from Chapter 3 are important for the realization of fast transformations with the special grouped index sets in order to achieve a fast approximation method.

In Section 4.1, we go into detail about the central least-squares problem which we use to approximate the function via the approximation of its basis coefficients. A main factor in these considerations is the amount of nodes compared to the amount of coefficients we aim to recover. This factor is also referred to as *oversampling factor*. If the factor is smaller than one, we are in an underdetermined setting and otherwise overdetermined. For the overdetermined setting, we investigate properties of the Moore-Penrose inverse and discuss the

necessary oversampling in order to achieve bounds on its spectral norm with high probability when we have nodes drawn at random. The results are based on the matrix Chernoff bound by Tropp in [Tro11]. In the underdetermined setting, we discuss the addition of Tikhonov regularization that simultaneously allows us to incorporate a priori smoothness information if it is known. Section 4.2 introduces the method which culminates in Algorithm 4.1. Here, we also discuss details of the interpretability and multiple ways to determine a subset of ANOVA terms with large importance to the function. Finally, Section 4.3 is concerned with the errors of the method in the case of function recovery. We first consider the setting of Sobolev type spaces and weighted Wiener spaces where we are looking for worst-case bounds on the L_2 error. We extend results from [KUV21, MU21] to our setting for the Sobolev type space achieve the bound in Theorem 4.10. Moreover, we are able to prove a new result for the L_2 worst-case error in weighted Wiener spaces in Theorem 4.11. Additionally, we are able to bound the L_2 and L_∞ error for individual function approximation in Theorem 4.12 and Theorem 4.13, respectively. Since there are no worst-case bounds in the L_∞ setting, we may use the individual results for functions in smoothness spaces yielding Corollary 4.14 and Corollary 4.15.

4.1 Least-Squares Approximation with Regularization

In this section, we discuss the crucial part for our approximation framework which we will present in Section 4.2. We consider a product space $L_2(\mathbb{D}^d, \omega^{(d)})$ from Definition 2.1 with an orthonormal basis $(\varphi_{\boldsymbol{k}}^{(d)})_{\boldsymbol{k}\in\mathbb{Z}^d}$ of continuous functions. Note that the we require the system to be a bounded orthonormal system (BOS) with BOS constant

$$C_{\mathrm{BOS}} \coloneqq \sup_{\boldsymbol{k}\in\mathbb{Z}^d} \left\| \varphi_{\boldsymbol{k}}^{(d)} \right\|_{L_\infty(\mathbb{D}^d)} < \infty \tag{4.1}$$

which all of the examples from Section 2.1.2 are. For now, we assume that there is a fixed subset of ANOVA terms $U \subseteq \mathcal{P}([d])$ and a finite

grouped index set $\mathcal{I}_N(U)$ with parameter vector $\boldsymbol{N} = (N_{\boldsymbol{u}})_{\boldsymbol{u}\in U}$, cf. Definition 3.3. Here, the additional constant

$$C_{\text{supp}} \coloneqq \sup_{\boldsymbol{k}\in\mathcal{I}_N(U)} \left\| \varphi_{\boldsymbol{k}}^{(d)} \right\|_{\mathrm{L}_\infty(\mathbb{D}^d)} < C_{\text{BOS}} \tag{4.2}$$

which can always be estimated by the BOS constant will be relevant.

Remark 4.1. *For the examples from Section 2.1.2, we have*

$$C_{\text{BOS}} = \begin{cases} 1 & : \varphi_{\boldsymbol{k}}^{(d)} = \varphi^{(d),\exp}, \\ \sqrt{2}^d & : \varphi_{\boldsymbol{k}}^{(d)} = \varphi^{(d),\text{cheb}}, \\ \sqrt{2}^d & : \varphi_{\boldsymbol{k}}^{(d)} = \varphi^{(d),\cos}, \\ \sqrt{2}^d & : \varphi_{\boldsymbol{k}}^{(d)} = \varphi^{(d),\text{std}}, \end{cases} \quad \textit{and}$$

$$C_{\text{supp}} = \begin{cases} 1 & : \varphi_{\boldsymbol{k}}^{(d)} = \varphi^{(d),\exp}, \\ \sqrt{2}^s & : \varphi_{\boldsymbol{k}}^{(d)} = \varphi^{(d),\text{cheb}}, \\ \sqrt{2}^s & : \varphi_{\boldsymbol{k}}^{(d)} = \varphi^{(d),\cos}, \\ \sqrt{2}^s & : \varphi_{\boldsymbol{k}}^{(d)} = \varphi^{(d),\text{std}}. \end{cases}$$

with $s = \max_{\mathcal{I}_N(U)} |\operatorname{supp} \boldsymbol{k}|$. *In the special case of* $U = U^{(d,d_s)}$, *we get* $s = d_s$ *for superposition threshold* d_s.

In Section 2.3, we have seen that we are able to truncate the ANOVA decomposition of a function $f : \mathbb{D}^d \to \mathbb{C}$ in $\mathrm{L}_2(\mathbb{D}^d, \omega^{(d)})$ such that

$$f \approx \mathrm{T}_U f = \sum_{\boldsymbol{u}\in U} f_{\boldsymbol{u}} = \sum_{\substack{\boldsymbol{k}\in\mathbb{Z}^d \\ \operatorname{supp}\boldsymbol{k}\in U}} \mathrm{c}_{\boldsymbol{k}}(f)\, \varphi_{\boldsymbol{k}}^{(d)}.$$

However, we have infinitely many indices in the set $\{\boldsymbol{k} \in \mathbb{Z}^d : \operatorname{supp}\boldsymbol{k} \in U\}$ and therefore infinitely many basis coefficients $\mathrm{c}_{\boldsymbol{k}}(f)$. Using our grouped index set

$$\mathcal{I}_N(U) \subseteq \{\boldsymbol{k} \in \mathbb{Z}^d : \operatorname{supp}\boldsymbol{k} \in U\},$$

we truncate the basis expansion of $\mathrm{T}_U f$ to a finite linear combination of basis functions. This yields the partial sum, cf. Section 2.1.3,

$$\mathrm{T}_U f \approx \mathrm{S}_{\mathcal{I}_N(U)} f = \sum_{\boldsymbol{k} \in \mathcal{I}_N(U)} \mathrm{c}_{\boldsymbol{k}}(f)\, \varphi_{\boldsymbol{k}}^{(d)}.$$

Here, we have combined the ANOVA truncation with our grouped index set to a combined truncation operation.

Our scenario is scattered data approximation using a set of $M \in \mathbb{N}$ arbitrary nodes $\mathcal{X} \coloneqq \{\boldsymbol{x}_1, \boldsymbol{x}_2, \dots, \boldsymbol{x}_M\} \subseteq \mathbb{D}^d$ and a vector of function evaluations $\boldsymbol{f} = (f(\boldsymbol{x}_j))_{j=1}^M \in \mathbb{C}^M$. It is our goal to find an approximation for the function f, i.e., approximations for the coefficients $\mathrm{c}_{\boldsymbol{k}}(f)$, $\boldsymbol{k} \in \mathcal{I}_N(U)$.

First of all, we notice that we may write the evaluation of the partial sum $\mathrm{S}_{\mathcal{I}_N(U)} f$ at the nodes $\mathcal{X}$ as a matrix-vector multiplication

$$\left(\mathrm{S}_{\mathcal{I}_N(U)} f(\boldsymbol{x})\right)_{\boldsymbol{x} \in \mathcal{X}} = \boldsymbol{F}_{\mathcal{I}_N(U)}^{\mathcal{X}}\, \hat{\boldsymbol{c}}$$
$$\text{with matrix} \quad \boldsymbol{F}_{\mathcal{I}_N(U)}^{\mathcal{X}} = \left(\varphi_{\boldsymbol{k}}^{(d)}(\boldsymbol{x})\right)_{\boldsymbol{x} \in \mathcal{X}, \boldsymbol{k} \in \mathcal{I}_N(U)},$$

and coefficients $\hat{\boldsymbol{c}} = (\mathrm{c}_{\boldsymbol{k}}(f))_{\boldsymbol{k} \in \mathcal{I}_N(U)}$, see also (3.15). Since we assume that $\mathrm{S}_{\mathcal{I}_N(U)} f \approx f$, we may also assume that $\mathrm{S}_{\mathcal{I}_N(U)} f(\boldsymbol{x}) \approx f(\boldsymbol{x})$ for $\boldsymbol{x} \in \mathcal{X}$. The errors caused by this truncation will be addressed in Section 4.3. Now, it is our goal to determine the approximation via solving the least-squares problem

$$\min_{\hat{\boldsymbol{f}} \in \mathbb{C}^{|\mathcal{I}_N(U)|}} \left\| \boldsymbol{f} - \boldsymbol{F}_{\mathcal{I}_N(U)}^{\mathcal{X}}\, \hat{\boldsymbol{f}} \right\|_{\ell_2}^2. \tag{4.3}$$

We denote its solution as $\hat{\boldsymbol{f}}_{\mathrm{sol}} = (\hat{f}_{\boldsymbol{k}})_{\boldsymbol{k} \in \mathcal{I}_N(U)}$ and call $\hat{f}_{\boldsymbol{k}}$, $\boldsymbol{k} \in \mathcal{I}_N(U)$, *approximate coefficients* since ideally we have $\hat{f}_{\boldsymbol{k}} \approx \mathrm{c}_{\boldsymbol{k}}(f)$. Then the linear combination

$$\mathrm{S}_{\mathcal{I}_N(U)}^{\mathcal{X}} f \coloneqq \sum_{\boldsymbol{k} \in \mathcal{I}_N(U)} \hat{f}_{\boldsymbol{k}}\, \varphi_{\boldsymbol{k}}^{(d)} \tag{4.4}$$

will be referred to as *approximate partial sum* since $\mathrm{S}_{\mathcal{I}_N(U)}^{\mathcal{X}} f \approx \mathrm{S}_{\mathcal{I}_N(U)} f$.

Solving the problem (4.3) is equivalent to solving the normal equations

$$\left(\boldsymbol{F}^{\mathcal{X}}_{\mathcal{I}_N(U)}\right)^{\mathsf{H}} \boldsymbol{F}^{\mathcal{X}}_{\mathcal{I}_N(U)}\, \hat{\boldsymbol{f}}_{\text{sol}} = \left(\boldsymbol{F}^{\mathcal{X}}_{\mathcal{I}_N(U)}\right)^{\mathsf{H}} \boldsymbol{f}. \tag{4.5}$$

If the matrix $(\boldsymbol{F}^{\mathcal{X}}_{\mathcal{I}_N(U)})^{\mathsf{H}}\boldsymbol{F}^{\mathcal{X}}_{\mathcal{I}_N(U)}$ is invertible, the unique solution is given as

$$\hat{\boldsymbol{f}}_{\text{sol}} = \underbrace{\left(\left(\boldsymbol{F}^{\mathcal{X}}_{\mathcal{I}_N(U)}\right)^{\mathsf{H}} \boldsymbol{F}^{\mathcal{X}}_{\mathcal{I}_N(U)}\right)^{-1} \left(\boldsymbol{F}^{\mathcal{X}}_{\mathcal{I}_N(U)}\right)^{\mathsf{H}}}_{=:\left(\boldsymbol{F}^{\mathcal{X}}_{\mathcal{I}_N(U)}\right)^{\dagger}} \boldsymbol{f}$$

with $(\boldsymbol{F}^{\mathcal{X}}_{\mathcal{I}_N(U)})^{\dagger}$ being the Moore-Penrose inverse. In Section 4.1.1 we consider when the matrix $(\boldsymbol{F}^{\mathcal{X}}_{\mathcal{I}_N(U)})^{\mathsf{H}}\boldsymbol{F}^{\mathcal{X}}_{\mathcal{I}_N(U)}$ is invertible under the condition that we are in the overdetermined case, i.e., we have $|\mathcal{X}| \geq |\mathcal{I}_N(U)|$. For the underdetermined case, $|\mathcal{X}| < |\mathcal{I}_N(U)|$, we modify the problem (4.3) and introduce Tikhonov regularization in Section 4.1.2.

For now, we assume that problem (4.3) has a unique solution. We determine that solution using the well-known iterative LSQR algorithm from Paige and Saunders, see [PS82, Bjö96]. The algorithm is an adaption of the conjugate gradients method, see e.g. [HS52], for rectangular matrices. While the residuals are the same as applying the conjugate gradient method to the normal equations (4.5), LSQR has better numeric properties and is more reliable in this case, cf. [BBC+94]. A main advantage we are able to exploit is that LSQR does not need the system matrix $\boldsymbol{F}^{\mathcal{X}}_{\mathcal{I}_N(U)}$ itself. We only need two *oracle functions*: the first function returns the result of the multiplication of $\boldsymbol{F}^{\mathcal{X}}_{\mathcal{I}_N(U)}$ with a given vector and the second function does the same for the adjoint (or transposed) $(\boldsymbol{F}^{\mathcal{X}}_{\mathcal{I}_N(U)})^{\mathsf{H}}$. For this we may rely on the grouped transformation, see Algorithm 3.1, and its adjoint version, see Algorithm 3.2. One iteration of the LSQR algorithm is therefore in the same complexity class as the grouped transformation.

4.1.1 The Overdetermined Case

In this section, we consider the *overdetermined* case for problem (4.3), i.e., we have more nodes in $\mathcal{X}$ than indices in $\mathcal{I}_{\boldsymbol{N}}(U)$, i.e.,

$$M = |\mathcal{X}| \geq |\mathcal{I}_{\boldsymbol{N}}(U)| = 1 + \sum_{\emptyset \neq \boldsymbol{u} \in U} (N_{\boldsymbol{u}} - 1)^{|\boldsymbol{u}|},$$

see Lemma 3.4. The ratio $|\mathcal{X}| / |\mathcal{I}_{\boldsymbol{N}}(U)|$ will be referred to as the *oversampling factor*. In this case, our problem has a unique solution when the matrix $\boldsymbol{F}^{\mathcal{X}}_{\mathcal{I}_{\boldsymbol{N}}(U)}$ has full rank since we then have that $\left(\boldsymbol{F}^{\mathcal{X}}_{\mathcal{I}_{\boldsymbol{N}}(U)}\right)^{\mathsf{H}} \boldsymbol{F}^{\mathcal{X}}_{\mathcal{I}_{\boldsymbol{N}}(U)}$ is invertible. In the following, we aim to consider requirements on the nodes $\mathcal{X}$ and the parameter vector $\boldsymbol{N}$ such that we can prove with high probability that $\boldsymbol{F}^{\mathcal{X}}_{\mathcal{I}_{\boldsymbol{N}}(U)}$ has full rank.

Here, we discuss the properties of our random matrix $\boldsymbol{F}^{\mathcal{X}}_{\mathcal{I}_{\boldsymbol{N}}(U)}$, i.e., the nodes $\mathcal{X}$ have been drawn i.i.d. at random according to a probability distribution. One requirement on the space $\mathrm{L}_2(\mathbb{D}^d, \omega^{(d)})$ from Chapter 2 is that the density $\omega^{(d)}$ has to be a probability density. We make the connection in the sense that we consider the properties of the matrix $\boldsymbol{F}^{\mathcal{X}}_{\mathcal{I}_{\boldsymbol{N}}(U)}$ if the nodes $\mathcal{X}$ have been drawn according to the distribution defined by the density $\omega^{(d)}$. In the case $\omega^{(d)} \equiv 1$, we would obtain uniformly distributed nodes. With this setting we are in a special case of [KUV21] and [MU21] which dealt thoroughly with the properties of such matrices making use of concentration inequalities and specifically the matrix Chernoff bound by Tropp, cf. [Tro11].

We approach the problem by considering the matrix

$$\boldsymbol{H}^{\mathcal{X}}_{\mathcal{I}_{\boldsymbol{N}}(U)} \coloneqq \frac{1}{|\mathcal{X}|} \left(\boldsymbol{F}^{\mathcal{X}}_{\mathcal{I}_{\boldsymbol{N}}(U)}\right)^{\mathsf{H}} \boldsymbol{F}^{\mathcal{X}}_{\mathcal{I}_{\boldsymbol{N}}(U)}.$$

If we are able to bound its eigenvalues, we immediately obtain a bound on the spectral norm of the Moore-Penrose inverse of $\boldsymbol{F}^{\mathcal{X}}_{\mathcal{I}_{\boldsymbol{N}}(U)}$.

Theorem 4.2. *Let all of the nodes in $\mathcal{X}$ be drawn i.i.d. at random according to the probability density $\omega^{(d)}$. For an $r > 0$ the eigenvalues of the matrix*

$\boldsymbol{H}^{\mathcal{X}}_{\mathcal{I}_N(U)}$ *are greater than* $1/2$ *with probability at least* $1 - |\mathcal{X}|^{-r}$ *if*

$$|\mathcal{I}_N(U)| \leq \frac{|\mathcal{X}|}{7\, C_{\text{supp}}^2\, (r+1)\, \log|\mathcal{X}|} \tag{4.6}$$

with C_{supp} *from* (4.2)*. In particular, we obtain an upper bound on the spectral norm of the Moore-Penrose inverse*

$$\left\| \left(\boldsymbol{F}^{\mathcal{X}}_{\mathcal{I}_N(U)} \right)^{\dagger} \right\|_{\ell_2 \to \ell_2} \leq \sqrt{\frac{2}{|\mathcal{X}|}}.$$

Proof. The theorem is an application of [MU21, Theorem 2.3]. They use the value

$$N(\mathcal{I}_N(U)) \coloneqq \sup_{\boldsymbol{x} \in \mathbb{D}^d} \sum_{\boldsymbol{k} \in \mathcal{I}_N(U)} \left| \varphi^{(d)}_{\boldsymbol{k}}(\boldsymbol{x}) \right|^2,$$

see also [Nev79]. In our case, we may estimate it by the constant C_{supp} from (4.2) as follows

$$\begin{aligned} \sup_{\boldsymbol{x} \in \mathbb{D}^d} \sum_{\boldsymbol{k} \in \mathcal{I}_N(U)} \left| \varphi^{(d)}_{\boldsymbol{k}}(\boldsymbol{x}) \right|^2 &\leq \sum_{\boldsymbol{k} \in \mathcal{I}_N(U)} \sup_{\boldsymbol{x} \in \mathbb{D}^d} \left| \varphi^{(d)}_{\boldsymbol{k}}(\boldsymbol{x}) \right|^2 \leq \sum_{\boldsymbol{k} \in \mathcal{I}_N(U)} C_{\text{supp}}^2 \\ &= C_{\text{supp}}^2 \cdot |\mathcal{I}_N(U)|. \end{aligned}$$

This yields our desired result. ∎

Clearly, a direct consequence of Theorem 4.2 is that the matrix $\left(\boldsymbol{F}^{\mathcal{X}}_{\mathcal{I}_N(U)} \right)^{\mathsf{H}} \boldsymbol{F}^{\mathcal{X}}_{\mathcal{I}_N(U)}$ is invertible. Simultaneously, we have obtained an upper bound on the spectral norm of the Moore-Penrose inverse $\left(\boldsymbol{F}^{\mathcal{X}}_{\mathcal{I}_N(U)} \right)^{\dagger}$ which will be useful when considering approximation errors in Section 4.3. The following corollary provides a lower bound on the spectral norm of the Moore-Penrose inverse.

Corollary 4.3. *Let all of the nodes in* $\mathcal{X}$ *be drawn i.i.d. at random according to the probability density* $\omega^{(d)}$*. Let* $r > 0$ *with*

$$|\mathcal{I}_N(U)| \leq \frac{|\mathcal{X}|}{10\, C_{\text{supp}}^2\, (r+1)\, \log|\mathcal{X}|} \tag{4.7}$$

with C_{supp} *from* (4.2). *Then we obtain the lower bound on the spectral norm of the Moore-Penrose inverse*

$$\left\| \left(\boldsymbol{F}^{\mathcal{X}}_{\mathcal{I}_N(U)} \right)^{\dagger} \right\|_{\ell_2 \to \ell_2} \geq \sqrt{\frac{2}{3\,|\mathcal{X}|}}$$

with probability at least $1 - |\mathcal{X}|^{-r}$.

Proof. This is the application of [MU21, Corollary 2.4] as a consequence of [KUV21, Proposition 3.1]. ■

Both results are based on the matrix Chernoff bound by Tropp, see [Tro11]. The difference between lies in the constant factor 1/7 in (4.6) and 1/10 in (4.7). In summary, we have shown that the problem has a unique solution with high-probability if the oversampling factor is large enough.

The important message from Theorem 4.2 and Corollary 4.3 is that if the nodes in $\mathcal{X}$ are distributed according to the probability density $\omega^{(d)}$ of our space $\mathrm{L}_2(\mathbb{D}^d, \omega^{(d)})$, then our matrix is well-conditioned. In our setting, we even obtain an improvement to [MU21] since we need less oversampling because of our constant $C_{\text{supp}} < C_{\text{BOS}}$. In the periodic case with the Fourier system from Section 2.1.2.1 as well as in the non-periodic case with the half-period cosine basis from Section 2.1.2.3, we assume uniformly distributed nodes. For the Chebyshev system from Section 2.1.2.2, we assume a distribution according to the Chebyshev density. For the transformed cosine from Section 2.1.2.4, this was a main motivation to even consider this system. The space has the probability density function of the standard normal distribution and can therefore deal with data that has zero mean and variance one. This fact will be discussed more thoroughly in Section 4.2.

Remark 4.4. *In [PS22a] the Chebyshev system from Section 2.1.2.2 was considered. Here, we need our nodes* $\mathcal{X}$ *to be distributed according to Chebyshev probability density*

$$\omega^{(d),\,\text{cheb}}(\boldsymbol{x}) = \prod_{s=1}^{d} \frac{1}{\pi\sqrt{1 - x_s^2}}.$$

However, it was investigated how one could modify the least-squares system in order to use uniformly distributed nodes $\mathcal{X}$ together with the Chebyshev system. The idea is to introduce a padding parameter $\theta \in (0,1)$ and use uniformly distributed data in $[-1+\theta, 1-\theta]$. Then we apply a preconditioner that has the Chebyshev density on the diagonal to the system matrix. The choice of θ influences both the condition of the matrix and the necessary oversampling. A larger θ will have a negative effect on the condition number while a smaller theta requires a higher oversampling.

4.1.2 The Underdetermined Case and Smoothness Information

In this section, we consider the case of oversampling factor $|\mathcal{X}|/|\mathcal{I}_N(U)|$ smaller than one, i.e.,

$$M = |\mathcal{X}| < |\mathcal{I}_N(U)| = 1 + \sum_{\emptyset \neq \boldsymbol{u} \in U} (N_{\boldsymbol{u}} - 1)^{|\boldsymbol{u}|}.$$

In other words, we aim to reconstruct more coefficients $|\mathcal{I}_N(U)|$ than we have available data points $\mathcal{X}$. We approach this by modifying problem (4.3) and add a regularization term, cf. [BPS22], to obtain the new problem

$$\min_{\hat{f} \in \mathbb{C}^{|\mathcal{I}_N(U)|}} \left\| f - \boldsymbol{F}^{\mathcal{X}}_{\mathcal{I}_N(U)} \hat{f} \right\|_{\ell_2}^2 + \lambda \left\| \hat{f} \right\|_{\boldsymbol{W}}^2 \tag{4.8}$$

for a regularization parameter $\lambda > 0$. Here, for a weight function $w \colon \mathcal{I}_N(U) \to [1, \infty)$, we define the diagonal matrix

$$\boldsymbol{W} = \operatorname{diag}(\, w(\boldsymbol{k}) \,)_{\boldsymbol{k} \in \mathcal{I}_N(U)} \tag{4.9}$$

and the weighted norm

$$\left\| \hat{f} \right\|_{\boldsymbol{W}} := \sqrt{\hat{f}^{\mathsf{T}} \boldsymbol{W} \hat{f}}.$$

For our diagonal matrix $\boldsymbol{W}$ with entries larger than one, we have the equality

$$\left\| \hat{f} \right\|_{\boldsymbol{W}} = \sqrt{\left(\sqrt{\boldsymbol{W}}\, \hat{f} \right)^{\mathsf{T}} \sqrt{\boldsymbol{W}}\, \hat{f}} = \left\| \sqrt{\boldsymbol{W}}\, \hat{f} \right\|_{\ell_2}$$

where $\sqrt{\boldsymbol{W}}$ is the element-wise square-root of $\boldsymbol{W}$. This weighted norm introduces the possibility for us to incorporate a-priori smoothness information about our problem. If nothing is known, we may choose $w \equiv 1$ and obtain a standard Tikhonov regularization, cf. [ORA16]. However, if we know that f is an element of a Sobolev type space, i.e., $f \in \mathrm{H}^v(\mathbb{D}^d, \omega^{(d)})$ for a weight $v\colon \mathbb{Z}^d \to [1, \infty)$, we may define $w(\boldsymbol{k}) = v(\boldsymbol{k})$ on $\mathcal{I}_{\boldsymbol{N}}(U)$. Using such a smoothness weight leads to a smaller *search space* which can be seen by using the equivalent Ivanov formulation of the regularization functional, cf. [ORA16], where we minimize the data fitting term subject to a bound on the Sobolev norm. This may compensate the lack of information from a small node set, i.e., a small oversampling factor.

Problem (4.8) is equivalent to

$$\min_{\hat{f} \in \mathbb{C}^{|\mathcal{I}_{\boldsymbol{N}}(U)|}} \left\| \begin{pmatrix} \boldsymbol{f} \\ \boldsymbol{0} \end{pmatrix} - \begin{pmatrix} \boldsymbol{F}^{\mathcal{X}}_{\mathcal{I}_{\boldsymbol{N}}(U)} \\ \sqrt{\lambda}\sqrt{\boldsymbol{W}} \end{pmatrix} \hat{f} \right\|_{\ell_2}^2 .$$

and therefore the normal equations become

$$\left(\left(\boldsymbol{F}^{\mathcal{X}}_{\mathcal{I}_{\boldsymbol{N}}(U)} \right)^{\mathsf{H}} \boldsymbol{F}^{\mathcal{X}}_{\mathcal{I}_{\boldsymbol{N}}(U)} + \lambda \boldsymbol{W} \right) \hat{f}_{\mathrm{sol}} = \left(\boldsymbol{F}^{\mathcal{X}}_{\mathcal{I}_{\boldsymbol{N}}(U)} \right)^{\mathsf{H}} \boldsymbol{f}.$$

This problem always has a unique solution since the matrix on the left-hand side is a symmetric positive definite matrix. We have achieved this trough shifting the eigenvalues away from zero. However, the solution does now depend on the regularization parameter λ. In the general case, the optimal choice for λ will be determined using cross-validation techniques, e.g., with the methods in [BHP20] which allow for fast computation of the cross-validation score for leave-one out cross validation in a periodic setting. This score can then be used to choose a λ which will be close to the optimal one, i.e., avoiding over- or underfitting effects. While we introduced this form of regularization for the underdetermined setting, it may of course also be beneficial if we are in the overdetermined setting.

Remark 4.5. *If we apply the method to a* synthetic *test function $f : \mathbb{D}^d \to \mathbb{C}$, i.e., we have the norm $\|f\|_{\mathrm{L}_2(\mathbb{D}^d,\omega^{(d)})}$ of the function as well as the basis coefficients $\mathrm{c}_{\boldsymbol{k}}(f)$, $\boldsymbol{k} \in \mathcal{I}_{\boldsymbol{N}}(U)$, available, it is possible to compute the error*

$$\begin{aligned}\left\| f - \mathrm{S}^{\mathcal{X}}_{\mathcal{I}_{\boldsymbol{N}}(U)} f \right\|^2_{\mathrm{L}_2(\mathbb{D}^d,\omega^{(d)})} \\ = \|f\|^2_{\mathrm{L}_2(\mathbb{D}^d,\omega^{(d)})} + \sum_{\boldsymbol{k}\in\mathcal{I}_{\boldsymbol{N}}(U)} \left|\hat{f}_{\boldsymbol{k}} - \mathrm{c}_{\boldsymbol{k}}(f)\right|^2 - \sum_{\boldsymbol{k}\in\mathcal{I}_{\boldsymbol{N}}(U)} |\mathrm{c}_{\boldsymbol{k}}(f)|^2 .\end{aligned}$$

Choosing λ according to this error will clearly yield the better choice. However, this error is in general not available and the strategy therefore not always feasible.

If we choose $w \equiv 1$ and therefore a Tikhonov regularization, we have for the norm of the Moore-Penrose inverse

$$\left\| \left(\left(\boldsymbol{F}^{\mathcal{X}}_{\mathcal{I}_{\boldsymbol{N}}(U)} \right)^{\mathsf{H}} \boldsymbol{F}^{\mathcal{X}}_{\mathcal{I}_{\boldsymbol{N}}(U)} + \lambda \boldsymbol{I} \right)^{-1} \left(\boldsymbol{F}^{\mathcal{X}}_{\mathcal{I}_{\boldsymbol{N}}(U)} \right)^{\mathsf{H}} \right\|_{\ell_2} = \max_{i=1,2,\ldots,|\mathcal{I}_{\boldsymbol{N}}(U)|} \frac{\mu_i}{\mu_i^2 + \lambda}$$

with $\mu_1, \mu_2, \ldots, \mu_{|\mathcal{I}_{\boldsymbol{N}}(U)|}$ the singular values of $\boldsymbol{F}^{\mathcal{X}}_{\mathcal{I}_{\boldsymbol{N}}(U)}$.

Remark 4.6. *It is possible to use different forms of regularization for our least-squares problem. In [BPS22] the use of a group lasso approach, see e.g. [YL06], was discussed. This regularization promotes sparsity in the ANOVA terms $f_{\boldsymbol{u}}$, $\boldsymbol{u} \in U$, and may therefore discard unimportant terms.*

4.2 Explainable Method, Attribute Ranking and Active Set Detection

With every preparation complete and every prerequisite discussed, we now introduce the explainable ANOVA approximation method for high-dimensional functions in the scattered data setting. First of all, we assume that we have a given set of M scattered data nodes $\mathcal{X} \coloneqq \{\boldsymbol{x}_1, \boldsymbol{x}_2, \dots, \boldsymbol{x}_M\} \subseteq \mathbb{D}^d$ and values $\boldsymbol{y} = (y_i)_{i=1}^M \in \mathbb{C}^M$. We denote the data also as tuples

$$D \coloneqq \{(\boldsymbol{x}_1, y_1), (\boldsymbol{x}_2, y_2), \dots, (\boldsymbol{x}_M, y_M)\} \subseteq \mathbb{D}^d \times \mathbb{C}. \tag{4.10}$$

We then assume that there exists a continuous function $f : \mathbb{D}^d \to \mathbb{C}$ in $\mathrm{L}_2(\mathbb{D}^d, \omega^{(d)})$ such that $f(\boldsymbol{x}_i) \approx \boldsymbol{y}_i$. This is already a very crucial part in the method. If we aim to approximate a function f and we know that f is in a certain space $\mathrm{L}_2(\mathbb{D}^d, \omega^{(d)})$, the setting is clear. However, in applications we are provided some form of nodes $\tilde{\mathcal{X}} \subseteq \mathbb{R}^d$ and values in $\mathbb{C}$ (or $\mathbb{R} \subseteq \mathbb{C}$) and we do not have any information what may be the best choice of space and subsequently basis. In parts, this issue has been discussed in [PS21b] and [PS22b]. After some necessary preprocessing, we have the option to apply normalization.

In machine learning, the scale of our features is a key component in building models. Let us, e.g., take recommendations in online shopping. We are only able to analyze the customers that actually exist and what they bought in the shop. However, the features may lie on immensely different scales. If we measure, e.g., the time a customer spent in the shop in seconds as well as their age in years, the result will be a scale that contains values with thousands of seconds and a scale ranging from up to 90 years. Bringing those features on similar scales trough normalization may significantly improve performance of our model. Two common methods for data normalization are min-max-normalization and Z-score normalization, see e.g. [HTF13]. The former method will yield data in the interval $[0, 1]$ and is especially useful if there is an intrinsic upper and lower bound for the values, e.g., when considering age. If we come back to our previous example,

the time a customer spends in the shop would be less suitable since the values may have a wide range and we will probably have very few people with a significantly small or large time. In this case, the Z-score normalization makes much more sense. It tells us how many standard deviations our value lies away from the mean of the data resulting in a distribution with zero mean and variance one. In summary, if we apply min-max-normalization to the nodes $\tilde{\mathcal{X}}$, we obtain $\mathcal{X} \subseteq [0,1]^d$ and may use the half-period cosine basis from Section 2.1.2.3. Should we apply Z-score normalization to $\tilde{\mathcal{X}}$, we obtain $\mathcal{X} \subseteq \mathbb{R}^d$ with mean zero and variance one resulting in the applicability of the transformed cosine basis from Section 2.1.2.4.

The first step in our method is to truncate the ANOVA decomposition of our function $f : \mathbb{D}^d \to \mathbb{C}$. We choose truncation by a superposition threshold $d_s \in [d]$ such that we obtain

$$f = \sum_{\boldsymbol{u} \subseteq [d]} f_{\boldsymbol{u}} \approx \sum_{\substack{\boldsymbol{u} \subseteq [d] \\ |\boldsymbol{u}| \leq d_s}} f_{\boldsymbol{u}} = \mathrm{T}_{d_s} f .$$

This has been discussed thoroughly in Section 2.3. A truncation of this type makes sense if the function f has a low superposition dimension $d^{(\mathrm{sp})}(\delta)$ for high accuracy δ, see (2.26). Then we may choose $d_s = d^{(\mathrm{sp})}$. However, the superposition dimension is in general unknown. Here, we distinguish again between two main cases. If it is our goal to approximate a function where the smoothness is known, we may compute the worst-case superposition dimension (2.30) or use the bounds on it as in Section 2.3. This works, e.g., for the functions of dominating-mixed and isotropic smoothness. Then we can assume a low superposition dimension. If we do not have any a-priori information about the function, we have to choose a superposition threshold $d_s \in [d]$ or possibly determine one via cross-validation. The second major case is real data from applications where we just have the nodes $\mathcal{X}$ and values $\boldsymbol{y}$. Here, the situation is very different. For the complete generality of problems one cannot make the assumption that we have a low superposition dimension. However, there are many application scenarios where numerical experiments successfully showed that this

is indeed the case, see e.g. [CMO97, HSS+21]. Moreover, it has been theorized that most real world applications consist only of low-order interactions relating to sparsity-of-effects, cf. [WH11], or the Pareto principle. Since we generally do not have a-priori information in this scenario, we work with low superposition thresholds d_s and use cross-validation to improve the choice.

The next step is to truncate the basis expansion of f or $\mathrm{T}_{d_s} f$ to achieve a finite amount of basis functions $\varphi_{\boldsymbol{k}}^{(d)}$ and therefore coefficients $\mathrm{c}_{\boldsymbol{k}}(f)$. To this end, we choose a grouped index set $\mathcal{I}_{\boldsymbol{N}}(U^{(d,d_s)})$ with bandwidth parameters $\boldsymbol{N} = (N_j)_{j=1}^{d_s} \in \mathbb{N}^{d_s}$ according to Definition 3.3. We then have an approximation by a partial sum

$$f \approx \mathrm{T}_{d_s} f \approx \mathrm{S}_{\mathcal{I}_{\boldsymbol{N}}(U^{(d,d_s)})} f = \sum_{\boldsymbol{k} \in \mathcal{I}_{\boldsymbol{N}}(U^{(d,d_s)})} \mathrm{c}_{\boldsymbol{k}}(f)\, \varphi_{\boldsymbol{k}}^{(d)},$$

see also Section 2.1.3. The choice of $\boldsymbol{N}$ is again an interesting issue. Any a-priori information may possibly help this choice. If we have information about the smoothness of the function, we can find upper bounds on the truncation error based on the choice of $\boldsymbol{N}$. This will be discussed in detail in Section 4.3. In the general case without a-priori information, this parameter has to be chosen via cross-validation techniques again. However, experiments with real data from applications show that low bandwidths achieve good results, cf. the experiments in Chapter 6.

Now, we determine approximations for the basis coefficients $\mathrm{c}_{\boldsymbol{k}}(f)$, $\boldsymbol{k} \in \mathcal{I}_{\boldsymbol{N}}(U^{(d,d_s)})$, as the solution of the (regularized) least-squares problem

$$\hat{\boldsymbol{f}}_{\mathrm{sol}} = (\hat{f}_{\boldsymbol{k}})_{\boldsymbol{k} \in \mathcal{I}_{\boldsymbol{N}}(U^{(d,d_s)})} = \underset{\hat{\boldsymbol{f}} \in \mathbb{C}^{\left|\mathcal{I}_{\boldsymbol{N}}(U^{(d,d_s)})\right|}}{\arg\min} \left\| \boldsymbol{y} - \boldsymbol{F}^{\mathcal{X}}_{\mathcal{I}_{\boldsymbol{N}}(U^{(d,d_s)})} \hat{\boldsymbol{f}} \right\|_{\ell_2}^2 + \lambda \left\| \hat{\boldsymbol{f}} \right\|_{\boldsymbol{W}}^2, \tag{4.11}$$

cf. (4.8), such that $\hat{f}_{\boldsymbol{k}} \approx \mathrm{c}_{\boldsymbol{k}}(f)$, $\boldsymbol{k} \in \mathcal{I}_{\boldsymbol{N}}(U^{(d,d_s)})$. A detailed description of the solution can be found in Section 4.1. Depending on the oversampling factor $|\mathcal{X}| / \left|\mathcal{I}_{\boldsymbol{N}}(U^{(d,d_s)})\right|$ we can decide if we use regularization, i.e., $\lambda > 0$, or not. If a priori smoothness information is available, it

can be incorporated via $\boldsymbol{W}$, see Section 4.1.2. We have obtained the approximation

$$f \approx \mathrm{T}_{d_s} f \approx \mathrm{S}_{\mathcal{I}_N(U^{(d,d_s)})} f \approx \mathrm{S}^{\mathcal{X}}_{\mathcal{I}_N(U^{(d,d_s)})} f = \sum_{\boldsymbol{k} \in \mathcal{I}_N(U^{(d,d_s)})} \hat{f}_{\boldsymbol{k}} \, \varphi^{(d)}_{\boldsymbol{k}}.$$

In the next step, we interpret our approximation $\mathrm{S}^{\mathcal{X}}_{\mathcal{I}_N(U^{(d,d_s)})} f$ using the techniques presented in Section 4.2.1. The goal is to reduce the number of ANOVA terms such that we may choose more indices for important terms. In general, the methods from Section 4.2.1 lead to a subset $U^{(\mathrm{active})} \subseteq U^{(d,d_s)}$. The special case of incremental expansion does both, remove certain terms and also add others of higher order. Regardless of the specifics, we have obtained a new subset of ANOVA terms $U^{(\mathrm{active})} \subseteq \mathcal{P}([d])$. In Figure 4.1 we have visualized the process for a 4-dimensional function.

Why does it make sense to reduce the number of ANOVA terms? The oversampling factor $|\mathcal{X}| / |\mathcal{I}_N(U)|$ directly influences the quality of our model. If the factor is low, i.e., we have a small number of nodes compared to our number of indices, the model may not yield a good approximation error, see also Section 4.3. By reducing the number of ANOVA terms to an active set $U^{(\mathrm{active})}$, we increase this factor. Moreover, if some terms are removed, it is also possible to increase the bandwidth parameters $N_{\boldsymbol{u}}$ for terms $\boldsymbol{u} \in U^{(\mathrm{active})}$. This may bring benefits since those terms have in some way been determined to be important.

Using the set $U^{(\mathrm{active})}$, we perform a *refitting*, i.e., we solve the new least-squares problem

$$\hat{\boldsymbol{g}}_{\mathrm{sol}} = (\hat{g}_{\boldsymbol{k}})_{\boldsymbol{k} \in \mathcal{I}_{\boldsymbol{M}}(U^{(\mathrm{active})})} = \underset{\hat{\boldsymbol{g}} \in \mathbb{C}^{\left|\mathcal{I}_{\boldsymbol{M}}(U^{(\mathrm{active})})\right|}}{\arg\min} \left\| \boldsymbol{f} - \boldsymbol{F}^{\mathcal{X}}_{\mathcal{I}_{\boldsymbol{M}}(U^{(\mathrm{active})})} \hat{\boldsymbol{g}} \right\|_{\ell_2}^2 + \theta \, \|\hat{\boldsymbol{g}}\|_{\boldsymbol{W}}^2 , \tag{4.12}$$

as a modified version of (4.11) with different regularization parameter θ. Here, we have the grouped index set $\mathcal{I}_{\boldsymbol{M}}(U^{(\mathrm{active})})$ with new bandwidths $\boldsymbol{M} = (M_{\boldsymbol{u}})_{\boldsymbol{u} \in U^{(\mathrm{active})}} \in \mathbb{N}^{\left|U^{(\mathrm{active})}\right|}$ as in Definition 3.3. Note that also the matrix $\boldsymbol{W}$ now only contains the weights for the indices in $\mathcal{I}_{\boldsymbol{M}}(U^{(\mathrm{active})})$.

Finally, we have obtained the approximation

$$f \approx \mathrm{S}^{X}_{\mathcal{I}_M(U^{(\mathrm{active})})} f = \sum_{\boldsymbol{k} \in \mathcal{I}_M(U^{(\mathrm{active})})} \hat{g}_{\boldsymbol{k}} \, \varphi^{(d)}_{\boldsymbol{k}}. \tag{4.13}$$

Algorithm 4.1 describes the complete approximation procedure using a cut-off for the terms by global sensitivity indices as described in Section 4.2.1 as an example. Note that it is possible to choose any of the strategies in Section 4.2.1 for obtaining an active set. Moreover, we can iterate the procedures to obtain an active set multiple times. In this case, we have to solve a new least-squares problem for every new active set $U^{(\mathrm{active})}$. The method has been implemented as a Julia package, see [Scha] with all available bases from Section 2.1.2.

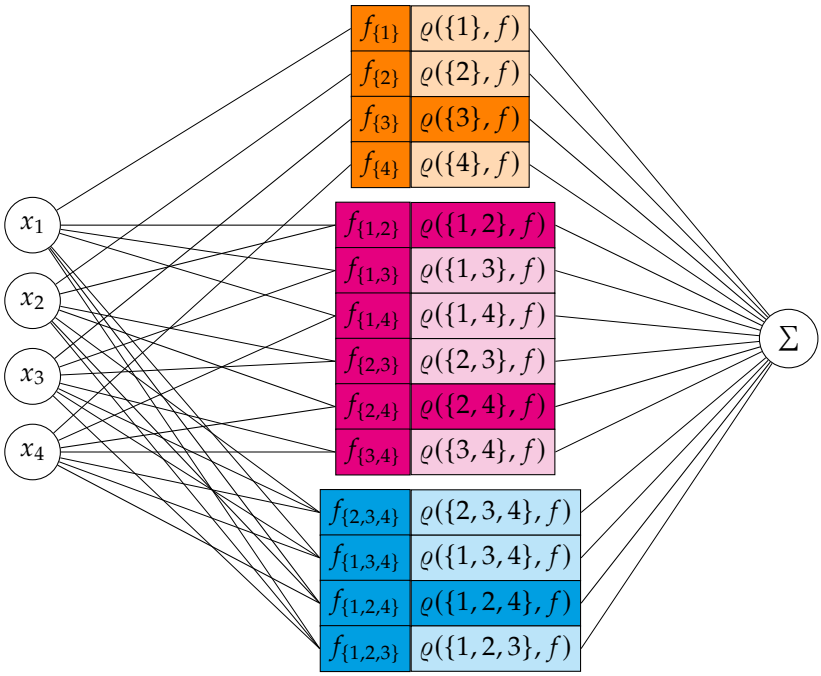

Figure 4.1: Explainable ANOVA network of a function $f : \mathbb{D}^4 \to \mathbb{C}$ for superposition threshold $d_s = 3$. We visualize the different ANOVA terms $f_{\boldsymbol{u}}$ for $|\boldsymbol{u}| = 1$ in orange, $|\boldsymbol{u}| = 2$ in magenta and for $|\boldsymbol{u}| = 3$ in blue. The related global sensitivity indices $\varrho(\boldsymbol{u}, f)$ serve as interpretable quantity for the ANOVA term.

Algorithm 4.1 ANOVA approximation method

Input: $\mathcal{X} \subseteq \mathbb{D}^d$ finite node set, $|\mathcal{X}| = M$
$\boldsymbol{y} \in \mathbb{C}^M$ function values
$d_s \in [d]$ superposition threshold
$\mathrm{L}_2(\mathbb{D}^d, \omega^{(d)})$ space with complete ONS, cf. Sec. 2.1.2

Choose bandwidth parameters $\boldsymbol{N} = (N_j)_{j=1}^{d_s}$.
Choose regularization parameters $\lambda_i \in [0, \infty)$, $i = 1, 2, \ldots, n$.
if a priori smoothness information via weight $w \colon \mathbb{Z}^d \to [1, \infty)$ is known **then**
    $\boldsymbol{w} \longleftarrow (w(\boldsymbol{k}))_{\boldsymbol{k} \in I_{\boldsymbol{N}}(U^{(d,d_s)})}$
else
    $\boldsymbol{w} \longleftarrow (1)_{\boldsymbol{k} \in I_{\boldsymbol{N}}(U^{(d,d_s)})}$
end if
$\boldsymbol{W} \longleftarrow \operatorname{diag} \boldsymbol{w}$
Apply cross-validation to determine best regularization parameter λ via solving (4.11):
$\hat{\boldsymbol{f}}_{\mathrm{sol}} = (\hat{f}_{\boldsymbol{k}})_{\boldsymbol{k} \in I_{\boldsymbol{N}}(U^{(d,d_s)})} = \arg\min_{\hat{\boldsymbol{f}} \in \mathbb{C}^{\left|I_{\boldsymbol{N}}(U^{(d,d_s)})\right|}} \left\| \boldsymbol{y} - \boldsymbol{F}^{\mathcal{X}}_{I_{\boldsymbol{N}}(U^{(d,d_s)})} \hat{\boldsymbol{f}} \right\|_{\ell_2}^2 + \lambda \left\| \hat{\boldsymbol{f}} \right\|_{\boldsymbol{W}}^2$
Compute global sensitivity indices for approximation $\mathrm{S}^{\mathcal{X}}_{I_{\boldsymbol{N}}(U^{(d,d_s)})} f$ using (4.14):
for $\boldsymbol{u} \in U^{(d,d_s)} \setminus \{\boldsymbol{0}\}$ **do**
    $\varrho(\boldsymbol{u}, \mathrm{S}^{\mathcal{X}}_{I_{\boldsymbol{N}}(U^{(d,d_s)})} f) \longleftarrow \left(\sum_{\boldsymbol{k} \in I_{\boldsymbol{u}, N_{\boldsymbol{u}}}} \left| \hat{f}_{\boldsymbol{k}} \right|^2 \right) / \left(\sum_{\boldsymbol{k} \in I_{\boldsymbol{N}}(U^{(d,d_s)}) \setminus \{\boldsymbol{0}\}} \left| \hat{f}_{\boldsymbol{k}} \right|^2 \right)$
end for
Choose threshold vector $\boldsymbol{\varepsilon} \in [0,1]^{d_s}$ and build active set through thresholding:
$U^{(\mathrm{gsi},\varepsilon)} \longleftarrow \emptyset \cup \left\{ \boldsymbol{u} \in U^{(d,d_s)} \colon \varrho(\boldsymbol{u}, \mathrm{S}^{\mathcal{X}}_{I_{\boldsymbol{N}}(U^{(d,d_s)})} f) > \varepsilon_{|\boldsymbol{u}|} \right\}$
Adjust bandwidth parameters $\boldsymbol{M} = (M_j)_{j=1}^{\left|U^{(\mathrm{gsi},\varepsilon)}\right|}$.
Adjust regularization parameters $\theta_i \in [0, \infty)$, $i = 1, 2, \ldots, n$.
if a priori smoothness information via weight $w \colon \mathbb{Z}^d \to [1, \infty)$ is known **then**
    $\boldsymbol{w} \longleftarrow (w(\boldsymbol{k}))_{\boldsymbol{k} \in I_{\boldsymbol{M}}(U^{(\mathrm{gsi},\varepsilon)})}$
else
    $\boldsymbol{w} \longleftarrow (1)_{\boldsymbol{k} \in I_{\boldsymbol{M}}(U^{(\mathrm{gsi},\varepsilon)})}$
end if
$\boldsymbol{W} \longleftarrow \operatorname{diag} \boldsymbol{w}$
Apply cross-validation to determine best regularization parameter θ via solving (4.12):
$\hat{\boldsymbol{g}}_{\mathrm{sol}} = (\hat{g}_{\boldsymbol{k}})_{\boldsymbol{k} \in I_{\boldsymbol{M}}(U^{(\mathrm{gsi},\varepsilon)})} = \arg\min_{\hat{\boldsymbol{g}} \in \mathbb{C}^{\left|I_{\boldsymbol{M}}(U^{(\mathrm{gsi},\varepsilon)})\right|}} \left\| \boldsymbol{y} - \boldsymbol{F}^{\mathcal{X}}_{I_{\boldsymbol{M}}(U^{(\mathrm{gsi},\varepsilon)})} \hat{\boldsymbol{g}} \right\|_{\ell_2}^2 + \theta \left\| \hat{\boldsymbol{g}} \right\|_{\boldsymbol{W}}^2$

Output: $\hat{g}_{\boldsymbol{k}} \in \mathbb{C}, \boldsymbol{k} \in I_{\boldsymbol{M}}(U^{(\mathrm{active})})$ approximations to basis coefficients $\mathrm{c}_{\boldsymbol{k}}(f)$

4.2.1 Attribute Ranking and Active Set Detection

This section is concerned with the question: *How can we interpret the approximation and which insights does it give us into the data?* The following statements hold for a general $U \subseteq \mathcal{P}([d])$ with $U = U^{(d,d_s)}$ as a special case. The grouped index set is a union such that we have

$$\mathcal{I}_{\boldsymbol{N}}(U) = \mathcal{I}_{\emptyset} \cup \bigcup_{\boldsymbol{u} \in U \setminus \{\emptyset\}} \mathcal{I}_{\boldsymbol{u},N_{\boldsymbol{u}}}$$

as in Definition 3.3. Therefore, we can directly compute the global sensitivity indices or Sobol indices of the approximation $\mathrm{S}^{\mathcal{X}}_{\mathcal{I}_{\boldsymbol{N}}(U)} f$ as

$$\varrho(\boldsymbol{u}, \mathrm{S}^{\mathcal{X}}_{\mathcal{I}_{\boldsymbol{N}}(U)} f) = \frac{\sum_{\boldsymbol{k} \in \mathcal{I}_{\boldsymbol{u},N_{\boldsymbol{u}}}} \left|\hat{f}_{\boldsymbol{k}}\right|^2}{\sum_{\boldsymbol{k} \in \mathcal{I}_{\boldsymbol{N}}(U)} \left|\hat{f}_{\boldsymbol{k}}\right|^2}. \tag{4.14}$$

Since all sensitivity indices add up to one, we may choose a dimension-wise cut-off percentage $\boldsymbol{\varepsilon} = (\varepsilon_s)_{s=1}^{\max_{\boldsymbol{u} \in U} |\boldsymbol{u}|} \in (0,1)^{\max_{\boldsymbol{u} \in U} |\boldsymbol{u}|}$ such that we choose the *active set*

$$U^{(\mathrm{gsi},\boldsymbol{\varepsilon})} \coloneqq \emptyset \cup \left\{ \boldsymbol{u} \in U \colon \varrho(\boldsymbol{u}, \mathrm{S}^{\mathcal{X}}_{\mathcal{I}_{\boldsymbol{N}}(U)} f) > \varepsilon_{|\boldsymbol{u}|} \right\} \subseteq U. \tag{4.15}$$

In other words, this throws away every ANOVA term with a small contribution to the variance of the approximation with respect to $\boldsymbol{\varepsilon}$. A dimension-dependent choice of $\boldsymbol{\varepsilon}$ may be favourable in some cases, but it is always possible to choose every entry to be equal.

If we are interested in how much one variable $i \in [d]$ adds to the variance of the function, i.e., how important it is, we sum over all of the contributing sensitivity indices $\varrho(\boldsymbol{u}, \mathrm{S}^{\mathcal{X}}_{\mathcal{I}_{\boldsymbol{N}}(U)} f)$ with $i \in \boldsymbol{u}$. This leads to the sum

$$\sum_{\boldsymbol{u} \in \{\boldsymbol{v} \in U \colon i \in \boldsymbol{v}\}} \varrho(\boldsymbol{u}, \mathrm{S}^{\mathcal{X}}_{\mathcal{I}_{\boldsymbol{N}}(U)} f).$$

In order to obtain a ranking score, we weigh the sensitivity indices by the number of sets $\boldsymbol{v} \in U$ with $|\boldsymbol{u}| = |\boldsymbol{v}|$ and $i \in \boldsymbol{v}$. This counteracts

an effect that makes a variable seem important if it occurs in many unimportant terms of the same order in contrast to other variables with some terms of that order not appearing in U. We obtain the ranking score

$$r(i) = \frac{\sum_{\boldsymbol{u} \in \{\boldsymbol{v} \in U\colon i \in \boldsymbol{v}\}} |\{\boldsymbol{v} \in U\colon |\boldsymbol{u}| = |\boldsymbol{v}|, i \in \boldsymbol{v}\}|^{-1} \varrho(\boldsymbol{u}, \mathrm{S}^{\mathcal{X}}_{\mathcal{I}_N(U)} f)}{\sum_{\boldsymbol{u} \in U} \left(\sum_{i \in \boldsymbol{u}} |\{\boldsymbol{v} \in U\colon |\boldsymbol{u}| = |\boldsymbol{v}|, i \in \boldsymbol{v}\}|^{-1}\right) \varrho(\boldsymbol{u}, \mathrm{S}^{\mathcal{X}}_{\mathcal{I}_N(U)} f)}. \quad (4.16)$$

In the denominator we added normalization such that $\sum_{i \in [d]} r(i) = 1$. Computing every score $r(i)$, $i \in [d]$ provides an *attribute ranking* with respect to U showing the percentage that every variable adds to the variance of the approximation. This allows for the conclusion that if we have a good approximation $\mathrm{S}^{\mathcal{X}}_{\mathcal{I}_N(U)} f$, its attribute ranking will be close to the attribute ranking of the function f. The obvious option is now to reduce the dimensionality of the problem by removing the influence of variables with a low attribute ranking score. Choosing a cut-off $\varepsilon > 0$, this yields a subset

$$U^{(\mathrm{ar},\varepsilon)} := \emptyset \cup \{\boldsymbol{u} \in U\colon r(i) > \varepsilon \quad \text{for all} \quad i \in \boldsymbol{u}\} \subseteq U. \quad (4.17)$$

This idea is related to the concept of truncation dimension (2.27).

A final method we propose is *incremental expansion*. This method is advantageous if the model function is already very complex with a small superposition threshold d_s which may occur if we are dealing with an especially large spatial dimension d. Here, we start with a small d_s, e.g., $d_s = 1$ or $d_s = 2$. A reduction in the ANOVA terms can be performed by either of the two previous approaches. Now, one chooses a $\theta \in (0, 1)$ and determines the subset

$$\boldsymbol{v} := \{i \in [d]\colon r(i) > \theta\}.$$

If we assume that additional interactions of the important variables might also be significant to the variance, we may add interactions of size up to $n \in [d]$, $n > d_s$. This translates to considering the subset

$$U^{(\mathrm{ie},\theta,n)} := U \cup \{\boldsymbol{u} \in \mathcal{P}(\boldsymbol{v})\colon d_s < |\boldsymbol{u}| \leq n\}.$$

This will be a beneficial way to improve the accuracy of the model if higher-order interactions play a role. However, if this method is used without reducing the complexity with any of the previous approaches, the overall complexity of the model will be significantly larger.

4.3 Approximation Errors

In this section, we consider the approximation error of the ANOVA approximation method in the case of approximating a function $f : \mathbb{D}^d \to \mathbb{C}$. Mainly, we are interested in the errors

$$\left\| f - \mathrm{S}^{\mathcal{X}}_{\mathcal{I}_N(U)} f \right\|_{\mathrm{L}_2(\mathbb{D}^d, \omega^{(d)})} \quad \text{and} \quad \left\| f - \mathrm{S}^{\mathcal{X}}_{\mathcal{I}_N(U)} f \right\|_{\mathrm{L}_\infty(\mathbb{D}^d)}.$$

Here, $\mathrm{S}^{\mathcal{X}}_{\mathcal{I}_N(U)} f$ is the approximate partial sum we have obtained by approximating our coefficients $\mathrm{c}_{\boldsymbol{k}}(f)$ with the least-squares method. This error can be considered in different ways. If we are aware of the regularity, e.g., considering Sobolev type spaces $\mathrm{H}^w(\mathbb{D}^d, \omega^{(d)})$ or weighted Wiener spaces $\mathcal{A}^w(\mathbb{D}^d, \omega^{(d)})$ with a weight function $w : \mathbb{Z}^d \to [1, \infty)$, we may ask for the worst-case error in this respective space. For the L_2 error, this will be considered in Section 4.3.1 for both spaces. If we do not have regularity information, we are interested in the individual error of approximating one function which we consider in Section 4.3.2. Since we do not have bounds for the L_∞ error in the worst-case setting, we use the results in the individual setting to obtain such statements again, but there is an difference in the node set $\mathcal{X}$. In the worst-case setting, we need to draw our nodes at random only once for the entire class. However, in the individual setting, we need to draw them for each function. In the setting of reproducing kernel Hilbert spaces, similar worst-case errors have been considered in [KUV21, MU21]. An individual approximation error for hyperbolic wavelet regression and scattered data was proposed in [LPU21]. If we consider sparse grids as a sampling scheme, we have the results in [Boh17] for the individual error as well as the recent work [KLT21] for weighted Wiener spaces in the worst-case setting.

4.3.1 Worst-Case Error

We begin by considering the worst-case L_2 error for Sobolev type spaces $\mathrm{H}^w(\mathbb{D}^d, \omega^{(d)})$ and weighted Wiener spaces $\mathcal{A}^w(\mathbb{D}^d, \omega^{(d)})$ with weight function $w : \mathbb{Z}^d \to [1, \infty)$. In the periodic case, this has been

done for Sobolev type spaces in [PS21a]. Here, we generalize the results. We assume a product space $\mathrm{L}_2(\mathbb{D}^d, \omega^{(d)})$ as in Definition 2.1 with orthonormal basis $(\varphi_{\boldsymbol{k}}^{(d)})_{\boldsymbol{k}\in\mathbb{Z}^d}$ that is a bounded orthonormal system (BOS) with BOS constant C_{BOS} from (4.1). This if fulfilled for all examples in Section 2.1.2. We also assume a fixed set of ANOVA terms $U \subseteq \mathcal{P}([d])$ and a corresponding grouped index set $\mathcal{I}_N(U)$ from Definition 3.3 with bandwidths $\boldsymbol{N} = (N_{\boldsymbol{u}})_{\boldsymbol{u}\in U} \in \mathbb{N}^{|U|}$. The infinite complement of this finite index set will be denoted as

$$\mathcal{I}_N^{\mathrm{C}}(U) \coloneqq \mathbb{Z}^d \setminus \mathcal{I}_N(U).$$

A key part will be the necessary oversampling of our function where the additional constant C_{supp} from (4.2) plays a role. This constant can always be estimated by the BOS constant, but may be significantly smaller which yields an improvement in the required oversampling of Theorem 4.2 which we are going to need in this section.

The error caused by the truncation with our index set $\mathcal{I}_N(U)$ is going to play a major part in the approximation error. In the following two lemmas, we are considering the worst-case truncation error for L_2 in a Sobolev type space and L_∞ in the weighted Wiener space.

Lemma 4.7. *Let* $\mathrm{H}^w(\mathbb{D}^d, \omega^{(d)})$ *be a Sobolev type space with weight function* $w\colon \mathbb{Z}^d \to [1,\infty)$. *Then*

$$\sup_{\|f\|_{\mathrm{H}^w(\mathbb{D}^d,\omega^{(d)})}\leq 1} \left\|f - \mathrm{S}_{\mathcal{I}_N(U)} f\right\|^2_{\mathrm{L}_2(\mathbb{D}^d,\omega^{(d)})} \leq \frac{1}{\inf_{\boldsymbol{k}\in\mathcal{I}_N^{\mathrm{C}}(U)} w^2(\boldsymbol{k})}.$$

Proof. For the proof, we apply Parseval's identity and incorporate our

weight function w to obtain

$$\begin{aligned}\left\|f - \mathrm{S}_{\mathcal{I}_N(U)} f\right\|^2_{\mathrm{L}_2(\mathbb{D}^d,\omega^{(d)})} &= \sum_{\boldsymbol{k}\in\mathcal{I}_N^{\mathrm{C}}(U)} |\mathrm{c}_{\boldsymbol{k}}(f)|^2 = \sum_{\boldsymbol{k}\in\mathcal{I}_N^{\mathrm{C}}(U)} \frac{w^2(\boldsymbol{k})}{w^2(\boldsymbol{k})}\,|\mathrm{c}_{\boldsymbol{k}}(f)|^2 \\ &\le \frac{1}{\inf_{\boldsymbol{k}\in\mathcal{I}_N^{\mathrm{C}}(U)} w^2(\boldsymbol{k})} \sum_{\boldsymbol{k}\in\mathcal{I}_N^{\mathrm{C}}(U)} w^2(\boldsymbol{k})\,|\mathrm{c}_{\boldsymbol{k}}(f)|^2 \\ &= \frac{\|f\|^2_{\mathrm{H}^w(\mathbb{D}^d,\omega^{(d)})}}{\inf_{\boldsymbol{k}\in\mathcal{I}_N^{\mathrm{C}}(U)} w^2(\boldsymbol{k})}.\end{aligned}$$

The result follows by taking the supremum. ∎

Lemma 4.8. *Let $\mathcal{A}^w(\mathbb{D}^d,\omega^{(d)})$ be a weighted Wiener space with weight function $w\colon\mathbb{Z}^d\to[1,\infty)$. Then*

$$\sup_{\|f\|_{\mathcal{A}^w(\mathbb{D}^d,\omega^{(d)})}\le 1} \left\|f - \mathrm{S}_{\mathcal{I}_N(U)} f\right\|_{\mathrm{L}_\infty(\mathbb{D}^d,)} \le \frac{C_{\mathrm{BOS}}}{\inf_{\boldsymbol{k}\in\mathcal{I}_N^{\mathrm{C}}(U)} w(\boldsymbol{k})}$$

with the BOS constant C_{BOS} from (4.1).

Proof. For the proof, we estimate the absolute values of the basis functions by the BOS constant and incorporate our weight function w to obtain

$$\begin{aligned}\left\|f - \mathrm{S}_{\mathcal{I}_N(U)} f\right\|_{\mathrm{L}_\infty(\mathbb{D}^d,\omega^{(d)})} &= \operatorname*{ess\,supp}_{\boldsymbol{x}\in\mathbb{D}^d} \left|\sum_{\boldsymbol{k}\in\mathcal{I}_N^{\mathrm{C}}(U)} \mathrm{c}_{\boldsymbol{k}}(f)\,\varphi_{\boldsymbol{k}}^{(d)}(\boldsymbol{x})\right| \\ &\le C_{\mathrm{BOS}} \sum_{\boldsymbol{k}\in\mathcal{I}_N^{\mathrm{C}}(U)} |\mathrm{c}_{\boldsymbol{k}}(f)| \\ &= C_{\mathrm{BOS}} \sum_{\boldsymbol{k}\in\mathcal{I}_N^{\mathrm{C}}(U)} \frac{w(\boldsymbol{k})}{w(\boldsymbol{k})}\,|\mathrm{c}_{\boldsymbol{k}}(f)| \\ &\le \frac{C_{\mathrm{BOS}}\,\|f\|_{\mathcal{A}^w(\mathbb{D}^d,\omega^{(d)})}}{\inf_{\boldsymbol{k}\in\mathcal{I}_N^{\mathrm{C}}(U)} w(\boldsymbol{k})}.\end{aligned}$$

The result follows by taking the supremum. ∎

For the least-squares error, we rely on similar techniques as in [MU21] and [KUV21] that have been used for the setting of reproducing kernel Hilbert spaces. We consider the case where the nodes $\mathcal{X}$ are drawn i.i.d. at random according to the probability density $\omega^{(d)}$ of our space and we have given function values $\boldsymbol{f} = (f(\boldsymbol{x}))_{\boldsymbol{x}\in\mathcal{X}}$. Before we consider the actual L_2 error bound, it is necessary to discuss properties of the infinite matrix

$$\boldsymbol{\Phi}^{\mathcal{X}}_{\mathcal{I}_N^{\mathrm{C}}(U)} \coloneqq \left(\frac{1}{w(\boldsymbol{k})}\,\varphi_{\boldsymbol{k}}^{(d)}(\boldsymbol{x})\right)_{\boldsymbol{x}\in\mathcal{X},\boldsymbol{k}\in\mathcal{I}_N^{\mathrm{C}}(U)} \tag{4.18}$$

that will play an important role in the proof. Specifically, we are interested in the spectral norm of this operator. In order to determine a bound for this norm, we require the use concentration inequalities.

Lemma 4.9. *Let $\mathrm{H}^w(\mathbb{D}^d, \omega^{(d)})$ be a Sobolev type space with weight function $w\colon \mathbb{Z}^d \to [1,\infty)$ such that*

$$\sum_{\boldsymbol{k}\in\mathbb{Z}^d} \frac{1}{w^2(\boldsymbol{k})} < \infty.$$

Moreover, let $\mathcal{X} \subseteq \mathbb{D}^d$ be a set of $|\mathcal{X}| > 3$ nodes drawn i.i.d. at random according to the probability density $\omega^{(d)}$, and let $r > 0$. Then for the infinite matrix $\boldsymbol{\Phi}^{\mathcal{X}}_{\mathcal{I}_N^{\mathrm{C}}(U)}$ from (4.18)*, we have*

$$\mathbb{P}\left(\left\|\left(\boldsymbol{\Phi}^{\mathcal{X}}_{\mathcal{I}_N^{\mathrm{C}}(U)}\right)^{\mathsf{H}} \boldsymbol{\Phi}^{\mathcal{X}}_{\mathcal{I}_N^{\mathrm{C}}(U)} - \boldsymbol{\Lambda}\right\|_{\ell_2\to\ell_2} \geq F\right) \leq 2^{\frac{3}{4}}\,|\mathcal{X}|^{-r}$$

where

$$\boldsymbol{\Lambda} \coloneqq \mathbb{E}\left(\left(\boldsymbol{\Phi}^{\mathcal{X}}_{\mathcal{I}_N^{\mathrm{C}}(U)}\right)^{\mathsf{H}} \boldsymbol{\Phi}^{\mathcal{X}}_{\mathcal{I}_N^{\mathrm{C}}(U)}\right) = \operatorname{diag}\left(\frac{1}{w^2(\boldsymbol{k})}\right)_{\boldsymbol{k}\in\mathcal{I}_N^{\mathrm{C}}(U)}$$

and

$$F := \max\left\{ \frac{8(r+1)\log|\mathcal{X}|}{|\mathcal{X}|}\, C_{\mathrm{BOS}}^2\, \kappa^2 \sum_{\boldsymbol{k}\in\mathcal{I}_N^{\mathrm{C}}(U)} \frac{1}{w^2(\boldsymbol{k})},\ \sup_{\boldsymbol{k}\in\mathcal{I}_N^{\mathrm{C}}(U)} \frac{1}{w^2(\boldsymbol{k})} \right\}$$

with $\kappa = (1+\sqrt{5})/2$*, and constant* C_{BOS} *from* (4.1).

Proof. For the details of this proof we refer to [MU21, Proposition 3.8]. This lemma is an application of the proposition for our special setting. ∎

The following theorem considers the L_2 approximation error in a Sobolev type space where the basis coefficients are approximated by least-squares. Here, we incorporate the bound on the spectral norm of the Moore-Penrose inverse from Theorem 4.2 as well as the bound on the spectral norm of our infinite matrix $\boldsymbol{\Phi}^{\mathcal{X}}_{\mathcal{I}_N^{\mathrm{C}}(U)}$ from Lemma 4.9.

Theorem 4.10. *Let* $\mathrm{H}^w(\mathbb{D}^d, \omega^{(d)})$ *be a Sobolev type space with a square-summable weight function* $w\colon \mathbb{Z}^d \to [1,\infty)$ *such that* $(w^{-1}(\boldsymbol{k}))_{\boldsymbol{k}\in\mathbb{Z}^d} \in \ell_2$*. Moreover, let* $\mathcal{X} \subseteq \mathbb{D}^d$ *be a set of* $|\mathcal{X}| > 3$ *nodes each drawn i.i.d. at random according to the probability density* $\omega^{(d)}$ *such that*

$$|\mathcal{I}_N(U)| \le \frac{|\mathcal{X}|}{10\, C_{\mathrm{supp}}^2\, (r+1)\, \log|\mathcal{X}|} \tag{4.19}$$

for an $r > 0$ *with* C_{supp} *from* (4.2)*. Let* $\boldsymbol{f} = (f(\boldsymbol{x}))_{\boldsymbol{x}\in\mathcal{X}}$ *be evaluations of* $f \in \mathrm{H}^w(\mathbb{D}^d, \omega^{(d)})$*, and let* $\mathrm{S}^{\mathcal{X}}_{\mathcal{I}_N(U)} f$ *be the approximate partial sum obtained by approximating the basis coefficients* $\mathrm{c}_{\boldsymbol{k}}(f)$ *via solving the least-squares system* (4.3)*. Then we have for the error*

$$\sup_{\|f\|_{\mathrm{H}^w(\mathbb{D}^d,\omega^{(d)})}\le 1} \left\| f - \mathrm{S}^{\mathcal{X}}_{\mathcal{I}_N(U)} f \right\|^2_{\mathrm{L}_2(\mathbb{D}^d,\omega^{(d)})} \tag{4.20}$$

$$\le 5\max\left\{ \frac{4C_{\mathrm{BOS}}^2\,\kappa^2}{5C_{\mathrm{supp}}^2\,|\mathcal{I}_N(U)|} \sum_{\boldsymbol{k}\in\mathcal{I}_N^{\mathrm{C}}(U)} \frac{1}{w^2(\boldsymbol{k})},\ \frac{1}{\inf_{\boldsymbol{k}\in\mathcal{I}_N^{\mathrm{C}}(U)} w^2(\boldsymbol{k})} \right\}$$

with probability at least $1 - (2^{3/4} + 1)\,|\mathcal{X}|^{-r}$ *for* $\kappa = (1 + \sqrt{5})/2$, *and* C_{BOS} *the BOS constant from* (4.1).

Proof. Let $\hat{f} \in \mathbb{C}^{|\mathcal{I}_N(U)|}$ be the approximate coefficients obtained by solving the least-squares problem (4.3), i.e.,

$$\hat{f} = (\hat{f}_{\boldsymbol{k}})_{\boldsymbol{k} \in \mathcal{I}_N(U)} = \left(\boldsymbol{F}^{\mathcal{X}}_{\mathcal{I}_N(U)}\right)^{\dagger} \boldsymbol{f}.$$

Moreover, we collect the exact coefficient as $\hat{\boldsymbol{c}} = (\mathrm{c}_{\boldsymbol{k}}(f))_{\boldsymbol{k} \in \mathcal{I}_N(U)}$. Then we may rewrite the error and apply Theorem 4.2 to obtain

$$\begin{aligned}
\left\| \mathrm{S}_{\mathcal{I}_N(U)} f - \mathrm{S}^{\mathcal{X}}_{\mathcal{I}_N(U)} f \right\|^2_{\mathrm{L}_2(\mathbb{D}^d, \omega^{(d)})} &= \sum_{\boldsymbol{k} \in \mathcal{I}_N(U)} \left| \hat{f}_{\boldsymbol{k}} - \mathrm{c}_{\boldsymbol{k}}(f) \right|^2 = \left\| \hat{\boldsymbol{f}} - \hat{\boldsymbol{c}} \right\|^2_{\ell_2} \\
&= \left\| \left(\boldsymbol{F}^{\mathcal{X}}_{\mathcal{I}_N(U)}\right)^{\dagger} \boldsymbol{f} - \hat{\boldsymbol{c}} \right\|^2_{\ell_2} \\
&= \left\| \left(\boldsymbol{F}^{\mathcal{X}}_{\mathcal{I}_N(U)}\right)^{\dagger} \left(\boldsymbol{f} - \boldsymbol{F}^{\mathcal{X}}_{\mathcal{I}_N(U)} \hat{\boldsymbol{c}} \right) \right\|^2_{\ell_2} \\
&\leq \left\| \left(\boldsymbol{F}^{\mathcal{X}}_{\mathcal{I}_N(U)}\right)^{\dagger} \right\|^2_{\ell_2 \to \ell_2} \left\| \boldsymbol{f} - \boldsymbol{F}^{\mathcal{X}}_{\mathcal{I}_N(U)} \hat{\boldsymbol{c}} \right\|^2_{\ell_2}.
\end{aligned}$$

In the next step, we consider the quantity

$$\frac{1}{|\mathcal{X}|} \left\| \boldsymbol{f} - \boldsymbol{F}^{\mathcal{X}}_{\mathcal{I}_N(U)} \hat{\boldsymbol{c}} \right\|^2_{\ell_2} = \frac{1}{|\mathcal{X}|} \sum_{\boldsymbol{x} \in \mathcal{X}} \left| f(\boldsymbol{x}) - \mathrm{S}_{\mathcal{I}_N(U)} f(\boldsymbol{x}) \right|^2.$$

Using the basis $\tilde{\varphi}^{(d)}_{\boldsymbol{k}}(\boldsymbol{x}) \coloneqq \frac{1}{w(\boldsymbol{k})}\, \varphi^{(d)}_{\boldsymbol{k}}(\boldsymbol{x})$, $\boldsymbol{k} \in \mathbb{Z}^d$, of $\mathrm{H}^w(\mathbb{D}^d, \omega^{(d)})$, we can write

$$f(\boldsymbol{x}) - \mathrm{S}_{\mathcal{I}_N(U)} f(\boldsymbol{x}) = \sum_{\boldsymbol{k} \in \mathcal{I}^{\mathrm{C}}_N(U)} \langle f, \tilde{\varphi}^{(d)}_{\boldsymbol{k}} \rangle_{\mathrm{H}^w(\mathbb{D}^d, \omega^{(d)})} \tilde{\varphi}^{(d)}_{\boldsymbol{k}}$$

with coefficients

$$\tilde{\tilde{\boldsymbol{c}}} \coloneqq \left(\langle f, \tilde{\varphi}^{(d)}_{\boldsymbol{k}} \rangle_{\mathrm{H}^w(\mathbb{D}^d, \omega^{(d)})} \right)_{\boldsymbol{k} \in \mathcal{I}^{\mathrm{C}}_N(U)}.$$

Using the infinite matrix $\boldsymbol{\Phi}^{\mathcal{X}}_{\mathcal{I}_N^{\mathsf{C}}(\mathcal{U})}$ from (4.18), we obtain

$$\begin{aligned}\frac{1}{|\mathcal{X}|}\left\|f - \boldsymbol{F}^{\mathcal{X}}_{\mathcal{I}_N(\mathcal{U})}\hat{\boldsymbol{c}}\right\|_{\ell_2}^2 &= \frac{1}{|\mathcal{X}|}\left\|\boldsymbol{\Phi}^{\mathcal{X}}_{\mathcal{I}_N^{\mathsf{C}}(\mathcal{U})}\tilde{\hat{\boldsymbol{c}}}\right\|_{\ell_2}^2 \leq \frac{1}{|\mathcal{X}|}\left\|\boldsymbol{\Phi}^{\mathcal{X}}_{\mathcal{I}_N^{\mathsf{C}}(\mathcal{U})}\right\|_{\ell_2\to\ell_2}^2 \left\|\tilde{\hat{\boldsymbol{c}}}\right\|_{\ell_2}^2 \\ &= \frac{1}{|\mathcal{X}|}\left\|\left(\boldsymbol{\Phi}^{\mathcal{X}}_{\mathcal{I}_N^{\mathsf{C}}(\mathcal{U})}\right)^{\mathsf{H}}\boldsymbol{\Phi}^{\mathcal{X}}_{\mathcal{I}_N^{\mathsf{C}}(\mathcal{U})}\right\|_{\ell_2\to\ell_2}\left\|\tilde{\hat{\boldsymbol{c}}}\right\|_{\ell_2}^2.\end{aligned}$$

We then define two random events

$$\begin{aligned}A &:= \left\{\frac{1}{|\mathcal{X}|}\left\|\left(\boldsymbol{\Phi}^{\mathcal{X}}_{\mathcal{I}_N^{\mathsf{C}}(\mathcal{U})}\right)^{\mathsf{H}}\boldsymbol{\Phi}^{\mathcal{X}}_{\mathcal{I}_N^{\mathsf{C}}(\mathcal{U})}\right\|_{\ell_2\to\ell_2} \leq F + \sup_{\boldsymbol{k}\in\mathcal{I}_N^{\mathsf{C}}(\mathcal{U})}\frac{1}{w^2(\boldsymbol{k})}\right\} \\ B &:= \left\{\left\|\left(\boldsymbol{F}^{\mathcal{X}}_{\mathcal{I}_N(\mathcal{U})}\right)^{\dagger}\right\|_{\ell_2\to\ell_2}^2 \leq \frac{2}{|\mathcal{X}|}\right\}.\end{aligned}$$

From Theorem 4.2 we know that $\mathbb{P}(B^{\mathsf{C}}) \leq |\mathcal{X}|^{-r}$. Moreover, Lemma 4.9 implies that

$$\begin{aligned}&\mathbb{P}\left(\frac{1}{|\mathcal{X}|}\left\|\left(\boldsymbol{\Phi}^{\mathcal{X}}_{\mathcal{I}_N^{\mathsf{C}}(\mathcal{U})}\right)^{\mathsf{H}}\boldsymbol{\Phi}^{\mathcal{X}}_{\mathcal{I}_N^{\mathsf{C}}(\mathcal{U})}\right\|_{\ell_2\to\ell_2} > F + \|\boldsymbol{\Lambda}\|_{\ell_2}\right) \\ &\qquad\leq \mathbb{P}\left(\left\|\left(\boldsymbol{\Phi}^{\mathcal{X}}_{\mathcal{I}_N^{\mathsf{C}}(\mathcal{U})}\right)^{\mathsf{H}}\boldsymbol{\Phi}^{\mathcal{X}}_{\mathcal{I}_N^{\mathsf{C}}(\mathcal{U})} - \boldsymbol{\Lambda}\right\|_{\ell_2\to\ell_2} \geq F\right) \leq 2^{\frac{3}{4}}|\mathcal{X}|^{-r}\end{aligned}$$

and therefore $\mathbb{P}(A^{\mathsf{C}}) \leq 2^{\frac{3}{4}}|\mathcal{X}|^{-r}$. In total, we have

$$1 - \mathbb{P}(A \cap B) \leq \mathbb{P}(A^{\mathsf{C}}) + \mathbb{P}(B^{\mathsf{C}}) \leq \left(1 + 2^{\frac{3}{4}}\right)|\mathcal{X}|^{-r}.$$

If the events A and B happen simultaneously, we have for the error

$$\begin{aligned}
&\left\| \mathrm{S}_{\mathcal{I}_N(U)} f - \mathrm{S}^{\mathcal{X}}_{\mathcal{I}_N(U)} f \right\|^2_{\mathrm{L}_2(\mathbb{D}^d,\omega^{(d)})} \leq \left\| \left(\boldsymbol{F}^{\mathcal{X}}_{\mathcal{I}_N(U)} \right)^{\dagger} \right\|^2_{\ell_2 \to \ell_2} \left\| f - \boldsymbol{F}^{\mathcal{X}}_{\mathcal{I}_N(U)} \hat{\boldsymbol{c}} \right\|^2_{\ell_2} \\
&\quad \leq \frac{2}{|\mathcal{X}|} \left\| \boldsymbol{\Phi}^{\mathcal{X}}_{\mathcal{I}_N^{\mathrm{C}}(U)} \right\|^2_{\ell_2 \to \ell_2} \left\| \tilde{\hat{\boldsymbol{c}}} \right\|^2_{\ell_2} \leq 2 \left(F + \sup_{\boldsymbol{k} \in \mathcal{I}_N^{\mathrm{C}}(U)} \frac{1}{w^2(\boldsymbol{k})} \right) \|f\|^2_{\mathrm{H}^w(\mathbb{D}^d,\omega^{(d)})} \\
&\quad \leq 4 \, \|f\|^2_{\mathrm{H}^w(\mathbb{D}^d,\omega^{(d)})} \\
&\qquad \cdot \max \left\{ \frac{8(r+1)\log|\mathcal{X}|}{|\mathcal{X}|} \, C^2_{\mathrm{BOS}} \, \kappa^2 \sum_{\boldsymbol{k} \in \mathcal{I}_N^{\mathrm{C}}(U)} \frac{1}{w^2(\boldsymbol{k})}, \sup_{\boldsymbol{k} \in \mathcal{I}_N^{\mathrm{C}}(U)} \frac{1}{w^2(\boldsymbol{k})} \right\}.
\end{aligned}$$

By the requirement on the oversampling, we get the estimate

$$\frac{\log|\mathcal{X}|}{|\mathcal{X}|} \leq \frac{1}{10 \, C^2_{\mathrm{supp}} \, (r+1) \, |\mathcal{I}_N(U)|}.$$

Finally, we may combine this with the truncation error result of Lemma 4.7 to obtain

$$\begin{aligned}
&\left\| f - \mathrm{S}^{\mathcal{X}}_{\mathcal{I}_N(U)} f \right\|^2_{\mathrm{L}_2(\mathbb{D}^d,\omega^{(d)})} \\
&= \left\| f - \mathrm{S}_{\mathcal{I}_N(U)} f \right\|^2_{\mathrm{L}_2(\mathbb{D}^d,\omega^{(d)})} + \left\| \mathrm{S}_{\mathcal{I}_N(U)} f - \mathrm{S}^{\mathcal{X}}_{\mathcal{I}_N(U)} f \right\|^2_{\mathrm{L}_2(\mathbb{D}^d,\omega^{(d)})} \\
&\leq \frac{\|f\|^2_{\mathrm{H}^w(\mathbb{D}^d,\omega^{(d)})}}{\inf_{\boldsymbol{k} \in \mathcal{I}_N^{\mathrm{C}}(U)} w^2(\boldsymbol{k})} + \left\| \mathrm{S}_{\mathcal{I}_N(U)} f - \mathrm{S}^{\mathcal{X}}_{\mathcal{I}_N(U)} f \right\|^2_{\mathrm{L}_2(\mathbb{D}^d,\omega^{(d)})} \\
&\leq 5 \, \|f\|^2_{\mathrm{H}^w(\mathbb{D}^d,\omega^{(d)})} \\
&\qquad \cdot \max \left\{ \frac{8(r+1)\log|\mathcal{X}|}{|\mathcal{X}|} \, C^2_{\mathrm{BOS}} \, \kappa^2 \sum_{\boldsymbol{k} \in \mathcal{I}_N^{\mathrm{C}}(U)} \frac{1}{w^2(\boldsymbol{k})}, \frac{1}{\inf_{\boldsymbol{k} \in \mathcal{I}_N^{\mathrm{C}}(U)} w^2(\boldsymbol{k})} \right\}.
\end{aligned}$$

■

Theorem 4.10 gives us insight into our approximation error if we can guarantee the necessary oversampling (4.19), i.e., logarithmic oversampling. We also have detailed knowledge about our constants.

Under the same requirements on the oversampling and with a similar approach, we are able to achieve a new bound on the L_2 error in the least-squares setting if we are in the weighted Wiener space $\mathcal{A}^w(\mathbb{D}^d, \omega^{(d)})$, i.e., we require more regularity.

Theorem 4.11. *Let $\mathcal{A}^w(\mathbb{D}^d, \omega^{(d)})$ be a weighted Wiener space with weight function $w\colon \mathbb{Z}^d \to [1, \infty)$. Moreover, let $\mathcal{X} \subseteq \mathbb{D}^d$ be a set of $|\mathcal{X}| > 3$ nodes each drawn i.i.d. at random according to the probability density $\omega^{(d)}$ such that*

$$|\mathcal{I}_N(U)| \leq \frac{|\mathcal{X}|}{10\, C_{\text{supp}}^2\, (r+1)\, \log|\mathcal{X}|}$$

for an $r > 0$ and C_{supp} from (4.2). Let $\boldsymbol{f} = (f(\boldsymbol{x}))_{\boldsymbol{x}\in\mathcal{X}}$ be evaluations of $f \in \mathcal{A}^w(\mathbb{D}^d, \omega^{(d)})$, and let $\mathrm{S}^{\mathcal{X}}_{\mathcal{I}_N(U)} f$ be the approximate partial sum obtained by approximating the basis coefficients $\mathrm{c}_{\boldsymbol{k}}(f)$ via solving the least-squares system (4.3). Then we have for the error

$$\sup_{\|f\|_{\mathcal{A}^w(\mathbb{D}^d,\omega^{(d)})}\leq 1} \left\| f - \mathrm{S}^{\mathcal{X}}_{\mathcal{I}_N(U)} f \right\|_{\mathrm{L}_2(\mathbb{D}^d,\omega^{(d)})} \leq \frac{\sqrt{3}\; C_{\text{BOS}}}{\inf_{\boldsymbol{k}\in\mathcal{I}_N^{\mathrm{C}}(U)} w(\boldsymbol{k})} \tag{4.21}$$

with probability at least $1 - (2^{3/4}+1)\,|\mathcal{X}|^{-r}$ for $\kappa = (1+\sqrt{5})/2$, and C_{BOS} the BOS constant (4.1).

Proof. From the proof of Theorem 4.10, we know that

$$\begin{aligned}\left\| \mathrm{S}_{\mathcal{I}_N(U)} f - \mathrm{S}^{\mathcal{X}}_{\mathcal{I}_N(U)} f \right\|^2_{\mathrm{L}_2(\mathbb{D}^d,\omega^{(d)})} \\ \leq \left\| \left(\boldsymbol{F}^{\mathcal{X}}_{\mathcal{I}_N(U)} \right)^{\dagger} \right\|^2_{\ell_2\to\ell_2} \sum_{\boldsymbol{x}\in\mathcal{X}} \left| f(\boldsymbol{x}) - \mathrm{S}_{\mathcal{I}_N(U)} f(\boldsymbol{x}) \right|^2 .\end{aligned}$$

The sum can be estimated by the L_∞ norm as follows

$$\begin{aligned}\sum_{\boldsymbol{x}\in\mathcal{X}} \left|f(\boldsymbol{x}) - S_{\mathcal{I}_N(U)} f(\boldsymbol{x})\right|^2 &\leq \sum_{\boldsymbol{x}\in\mathcal{X}} \left\|f - S_{\mathcal{I}_N(U)} f\right\|^2_{L_\infty(\mathbb{D}^d)} \\ &= |\mathcal{X}| \left\|f - S_{\mathcal{I}_N(U)} f\right\|^2_{L_\infty(\mathbb{D}^d)}.\end{aligned}$$

Lemma 4.8 tells us that

$$\left\|f - S_{\mathcal{I}_N(U)} f\right\|_{L_\infty(\mathbb{D}^d)} \leq \frac{C_{\mathrm{BOS}} \|f\|_{\mathcal{A}^w(\mathbb{D}^d,\omega^{(d)})}}{\inf_{\boldsymbol{k}\in\mathcal{I}_N^C(U)} w(\boldsymbol{k})}.$$

Moreover, Theorem 4.2 implies that

$$\left\|\left(\boldsymbol{F}^{\mathcal{X}}_{\mathcal{I}_N(U)}\right)^\dagger\right\|^2_{\ell_2\to\ell_2} \leq \frac{2}{|\mathcal{X}|}$$

with probability $1 - |\mathcal{X}|^{-r}$. In summary, we obtain

$$\begin{aligned}&\sup_{\|f\|_{\mathcal{A}^w(\mathbb{D}^d,\omega^{(d)})}\leq 1} \left\|f - S^{\mathcal{X}}_{\mathcal{I}_N(U)} f\right\|^2_{L_2(\mathbb{D}^d,\omega^{(d)})} \\ &\quad= \left\|f - S_{\mathcal{I}_N(U)} f\right\|^2_{L_2(\mathbb{D}^d,\omega^{(d)})} + \left\|S_{\mathcal{I}_N(U)} f - S^{\mathcal{X}}_{\mathcal{I}_N(U)} f\right\|^2_{L_2(\mathbb{D}^d,\omega^{(d)})} \\ &\quad\leq \left\|f - S_{\mathcal{I}_N(U)} f\right\|^2_{L_\infty(\mathbb{D}^d)} + 2\left\|f - S_{\mathcal{I}_N(U)} f\right\|^2_{L_\infty(\mathbb{D}^d)} \\ &\quad\leq \frac{3C^2_{\mathrm{BOS}}}{\inf_{\boldsymbol{k}\in\mathcal{I}_N^C(U)} w^2(\boldsymbol{k})}\end{aligned}$$

also with probability $1 - |\mathcal{X}|^{-r}$. ■

In the recent paper [KLT21], L_2 error bounds have been considered for weighted Wiener spaces using sparse grids as sampling schemes. Here, we have collected counterparts for these results in our setting for least-squares approximation with Theorem 4.11 being a wholly new result. It shows that the L_∞ truncation error from Lemma 4.8 and the

L_2 approximation error from Theorem 4.11 are of the same order in weighted Wiener spaces.

Let us consider the previous bounds in a special setting to better understand their impact. We consider space $L_2(\mathbb{T}^d)$ of periodic functions with spatial dimension $d \in \mathbb{N}$ and the Fourier system $\varphi_{\boldsymbol{k}}^{(d),\exp}$, $\boldsymbol{k} \in \mathbb{Z}^d$, as an orthonormal basis such that $C_{\mathrm{BOS}} = C_{\mathrm{supp}} = 1$ for the constants (4.1) and (4.2). The functions of dominating-mixed smoothness represent an important class of functions used in many different applications, see e.g. [DTU18], which is why we choose the weights

$$w(\boldsymbol{k}) \coloneqq w_\beta(\boldsymbol{k}) \coloneqq \prod_{s=1}^{d} (1 + |k_s|)^\beta$$

with dominating-mixed smoothness parameter $\beta > 0$. Note that this is a special setting of our more general weights from (2.5). For the ANOVA truncation, we choose a subset of ANOVA terms $U = U^{(d,d_s)}$ with superposition threshold $d_s \in [d]$ and a grouped index set $\mathcal{I}_N(U^{(d,d_s)})$ with bandwidths $\boldsymbol{N} \in (2\mathbb{N})^{d_s}$, cf. Definition 3.3.

We first consider the sum appearing in the bound in Theorem 4.10 which we split as follows

$$\sum_{\boldsymbol{k} \in \mathcal{I}_{\boldsymbol{N}}^{\mathrm{C}}(U^{(d,d_s)})} \frac{1}{w^2(\boldsymbol{k})} = \sum_{\substack{\boldsymbol{k} \in \mathbb{Z}^d \\ |\operatorname{supp} \boldsymbol{k}| > d_s}} \frac{1}{w^2(\boldsymbol{k})} + \sum_{n=1}^{d_s} \binom{d}{n} \sum_{\boldsymbol{k} \in (\mathbb{Z}\setminus\{0\})^n \setminus \mathcal{I}_{N_n}^n} \frac{1}{w^2(\boldsymbol{k})}$$

with index sets $\mathcal{I}_{N_n}^n$ from (3.7). The first sum is only related to the ANOVA truncation and appeared already in L_∞ bound in Corollary 2.32. It can be expressed explicitly as

$$\sum_{\substack{\boldsymbol{k} \in \mathbb{Z}^d \\ |\operatorname{supp} \boldsymbol{k}| > d_s}} \frac{1}{w_\beta^2(\boldsymbol{k})} = \sum_{n=d_s+1}^{d} \zeta_\beta^n = \frac{\zeta_\beta^{d_s+1} - \zeta_\beta^{d+1}}{1 - \zeta_\beta}, \quad \zeta_\beta \coloneqq 2\zeta(2\beta) - 2,$$

with ζ being the Riemann zeta function. The second sum appears in the truncation of the basis expansion to our index set $\mathcal{I}_{\boldsymbol{N}}(U^{(d,d_s)})$ which

we can express as follows

$$\sum_{\boldsymbol{k}\in(\mathbb{Z}\setminus\{0\})^n\setminus\mathcal{I}_{N_n}^n}\frac{1}{w_\beta^2(\boldsymbol{k})} = \sum_{\boldsymbol{k}\in(\mathbb{Z}\setminus\{0\})^n}\frac{1}{w_\beta^2(\boldsymbol{k})} - \sum_{\boldsymbol{k}\in\mathcal{I}_{N_n}^n}\frac{1}{w_\beta^2(\boldsymbol{k})}$$
$$= \zeta_\beta^n - \left(\sum_{k\in\mathcal{I}_{N_n}}\frac{1}{(1+|k|)^{2\beta}}\right)^n.$$

The remaining quantity can be expressed using the generalized harmonic number $\mathcal{H}_{\frac{N}{2},2\beta}$ to obtain

$$\sum_{k\in\mathcal{I}_{N_n}}\frac{1}{(1+|k|)^{2\beta}} = 2\sum_{k=1}^{N/2-1}\frac{1}{(1+k)^{2\beta}} + \frac{1}{(\frac{N}{2}+1)^{2\beta}} = 2\mathcal{H}_{\frac{N}{2},2\beta} - 2 + \frac{1}{(\frac{N}{2}+1)^{2\beta}}.$$

In summary, we get an explicit form

$$\mathcal{S}(\beta, d_s, d, \boldsymbol{N}) \coloneqq \sum_{\boldsymbol{k}\in\mathcal{I}_{\boldsymbol{N}}^{\mathrm{C}}(U^{d,d_s})}\frac{1}{w^2(\boldsymbol{k})} \tag{4.22}$$
$$= \frac{\zeta_\beta^{d_s+1} - \zeta_\beta^{d+1}}{1-\zeta_\beta}\sum_{n=1}^{d_s}\binom{d}{n}\left[\zeta_\beta^n - \left(2\mathcal{H}_{\frac{N}{2},2\beta} - 2 + \frac{1}{(\frac{N}{2}+1)^{2\beta}}\right)^n\right].$$

Considering the bound (4.20), we obtain for the first quantity in the maximum

$$\mathcal{B}_1(\beta, d_s, d, \boldsymbol{N}) \coloneqq \frac{4\kappa^2\mathcal{S}(\beta, d_s, d, \boldsymbol{N})}{1+\sum_{i=1}^{d_s}\binom{d}{i}(N_i-1)^i}. \tag{4.23}$$

The second part of the maximum in (4.20) can be computed as follows

$$\mathcal{B}_2(\beta, d_s, \boldsymbol{N}) \coloneqq \frac{5}{\inf_{\boldsymbol{k}\in\mathcal{I}_{\boldsymbol{N}}^{\mathrm{C}}(U)} w^2(\boldsymbol{k})}$$
$$= \frac{5}{\min\{2^{2\beta(d_s+1)}, (1+\frac{N_1}{2})^{2\beta}, (1+\frac{N_2}{2})^{4\beta}, \ldots, (1+\frac{N_{d_s}}{2})^{2d_s\beta}\}} \tag{4.24}$$

since the minimum is either attained through the ANOVA truncation which yields the term $2^{2\beta(d_s+1)}$ or through the index set truncation which yields $(1+\frac{N_i}{2})^{2\cdot i\beta}$, $i = 1, 2, \ldots, d_s$. Note that this quantity does not depend on the spatial dimension d which is fact was already discovered in Section 2.3 for the ANOVA truncation part. If the minimum is attained at $2^{2\beta(d_s+1)}$, the bound $\mathcal{B}_2$ is dominated by the ANOVA truncation and is therefore of the same order. Note that the quantity $\mathcal{B}_2$ appears up to a constant also in our L_∞ error bound (4.21) in Theorem 4.11.

Figure 4.2 shows the quantity $\mathcal{B}_1(\beta, d_s, d, \boldsymbol{N})$ from Theorem 4.10 and $\mathcal{B}_2(\beta, d_s, \boldsymbol{N})$ from Theorem 4.10 and Theorem 4.10. We visualize them depending on the smoothness β for exemplary choices of spatial dimension d, superposition threshold d_s and bandwidths $\boldsymbol{N}$. We observe the dependence of $\mathcal{B}_1$ on the choice of the bandwidths where a larger choice of bandwidth leads to a steeper descent. However, except for a small interval near $\beta = 1$, the maximum in the bound (4.20) is always dominated by the dimension independent $\mathcal{B}_2$. In general, we notice a good worst-case bound for our approximation error which implies the applicability of our methods for the important class of functions with dominating-mixed smoothness.

4.3.2 Individual Error

In the following, we leave the area of worst-case error and consider the recovery of individual functions. Note that there is an important difference in the approximation operator $S^{\mathcal{X}}_{\mathcal{I}_N(U)}$. In the previous Section 4.3.1, we may draw the node set $\mathcal{X}$ once for the entire class of functions and now we draw the node set $\mathcal{X}$ once for each function to be exact. As an assumption, we always use that our function f is an element of the Lebesgue product space $L_2(\mathbb{D}^d, \omega^{(d)})$ with complete orthonormal system $(\varphi^{(d)}_{\boldsymbol{k}})_{\boldsymbol{k}\in\mathbb{Z}^d}$. Here, we do not necessarily require it to be a bounded orthonormal system unless stated explicitly in the respective theorem. We additionally assume that f is continuous and if the domain is $\mathbb{D} = \mathbb{R}$, we require f to be bounded such that we always ensure $f \in L_\infty(\mathbb{D}^d)$.

We begin by proving a general probabilistic result using Bernstein's

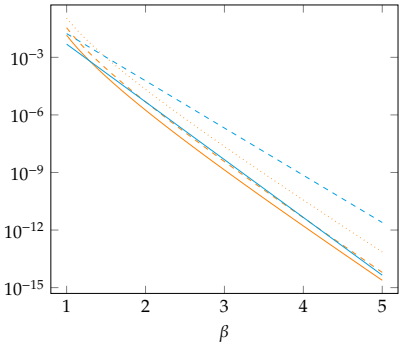

Figure 4.2: Bound $\mathcal{B}_1(\beta, 4, 9, \boldsymbol{N})$ from (4.23) for $\boldsymbol{N}_1 = [128, 32, 16, 4]$ (solid), and $\boldsymbol{N}_2 = [64, 24, 12, 4]$ (dashed), $\boldsymbol{N}_3 = [32, 16, 8, 4]$ (dotted) in orange and bound $\mathcal{B}_2(\beta, 4, 9, \boldsymbol{N})$ from (4.24) for $\boldsymbol{N}_1$, $\boldsymbol{N}_2$ (solid), and $\boldsymbol{N}_3$ (dashed) in cyan. Note that $\mathcal{B}_2(\beta, 4, 9, \boldsymbol{N}_1) = \mathcal{B}_2(\beta, 4, 9, \boldsymbol{N}_2)$ since the minimum in (4.24) is realized at $2^{10\beta}$.

inequality, see [SC08, Chapter 6]. A similar approach was first used in [LPU21] for hyperbolic wavelet regression. For independent random variables $\xi_1, \xi_2, \dots, \xi_M$, $M \geq 1$, with $\|\xi_i\|_\infty \leq C$ and $\mathbb{E}(\xi_i^2) \leq \sigma^2$, Bernstein's inequality states that

$$\mathbb{P}\left(\frac{1}{M}\sum_{i=1}^{M} \xi_i \geq \sqrt{\frac{2\sigma^2\tau}{M}} + \frac{2C\tau}{3M}\right) \leq \mathrm{e}^{-\tau} \quad \text{for any} \quad \tau > 0. \tag{4.25}$$

In the following, we denote the individual truncation errors in L_2 and L_∞ as

$$e_2 \coloneqq \left\| f - \mathrm{S}_{I_N(U)} f \right\|_{\mathrm{L}_2(\mathbb{D}^d, \omega^{(d)})} \quad \text{and} \quad e_\infty \coloneqq \left\| f - \mathrm{S}_{I_N(U)} f \right\|_{\mathrm{L}_\infty(\mathbb{D}^d)}. \tag{4.26}$$

Theorem 4.12. *Let $f \in \mathrm{L}_2(\mathbb{D}^d, \omega^{(d)})$ be a bounded and continuous function, let $\mathcal{X} \subseteq \mathbb{D}^d$ be a set of $|\mathcal{X}| > 3$ nodes each drawn i.i.d. at random according to*

the probability density $\omega^{(d)}$ *such that*

$$|\mathcal{I}_N(U)| \leq \frac{|\mathcal{X}|}{10\, C_{\text{supp}}^2\, (r+1)\, \log|\mathcal{X}|}$$

for $r > 0$ *and* $C_{\text{supp}} < \infty$ *from* (4.2). *Let* $\boldsymbol{f} = (f(\boldsymbol{x}))_{\boldsymbol{x}\in\mathcal{X}}$ *be evaluations of* f, *and let* $\mathrm{S}^{\mathcal{X}}_{\mathcal{I}_N(U)} f$ *be the approximate partial sum obtained by approximating the basis coefficients* $\mathrm{c}_{\boldsymbol{k}}(f)$ *via solving the least-squares system* (4.3). *Then we have for the error*

$$\left\| f - \mathrm{S}^{\mathcal{X}}_{\mathcal{I}_N(U)} f \right\|^2_{\mathrm{L}_2(\mathbb{D}^d,\omega^{(d)})} \leq 3e_2^2 + \frac{2e_2 e_\infty}{C_{\text{supp}}\sqrt{5\,|\mathcal{I}_N(U)|}} + \frac{2e_\infty^2}{15 C_{\text{supp}}^2\,|\mathcal{I}_N(U)|}$$

with probability at least $1 - 2\,|\mathcal{X}|^{-r}$.

Proof. In order to apply Bernstein's inequality (4.25), we introduce the random variables

$$\begin{aligned} \eta_i &\coloneqq \left| f(\boldsymbol{x}_i) - \mathrm{S}_{\mathcal{I}_N(U)} f(\boldsymbol{x}_i) \right|^2, \quad \mathbb{E}\,(\eta_i) = e_2^2, \\ \xi_i &\coloneqq \eta_i - \mathbb{E}\,(\eta_i), \quad \mathbb{E}\,(\xi_i) = 0. \end{aligned}$$

We proceed to bound the variance of ξ_i as follows

$$\begin{aligned} \mathbb{E}\left(\xi_i^2\right) &= \mathbb{E}\left(\eta_i^2\right) - \mathbb{E}\,(\eta_i)^2 = \left\| f - \mathrm{S}_{\mathcal{I}_N(U)} f \right\|^4_{\mathrm{L}_4(\mathbb{D}^d,\omega^{(d)})} - e_2^4 \\ &\leq e_\infty^2 e_2^2 - e_2^4 \leq e_2^2\left(e_\infty^2 - e_2^2\right) \leq e_2^2 e_\infty^2. \end{aligned}$$

For the infinity norm, i.e., the constant C in (4.25), we get

$$\|\xi_i\|_\infty = \|\eta_i - \mathbb{E}\,(\eta_i)\|_\infty \leq \mathrm{e}_\infty^2.$$

Now, the application of Bernstein's inequality yields

$$\mathbb{P}\left(\frac{1}{|\mathcal{X}|} \sum_{i=1}^{|\mathcal{X}|} \xi_i \geq \sqrt{\frac{2e_2^2 e_\infty^2 (r+1)\log|\mathcal{X}|}{|\mathcal{X}|}} + \frac{2e_\infty^2 (r+1)\log|\mathcal{X}|}{3\,|\mathcal{X}|} \right) \leq |\mathcal{X}|^{-r-1} \tag{4.27}$$

for $r > 0$. In order to bound the approximation error, we start by following similar steps as in the proof of Theorem 4.10. Let $\hat{f} \in \mathbb{C}^{|\mathcal{I}_N(U)|}$ be the approximate coefficients obtained by solving the least-squares problem (4.3), i.e.,

$$\hat{f} = (\hat{f}_k)_{k \in \mathcal{I}_N(U)} = \left(\boldsymbol{F}^{\mathcal{X}}_{\mathcal{I}_N(U)}\right)^{\dagger} \boldsymbol{f}.$$

Moreover, we collect the exact coefficients as $\hat{\boldsymbol{c}} = (\mathrm{c}_k(f))_{k \in \mathcal{I}_N(U)}$. Then the error can be estimated as follows

$$\begin{aligned}\left\| \mathrm{S}^{\mathcal{X}}_{\mathcal{I}_N(U)} f - \mathrm{S}_{\mathcal{I}_N(U)} f \right\|^2_{\mathrm{L}_2(\mathbb{D}^d, \omega^{(d)})} \\ \leq \left\| \left(\boldsymbol{F}^{\mathcal{X}}_{\mathcal{I}_N(U)}\right)^{\dagger} \right\|^2_{\ell_2 \to \ell_2} \sum_{\boldsymbol{x} \in \mathcal{X}} \left| f(\boldsymbol{x}) - \mathrm{S}_{\mathcal{I}_N(U)} f(\boldsymbol{x}) \right|^2,\end{aligned}$$

see the proof of Theorem 4.10. Now, we define two random events

$$\begin{aligned} A &\coloneqq \left\{ \frac{1}{|\mathcal{X}|} \sum_{\boldsymbol{x} \in \mathcal{X}} \left| f(\boldsymbol{x}) - \mathrm{S}_{\mathcal{I}_N(U)} f(\boldsymbol{x}) \right|^2 \right. \\ &\qquad \left. \leq e_2^2 + \sqrt{\frac{e_2^2 e_\infty^2}{5 C_{\mathrm{supp}}^2 \, |\mathcal{I}_N(U)|}} + \frac{e_\infty^2}{15 C_{\mathrm{supp}}^2 \, |\mathcal{I}_N(U)|} \right\} \\ B &\coloneqq \left\{ \left\| \left(\boldsymbol{F}^{\mathcal{X}}_{\mathcal{I}_N(U)}\right)^{\dagger} \right\|^2_{\ell_2 \to \ell_2} \leq \frac{2}{|\mathcal{X}|} \right\}. \end{aligned}$$

From Theorem 4.2, we know that $\mathbb{P}(B) > 1 - |\mathcal{X}|^{-r}$ for any $r > 0$. Our oversampling requirement tells us that

$$\begin{aligned} e_2^2 + \sqrt{\frac{2 e_2^2 e_\infty^2 (r+1) \log |\mathcal{X}|}{|\mathcal{X}|}} + \frac{2 e_\infty^2 (r+1) \log |\mathcal{X}|}{3 \, |\mathcal{X}|} \\ \leq e_2^2 + \sqrt{\frac{e_2^2 e_\infty^2}{5 C_{\mathrm{supp}}^2 \, |\mathcal{I}_N(U)|}} + \frac{e_\infty^2}{15 C_{\mathrm{supp}}^2 \, |\mathcal{I}_N(U)|} \end{aligned}$$

which implies with (4.27) that $\mathbb{P}(A) > 1 - |\mathcal{X}|^{-r-1} > 1 - |\mathcal{X}|^{-r}$. In total, we get

$$\mathbb{P}(A \cap B) \geq 1 - \mathbb{P}(A^{\mathrm{C}}) - \mathbb{P}(B^{\mathrm{C}}) \geq 1 - 2\,|\mathcal{X}|^{-r}\,.$$

If both events happen, we obtain for the approximation error

$$\begin{aligned}\left\| f - \mathrm{S}^{\mathcal{X}}_{\mathcal{I}_N(U)} f \right\|^2_{\mathrm{L}_2(\mathbb{D}^d,\omega^{(d)})} &= e_2^2 + \left\| \mathrm{S}^{\mathcal{X}}_{\mathcal{I}_N(U)} f - \mathrm{S}_{\mathcal{I}_N(U)} f \right\|^2_{\mathrm{L}_2(\mathbb{D}^d,\omega^{(d)})} \\ &\leq e_2^2 + \frac{2}{|\mathcal{X}|} \sum_{\boldsymbol{x}\in\mathcal{X}} \left| f(\boldsymbol{x}) - \mathrm{S}_{\mathcal{I}_N(U)} f(\boldsymbol{x}) \right|^2 \\ &\leq e_2^2 + 2\left(e_2^2 + \sqrt{\frac{e_2^2 e_\infty^2}{5C_{\mathrm{supp}}^2\,|\mathcal{I}_N(U)|}} + \frac{e_\infty^2}{15C_{\mathrm{supp}}^2\,|\mathcal{I}_N(U)|} \right).\end{aligned}$$

■

This is always applicable since we do not make any regularity assumptions in terms of the decay of the coefficients as would be the case if we assume that the function lies in a Sobolev type space or a weighted Wiener space. In fact, it can be explicitly computed and compared to the error if the basis coefficients of the function are known. For a numerical experiments with a periodic function, we refer to Section 5.1. Now, we aim to obtain a similar bound error in the L_∞ norm.

Theorem 4.13. *Let $f \in \mathrm{L}_2(\mathbb{D}^d, \omega^{(d)})$ be a bounded and continuous function, let $\mathcal{X} \subseteq \mathbb{D}^d$ be a set of $|\mathcal{X}| > 3$ nodes each drawn i.i.d. at random according to the probability density $\omega^{(d)}$ such that*

$$|\mathcal{I}_N(U)| \leq \frac{|\mathcal{X}|}{10\,C_{\mathrm{supp}}^2\,(1+r)\,\log|\mathcal{X}|} \tag{4.28}$$

for $r > 0$ and $C_{\mathrm{supp}} < \infty$ from (4.2)*. Let $\boldsymbol{y} = (f(\boldsymbol{x}))_{\boldsymbol{x}\in\mathcal{X}}$ be evaluations of f, and let $\mathrm{S}^{\mathcal{X}}_{\mathcal{I}_N(U)} f$ be the approximate partial sum obtained by approximating the basis coefficients $\mathrm{c}_{\boldsymbol{k}}(f)$ via solving the least-squares system* (4.3)*. Then we*

have for the error

$$\left\| f - \mathrm{S}^{\mathcal{X}}_{\mathcal{I}_N(U)} f \right\|_{\mathrm{L}_\infty(\mathbb{D}^d)} \leq e_\infty + \sqrt{2C^2_{\mathrm{supp}} \left|\mathcal{I}_N(U)\right| e_2^2 + 2C_{\mathrm{supp}} \sqrt{\frac{\left|\mathcal{I}_N(U)\right|}{5}}\, e_2 e_\infty + \frac{2}{15} e_\infty^2}$$

with probability at least $1 - 2\left|\mathcal{X}\right|^{-r}$ *and* e_2, e_∞ *the truncation errors from* (4.26).

Proof. The idea of the proof is close to the previous theorem. We estimate the error using the triangle inequality as follows

$$\left\| f - \mathrm{S}^{\mathcal{X}}_{\mathcal{I}_N(U)} f \right\|_{\mathrm{L}_\infty(\mathbb{D}^d)} \leq e_\infty + \left\| \mathrm{S}_{\mathcal{I}_N(U)} f - \mathrm{S}^{\mathcal{X}}_{\mathcal{I}_N(U)} f \right\|_{\mathrm{L}_\infty(\mathbb{D}^d)}.$$

The second part can be bounded by applying the Cauchy-Schwarz inequality to obtain

$$\begin{aligned}
\left\| \mathrm{S}_{\mathcal{I}_N(U)} f - \mathrm{S}^{\mathcal{X}}_{\mathcal{I}_N(U)} f \right\|_{\mathrm{L}_\infty(\mathbb{D}^d)} &= \sup_{x \in \mathbb{D}^d} \left| \sum_{k \in \mathcal{I}_N(U)} \left(\hat{f}_k - \mathrm{c}_k(f) \right) \varphi_k^{(d)}(x) \right| \\
&\leq \sqrt{\sum_{k \in \mathcal{I}_N(U)} \left| \hat{f}_k - \mathrm{c}_k(f) \right|^2} \sup_{x \in \mathbb{D}^d} \sqrt{\sum_{k \in \mathcal{I}_N(U)} \left| \varphi_k^{(d)}(x) \right|^2} \\
&\leq \left\| \mathrm{S}_{\mathcal{I}_N(U)} f - \mathrm{S}^{\mathcal{X}}_{\mathcal{I}_N(U)} f \right\|_{\mathrm{L}_2(\mathbb{D}^d, \omega^{(d)})} \cdot \sqrt{C^2_{\mathrm{supp}} \left|\mathcal{I}_N(U)\right|}
\end{aligned}$$

Now, we apply the same steps as in the proof of Theorem 4.12 to obtain the estimate

$$\left\| \mathrm{S}_{\mathcal{I}_N(U)} f - \mathrm{S}^{\mathcal{X}}_{\mathcal{I}_N(U)} f \right\|_{\mathrm{L}_2(\mathbb{D}^d, \omega^{(d)})} \leq \sqrt{2e_2^2 + \frac{2e_2 e_\infty}{C_{\mathrm{supp}} \sqrt{5\left|\mathcal{I}_N(U)\right|}} + \frac{2e_\infty^2}{15 C^2_{\mathrm{supp}} \left|\mathcal{I}_N(U)\right|}}$$

with probability $1 - 2\,|\mathcal{X}|^{-r}$. This gives us

$$\left\| \mathrm{S}_{\mathcal{I}_N(U)} f - \mathrm{S}^{\mathcal{X}}_{\mathcal{I}_N(U)} f \right\|_{\mathrm{L}_\infty(\mathbb{D}^d)} \leq \sqrt{2C_{\mathrm{supp}}^2\,|\mathcal{I}_N(U)|\,e_2^2 + 2C_{\mathrm{supp}}\sqrt{\frac{|\mathcal{I}_N(U)|}{5}}\;e_2 e_\infty + \frac{2}{15}e_\infty^2}$$

which proves our result. ∎

This L_∞ bound may help us again in a setting where we know regularity, e.g., in a Sobolev type space or a weighted Wiener space, but we do not have any statements about the worst-case error in L_∞. In the following, we consider two corollaries for this setting.

Corollary 4.14. *Let $0 \neq f \in \mathrm{H}^w(\mathbb{D}^d, \omega^{(d)})$ with a weight function $w\colon \mathbb{Z}^d \to [1,\infty)$ that is square-summable, i.e., $(w^{-1}(\boldsymbol{k}))_{\boldsymbol{k}\in\mathbb{Z}^d} \in \ell_2$. Moreover, let $\mathcal{X} \subseteq \mathbb{D}^d$ be a set of $|\mathcal{X}| > 3$ nodes each drawn i.i.d. at random according to the probability density $\omega^{(d)}$ such that*

$$|\mathcal{I}_N(U)| \leq \frac{|\mathcal{X}|}{10\,C_{\mathrm{supp}}^2\,(1+r)\,\log|\mathcal{X}|}$$

for $r > 0$ and $C_{\mathrm{supp}} < \infty$ from (4.2)*. Let $\boldsymbol{f} = (f(\boldsymbol{x}))_{\boldsymbol{x}\in\mathcal{X}}$ be evaluations of f, and let $\mathrm{S}^{\mathcal{X}}_{\mathcal{I}_N(U)} f$ be the approximate partial sum obtained by approximating the basis coefficients $\mathrm{c}_{\boldsymbol{k}}(f)$ via solving the least-squares system* (4.3)*. Then we have for the error*

$$\frac{\left\| f - \mathrm{S}^{\mathcal{X}}_{\mathcal{I}_N(U)} f \right\|_{\mathrm{L}_\infty(\mathbb{D}^d)}}{\|f\|_{\mathrm{H}^w(\mathbb{D}^d,\omega^{(d)})}} \leq C_{\mathrm{BOS}} \sqrt{\sum_{\boldsymbol{k}\in\mathcal{I}_N^C(U)} \frac{1}{w^2(\boldsymbol{k})}} \cdot \left(1 + \sqrt{2C_{\mathrm{supp}}^2\,|\mathcal{I}_N(U)| + 2C_{\mathrm{supp}}\sqrt{\frac{|\mathcal{I}_N(U)|}{5}} + \frac{2}{15}}\right)$$

with probability at least $1 - 2\,|\mathcal{X}|^{-r}$ and $C_{\mathrm{BOS}} < \infty$ from (4.1)*.*

Proof. Following the same arguments as in the proof of Theorem 2.30, we obtain

$$\mathrm{e}_\infty \le C_{\mathrm{BOS}} \, \|f\|_{\mathrm{H}^w(\mathbb{D}^d,\omega^{(d)})} \sqrt{\sum_{\boldsymbol{k}\in\mathcal{I}_N^C(U)} \frac{1}{w^2(\boldsymbol{k})}}.$$

If we roughly estimate the e_2 truncation error by e_∞, we get

$$\mathrm{e}_2 \le \mathrm{e}_\infty \le C_{\mathrm{BOS}} \, \|f\|_{\mathrm{H}^w(\mathbb{D}^d,\omega^{(d)})} \sqrt{\sum_{\boldsymbol{k}\in\mathcal{I}_N^C(U)} \frac{1}{w^2(\boldsymbol{k})}}.$$

Applying this to Theorem 4.13 yields the result. ∎

Corollary 4.15. *Let $0 \neq f \in \mathcal{A}^w(\mathbb{D}^d, \omega^{(d)})$ with a weight function $w\colon \mathbb{Z}^d \to [1,\infty)$, let $\mathcal{X} \subseteq \mathbb{D}^d$ be a set of $|\mathcal{X}| > 3$ nodes each drawn i.i.d. at random according to the probability density $\omega^{(d)}$ such that*

$$|\mathcal{I}_N(U)| \le \frac{|\mathcal{X}|}{10\, C_{\mathrm{supp}}^2\,(1+r)\,\log|\mathcal{X}|}$$

for $r > 0$ and $C_{\mathrm{supp}} < \infty$ from (4.2)*. Let $\boldsymbol{f} = (f(\boldsymbol{x}))_{\boldsymbol{x}\in\mathcal{X}}$ be evaluations of f, and let $\mathrm{S}^{\mathcal{X}}_{\mathcal{I}_N(U)} f$ be the approximate partial sum obtained by approximating the basis coefficients $\mathrm{c}_{\boldsymbol{k}}(f)$ via solving the least-squares system* (4.3)*. Then we have for the error*

$$\frac{\left\| f - \mathrm{S}^{\mathcal{X}}_{\mathcal{I}_N(U)} f \right\|_{\mathrm{L}_\infty(\mathbb{D}^d)}}{\|f\|_{\mathcal{A}^w(\mathbb{D}^d,\omega^{(d)})}} \le \frac{C_{\mathrm{BOS}}}{\inf_{\boldsymbol{k}\in\mathcal{I}_N^C(U)} w(\boldsymbol{k})} \cdot \left(1 + \sqrt{2C_{\mathrm{supp}}^2\,|\mathcal{I}_N(U)| + 2C_{\mathrm{supp}}\sqrt{\frac{|\mathcal{I}_N(U)|}{5}} + \frac{2}{15}}\right)$$

with probability at least $1 - 2\,|\mathcal{X}|^{-r}$ and $C_{\mathrm{BOS}} < \infty$ from (4.1)*.*

Proof. We use the same arguments as in the proof of Lemma 4.8 to obtain

$$\mathrm{e}_\infty \le \frac{C_{\mathrm{BOS}} \, \|f\|_{\mathcal{A}^w(\mathbb{D}^d,\omega^{(d)})}}{\inf_{\boldsymbol{k}\in\mathcal{I}_N^C(U)} w(\boldsymbol{k})}.$$

If we estimate the truncation error e_2 by e_∞ and apply Theorem 4.13, we have proven the statement. ■

Corollary 4.14 and Corollary 4.15 give us bounds on the L_∞ error for Sobolev type spaces and weighted Wiener spaces in an individual setting where we do not have worst-case results. We observe that these errors scale in the size of the index set $\mathcal{I}_N(U)$. For the well-known case of dominating-mixed smoothness, the quantities

$$\sqrt{\sum_{\boldsymbol{k}\in\mathcal{I}_N^{\mathrm{C}}(U)} \frac{1}{w^2(\boldsymbol{k})}} \quad \text{and} \quad \frac{1}{\inf_{\boldsymbol{k}\in\mathcal{I}_N^{\mathrm{C}}(U)} w(\boldsymbol{k})}$$

have been computed in the previous Section 4.3.1, see (4.22) and (4.24).

In the following, we study how certain requirements in our ANOVA language may lead to upper bounds on the errors e_2 and e_∞ from (4.26) under certain conditions that allow us to separate the truncation of the ANOVA decomposition and the truncation with the grouped index set $\mathcal{I}_N(U)$. We start by considering e_2 and the superposition dimension as well as global sensitivity indices.

Theorem 4.16. *Let $f \in \mathrm{L}_2(\mathbb{D}^d, \omega^{(d)})$ with superposition dimension $d_s \coloneqq d^{(\mathrm{sp})}(\delta) \in [d]$ for accuracy $\delta \in (0,1)$. Moreover, we have a subset of ANOVA terms $U \subseteq U^{(d,d_s)}$ with*

$$\varrho(\boldsymbol{u}, f) \le \varepsilon_{|\boldsymbol{u}|} \quad \text{for} \quad \boldsymbol{u} \in U^{(d,d_s)} \setminus U \quad \text{and} \quad \boldsymbol{\varepsilon} \in (0,1)^{d_s}.$$

Then the error e_2 from (4.26) *can be bounded by*

$$e_2^2 \le \left(1 - \delta + \sum_{\boldsymbol{u}\in U^{(d,d_s)}\setminus U} \varepsilon_{|\boldsymbol{u}|}\right) \sigma^2(f) + \left\| \mathrm{T}_U f - \mathrm{S}_{\mathcal{I}_N(U)} f \right\|^2_{\mathrm{L}_2(\mathbb{D}^d,\omega^{(d)})}.$$

Proof. We use orthogonality to split the error as follows

$$\begin{aligned}
&\left\|f - \mathrm{S}_{\mathcal{I}_N(U)} f\right\|^2_{\mathrm{L}_2(\mathbb{D}^d,\omega^{(d)})} \\
&\quad = \|f - \mathrm{T}_U f\|^2_{\mathrm{L}_2(\mathbb{D}^d,\omega^{(d)})} + \left\|\mathrm{T}_U f - \mathrm{S}_{\mathcal{I}_N(U)} f\right\|^2_{\mathrm{L}_2(\mathbb{D}^d,\omega^{(d)})} \\
&\quad = \|f - \mathrm{T}_{U^{(d,d_s)}} f\|^2_{\mathrm{L}_2(\mathbb{D}^d,\omega^{(d)})} + \|\mathrm{T}_{U^{(d,d_s)}} f - \mathrm{T}_U f\|^2_{\mathrm{L}_2(\mathbb{D}^d,\omega^{(d)})} \\
&\qquad + \left\|\mathrm{T}_U f - \mathrm{S}_{\mathcal{I}_N(U)} f\right\|^2_{\mathrm{L}_2(\mathbb{D}^d,\omega^{(d)})}.
\end{aligned}$$

The first part is smaller than or equal to $(1-\delta)\sigma^2(f)$ by the definition (2.26). For the second part, we have for $\boldsymbol{u} \in U^{(d,d_s)} \setminus U$ that $\varrho(\boldsymbol{u}, f) \leq \varepsilon_{|\boldsymbol{u}|}$ implies

$$\|f_{\boldsymbol{u}}\|^2_{\mathrm{L}_2(\mathbb{D}^d,\omega^{(d)})} \leq \varepsilon_{|\boldsymbol{u}|}\sigma^2(f).$$

As a consequence, we get

$$\begin{aligned}
\|\mathrm{T}_{U^{(d,d_s)}} f - \mathrm{T}_U f\|^2_{\mathrm{L}_2(\mathbb{D}^d,\omega^{(d)})} &= \sum_{\boldsymbol{u}\in U^{(d,d_s)}\setminus U} \|f_{\boldsymbol{u}}\|^2_{\mathrm{L}_2(\mathbb{D}^d,\omega^{(d)})} \\
&\leq \sigma^2(f) \sum_{\boldsymbol{u}\in U^{(d,d_s)}\setminus U} \varepsilon_{|\boldsymbol{u}|}
\end{aligned}$$

which yields our desired result. ∎

Finding a bound on e_∞ requires stronger assumptions on our function. Here, we assume $f \in \mathcal{A}(\mathbb{D}^d, \omega^{(d)})$. In fact, if we define a form of ℓ_1 equivalent to the sensitivity indices as

$$\theta(\boldsymbol{u}, f) \coloneqq \frac{1}{\|f\|_{\mathcal{A}(\mathbb{D}^d,\omega^{(d)})}} \sum_{\substack{\boldsymbol{k}\in\mathbb{Z}^d \\ \operatorname{supp}\boldsymbol{k}=\boldsymbol{u}}} |\mathrm{c}_{\boldsymbol{k}}(f)|,$$

we are able to determine similar bounds as in Theorem 4.16.

Theorem 4.17. *Let $f \in \mathcal{A}(\mathbb{D}^d, \omega^{(d)})$ with*

$$\sum_{\substack{\boldsymbol{u}\subseteq[d] \\ |\boldsymbol{u}|>d_s}} \theta(\boldsymbol{u}, f) \leq 1 - \delta$$

for accuracy $\delta \in (0,1)$. *Moreover, we have a subset of ANOVA terms* $U \subseteq U^{(d,d_s)}$ *with*

$$\theta(\boldsymbol{u}, f) \leq \varepsilon_{|\boldsymbol{u}|} \quad \text{for} \quad \boldsymbol{u} \in U^{(d,d_s)} \setminus U \quad \text{and} \quad \boldsymbol{\varepsilon} \in (0,1)^{d_s}. \tag{4.29}$$

Then the error e_∞ *from* (4.26) *can be bounded by*

$$e_\infty \leq C_{\mathrm{BOS}} \left(1 - \delta + \sum_{\boldsymbol{u} \in U^{(d,d_s)} \setminus U} \varepsilon_{|\boldsymbol{u}|}\right) \|f\|_{\mathcal{A}(\mathbb{D}^d, \omega^{(d)})} + \left\|\mathrm{T}_U f - \mathrm{S}_{\mathcal{I}_N(U)} f\right\|_{\mathrm{L}_\infty(\mathbb{D}^d)}$$

with C_{BOS} *from* (4.1).

Proof. We use the triangle inequality to split the error as follows

$$\begin{aligned}
\left\|f - \mathrm{S}_{\mathcal{I}_N(U)} f\right\|_{\mathrm{L}_\infty(\mathbb{D}^d)} &\leq \|f - \mathrm{T}_U f\|_{\mathrm{L}_\infty(\mathbb{D}^d)} + \left\|\mathrm{T}_U f - \mathrm{S}_{\mathcal{I}_N(U)} f\right\|_{\mathrm{L}_\infty(\mathbb{D}^d)} \\
&\leq \|f - \mathrm{T}_{U^{(d,d_s)}} f\|_{\mathrm{L}_\infty(\mathbb{D}^d)} \\
&\quad + \|\mathrm{T}_{U^{(d,d_s)}} f - \mathrm{T}_U f\|_{\mathrm{L}_\infty(\mathbb{D}^d)} \\
&\quad + \left\|\mathrm{T}_U f - \mathrm{S}_{\mathcal{I}_N(U)} f\right\|_{\mathrm{L}_\infty(\mathbb{D}^d)}
\end{aligned}$$

For the first part, we have

$$\|f - \mathrm{T}_{U^{(d,d_s)}} f\|_{\mathrm{L}_\infty(\mathbb{D}^d)} \leq C_{\mathrm{BOS}} \sum_{\substack{\boldsymbol{k} \in \mathbb{Z}^d \\ |\operatorname{supp} \boldsymbol{k}| > d_s}} |c_{\boldsymbol{k}}(f)| \leq C_{\mathrm{BOS}} (1-\delta) \|f\|_{\mathcal{A}(\mathbb{D}^d, \omega^{(d)})}$$

by (4.29). The second part can be estimated as follows

$$\begin{aligned}
\|\mathrm{T}_{U^{(d,d_s)}} f - \mathrm{T}_U f\|_{\mathrm{L}_\infty(\mathbb{D}^d)} &\leq C_{\mathrm{BOS}} \sum_{\boldsymbol{u} \in U^{(d,d_s)} \setminus U} \sum_{\substack{\boldsymbol{k} \in \mathbb{Z}^d \\ \operatorname{supp} \boldsymbol{k} = \boldsymbol{u}}} |c_{\boldsymbol{k}}(f)| \\
&\leq C_{\mathrm{BOS}} \|f\|_{\mathcal{A}(\mathbb{D}^d, \omega^{(d)})} \sum_{\boldsymbol{u} \in U^{(d,d_s)} \setminus U} \varepsilon_{|\boldsymbol{u}|}
\end{aligned}$$

which yields our desired result. ∎

This concludes our considerations of the least-squares error for worst-case recovery as well as individual function recovery. In summary, we obtained bounds in the worst-case setting for the L_2 error and in the individual recovery setting for the L_2 and L_∞ error.

5

Numerical Experiments with Synthetic Data

In this chapter, we perform numerical experiments on synthetic data, i.e., we want to approximate a function $f\colon \mathbb{D}^d \to \mathbb{C}$ that is an element of $\mathrm{L}_2(\mathbb{D}^d, \omega^{(d)})$. The available scattered data is

$$D := \{(\boldsymbol{x}, f(\boldsymbol{x}) + \eta_{\boldsymbol{x}})\colon \boldsymbol{x} \in \mathcal{X}\} \subseteq \mathbb{D}^d \times \mathbb{C} \tag{5.1}$$

with $\mathcal{X} \subseteq \mathbb{D}^d$ being a finite set of nodes drawn i.i.d. at random according to the probability density $\omega^{(d)}$. In some cases, we add Gaussian noise $\eta_{\boldsymbol{x}}$, otherwise we have $\eta_{\boldsymbol{x}} \equiv 0$. Our goal is to recover the function f from the data D, i.e., determine approximations for basis coefficients $\mathrm{c}_{\boldsymbol{k}}(f)$ on grouped index sets $\mathcal{I}_{\boldsymbol{N}}(U)$ with bandwidths $\boldsymbol{N}$ from Definition 3.3 by applying the method from Section 4.2. Initially, we choose a superposition threshold $d_s \in [d]$ and use the set of ANOVA terms $U^{(d,d_s)}$ which we reduce to an *active set* $U^* \subseteq U^{(d,d_s)}$ via one or multiple ideas from Section 4.2.1. This requires us to compute approximations of the type

$$\mathrm{S}^{\mathcal{X}}_{\mathcal{I}_{\boldsymbol{N}}(U)} f = \sum_{\boldsymbol{k} \in \mathcal{I}_{\boldsymbol{N}}(U)} \hat{f}_{\boldsymbol{k}}\, \varphi^{(d)}_{\boldsymbol{k}},$$

see e.g. (4.4), for a general $U \subseteq \mathcal{P}([d])$ by solving the least-squares problem (4.3) or its regularized variant (4.8) with parameters $\lambda \geq 0$ and $\boldsymbol{W}$ a diagonal weight matrix. We specifically choose test functions with sparse ANOVA decompositions such that we have $f_{\boldsymbol{u}} \neq 0$ only for a subset $U^* \subseteq \mathcal{P}([d])$ of ANOVA terms. This has the goal to demonstrate the applicability of tools from Section 4.2.1.

We are going to use two kinds of error measures. The first one is the L_2 approximation error which can only be calculated if we have an explicit form for the norm $\|f\|_{L_2(\mathbb{D}^d,\omega^{(d)})}$ and the basis coefficients $c_{\boldsymbol{k}}(f)$. Then we define the error as

$$e_{L_2}(f, D, \mathcal{I}_{\boldsymbol{N}}(U)) \coloneqq \frac{\left\| f - S^{\mathcal{X}}_{\mathcal{I}_{\boldsymbol{N}}(U)} f \right\|_{L_2(\mathbb{D}^d,\omega^{(d)})}}{\|f\|_{L_2(\mathbb{D}^d,\omega^{(d)})}} \tag{5.2}$$
$$= \sqrt{1 - \frac{\sum_{\boldsymbol{k}\in\mathcal{I}_{\boldsymbol{N}}(U)} \left(\left| \hat{f}_{\boldsymbol{k}} - c_{\boldsymbol{k}}(f) \right|^2 - |c_{\boldsymbol{k}}(f)|^2 \right)}{\|f\|^2_{L_2(\mathbb{D}^d,\omega^{(d)})}}}.$$

This error can be regarded as a *generalization error* since it measures the deviation in the basis coefficients of the function f, i.e., the error itself has no random component. However, it is not always possible to compute it since the norm or the basis coefficients may not be known explicitly. In this case, we have to consider empirical errors, i.e., errors computed on a second set of nodes that have not been used in computing the approximation. We denote this set with

$$D_{\text{test}} \coloneqq \{(\boldsymbol{x}, f(\boldsymbol{x}) + \eta_{\boldsymbol{x}}) \colon \boldsymbol{x} \in \mathcal{X}_{\text{test}}\} \subseteq \mathbb{D}^d \times \mathbb{C} \tag{5.3}$$

since it is used to *test* the approximation. Here, $\mathcal{X}_{\text{test}}$ is again a finite set of nodes drawn i.i.d. at random according to $\omega^{(d)}$ and $\eta_{\boldsymbol{x}}$ is again Gaussian noise or $\eta_{\boldsymbol{x}} \equiv 0$. We define the *mean square error* (MSE) as

$$e_{\text{MSE}}(f, D, \mathcal{I}_{\boldsymbol{N}}(U), D_{\text{test}}) \coloneqq \frac{1}{|D_{\text{test}}|} \sum_{(\boldsymbol{x},y)\in D_{\text{test}}} \left| S^{\mathcal{X}}_{\mathcal{I}_{\boldsymbol{N}}(U)} f(\boldsymbol{x}) - y \right|^2. \tag{5.4}$$

This error contains a random component since it depends on the test set D_{test}. It represents an approximation on the L_2 error since we have for the expected value

$$\mathbb{E}\left[e_{\text{MSE}}(f, D, \mathcal{I}_{\boldsymbol{N}}(U), D_{\text{test}})\right] = \left\| f - S^{X}_{\mathcal{I}_{\boldsymbol{N}}(U)} f \right\|^2_{L_2(\mathbb{D}^d, \omega^{(d)})}.$$

Table 5.1 provides an overview of our experiments with synthetic data including references to the functions we used, whether we used noise and/or regularization, and the spatial dimension as well as the number of nodes.

d	$\lvert D\rvert$	noise	space	regularization	references	section
9	10000	no	$L_2(\mathbb{T}^9)$	$\boldsymbol{W} \neq \boldsymbol{I}$	[PV16, PS21a, BPS22]	5.1
8	10000	no	$L_2([-1,1]^8, \omega^{(d),\text{cheb}})$	no	[PV17, PS22a]	5.2
10	200	yes	$L_2([0,1]^{10})$	$\boldsymbol{W} = \boldsymbol{I}$	[MLH03, PS21b]	5.3.1
4	200	yes	$L_2([0,1]^4)$	$\boldsymbol{W} = \boldsymbol{I}$	[MLH03, PS21b]	5.3.2
4	200	yes	$L_2([0,1]^4)$	$\boldsymbol{W} = \boldsymbol{I}$	[MLH03, PS21b]	5.3.3

Table 5.1: Overview of the experiments with synthetic data. In the column *regularization*, we refer to smoothness weights $\boldsymbol{W} \neq \boldsymbol{I}$ as in (4.9) or standard Tikhonov regularization with $\boldsymbol{W} = \boldsymbol{I}$ otherwise. The spaces and their respective bases have been considered in Section 2.1.2.

5.1 Periodic B-Spline Function

In this section, we consider the 9-dimensional 1-periodic function

$$\begin{aligned} f &: \mathbb{T}^9 \to \mathbb{R}, \\ \boldsymbol{x} &\mapsto B_2(x_1)B_4(x_3)B_6(x_8) + B_2(x_2)B_4(x_5)B_6(x_6) + B_2(x_4)B_4(x_7)B_6(x_9), \end{aligned} \tag{5.5}$$

where B_2, B_4 and B_6 are parts of univariate, shifted, scaled, and dilated B-splines of order 2, 4, and 6, respectively. The function f is an element of the space $\mathrm{L}_2(\mathbb{T}^9)$. The Fourier series of the B-splines is given by

$$B_j(x) \coloneqq c_j \sum_{k\in\mathbb{Z}} \operatorname{sinc}^j\left(\frac{\pi\cdot k}{j}\right)\cos(\pi\cdot k)\,\mathrm{e}^{2\pi\mathrm{i}k\cdot x} \quad \text{for} \quad j = 2,4,6,$$

with $\operatorname{sinc}(x) \coloneqq \sin(x)/x$ and the three normalization constants

$$c_2 \coloneqq \sqrt{\frac{3}{4}}, \quad c_4 \coloneqq \sqrt{\frac{315}{604}}, \quad \text{and} \quad c_6 \coloneqq \sqrt{\frac{277200}{655177}}$$

such that $\left\|B_j\right\|_{\mathrm{L}_2(\mathbb{T})} = 1$, $j = 2,4,6$.

For this function, we have an explicit form for the Fourier coefficients $\mathrm{c}_{\boldsymbol{k}}(f)$ and the norm $\|f\|_{\mathrm{L}_2(\mathbb{T}^9)}$, i.e., the generalization error e_{L_2} from (5.2) can be computed. Moreover, the function f has superposition dimension $d^{(\mathrm{sp})}(\delta) = 3$, see (2.26), for $\delta = 1$, i.e., it can be represented by at most three-dimensional ANOVA terms with $f = \mathrm{T}_3 f$. This leads to $d_s = 3$ being the optimal choice for the superposition threshold with no error caused by the ANOVA truncation. We have the active set of terms

$$U^* \coloneqq \mathcal{P}(\{1,3,8\}) \cup \mathcal{P}(\{2,5,6\}) \cup \mathcal{P}(\{4,7,9\})$$

with $f_{\boldsymbol{u}} \equiv 0$ for $\boldsymbol{u} \notin U^*$. The function also has dominating-mixed smoothness of $3/2 - \varepsilon$ for every $\varepsilon > 0$, i.e., $f \in \mathrm{H}^{\omega_\varepsilon}(\mathbb{T}^9)$ with

$$\omega_\varepsilon(\boldsymbol{k}) = \prod_{j\in\operatorname{supp}\boldsymbol{k}} (1 + |k_j|)^{\frac{3}{2}-\varepsilon}.$$

In [PV16, PS21a, BPS22] a test function similar to f was also considered as a benchmark function for different methods. Note that [PV16] dealt with the problem of *active learning* or *black-box approximation* where the function is given as a black-box and can be evaluated anywhere. They made use of rank-1 lattices as sampling schemes.

The ANOVA terms $f_{\boldsymbol{u}}$ can be computed analytically such that we obtain

$$f_{\emptyset} = 3 \prod_{j \in \{2,4,6\}} c_j$$
$$f_{\{i\}}(x_i) = \frac{\prod_{j \in \{2,4,6\}} c_j}{c_{\mathrm{o}(i)}} \left(B_{\mathrm{o}(i)}(x_i) - c_{\mathrm{o}(i)} \right) \tag{5.6}$$

for the constant and the one-dimensional terms with $i = 1, 2, \ldots, 9$ and

$$\mathrm{o}(i) \coloneqq \begin{cases} 2 & : i \in \{1,2,4\}, \\ 4 & : i \in \{3,5,7\}, \\ 6 & : i \in \{8,6,9\}. \end{cases}$$

We find for the two-dimensional terms $f_{\boldsymbol{u}}$, $\boldsymbol{u} = \{i, j\}$, $i, j \in \{1, 2, \ldots, 9\}$, that $f_{\{i,j\}} \equiv 0$ for $\boldsymbol{u} \notin U^*$ and

$$f_{\{i,j\}}(x_{\{i,j\}}) = \frac{\prod_{j \in \{2,4,6\}} c_j}{c_{\mathrm{o}(i)} c_{\mathrm{o}(j)}} \left(B_{\mathrm{o}(i)}(x_i) - c_{\mathrm{o}(i)} \right) \left(B_{\mathrm{o}(j)}(x_j) - c_{\mathrm{o}(j)} \right) \tag{5.7}$$

for $\boldsymbol{u} \in U^*$. Finally, we get for the three-dimensional terms $f_{\boldsymbol{u}}$, $\boldsymbol{u} = \{i, j, \ell\}$, $i, j, \ell \in \{1, 2, \ldots, 9\}$, that $f_{\boldsymbol{u}} \equiv 0$ again for $\boldsymbol{u} \notin U^*$ and

$$f_{\{i,j,\ell\}}(x_{\{i,j,\ell\}}) = \left(B_{\mathrm{o}(i)}(x_i) - c_{\mathrm{o}(i)} \right) \left(B_{\mathrm{o}(j)}(x_j) - c_{\mathrm{o}(j)} \right) \left(B_{\mathrm{o}(\ell)}(x_\ell) - c_{\mathrm{o}(\ell)} \right) \tag{5.8}$$

for $\boldsymbol{u} \in U^*$.

As available data, we have

$$D = \{(\boldsymbol{x}, f(\boldsymbol{x})) \colon \boldsymbol{x} \in \mathcal{X}\},$$

cf. (5.1), with a node set $\mathcal{X} \subseteq \mathbb{T}^9$ of $|\mathcal{X}| = 10000$ nodes drawn i.i.d. uniformly at random. Using the ANOVA approximation method from Chapter 4, we aim to recover the information that U^* is the active set of terms as well as an approximation for f. We begin with no regularization, i.e., we solve least-squares problems of type (4.3). Any form of attribute ranking will not be able to detect the sparsity in the set

of ANOVA terms $U^{(9,3)}$ since every variable $x_1, x_2, \ldots, x_9$ itself plays a role.

We start by using grouped index sets $\mathcal{I}_{\boldsymbol{N}}(U^{(9,3)})$ with different bandwidth parameters $\boldsymbol{N}$. Here, we are for now not particularly interested in the error $e_{\mathrm{L}_2}(f, D, \mathcal{I}_{\boldsymbol{N}}(U^{(9,3)}))$, but the detection of the active set U^*. We aim to determine this set via the global sensitivity cut-off from (4.15). Therefore, we have to check the existence of a threshold vector $\boldsymbol{\varepsilon} \in (0,1)^3$ such that $U^{(\mathrm{gsi},\boldsymbol{\varepsilon})} = U^*$. The choice for the entries of $\boldsymbol{\varepsilon}$ lies in the intervals

$$\varepsilon_i \in I_i := \left(\max_{\substack{\boldsymbol{u} \in U^{(9,3)} \setminus U^* \\ |\boldsymbol{u}| = i}} \varrho(\boldsymbol{u}, \mathrm{S}^{\mathcal{X}}_{\mathcal{I}_{\boldsymbol{N}}(U)} f), \quad \min_{\substack{\boldsymbol{u} \in U^* \\ |\boldsymbol{u}| = i}} \varrho(\boldsymbol{u}, \mathrm{S}^{\mathcal{X}}_{\mathcal{I}_{\boldsymbol{N}}(U)} f) \right), \quad i = 1, 2, 3. \tag{5.9}$$

In other words, a larger interval I_i implies that the active terms in U^* are better separated from the inactive terms in the complement $U^{(9,3)} \setminus U^*$.

$\boldsymbol{N}$	$\lvert\mathcal{I}_{\boldsymbol{N}}\rvert$	e_{L_2}	I_1	I_2	I_3
$[16, 4, 2]$	544	$2.7 \cdot 10^{-1}$	$(0.0, 2.4 \cdot 10^{-2})$	$(2.2 \cdot 10^{-4}, 2.1 \cdot 10^{-2})$	$(6.5 \cdot 10^{-5}, 2.8 \cdot 10^{-3})$
$[32, 4, 2]$	688	$2.8 \cdot 10^{-1}$	$(0.0, 2.4 \cdot 10^{-2})$	$(2.2 \cdot 10^{-4}, 2.1 \cdot 10^{-2})$	$(6.8 \cdot 10^{-5}, 2.8 \cdot 10^{-3})$
$[64, 8, 2]$	2416	$2.5 \cdot 10^{-1}$	$(0.0, 2.3 \cdot 10^{-2})$	$(7.5 \cdot 10^{-4}, 2.1 \cdot 10^{-2})$	$(4.3 \cdot 10^{-5}, 2.6 \cdot 10^{-3})$
$[64, 8, 4]$	4600	$1.1 \cdot 10^{-1}$	$(0.0, 2.2 \cdot 10^{-2})$	$(1.3 \cdot 10^{-4}, 2.0 \cdot 10^{-2})$	$(8.0 \cdot 10^{-5}, 2.4 \cdot 10^{-2})$
$[64, 16, 4]$	10936	$3.9 \cdot 10^{-1}$	$(0.0, 1.8 \cdot 10^{-2})$	$(4.9 \cdot 10^{-3}, 2.0 \cdot 10^{-2})$	$(8.0 \cdot 10^{-4}, 1.9 \cdot 10^{-2})$

Table 5.2: Approximation of f from (5.5) with different bandwidth vectors $\boldsymbol{N}$ and grouped index set $\mathcal{I}_{\boldsymbol{N}} := \mathcal{I}_{\boldsymbol{N}}(U^{(9,3)})$. The generalization error is denoted as $e_{\mathrm{L}_2} := e_{\mathrm{L}_2}(f, D, \mathcal{I}_{\boldsymbol{N}}(U^{(9,3)}))$ and the intervals I_1, I_2, and I_3 from (5.9). All results are the average of running the experiment on 10 randomly generated data sets D.

Table 5.2 shows the results from experiments with different bandwidth vectors $\boldsymbol{N}$. Clearly, the approximation error $e_{\mathrm{L}_2}(f, D, \mathcal{I}_{\boldsymbol{N}}(U^{(9,3)}))$ itself is not great. However, the active terms are well-separated from the inactive terms for any of the bandwidths and we have large intervals I_i

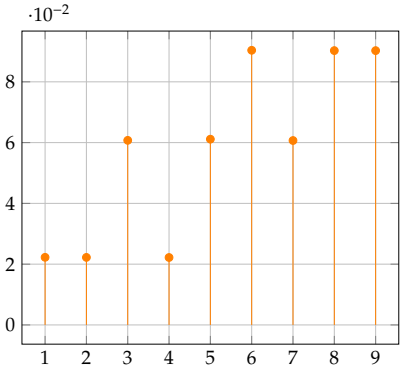

(a) $\varrho(\boldsymbol{u}, \mathrm{S}^{\mathcal{X}}_{\mathcal{I}_N(U^{(9,3)})} f)$ for $|\boldsymbol{u}| = 1$, $\binom{9}{1} = 9$ terms.

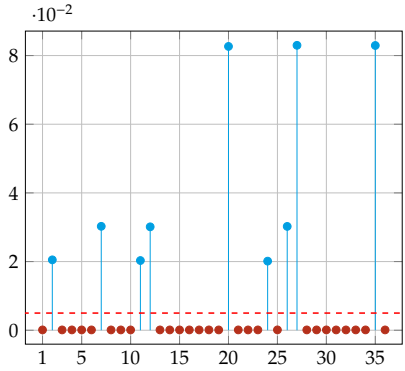

(b) $\varrho(\boldsymbol{u}, \mathrm{S}^{\mathcal{X}}_{\mathcal{I}_N(U^{(9,3)})} f)$ for $|\boldsymbol{u}| = 2$, $\binom{9}{2} = 26$ terms. Inactive terms with $\boldsymbol{u} \notin U^*$ in red.

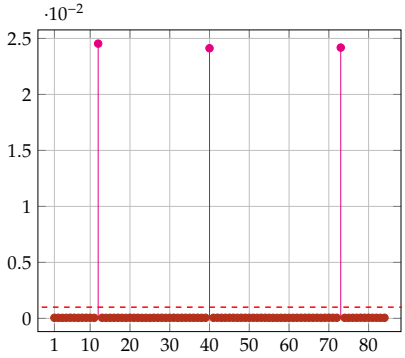

(c) $\varrho(\boldsymbol{u}, \mathrm{S}^{\mathcal{X}}_{\mathcal{I}_N(U^{(9,3)})} f)$ for $|\boldsymbol{u}| = 3$, $\binom{9}{3} = 84$ terms. Inactive terms with $\boldsymbol{u} \notin U^*$ in red.

Figure 5.1: Global sensitivity indices $\varrho(\boldsymbol{u}, \mathrm{S}^{\mathcal{X}}_{\mathcal{I}_N(U^{(9,3)})} f)$ for bandwidths $\boldsymbol{N} = [64, 8, 4]$.

to choose the threshold parameters ε_i such that we are able to detect the active set with $U^{(\mathrm{gsi},\varepsilon)} = U^*$. In summary, the first step of our method was successful and we were able to exactly determine U^*. Figure 5.1 depicts the global sensitivity indices for the experiment from Table 5.2 with bandwidths $\boldsymbol{N} = [64, 8, 4]$. If we compare to the one-dimensional indices in Figure 5.1a to the definition of the corresponding terms (5.6), we observe that we have three types of smoothness depending on the order of involved B-splines which results in the sensitivity indices being grouped around three values. The same connection between the smoothness of the terms and the groups can be observed for the two-dimensional terms (5.7) in Figure 5.1b and the three-dimensional terms (5.8) in Figure 5.1c.

For the second step, we now aim to obtain a good approximation on f. To this end, we choose to use a grouped index set $\mathcal{I}_{\boldsymbol{M}}(U^*)$ with larger bandwidths $\boldsymbol{M} \in (2\mathbb{N})^3$ than before. Note that we would also be able to choose individual bandwidths for each $\boldsymbol{u} \in U^*$. Table 5.3 shows the results of our experiments. Note that we were able to significantly increase the bandwidths from the previous experiments and as a result, we were able to decrease the error e_{L_2} about one order in the exponent. Therefore, our two step method was successful, i.e., we have not only detected the active set of terms U^*, but also approximated a 9-dimensional function using only 10000 data points with an error of about $1.4 \cdot 10^{-2}$. For this function, we are also able to compute the bound from Theorem 4.12 for individual function approximation. The truncation error e_2 from (4.26) can be computed explicitly while we estimate the truncation error e_∞ from (4.26) in L_∞ as

$$\tilde{e}_\infty \coloneqq \sum_{\boldsymbol{k} \in \mathbb{Z}^d \setminus \mathcal{I}} |\mathrm{c}_{\boldsymbol{k}}(f)| \geq e_\infty$$

for an index set $\mathcal{I} \subseteq \mathbb{Z}^d$. We have visualized the relative e_{L_2} error compared to the relative bound

$$\mathcal{B} = \frac{1}{\|f\|_{\mathrm{L}_2(\mathbb{T}^9)}} \left(3e_2^2 + \frac{2e_2\tilde{e}_\infty}{\sqrt{5\,|\mathcal{I}_{\boldsymbol{N}}(U)|}} + \frac{2\tilde{e}_\infty^2}{15\,|\mathcal{I}_{\boldsymbol{N}}(U)|} \right) \tag{5.10}$$

in Figure 5.2.

$\boldsymbol{M}$	$\lvert\mathcal{I}_{\boldsymbol{M}}(U^*)\rvert$	e_{L_2}
$[80, 16, 12]$	6730	$1.4 \cdot 10^{-2}$
$[90, 18, 14]$	9994	$1.7 \cdot 10^{-1}$
$[80, 14, 10]$	4420	$1.5 \cdot 10^{-2}$
$[80, 10, 10]$	3628	$1.9 \cdot 10^{-2}$
$[70, 16, 12]$	6640	$1.4 \cdot 10^{-2}$

Table 5.3: Approximation of f from (5.5) with different bandwidth vectors $\boldsymbol{M}$ and grouped index set $\mathcal{I}_{\boldsymbol{M}}(U^*)$. The generalization error is denoted as $e_{\mathrm{L}_2} \coloneqq e_{\mathrm{L}_2}(f, D, \mathcal{I}_{\boldsymbol{M}}(U^*))$. All results are the average over computing the approximation with 10 randomly generated data sets D.

We conclude our considerations of this test function by repeating the experiments using the weighted regularization idea from Section 4.1.2. Since we know that $f \in \mathrm{H}^{\omega_\varepsilon}(\mathbb{T}^9)$, we define the weight matrix

$$\boldsymbol{W}_{\mathcal{I}} = \operatorname{diag}\left(\prod_{j \in \operatorname{supp} \boldsymbol{k}} (1 + \left|k_j\right|)^{\frac{3}{2}}\right)_{\boldsymbol{k} \in \mathcal{I}}$$

for a finite index set $\mathcal{I}$. Now, we perform the experiments from Table 5.2 again, but this time we solve the regularized least-squares problem (4.8) and also add the larger bandwidths from Table 5.3 to the test in order to see the effect of reducing the search space with this type of regularization, cf. Section 4.1.2. In Table 5.4 we see that the regularization makes an enormous difference when it comes to the oversampling. While the error slightly improves in comparison to the results in Table 5.2, we even achieve comparable errors for around 200000 indices, i.e., 20 times more indices than nodes. In Table 5.5 we repeated the experiments of Table 5.3, showing the same phenomenon which also allows us to decrease the error slightly.

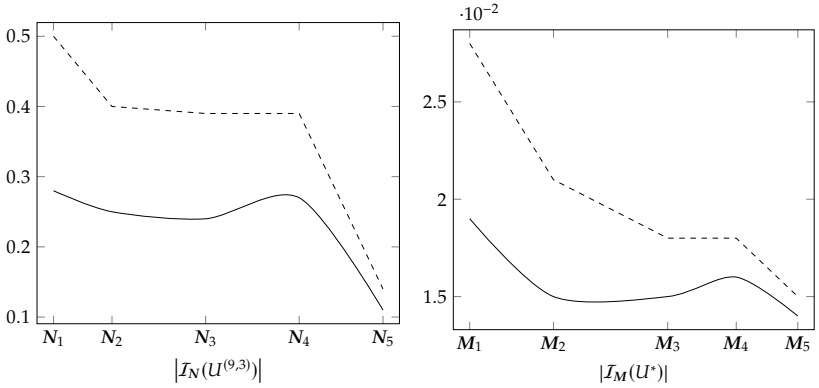

(a) Approximation error $e_{\mathrm{L}_2}(f, D, \mathcal{I}_N(U^{(9,3)}))$ (solid) and error bound $\mathcal{B}$ from (5.10) (dashed) for bandwidths $N_1 = [16, 4, 2]$, $N_2 = [32, 6, 4]$, $N_3 = [64, 8, 2]$, $N_4 = [64, 10, 2]$, and $N_5 = [64, 8, 4]$.

(b) Approximation error $e_{\mathrm{L}_2}(f, D, \mathcal{I}_M(U^*))$ (solid) and error bound $\mathcal{B}$ from (5.10) (dashed) for bandwidths $N_1 = [80, 10, 10]$, $N_2 = [80, 14, 10]$, $N_3 = [80, 18, 10]$, $N_4 = [80, 20, 10]$, and $N_5 = [80, 16, 12]$.

Figure 5.2: Visualization of approximation errors and the error bounds from Section 4.3.2.

$\boldsymbol{N}$	$\lvert\mathcal{I}_{\boldsymbol{N}}\rvert$	λ	e_{L_2}	I_1	I_2	I_3
[16, 4, 2]	544	e^3	$2.7 \cdot 10^{-1}$	$(0.0, 2.5 \cdot 10^{-2})$	$(2.1 \cdot 10^{-4}, 2.1 \cdot 10^{-2})$	$(6.1 \cdot 10^{-5}, 2.6 \cdot 10^{-3})$
[32, 4, 2]	688	e^4	$2.7 \cdot 10^{-1}$	$(0.0, 2.5 \cdot 10^{-2})$	$(2.1 \cdot 10^{-4}, 2.1 \cdot 10^{-2})$	$(6.0 \cdot 10^{-5}, 2.5 \cdot 10^{-3})$
[64, 8, 2]	2416	e^4	$2.4 \cdot 10^{-1}$	$(0.0, 2.4 \cdot 10^{-2})$	$(5.1 \cdot 10^{-4}, 2.0 \cdot 10^{-2})$	$(3.5 \cdot 10^{-5}, 2.2 \cdot 10^{-3})$
[64, 8, 4]	4600	e^3	$1.0 \cdot 10^{-1}$	$(0.0, 2.3 \cdot 10^{-2})$	$(9.6 \cdot 10^{-5}, 2.0 \cdot 10^{-2})$	$(5.7 \cdot 10^{-5}, 2.1 \cdot 10^{-2})$
[64, 16, 4]	10936	e^3	$1.2 \cdot 10^{-1}$	$(0.0, 2.3 \cdot 10^{-2})$	$(2.7 \cdot 10^{-4}, 2.0 \cdot 10^{-2})$	$(7.2 \cdot 10^{-5}, 1.9 \cdot 10^{-2})$
[80, 16, 12]	120616	e^0	$2.3 \cdot 10^{-1}$	$(0.0, 2.7 \cdot 10^{-2})$	$(3.0 \cdot 10^{-4}, 1.6 \cdot 10^{-2})$	$(2.6 \cdot 10^{-4}, 9.4 \cdot 10^{-3})$
[90, 18, 14]	195754	e^0	$2.5 \cdot 10^{-1}$	$(0.0, 2.7 \cdot 10^{-2})$	$(3.3 \cdot 10^{-4}, 1.6 \cdot 10^{-2})$	$(2.7 \cdot 10^{-4}, 8.1 \cdot 10^{-3})$

Table 5.4: Approximation of f from (5.5) with different bandwidth vectors $\boldsymbol{N}$ and grouped index set $\mathcal{I}_{\boldsymbol{N}} := \mathcal{I}_{\boldsymbol{N}}(U^{(9,3)})$. The generalization error is denoted as $e_{\mathrm{L}_2} := e_{\mathrm{L}_2}(f, D, \mathcal{I}_{\boldsymbol{N}}(U^{(9,3)}))$ and the intervals I_1, I_2, and I_3 from (5.9). We apply weighted regularization with $\boldsymbol{W}_{\mathcal{I}_{\boldsymbol{N}}}$ as in (4.8) with λ being the best choice of regularization parameter from $\mathrm{e}^t, t = 0, 1, \ldots, 5$. All results are the average of running the experiment on 10 randomly generated data sets D.

$\boldsymbol{M}$	$\lvert\mathcal{I}_{\boldsymbol{M}}(U^*)\rvert$	λ	e_{L_2}
[80, 16, 12]	6730	e^0	$1.3 \cdot 10^{-2}$
[90, 18, 14]	9994	e^0	$1.4 \cdot 10^{-2}$
[80, 14, 10]	4420	e^0	$1.5 \cdot 10^{-2}$
[80, 10, 10]	3628	e^1	$1.8 \cdot 10^{-2}$
[70, 16, 12]	6640	e^0	$1.3 \cdot 10^{-2}$
[100, 20, 14]	10732	e^0	$1.4 \cdot 10^{-2}$
[120, 24, 16]	15958	e^0	$1.7 \cdot 10^{-2}$

Table 5.5: Approximation of f from (5.5) with different bandwidth vectors $\boldsymbol{M}$ and grouped index set $\mathcal{I}_{\boldsymbol{M}}(U^*)$. The generalization error is denoted as $e_{\mathrm{L}_2} := e_{\mathrm{L}_2}(f, D, \mathcal{I}_{\boldsymbol{M}}(U^*))$. All results are the average over computing the approximation with 10 randomly generated data sets D.

5.2 Non-Periodic B-Spline Function

In this section, we consider the non-periodic function

$$f\colon [-1,1]^8 \to \mathbb{R}, \qquad (5.11)$$
$$f(\boldsymbol{x}) = B_2(x_1)B_4(x_5) + B_2(x_2)B_4(x_6) + B_2(x_3)B_4(x_7) + B_2(x_4)B_4(x_8),$$

with B_2 and B_4 being parts of the univariate shifted, scaled and dilated B-splines from the previous Section 5.1. We have visualized the two B-splines in Figure 5.3. The function f is an element of $\mathrm{L}_2([-1,1]^8, \omega^{(d),\,\mathrm{cheb}})$ and we have normalized the splines such that $\|B_2\|_{\mathrm{L}_2([-1,1]^8,\omega^{(d),\,\mathrm{cheb}})} = \|B_4\|_{\mathrm{L}_2([-1,1]^8,\omega^{(d),\,\mathrm{cheb}})} = 1$.

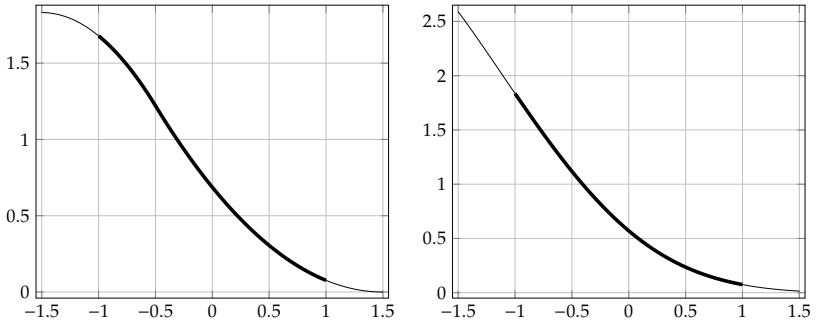

(a) $B_2\colon [-1,1] \to \mathbb{R}$ highlighted in bold.

(b) $B_4\colon [-1,1] \to \mathbb{R}$ highlighted in bold.

Figure 5.3: B-Splines B_2 and B_4 from (5.11).

For this function, we have an active set

$$U^* \coloneqq \emptyset \cup \mathcal{P}(\{1,5\}) \cup \mathcal{P}(\{2,6\}) \cup \mathcal{P}(\{3,7\}) \cup \mathcal{P}(\{4,8\})$$

such that $f_{\boldsymbol{u}} \equiv 0$ for $\boldsymbol{u} \in \mathcal{P}([d]) \setminus U^*$. This implies that we have the superposition dimension $d^{(\mathrm{sp})}(\delta) = 2$ for $\delta = 1$, i.e., $f = \mathrm{T}_2 f$, see (2.26). We can also explicitly compute the basis coefficients

$$\mathrm{c}_{\boldsymbol{k}}(f) = \langle f, \varphi_{\boldsymbol{k}}^{(d),\,\mathrm{cheb}} \rangle_{\mathrm{L}_2([-1,1]^8,\omega^{(d),\,\mathrm{cheb}})}$$

and the norm $\|f\|_{L_2([-1,1]^8,\omega^{(d),\,\mathrm{cheb}})}$, i.e., the generalization error e_{L_2} from (5.2) is available.

As for the periodic function in Section 5.1, it is our goal to recover the active set U^* and obtain a good approximation for f from the data

$$D = \{(\boldsymbol{x}, f(\boldsymbol{x})) \colon \boldsymbol{x} \in \mathcal{X}\}\,.$$

Here, we have a set $\mathcal{X} \subseteq [-1,1]^8$ of $|\mathcal{X}| = 10000$ nodes drawn i.i.d. at random according to the Chebyshev probability density $\omega^{(d),\,\mathrm{cheb}}$. The superposition threshold will be set to $d_s = 3$, i.e., we start by taking also 3-dimensional terms into account. We do this to show that starting with a higher superposition threshold d_s will still lead to the correct active set U^*. We use the global sensitivity cut-off method from (4.15), i.e., we are looking for a threshold vector $\boldsymbol{\varepsilon} \in (0,1)^3$ such that $U^{(\mathrm{gsi},\varepsilon)} = U^*$. The choice for the entries of $\boldsymbol{\varepsilon}$ lie in the intervals

$$\varepsilon_i \in I_i \coloneqq \left(\max_{\substack{\boldsymbol{u} \in U^{(8,3)} \setminus U^* \\ |\boldsymbol{u}| = i}} \varrho(\boldsymbol{u}, \mathrm{S}^{\mathcal{X}}_{\mathcal{I}_N(U)} f), \quad \min_{\substack{\boldsymbol{u} \in U^* \\ |\boldsymbol{u}| = i}} \varrho(\boldsymbol{u}, \mathrm{S}^{\mathcal{X}}_{\mathcal{I}_N(U)} f) \right), \quad i = 1, 2. \tag{5.12}$$

A larger interval I_i implies that the active terms in U^* are better separated from the inactive terms in the complement $U^{(8,3)} \setminus U^*$. For $|\boldsymbol{u}| = 3$ we are hoping that the value

$$\varrho_3 \coloneqq \max_{\substack{\boldsymbol{u} \in U^{(8,3)} \setminus U^* \\ |\boldsymbol{u}| = 3}} \varrho(\boldsymbol{u}, \mathrm{S}^{\mathcal{X}}_{\mathcal{I}_N(U)} f) \tag{5.13}$$

is small in order to correctly recognize that there are no terms $\boldsymbol{u} \in U^*$ with $|\boldsymbol{u}| = 3$.

The experiments from Table 5.6 show promising results already for the generalization error as well as the active set detection. We have a clear separation of active terms in U^* and inactive terms in its complement yielding large intervals I_1 and I_2. The 3-dimensional terms are correctly not attributed any importance with the quantity ϱ_3 being in the range of 10^{-10}. The global sensitivity indices are also visualized in Figure 5.4.

Now, we choose to use a grouped index set $\mathcal{I}_{\boldsymbol{M}}(U^*)$ with larger bandwidths $\boldsymbol{M} \in \mathbb{N}^2$ than before to obtain a better approximation. Note that $\boldsymbol{M}$ now only has two entries since there is no three-dimensional term in the active set U^*. The results of the experiments are displayed in Table 5.7. We observe that we can decrease the generalization error further obtaining a final approximation with $e_{\mathrm{L}_2}(f, D, \mathcal{I}_{\boldsymbol{M}}(U^*)) \approx 3.3 \cdot 10^{-4}$.

$\boldsymbol{N}$	$\lvert\mathcal{I}_{\boldsymbol{N}}\rvert$	e_{L_2}	I_1	I_2	ϱ_3
$[16, 8, 2]$	1549	$7.0 \cdot 10^{-4}$	$(0.0, 8.6 \cdot 10^{-2})$	$(9.8 \cdot 10^{-9}, 5.9 \cdot 10^{-2})$	$8.2 \cdot 10^{-10}$
$[16, 16, 2]$	6477	$4.3 \cdot 10^{-4}$	$(0.0, 8.6 \cdot 10^{-2})$	$(6.4 \cdot 10^{-9}, 5.9 \cdot 10^{-2})$	$1.7 \cdot 10^{-10}$
$[32, 8, 2]$	1677	$7.0 \cdot 10^{-4}$	$(0.0, 8.6 \cdot 10^{-2})$	$(9.4 \cdot 10^{-9}, 5.9 \cdot 10^{-2})$	$8.1 \cdot 10^{-10}$
$[32, 16, 2]$	6605	$3.8 \cdot 10^{-4}$	$(0.0, 8.6 \cdot 10^{-2})$	$(2.9 \cdot 10^{-9}, 5.9 \cdot 10^{-2})$	$7.2 \cdot 10^{-11}$
$[16, 8, 4]$	3005	$7.6 \cdot 10^{-4}$	$(0.0, 8.6 \cdot 10^{-2})$	$(1.2 \cdot 10^{-8}, 5.9 \cdot 10^{-2})$	$8.6 \cdot 10^{-9}$

Table 5.6: Approximation of f from (5.11) with different bandwidth vectors $\boldsymbol{N}$ and grouped index set $\mathcal{I}_{\boldsymbol{N}} \coloneqq \mathcal{I}_{\boldsymbol{N}}(U^{(8,3)})$. The generalization error is denoted as $e_{\mathrm{L}_2} \coloneqq e_{\mathrm{L}_2}(f, D, \mathcal{I}_{\boldsymbol{N}}(U^{(8,3)}))$ and the intervals I_1, I_2 from (5.12), and ϱ_3 from (5.13). All results are the average of running the experiment on 10 randomly generated sets of nodes $\mathcal{X}$.

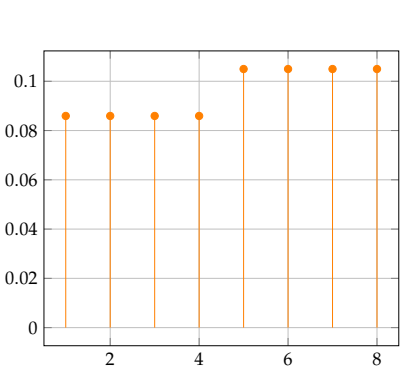

(a) $\varrho(\boldsymbol{u}, \mathrm{S}^{\mathcal{X}}_{\mathcal{I}_N(U^{(8,3)})} f)$ for $|\boldsymbol{u}| = 1$, $\binom{8}{1} = 8$ terms.

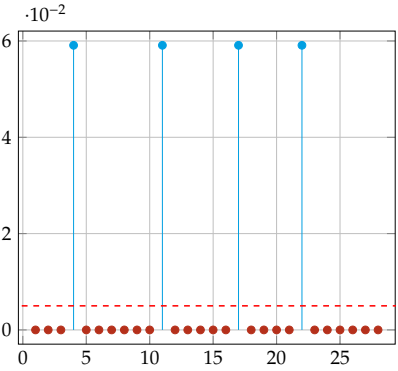

(b) $\varrho(\boldsymbol{u}, \mathrm{S}^{\mathcal{X}}_{\mathcal{I}_N(U^{(8,3)})} f)$ for $|\boldsymbol{u}| = 2$, $\binom{8}{2} = 28$ terms. Inactive terms with $\boldsymbol{u} \notin U^*$ in red.

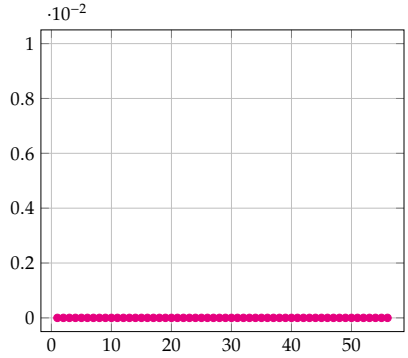

(c) $\varrho(\boldsymbol{u}, \mathrm{S}^{\mathcal{X}}_{\mathcal{I}_N(U^{(8,3)})} f)$ for $|\boldsymbol{u}| = 3$, $\binom{8}{3} = 56$ terms. All terms are inactive with $\boldsymbol{u} \notin U^*$.

Figure 5.4: Global sensitivity indices $\varrho(\boldsymbol{u}, \mathrm{S}^{\mathcal{X}}_{\mathcal{I}_N(U^{(8,3)})} f)$ for bandwidths $\boldsymbol{N} = [32, 16, 2]$.

$\boldsymbol{M}$	$\lvert\mathcal{I}_{\boldsymbol{M}}(U^*)\rvert$	e_{L_2}
$[60, 30]$	3837	$3.4 \cdot 10^{-4}$
$[60, 36]$	5373	$3.3 \cdot 10^{-4}$
$[60, 42]$	7197	$1.0 \cdot 10^{-3}$
$[80, 30]$	3997	$3.4 \cdot 10^{-4}$
$[80, 36]$	5533	$3.3 \cdot 10^{-4}$
$[80, 42]$	7357	$1.4 \cdot 10^{-3}$

Table 5.7: Approximation of f from (5.11) with different bandwidth vectors $\boldsymbol{M}$ and grouped index set $\mathcal{I}_{\boldsymbol{M}}(U^*)$. The generalization error is denoted as $e_{\mathrm{L}_2} \coloneqq e_{\mathrm{L}_2}(f, D, \mathcal{I}_{\boldsymbol{M}}(U^*))$. All results are the average over computing the approximation with 10 randomly generated data sets D.

5.3 Friedman Functions

The Friedman functions are a class of functions used for benchmarking scattered data approximation, see e.g. [MLH03, BGM09, BDL11]. We start by defining the three non-periodic Friedman functions over $[0,1]^d$.

The Friedman 1 function

$$f_1 \colon [0,1]^{10} \to \mathbb{R},\ f_1(\boldsymbol{x}) = 10\sin(\pi x_1 x_2) + 20(x_3 - 0.5)^2 + 10x_4 + 5x_5$$

has spatial dimension $d = 10$. However, only five of the ten variables have any influence on the function which is the most important information we aim to find with an attribute ranking. Additionally, we have the superposition dimension $d^{(\mathrm{sp})}(\delta) = 2$ for $\delta = 1$, i.e., $\mathrm{T}_2 f = f$, see (2.26). The Friedman 2 function

$$f_2 \colon [0,1]^4 \to \mathbb{R},\ f_2(\boldsymbol{x}) = \sqrt{s_1^2(x_1) + \left(s_2(x_2)\cdot x_3 - \frac{1}{s_2(x_2)\cdot s_4(x_4)}\right)^2}$$

has spatial dimension 4 and contains the variable scalings $s_1(x_1) = 100x_1$, $s_2(x_2) = 520\pi x_2 + 40\pi$, and $s_4(x_4) = 10x_4 + 1$. The scalings ensure that we have $x_i \in [0,1]$, $i = 1,2,3,4$. The third and last Friedman function is given by

$$f_3 \colon [0,1]^4 \to \mathbb{R},\ f_3(\boldsymbol{x}) = \arctan\left(\frac{s_2(x_2)\cdot x_3 - (s_2(x_2)\cdot s_4(x_4))^{-1}}{s_1(x_1)}\right)$$

again with spatial dimension $d = 4$ and the same scalings s_1, s_2, and s_4 as before. Here, every term is (analytically) non-zero which means that entire function can only be reconstructed for a superposition threshold $d_s = 4$ without an ANOVA truncation error.

The three functions f_1, f_2, and f_3 are elements of the space $\mathrm{L}_2([0,1]^d)$ for their respective spatial domain d. However, we do not have access to an explicit form of the norm $\|f\|_{\mathrm{L}_2([0,1]^d)}$ and the basis coefficients $\mathrm{c}_{\boldsymbol{k}}(f) = \langle f, \varphi_{\boldsymbol{k}}^{(d),\cos}\rangle_{\mathrm{L}_2([0,1]^d)}$, i.e., we have to rely on the empirical error. Since it is our goal to compare to the results in [MLH03], we use the mean square error (MSE) $e_{\mathrm{MSE}}(f, D, \mathcal{I}_N(U), D_{\mathrm{test}})$ from (5.4). As in

[MLH03], our data D, cf. (5.1), will always consist of 200 nodes and noisy function evaluations. For the test data D_{test}, cf. (5.3), we validate our model on 1000 nodes and also apply noise to the evaluations.

Table 5.8 shows benchmark data from [MLH03] with a support vector machine (SVM), a linear model (LM), a neural network (MNET) and a random forest (RFORST) together with the results from our method (ANOVAapprox). In the following sections we present the detailed procedure on how to obtain the models for ANOVAapprox.

	SVM	LM	MNET	RFORST	ANOVAapprox
Friedman 1	4.36	7.71	9.21	6.02	**1.43**
Friedman 2 ($\cdot 10^3$)	18.13	36.15	19.61	21.50	**17.18**
Friedman 3 ($\cdot 10^{-3}$)	23.15	45.42	**18.12**	22.21	20.69

Table 5.8: Mean squared errors (MSE) for different methods when approximating Friedman functions in [MLH03] compared to ANOVAapprox. The value for ANOVAapprox was obtained by computing the approximation on 100 randomly generated data sets D and validating them on 100 randomly generated test sets D_{test}. All values are the medians of the mean square errors and the best value for every function is highlighted.

The results show that the ANOVA approximation method is competitive to the other approaches and delivers the best MSE for Friedman 1 and 2 as well as a close second best MSE for Friedman 3. Note that a set with 200 data points is rather small and other experiments used significantly more data, but we aimed to stay in the exact setting of [MLH03].

5.3.1 Friedman 1

The function f_1 provides a particular challenge for attribute ranking since it has spatial dimension 10, but only the variables x_1 to x_5 have an

influence on the function value. Moreover, we have an active set

$$U_1^* = \{\emptyset\} \cup \{\{1\}, \{2\}, \{3\}, \{4\}, \{5\}, \{1,2\}\}, \tag{5.14}$$

i.e., only one two-dimensional term is relevant to the function. For obtaining the approximation, we use the data

$$D = \{(\boldsymbol{x}, f_1(\boldsymbol{x}) + \eta_{\boldsymbol{x}}) \colon \boldsymbol{x} \in \mathcal{X}\}$$
$$D_{\text{test}} = \{(\boldsymbol{x}, f_1(\boldsymbol{x}) + \eta_{\boldsymbol{x}}) \colon \boldsymbol{x} \in \mathcal{X}_{\text{test}}\},$$

cf. (5.1) with a set $\mathcal{X} \subseteq [0,1]^{10}$ of $|\mathcal{X}| = 200$ uniformly distributed nodes drawn i.i.d. at random. Here, $\eta_{\boldsymbol{x}}$ is random Gaussian noise with expected value 0 and variance 1. For computing the MSE, we use a test set $\mathcal{X}_{\text{test}} \subseteq [0,1]^{10}$ of $|\mathcal{X}_{\text{test}}| = 1000$ uniformly distributed nodes drawn i.i.d. at random.

We choose as superposition threshold $d_s = 2$ and apply regularization, i.e., we solve problem (4.8) unweighted with regularization parameter $\lambda \geq 0$ and $\boldsymbol{W} = \boldsymbol{I}$ the identity. Our first goal is to approximate the function with a grouped index set $\mathcal{I}_{\boldsymbol{N}}(U^{(10,2)})$ for bandwidths $\boldsymbol{N} \in \mathbb{N}^2$. Here, we aim to find the information that the variables x_6 to x_{10} do not contribute to the function. The active set detection with attribute ranking provides a method for this, i.e., we want to find an $\varepsilon > 0$ such that

$$U^{(\text{ar},\varepsilon)} = \{\boldsymbol{u} \subseteq \{1,2,3,4,5\} \colon |\boldsymbol{u}| \leq 2\} = U^{(5,2)},$$

see (4.17). Since the emphasis lies on computing the attribute ranking, we choose small bandwidths $\boldsymbol{N} = [4,2]$ such that $\left|\mathcal{I}_{\boldsymbol{N}}(U^{(10,2)})\right| = 76$ and compute the approximation $\mathrm{S}^{\mathcal{X}}_{\mathcal{I}_{\boldsymbol{N}}(U^{(10,2)})} f_1$ with regularization parameter $\lambda \in [0,1,2,3,4,5]$. We then choose the λ that yields the lowest MSE. This procedure is iterated with 10 randomly generated pairs of data sets D and D_{test} in order to account for the variance in the data. The average of the mean square errors $e_{\text{MSE}}(f_1, D, \mathcal{I}_{\boldsymbol{N}}(U^{(10,2)}), D_{\text{test}})$ is 4.99 with $\lambda = 1$ turning out to be the choice for the regularization parameter. The average attribute ranking

$$\boldsymbol{r} = [0.22, 0.21, 0.090, 0.36, 0.099, 0.005, 0.003, 0.004, 0.004, 0.004]$$

is depicted in Figure 5.5a. The scores r_i, $i = 1, 2, \ldots, 10$, were computed according to (4.17). This implies a clear separation of active variables x_1 to x_5 and inactive variables x_6 to x_{10} such that we may choose the cut-off at 1% with $\varepsilon = 0.01$ and

$$U^{(\mathrm{ar},0.01)} = \{\boldsymbol{u} \subseteq \{1,2,3,4,5\} \colon |\boldsymbol{u}| \leq 2\} = U^{(5,2)}.$$

Now, we want to detect the active set of terms $U_1^* \subseteq U^{(\mathrm{ar},0.01)}$ from (5.14). To this end, we compute the approximation $\mathrm{S}^{\mathcal{X}}_{\mathcal{I}_N(U^{(\mathrm{ar},0.01)})} f_1$ with bandwidths $\boldsymbol{N} = [6, 4]$, i.e., an increase to the previous experiment, and $\lambda \in [0, 1, 2, 3, 4, 5]$ again. The approximation yields an average MSE $e_{\mathrm{MSE}}(f_1, D, \mathcal{I}_N(U^{(\mathrm{ar},0.01)}), D_{\mathrm{test}})$ of 3.17 on the 10 randomly generated pairs of data sets D and D_{test} with $\lambda = 1$. We depicted the global sensitivity indices in Figure 5.5b. Clearly, the active sets U_1^* are well-separated from the inactive sets such that we may apply a sensitivity cut-off with $U^{(\mathrm{gsi},[0.01,0.01])} = U_1^*$, cf. (4.15).

Finally, we have to determine a good choice of bandwidths $\boldsymbol{N}$ for the approximation $\mathrm{S}^{\mathcal{X}}_{\mathcal{I}_N(U_1^*)} f_1$. From the experiments in Table 5.9, we obtain that this choice is $\boldsymbol{N} = [6, 4]$ yielding an average MSE $e_{\mathrm{MSE}}(f_1, D, \mathcal{I}_N(U_1^*), D_{\mathrm{test}})$ of 1.47 on the 10 randomly generated pairs of data sets D and D_{test} with $\lambda = 0$. In order to obtain the value for Table 5.8, we have computed $\mathrm{S}^{\mathcal{X}}_{\mathcal{I}_{[6,4]}(U_1^*)} f_1$ on 100 randomly generated data sets D and took the MSE on 100 randomly generated data sets D_{test}. This is a replication of the setting in [MLH03] which yielded a median MSE of 1.43 for our setting. This is a significant improvement to the results obtained by the other methods, see Table 5.8.

There exist a number of other methods for attribute rankings or feature selection, see e.g. [GE03]. We conclude this section with a comparison to the well-known method of the estimation of mutual information. The mutual information between two random variables represents a measure for the dependency between the variables. For a pair of jointly continuous random variables (Z, Y) with values over the space $\mathcal{Z} \times \mathcal{Y}$, it is defined as

$$I(Z, Y) \coloneqq \int_{\mathcal{Z}} \int_{\mathcal{Y}} p_{(Z,Y)}(z, y) \log \frac{p_{(Z,Y)}(z, y)}{p_Z(z)\, p_Y(y)} \,\mathrm{d}z \,\mathrm{d}y$$

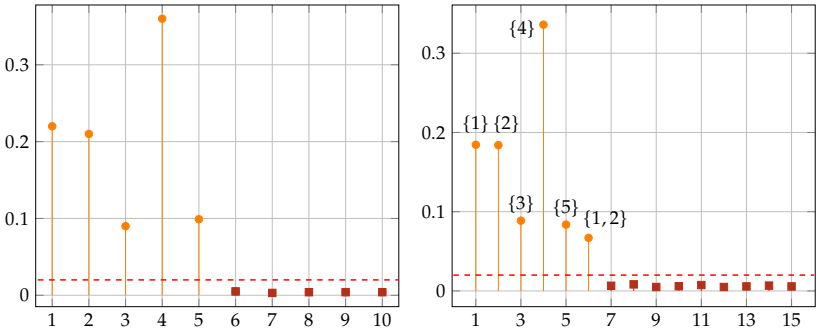

(a) Average of attribute rankings $r(i)$, $i = 1, 2, \ldots, 10$, of approximation $\mathrm{S}^{\mathcal{X}}_{\mathcal{I}_{[4,2]}(U^{(10,2)})} f_1$ on 10 randomly generated data sets D. Active variables x_1 to x_5 in orange and inactive variables x_6 to x_{10} in red.

(b) Average global sensitivity indices $\varrho(\boldsymbol{u}, \mathrm{S}^{\mathcal{X}}_{\mathcal{I}_{[6,4]}(U^{(\mathrm{ar},0.01)})} f_1)$ on 10 randomly generated data sets D. Active sets $\boldsymbol{u} \in U_1^*$ in orange and inactive sets $\boldsymbol{u} \notin U_1^*$ in red.

Figure 5.5: Analysis of the Friedman 1 function using attribute ranking and global sensitivity cut-off.

$\boldsymbol{N}$	$\left\lvert\mathcal{I}_{\boldsymbol{N}}(U_1^*)\right\rvert$	λ	e_{MSE}
$[4,4]$	25	0.0	1.65
$[6,4]$	35	0.0	1.47
$[8,4]$	45	0.0	1.52
$[10,4]$	55	1.0	1.59
$[4,6]$	41	0.0	1.71
$[6,6]$	51	0.0	1.52
$[8,6]$	61	0.0	1.63
$[10,6]$	71	0.0	1.70

Table 5.9: Approximation of f_1 with different bandwidth vectors $\boldsymbol{N}$, grouped index set $\mathcal{I}_{\boldsymbol{N}}(U_1^*)$ and regularization parameter λ. The mean square error $e_{\text{MSE}} \coloneqq e_{\text{MSE}}(f_1, D, \mathcal{I}_{\boldsymbol{N}}(U_1^*), D_{\text{test}})$ is the average over 10 randomly generated pairs of data sets D and D_{test}.

with $p_{(Z,Y)}$ the joint probability density function of Z and Y, and p_Z, p_Y the marginal probability density functions of Z and Y, respectively. We use the function SKLEARN.FEATURE_SELECTION.MUTUAL_INFO_REGRESSION from the scikit-learn Python library for the computations, see [PVG+11]. The estimation of the mutual information is based on the estimation of entropy from k-nearest neighbor distances, cf. [KSG04, Ros14].

Table 5.10 shows the results of our experiments with different values for the number of nearest neighbors k. The method has been applied to the data set D with noisy evaluations. We observe that it is not possible to clearly distinguish the active variables. The active variables x_3 and x_5 get attributed only a small influence while some unimportant variables get attributed a higher influence, e.g., the variable x_{10} in the test with $k = 5$. In contrast to the experiments with mutual information estimation, our model-based approach by estimating the global sensitivity indices delivers a clear distinction of the active variables.

k	x_1	x_2	x_3	x_4	x_5	x_6	x_7	x_8	x_9	x_{10}
3	0.14	0.15	0.00	0.21	0.10	0.00	0.00	0.01	0.04	0.05
5	0.17	0.11	0.05	0.23	0.07	0.00	0.00	0.00	0.00	0.11
7	0.14	0.12	0.04	0.25	0.05	0.00	0.03	0.02	0.00	0.04

Table 5.10: Attribute ranking obtained by mutual information estimation using the scikit-learn library. The parameter k represents the number of neighbors to use in the entropy estimation.

5.3.2 Friedman 2

Now, we consider the second Friedman function f_2 with spatial dimension $d = 4$. For this function, we do not have a clear active set of terms from an analytical viewpoint which means that we are going to determine one empirically from the approximation. As the data, we use a set $\mathcal{X} \subseteq [0,1]^4$ of $|\mathcal{X}| = 200$ uniformly distributed nodes drawn i.i.d. at random. For computing the mean square error, we use a test set $\mathcal{X}_{\text{test}} \subseteq [0,1]^4$ of $|\mathcal{X}_{\text{test}}| = 1000$ uniformly distributed nodes also drawn i.i.d. at random. This gives us the data

$$D = \{(\boldsymbol{x}, f_2(\boldsymbol{x}) + \eta_x) \colon \boldsymbol{x} \in \mathcal{X}\}$$
$$D_{\text{test}} = \{(\boldsymbol{x}, f_2(\boldsymbol{x}) + \eta_x) \colon \boldsymbol{x} \in \mathcal{X}_{\text{test}}\},$$

cf. (5.1), where η_x is Gaussian noise with mean zero and variance 125 as in [MLH03].

In order to determine an active set, we choose as superposition threshold $d_s = 2$ and compute the approximation $\mathrm{S}^{\mathcal{X}}_{\mathcal{I}_{[4,2]}(\mathcal{U}^{(4,2)})} f_2$ by solving the unweighted regularized least-squares problem (4.8) with regularization parameter $\lambda \in [0,1,2,3,4,5]$, $\boldsymbol{W} = \boldsymbol{I}$ the identity, and grouped index set $\mathcal{I}_{[4,2]}(\mathcal{U}^{(4,2)})$. This yielded an average for the mean square error $e_{\text{MSE}}(f_2, D, \mathcal{I}_{[4,2]}(\mathcal{U}^{(4,2)}), D_{\text{test}})$ of $18.2 \cdot 10^3$ on 10 randomly generated pairs of data sets D and D_{test} with $\lambda = 3$. The average global sensitivity indices are depicted in Figure 5.6. This is a rather surprising

result since the terms involving the variables x_1 and x_4 do not seem to contribute significantly to the variance of the function. We decided for a global sensitivity cut-off at 1% and subsequently obtained as the active set

$$U^{(\text{gsi},[0.01,0.01])} = \{\emptyset, \{2\}, \{3\}, \{2,3\}\} =: U_2^*$$

cf. (4.15).

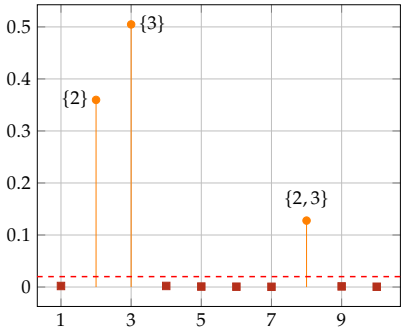

Figure 5.6: Average global sensitivity indices $\varrho(\boldsymbol{u}, \mathrm{S}^{\mathcal{X}}_{\mathcal{I}_{[4,2]}(U^{(4,2)})} f_2)$ on 10 randomly generated data sets D. Active sets $\boldsymbol{u} \in U_2^*$ in orange and inactive sets $\boldsymbol{u} \notin U_2^*$ in red.

For finding a good choice of bandwidths $\boldsymbol{N}$ in the approximation $\mathrm{S}^{\mathcal{X}}_{\mathcal{I}_{\boldsymbol{N}}(U_2^*)} f_2$, we performed the experiments in Table 5.11. The bandwidths $\boldsymbol{N} = [4, 2]$ yielded the best average MSE $e_{\text{MSE}}(f_2, D, \mathcal{I}_{\boldsymbol{N}}(U_2^*), D_{\text{test}})$ of $17.3 \cdot 10^3$ with regularization parameter $\lambda = 2$. Computing the approximation $\mathrm{S}^{\mathcal{X}}_{\mathcal{I}_{[4,2]}(U_2^*)} f_2$ on 100 randomly generated data sets D yielded a median MSE $e_{\text{MSE}}(f_2, D, \mathcal{I}_{\boldsymbol{N}}(U_2^*), D_{\text{test}})$ of $17.18 \cdot 10^3$ on 100 randomly generated test sets D_{test} which represents the value for Friedman 2 in Table 5.8.

$\boldsymbol{N}$	$\left\lvert\mathcal{I}_{\boldsymbol{N}}(U_2^*)\right\rvert$	λ	e_{MSE}
$[2,2]$	4	3.0	$18.3 \cdot 10^3$
$[2,4]$	12	2.0	$18.5 \cdot 10^3$
$[2,6]$	28	4.0	$20.1 \cdot 10^3$
$[4,2]$	8	2.0	$17.3 \cdot 10^3$
$[4,4]$	16	1.0	$17.5 \cdot 10^3$
$[4,6]$	32	2.0	$19.0 \cdot 10^3$
$[6,2]$	12	3.0	$17.6 \cdot 10^3$
$[6,4]$	20	3.0	$17.9 \cdot 10^3$
$[6,6]$	36	4.0	$19.3 \cdot 10^3$

Table 5.11: Approximation of f_2 with different bandwidth vectors $\boldsymbol{N}$, grouped index set $\mathcal{I}_{\boldsymbol{N}}(U_2^*)$ and regularization parameter λ. The mean square error $e_{\text{MSE}} \coloneqq e_{\text{MSE}}(f_2, D, \mathcal{I}_{\boldsymbol{N}}(U_2^*), D_{\text{test}})$ is the average over 10 randomly generated pairs of data sets D and D_{test}.

5.3.3 Friedman 3

Finally, we consider the third Friedman function f_3 with spatial dimension $d = 4$. This function is special since the inverse tangent arctan causes that we neither have an intrinsic sparsity in the ANOVA decomposition nor in the number of variables. As for Friedman 2, we have to determine an active set of terms empirically. The data will again be a set $\mathcal{X} \subseteq [0,1]^4$ of $|\mathcal{X}| = 200$ uniformly distributed nodes drawn i.i.d. at random. The mean square error will be computed on a test set $\mathcal{X}_{\text{test}} \subseteq [0,1]^4$ of $|\mathcal{X}_{\text{test}}| = 1000$ uniformly distributed nodes also drawn i.i.d. at random. As data we use

$$D = \{(\boldsymbol{x}, f_3(\boldsymbol{x}) + \eta_{\boldsymbol{x}}) \colon \boldsymbol{x} \in \mathcal{X}\}$$
$$D_{\text{test}} = \{(\boldsymbol{x}, f_3(\boldsymbol{x}) + \eta_{\boldsymbol{x}}) \colon \boldsymbol{x} \in \mathcal{X}_{\text{test}}\},$$

cf. (5.1), where $\eta_{\boldsymbol{x}}$ is Gaussian noise with mean zero and variance 0.1 as in [MLH03].

We start our experiments by choosing to use the full set of ANOVA terms $U^{(4,4)} = \mathcal{P}([4])$ and aim to determine an active set $U_3^* \subseteq U^{(4,4)}$ from there. We use bandwidths $\boldsymbol{N} = [4, 2, 2, 2]$ and compute the approximation $\mathrm{S}^{\mathcal{X}}_{\mathcal{I}_{[4,2,2,2]}(U^{(4,4)})} f_3$ by solving the unweighted regularized least-squares problem (4.8) with regularization parameter $\lambda \in [1, 2, 3, 4, 5]$ and $\boldsymbol{W} = \boldsymbol{I}$ the identity. When computed on 10 randomly generated data sets D, the approximation yielded an average MSE $e_{\mathrm{MSE}}(f_3, D, \mathcal{I}_{[4,2,2,2]}(U^{(4,4)}), D_{\mathrm{test}})$ of $33.3 \cdot 10^{-3}$ on 10 randomly generated test sets D_{test}. Figure 5.7 shows the average attribute ranking

$$\boldsymbol{r} = [0.166, 0.209, 0.612, 0.013]$$

for the approximation with r_i computed according to (4.16). We observe that the variable x_4 seems to have very little influence on the variance of the approximation. If we cut off at 5% importance, we get

$$U^{(\mathrm{ar},0.05)} = \mathcal{P}([3]),$$

see (4.17). However, we want to limit the interactions with superposition threshold $d_s = 2$ such that we choose the active set

$$U_3^* \coloneqq \{\boldsymbol{u} \subseteq [3] \colon |\boldsymbol{u}| \leq 2\} = U^{(3,2)}.$$

Now, we only need to find a suitable choice of bandwidths $\boldsymbol{N}$ in the final approximation $\mathrm{S}^{\mathcal{X}}_{\mathcal{I}_N(U_3^*)} f$. Table 5.12 shows the results of our experiments with different $\boldsymbol{N} \in \mathbb{N}^2$. Here, $\boldsymbol{N} = [12, 2]$ yielded the best average MSE $e_{\mathrm{MSE}}(f_3, D, \mathcal{I}_N(U_3^*), D_{\mathrm{test}})$ of $21.0 \cdot 10^{-3}$ with regularization parameter $\lambda = 4$. Finally, we compute the approximation $\mathrm{S}^{\mathcal{X}}_{\mathcal{I}_{[12,2]}(U_3^*)} f_3$ on 100 randomly generated data sets D yielding a median MSE $e_{\mathrm{MSE}}(f_3, D, \mathcal{I}_N(U_3^*), D_{\mathrm{test}})$ of $20.69 \cdot 10^{-3}$ on 100 randomly generated test sets D_{test} which is the value for Friedman 3 in Table 5.8.

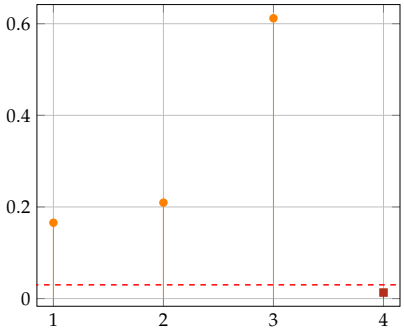

Figure 5.7: Average attribute ranking $r(i)$, $i = 1, 2, 3, 4$, for $S^{\mathcal{X}}_{\mathcal{I}_{[4,2,2,2]}(U^{(4,4)})} f_3$ computed on 10 randomly generated data sets D. Active variables x_1 to x_3 in orange and inactive variable x_4 in red.

$\boldsymbol{N}$	$\left\lvert\mathcal{I}_{\boldsymbol{N}}(U_3^*)\right\rvert$	λ	e_{MSE}
$[8, 2]$	25	3.0	$22.2 \cdot 10^{-3}$
$[8, 4]$	49	2.0	$22.7 \cdot 10^{-3}$
$[10, 2]$	31	4.0	$21.3 \cdot 10^{-3}$
$[10, 4]$	55	3.0	$21.8 \cdot 10^{-3}$
$[12, 2]$	37	4.0	$21.0 \cdot 10^{-3}$
$[12, 4]$	61	3.0	$21.6 \cdot 10^{-3}$

Table 5.12: Approximation of f_3 with different bandwidth vectors $\boldsymbol{N}$, grouped index set $\mathcal{I}_{\boldsymbol{N}}(U_3^*)$, and regularization parameter λ. The mean square error $e_{\text{MSE}} := e_{\text{MSE}}(f_3, D, \mathcal{I}_{\boldsymbol{N}}(U_3^*), D_{\text{test}})$ is the average over 10 randomly generated pairs of data sets D and D_{test}.

5.3.4 Runtime

We conclude this section with a runtime comparison of our methods for the experiments conducted with the Friedman functions. Here, we distinguish between an *init* step, i.e., the initialization and pre-computations of the grouped transform, and solving the regularized least-squares problem (4.8) with LSQR. Table 5.13 shows the runtimes for computing the approximations. Note that this is the computation for one specific choice of parameters λ, and $\boldsymbol{N}$. However, solving for additional regularization parameters λ does not require a repetition of the initialization. The experiments were conducted on a computer with an Intel Xeon Gold 6240 R CPU at 2.4 gigahertz. We used 12 cores for the parallelization of the grouped transformations. One observes a direct correlation from the number of involved ANOVA terms to the time for both the initialization and computation step. This is especially evident when comparing Friedman 1 with $d = 10$ to the other experiments.

function	$U \subseteq \mathcal{P}([d])$	$\boldsymbol{N}$	init time	LSQR time
Friedman 1	$U^{(10,2)}$	$[4, 2]$	31.6 ms	2.1 s
Friedman 1	$U^{(\mathrm{ar},0.01)}$	$[6, 4]$	6.2 ms	0.89 s
Friedman 1	U_1^*	$[6, 4]$	1.4 ms	54.0 ms
Friedman 2	$U^{(4,2)}$	$[4, 2]$	2.7 ms	85.3 ms
Friedman 2	U_2^*	$[4, 2]$	1.3 ms	15.1 ms
Friedman 3	$U^{(4,4)}$	$[4, 2, 2, 2]$	7.1 ms	0.17 s
Friedman 3	U_3^*	$[12, 2]$	1.8 ms	61.1 ms

Table 5.13: Runtimes of experiments with the Friedman functions using the ANOVAapprox method. The pre-computations and initialization is measured as *init time* and computing the solution of the corresponding least-squares problem as *LSQR time* ($\boldsymbol{N} = [N_1, N_2]$ or $\boldsymbol{N} = [N_1, N_2, N_3, N_4]$).

6

Numerical Experiments with Real Data

Now that we have shown the performance of the ANOVA approximation method from Chapter 4 for the recovery of functions, we focus on known data sets from applications. In this case, we have given data

$$D \coloneqq \{(\boldsymbol{x}_1, y_1), (\boldsymbol{x}_2, y_2), \dots, (\boldsymbol{x}_M, y_M)\}, \quad M \in \mathbb{N}, \tag{6.1}$$

with a set of nodes $\mathcal{X} = \{\boldsymbol{x}_1, \boldsymbol{x}_2, \dots, \boldsymbol{x}_M\} \subseteq \mathbb{R}^d$ and values $y_i \in \mathbb{R}$, $i = 1, 2, \dots, M$. The spatial dimension d is here the number of features of the data set. Note that we always apply a Z-score transformation or a min-max normalization beforehand, see e.g. [HTF13], such that we may assume that the nodes $\boldsymbol{x}_i$ are either from a standard normal distribution or uniformly distributed in $[0,1]^d$. In order to apply our method from Section 4.2, we assume that there exists either a continuous $f\colon \mathbb{R}^d \to \mathbb{R}$ from $\mathrm{L}_2(\mathbb{R}^d, \omega^{(d),\mathrm{std}})$, i.e., we use the transformed basis functions $\varphi^{(d),\mathrm{std}}$ from Section 2.1.2.4, or a continuous $f\colon [0,1]^d \to \mathbb{R}$ from $\mathrm{L}_2([0,1]^d)$, i.e., we use the half-period cosine basis $\varphi^{(d),\cos}$ from Section 2.1.2.3. Moreover, f should fit our data in the sense that $f(\boldsymbol{x}_i) \approx y_i$, $i = 1, 2, \dots, M$. We use the ANOVA approximation method to approximate this function f. We always start by choosing a low superposition threshold $d_s \in [d]$ to compute an approximation

$\mathrm{S}^{\mathcal{X}}_{\mathcal{I}_{\boldsymbol{N}}(U^{(d,d_s)})} f$ with grouped index set $\mathcal{I}_{\boldsymbol{N}}(U^{(d,d_s)})$, and bandwidths $\boldsymbol{N} \in \mathbb{N}$, see Definition 3.3, via solving the regularized least-squares problem (4.8) with regularization parameter $\lambda \geq 0$ and $\boldsymbol{W} = \boldsymbol{I}$ the identity. Then we perform an analysis using the methods from Section 4.2.1, e.g., via attribute ranking or global sensitivity indices, to obtain a subset $U^* \subseteq U^{(d,d_s)}$. In the end, we have to determine bandwidths $\boldsymbol{M} \in \mathbb{N}$ and obtain the final approximation $\mathrm{S}^{\mathcal{X}}_{\mathcal{I}_{\boldsymbol{M}}(U^*)} f$.

Since we only have the data set D available, we need to use it for training, i.e., obtaining the approximation, as well as for testing, i.e., evaluating the performance of the model. To this end, we apply a cross-validation procedure. For each data set we choose a split of the data into training and test set with the value $p_{\text{test}} \in (0,1)$ such that we have $\lfloor p_{\text{test}} \cdot M \rfloor$ data points for evaluating the model and $M - \lfloor p_{\text{test}} \cdot M \rfloor$ for obtaining the approximation. A common example is to reserve 10% for testing, i.e., $p_{\text{test}} = 0.1$. This yields a training set $D_{\text{train}} \subseteq D$ and a test set $D_{\text{test}} \subseteq D$ such that $D_{\text{train}} \cap D_{\text{test}} = \emptyset$ and $D_{\text{train}} \cup D_{\text{test}} = D$. However, it will not be sufficient to perform this procedure only once since it depends on which specific points we choose for D_{train} and D_{test}. We are going to apply a form of cross-validation where we randomly draw D_{train} and D_{test} from D a number of times. Cross-validation with 10 iterations therefore refers to drawing the training set and the test set 10 times at random.

In order to evaluate the model, we consider empirical generalization errors. The *root mean square error (RMSE)* is defined as

$$e_{\text{RMSE}}(D, \mathcal{I}_{\boldsymbol{N}}(U), D_{\text{test}}) \coloneqq \sqrt{\frac{1}{|D_{\text{test}}|} \sum_{(\boldsymbol{x},y)\in D_{\text{test}}} \left| \mathrm{S}^{\mathcal{X}}_{\mathcal{I}_{\boldsymbol{N}}(U)} f(\boldsymbol{x}) - y \right|^2}.$$

The *mean absolute deviation (MAD)* is an ℓ_1 error and given by

$$e_{\text{MAD}}(D, \mathcal{I}_{\boldsymbol{N}}(U), D_{\text{test}}) \coloneqq \frac{1}{|D_{\text{test}}|} \sum_{(\boldsymbol{x},y)\in D_{\text{test}}} \left| \mathrm{S}^{\mathcal{X}}_{\mathcal{I}_{\boldsymbol{N}}(U)} f(\boldsymbol{x}) - y \right|.$$

Finally, we have the relative ℓ_2 error

$$e_{\mathrm{rel}}(D, \mathcal{I}_{\boldsymbol{N}}(U), D_{\mathrm{test}}) \coloneqq \sqrt{\frac{\sum_{(\boldsymbol{x},y)\in D_{\mathrm{test}}} \left| \mathrm{S}^{\mathcal{X}}_{\mathcal{I}_{\boldsymbol{N}}(U)} f(\boldsymbol{x}) - y \right|^2}{\sum_{(\boldsymbol{x},y)\in D_{\mathrm{test}}} |y|^2}}.$$

Note that we are minimizing the ℓ_2 norm which corresponds to the RMSE and the relative ℓ_2 error. We do not minimize an ℓ_1 norm and therefore the MAD is more of a byproduct.

In order to compare our performance to other well-known methods, we chose data sets from the UCI machine learning repository [DG17] and the website [Tor]. An overview is provided in Table 6.1 with references where the data sets originate from and where else they have been considered. Note that the forest fires data set has been investigated with our method in [PS22b] and the other data sets in [PS21b]. Table 6.2 summarizes our numerical results from the following sections in comparison to the results from the literature. Our method does not only provide interpretable results, it also outperforms the other methods in the model accuracy.

Name	dimension	data points	references
Forest Fires (FIRES)	12	517	[CM07, DG17, PS22b]
Energy Efficiency Heating (ENH)	8	768	[GPT20, DG17, PS21b]
Energy Efficiency Cooling (ENC)	8	768	[GPT20, DG17, PS21b]
Airfoil Self-Noise (ASN)	5	1503	[HSS+21, DG17, PS21b]
California Housing (CH)	8	20640	[KM15, Tor, PS21b]
Ailerons (AIL)	40	13750	[KM15, Tor, PS21b]

Table 6.1: Application data sets for benchmarking the ANOVAapprox method with sources.

data set	error (type)	method (reference)	ANOVAapprox
FIRES	12.71 (MAD)	Support Vector Machine ([CM07])	12.65
ENC	1.79 (RMSE)	Gradient Boosting Machine ([GPT20])	1.49
ENH	0.48 (RMSE)	Random Forest ([GPT20])	0.44
ASN	0.0277 (relative ℓ_2)	Sparse Random Features ([HSS$^+$21])	0.0161
CH	0.11450 (RMSE)	Local Learning Reg. NN ([KM15])	0.10899
Ailerons	0.04601 (RMSE)	Local Learning Reg. NN ([KM15])	0.04569

Table 6.2: Result comparison for different data sets and approaches. The models for ANOVAapprox where validated using 100 random splits of training and test set. More details are discussed in the corresponding section. The ANOVAapprox error is compared to the best error found in the mentioned source together with the method used therein.

6.1 Forest Fires

The forest fires data set from the UCI repository [DG17] contains information about forest fires in the Montesinho national park in the Trás-os-Montes northeast region of Portugal from 2002 to 2003. The data set has $d = 12$ attributes about every fire with the target variable being the area of the forest that was destroyed. An efficient model for the prediction of this area can be used in predicting the occurrence of fires and preparing appropriate countermeasures. It is our goal to compare to the results from [CM07] and where this data set has been considered.

group	name	description
spatial (S)	X	x-coordinate (1 to 9)
	Y	y-coordinate (1 to 9)
temporal (T)	month	month of the year (1 to 12)
	day	day of the week (1 to 7)
FWI	FFMC	FFMC code
	DMC	DMC code
	DC	DC code
	ISI	ISI index
meteorological (M)	temp	outside temperature in °C
	RH	outside relative humidity in %
	wind	outside wind speed in km/h
	rain	outside rain in mm/m^2

Table 6.3: Attributes and their corresponding groups

Here, the 12 attributes are grouped into 4 categories as in [CM07], i.e., spatial, temporal, FWI system, and meteorological data, see Table 6.3. The Trás-os-Montes northeast region of Portugal has been divided into a 9 by 9 grid and the spatial attributes describe the location of the fire

in this grid. As temporal attributes, we have the month of the year and the day of the week when the fire occurred. The *forest fire weather index (FWI)*, cf. [TA06], is the Canadian system for rating fire danger. The FWI group contains four of its component, the FFMC code, the DMC code, the DC code, and the ISI index. Moreover, the meteorological group collects the four attributes temperature, humidity, wind, and rain.

For pre-processing, we apply a Z-score transformation to the the variables and the logarithmic transformation $\log(1+\cdot)$ to the burned area. The Z-score transformation achieves that we may assume our data stems from a standard normal distribution. The logarithmic transformation on the target is helpful since the variable shows a positive skew with a large number of fires that have a small size. We denote the data with D, cf. (6.1), and split it into 90% for the training set D_{train} and 10% for the test set D_{test}. In the following, we do not use all of the variables, but build models based only on some groups as denoted in Table 6.3, e.g., **STM** means that we use spatial, temporal and meteorological attributes without the FWI.

Table 6.4 shows the overall results of our experiment (ANOVA) combined with the benchmark data from [CM07]. Each value, our ANOVA results as well as the others, were obtained by averaging over executing a 10-fold cross-validation 30 times. This results in a total of 300 experiments. We used a superposition threshold of $d_s = 2$ and therefore needed to detect optimal choices for the bandwidths $\boldsymbol{N} \in \mathbb{N}$ in the grouped index sets $\mathcal{I}_{\boldsymbol{N}}(U^{(d,2)})$, see Table 6.5. We are able to outperform the previously applied methods for every subset of attributes in both average MAD $e_{\text{MAD}}(D, \mathcal{I}_{\boldsymbol{N}}(U^{(d,2)}), D_{\text{test}})$ and average RMSE $e_{\text{RMSE}}(D, \mathcal{I}_{\boldsymbol{N}}(U^{(d,2)}), D_{\text{test}})$ error. We also observe a significant better result in the RMSE which penalizes larger deviations stronger.

We replicated the setting of [CM07] for benchmark purposes. However, with our method, we should be able to detect the most important attributes for the forest fires ourselves. To this end, we use all 12 attributes of the data set in obtaining our approximation and subsequently interpret the results. Figure 6.1 shows the attribute ranking $r(i)$, $i = 1, 2, \ldots, 12$, as well as the global sensitivity indices for an

model	attribute selection S T FWI	S T M	FWI	M
Naive	18.61 (63.7)	18.61 (63.7)	18.61 (63.7)	18.61 (63.7)
MR	13.07 (64.5)	13.04 (64.4)	13.00 (64.5)	13.01 (64.5)
DT	13.46 (64.4)	13.43 (64.6)	13.24 (64.4)	13.18 (64.5)
RF	13.31 (64.3)	13.04 (64.5)	13.38 (64.0)	12.93 (64.4)
NN	13.09 (64.5)	13.92 (68.9)	13.08 (64.6)	13.71 (66.9)
SVM	13.07 (64.7)	13.13 (64.7)	12.86 (64.7)	12.71 (64.7)
ANOVA	**12.75** (**45.77**)	**12.81** (**46.7**)	**12.76** (**46.09**)	**12.65** (**45.69**)

Table 6.4: MAD and RMSE (in brackets) for the best performing model in the corresponding attribute subset (underline - overall best result, **bold** - best result for this selection).

attribute selection	N_1	N_2	$\lvert I\rvert$	λ
S T FWI	2	6	149	e^9
S T M	2	10	261	e^{10}
FWI	2	4	23	e^8
M	2	8	47	e^7

Table 6.5: Optimal parameter choices for the experiments from Table 6.4.

approximation with grouped index set $\mathcal{I}_{[2,2]}(U^{(12,2)})$ and regularization parameter $\lambda = 1$.

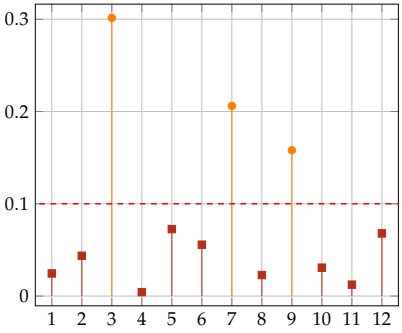

Figure 6.1: Attribute ranking $r(i)$, $i = 1, 2, \ldots, 12$, from (4.16) of our final model obtained for the prediction of the forest fire area.

We observe that the attributes 3, 7, and 9 are of the most importance to the prediction such that we have $U^{(\mathrm{ar},0.1)} =: U^*_{\mathrm{fires}} \subseteq U^{(12,2)}$, see (4.17). They represent the month of the year (3), the DC code of the FWI (7) and the outside temperature (9). We subsequently computed an approximation with only these three attributes and a superposition threshold $d_s = 2$. Here, we used the grouped index set $\mathcal{I}_{[2,10]}(U^*_{\mathrm{fires}})$ and regularization parameter $\lambda = \mathrm{e}^8$. The resulting model yielded an average MAD $e_{\mathrm{MAD}}(D, \mathcal{I}_{[2,10]}(U^*_{\mathrm{fires}}), D_{\mathrm{test}})$ of 12.64 and an average RMSE $e_{\mathrm{RMSE}}(D, \mathcal{I}_{[2,10]}(U^*_{\mathrm{fires}}), D_{\mathrm{test}})$ of 45.57 with 30 times of 10-fold cross validation as before. In summary, we know that the most important information of our problem is contained in only three attributes and we also obtained a better performing model using only these three attributes.

6.2 Energy Efficiency

This data set from the UCI repository [DG17] describes the energy efficiency of houses by $d = 8$ attributes and two values to predict, the cooling load and the heating load. Therefore, we have two problems ENC to predict the cooling load and ENH for the heating load. The data set D contains 768 data points from sample houses in both cases which we split 70% for the training set D_{train} and 30% for the test set D_{test}, i.e., $p_{\text{test}} = 0.3$. The data points have been normalized into the interval $[0, 1]$, i.e., we use the half-period cosine basis.

We start by considering the prediction of the heating load with a superposition threshold of $d_s = 2$. We have taken one randomly drawn pair of data sets D_{train} and D_{test} to detect an initial bandwidth vector $\boldsymbol{N} \in \mathbb{N}^2$ with

$$N_1 - 1 = (N_2 - 1)^2 \tag{6.2}$$

for the grouped index set $\mathcal{I}_{\boldsymbol{N}}(U^{(8,2)})$ as well as the threshold vector $\boldsymbol{\varepsilon} \in (0, 1)^2$ for the cut-off of the global sensitivity indices $U^{(\text{gsi},\varepsilon)}$, see (4.15). Note that we use (6.2) in order to have all ANOVA terms with the same number of indices which may create better conditions for the active set detection if no information is known. Here, it turned out that the bandwidths $\boldsymbol{N} = [26, 6]$ and the threshold vector $\boldsymbol{\varepsilon} = [0.001, 0.001]$ are opportune choices. This leads to an active set

$$U^{(\text{gsi},\varepsilon)} = U^*_{\text{heating}} \subseteq U^{(8,2)} \quad \text{with} \quad \left|U^*_{\text{heating}}\right| = 28$$

terms. Subsequently, we aim to determine bandwidths $\boldsymbol{M}$ for an approximation with grouped index $\mathcal{I}_{\boldsymbol{M}}(U^*_{\text{heating}})$. This is done via cross-validation with 20 iterations. The resulting bandwidth choice is $\boldsymbol{M} = [100, 6]$ and for the regularization parameter we have $\lambda = 20$. The model has then been trained on 100 randomly generated training sets D_{train} and validated on 100 corresponding test sets D_{test} which yielded a median for the RMSE $e_{\text{RMSE}}(D, \mathcal{I}_{\boldsymbol{M}}(U^*_{\text{heating}}), D_{\text{test}})$ of 0.44.

For the cooling problem, we proceed in a similar fashion. We set the superposition threshold to $d_s = 2$ and determine the bandwidths $\boldsymbol{N}$

with (6.2) for the grouped index set $\mathcal{I}_{\boldsymbol{N}}(U^{(8,2)})$ as well as the threshold vector $\boldsymbol{\varepsilon} \in (0,1)^2$ for the global sensitivity cut-off using one data pair D_{train} and D_{test}. Here, we obtain $\boldsymbol{N} = [10, 4]$, and $\boldsymbol{\varepsilon} = [0.002, 0.002]$ yielding the active set

$$U^{(\text{gsi},\boldsymbol{\varepsilon})} = U^*_{\text{cooling}} \subseteq U^{(8,2)} \quad \text{with} \quad \left|U^*_{\text{cooling}}\right| = 22$$

terms. Then we use 20 iterations of our cross-validation to obtain a good choice of bandwidths $\boldsymbol{M}$ for an approximation with grouped index set $\mathcal{I}_{\boldsymbol{M}}(U^*_{\text{cooling}})$. This yielded a bandwidth vector $\boldsymbol{M} = [30, 6]$ with regularization parameter $\lambda = 50$. As a result we obtained a model with a median RMSE $e_{\text{RMSE}}(D, \mathcal{I}_{\boldsymbol{M}}(U^*_{\text{cooling}}), D_{\text{test}})$ of 1.49 trained on 100 randomly generated training sets D_{train} and validated on 100 corresponding test sets D_{test}.

Figure 6.2 shows attribute rankings for our obtained models. For both problems Figure 6.2a, and Figure 6.2b, we notice that the attribute 5, i.e., the overall height of the building, is especially important for the prediction of the load.

6.3 Airfoil Self-Noise

This data set from the UCI repository [DG17] is provided by the NASA and describes experiments with airfoil blade section. The aerodynamic and acoustic tests have been conducted in an anechoic wind tunnel with different speeds and angles of attack. We aim to find a model that is able to predict the scaled sound pressure level of the self-noise in decibels, see [DG17]. The data set D has $d = 5$ attributes and contains 1503 nodes. We reserve 80% for the training set D_{train} and 20% for the test set D_{test} such that $p_{\text{test}} = 0.2$. The data points have been normalized into the interval $[0, 1]$, i.e., we use the half-period cosine basis. Since this data set has recently been used in [HSS+21] for experiments with sparse random features, we choose the same split to compare the results.

We use the same general procedure as before in Section 6.2. First, we approximate with a grouped index set $\mathcal{I}_{\boldsymbol{N}}(U^{(5,2)})$ and determine

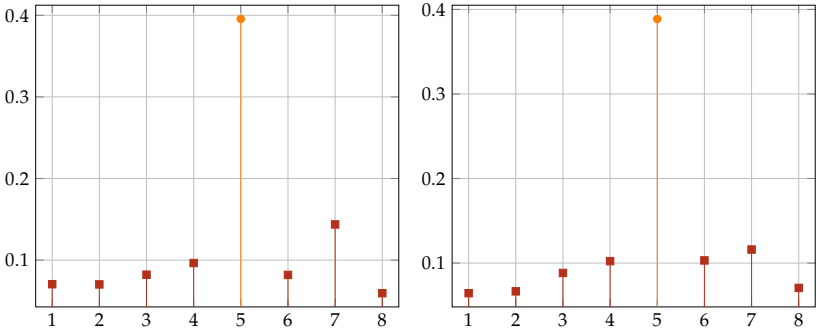

(a) Attribute ranking $r(i)$, $i = 1, 2, \ldots, 8$, from (4.16) of our final model obtained for the heating problem.

(b) Attribute ranking $r(i)$, $i = 1, 2, \ldots, 8$, from (4.16) of our final model obtained for the cooling problem.

Figure 6.2: Attribute rankings for the energy efficiency data set.

a good choice of bandwidths on a single pair of data sets D_{train} and D_{test} which yielded $\boldsymbol{N} = [170, 14]$ under condition (6.2). Analyzing the global sensitivity indices shows that it is best to choose a cut-off with $\boldsymbol{\varepsilon} = [0.01, 0.01]$ such that we obtain an active set

$$U^{(\text{gsi},\varepsilon)} = U^*_{\text{airfoil}} \subseteq U^{(5,2)} \quad \text{with} \quad \left|U^*_{\text{airfoil}}\right| = 15$$

terms. This means that we have only removed one term from $U^{(5,2)}$. Then we draw 20 pairs of D_{train} and D_{test} to use cross-validation in order to determine a good choice of bandwidths $\boldsymbol{M}$ for an approximation with grouped index set $\mathcal{I}_{\boldsymbol{M}}(U^*_{\text{airfoil}})$. This resulted in $\boldsymbol{M} = [200, 30]$ and regularization parameter $\lambda = 100$. The obtained model was then validated on 100 random pairs of training data D_{train} and test data D_{test} yielding a median relative error $e_{\text{rel}}(D, \mathcal{I}_{\boldsymbol{M}}(U^*_{\text{airfoil}}), D_{\text{test}})$ of 1.61%. In Figure 6.3 we have visualized the attribute ranking for our model. It shows that attributes 3 and 4, i.e., the chord length and the free-stream velocity have a large influence on the predictions.

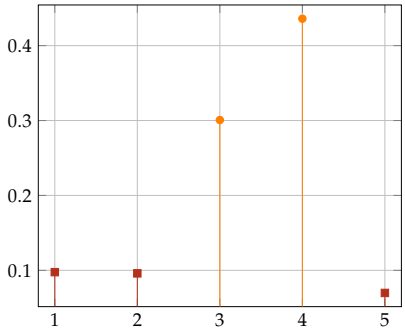

Figure 6.3: Attribute ranking $r(i)$, $i = 1, 2, \ldots, 8$, from (4.16) of our final model obtained for the prediction of the sound pressure level of airfoil blade sections.

6.4 California Housing

The data set from [Tor] describes the prices for houses in California from data about the block groups from the 1990 census. We have a data set D with $d = 8$ attributes and 20460 data points. It is our goal to create a model that is able to predict the median house price for the geographic area. Since we want to compare our results to [KM15], we split the data in 50% for the training set D_{train} and 50% for the test set D_{test} such that $p_{\text{test}} = 0.5$. Here, the nodes *as well as the values* have been transformed into $[0, 1]$ via a min-max-normalization. The normalization of the values is replicated from [KM15].

We start with a superposition threshold of $d_s = 2$ to obtain an approximation with the grouped index set $\mathcal{I}_{\boldsymbol{N}}(U^{(8,2)})$. Using one randomly drawn pair of data sets D_{train}, and D_{test}, we obtained $\boldsymbol{N} = [82, 10]$ under condition (6.2) for the bandwidth and $\boldsymbol{\varepsilon} = [0.02, 0.02]$ for the sensitivity cut-off yielding an active set

$$U^{(\text{gsi},\varepsilon)} = U^*_{\text{housing}} \subseteq U^{(8,2)} \quad \text{with} \quad \left|U^*_{\text{housing}}\right| = 21$$

terms. Subsequently, we computed an approximation with $\boldsymbol{M} \in \mathbb{N}^2$

and the grouped index set $\mathcal{I}_{\boldsymbol{M}}(U^*_{\text{housing}})$ where $\boldsymbol{M}$ was determined via cross-validation using 20 randomly drawn pairs of data sets D_{train}, and D_{test}. This yielded $\boldsymbol{M} = [120, 10]$ and the regularization parameter $\lambda = 100$. The model was subsequently validated on 100 randomly drawn pairs of training and test data which yielded a median for the RMSE

$$e_{\text{RMSE}}(D, \mathcal{I}_{\boldsymbol{M}}(U^*_{\text{housing}}), D_{\text{test}})$$

of 0.10899.

Figure 6.4a shows an attribute ranking for the obtained model. We observe that the variables 1, 2, and 6, i.e., the geographical longitude, the latitude, and the population count, are most important for the prediction. It is also evident from the global sensitivity indices, see Figure 6.4b, that the ANOVA term $f_{\{1,2\}}$ has significant importance which seems very plausible from an interpretation view since variable 1 is the longitude and variable 2 the latitude, i.e., together they represent the geographical location.

6.5 Ailerons

The Ailerons data set from [Tor] describes the control problem of flying an F16 aircraft. The attributes describe the status of the aircraft and it is our goal to predict the control action on its ailerons. The data set has $d = 40$ attributes and 13750 data points. We aim to replicate the setting in [KM15], which separates the data into 50% for the training set D_{train} and 50% for the test set D_{test} such that $p_{\text{test}} = 0.5$. Here, the nodes *as well as the values* have been transformed into $[0, 1]$ via a min-max-normalization. The normalization of the values is replicated from [KM15].

As a first step, we aim to consider an attribute ranking for superposition threshold $d_s = 1$ in order to determine whether some variables have little influence and can be omitted for the model. To this end, we are using the grouped index set $\mathcal{I}_{10}(U^{(40,1)})$ for approximation and average the attribute ranking over 100 randomly drawn pairs of data sets D_{train}

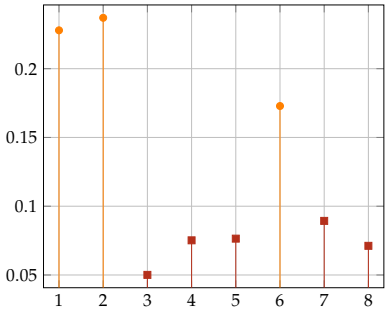

(a) Attribute ranking $r(i)$, $i = 1, 2, \ldots, 8$, from (4.16) of our final model obtained for the prediction of median house prices in California.

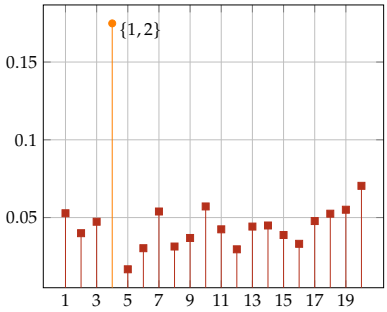

(b) Global sensitivity indices for the house price model. The geographical location term $\{1, 2\}$ is highlighted in orange.

Figure 6.4: Analysis of the ANOVAapprox model for the prediction of house prices.

and D_{test}. This lead us to eliminate 29 variables with a contribution smaller than $\varepsilon = 0.0185$ such that

$$U^{(\text{ar},\varepsilon)} =: U^{(\text{ar})}_{\text{ail}} \quad \text{with} \quad \left|U^{(\text{ar})}_{\text{ail}}\right| = 12$$

terms, see (4.17).

We proceeded with the $d^* = 11$ active variables and $d_s = 2$ such that we have the set of terms

$$U := \{\boldsymbol{u} \subseteq [11] \colon |\boldsymbol{u}| \leq 2\}.$$

We perform sensitivity analysis on an approximation with grouped index set $\mathcal{I}_{[12,2]}(U)$ which leads to an optimal cut-off vector $\varepsilon = [0.001, 0.001]$ such that we have an active set

$$U^{(\text{gsi},\varepsilon)} = U^*_{\text{ail}} \subseteq U \quad \text{with} \quad \left|U^*_{\text{ail}}\right| = 43$$

terms. The model was subsequently validated on 100 randomly drawn pairs of training set D_{train} and test set D_{test} yielding a median RMSE of 0.04569. In Figure 6.5 we have visualized the attribute ranking for our model. We observe that the variables 1, 2,and 8 are of greater importance. They correspond to the control variables 7, 3, and 30 of the original problem.

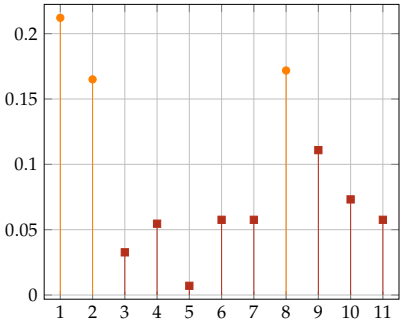

Figure 6.5: Attribute ranking $r(i)$, $i = 1, 2, \ldots, 11$, from (4.16) of our final model obtained for the prediction of the control actions on the ailerons of an F16 aircraft.

7 Conclusion

The main focus of this work was the introduction and analysis of the ANOVA approximation method. It includes considerations of the ANOVA decomposition in connection to orthonormal bases in the Lebesgue product space $L_2(\mathbb{D}^d, \omega^{(d)})$ as well as the introduction of grouped transformations as a general concept for the extension of the non-equispaced fast Fourier and fast cosine transforms to grouped index sets. The method is applicable for the approximation of functions as well as for regression problems with scattered data where one approximates an unknown underlying function that maps input data to output. Our main assumption is that the sparsity-of-effects principle is applicable, i.e., the function is dominated by low-order interactions which we related to both scenarios.

We considered the classical ANOVA decomposition with the integral projection operator in weighted Lebesgue spaces $L_2(\mathbb{D}^d, \omega^{(d)})$ with probability measures $\omega^{(d)}$ and found a new connection to complete orthonormal systems $(\varphi_{\boldsymbol{k}}^{(d)})_{\boldsymbol{k}\in\mathbb{Z}^d}$ with relationships to the basis coefficients. This connection provided a new access to the decomposition that simplified understanding properties like the inheritance of smoothness. With the goal of our approximation method in mind, we considered sparsity

of the decomposition and its truncation. Specifically, we focused on the concept of low superposition dimension, i.e., a large part of the variance is explained by interactions of low order. Since the number of ANOVA terms grows exponentially in the spatial dimension, this truncation provided us with a way to reduce it to polynomial growth as a way to circumvent the curse. We discussed how smoothness may be related to a low superposition dimension or its worst-case version. For Sobolev type spaces $\mathrm{H}^w(\mathbb{D}^d, \omega^{(d)})$ and weighted Wiener spaces $\mathcal{A}^w(\mathbb{D}^d, \omega^{(d)})$ with smoothness weight $w\colon \mathbb{Z}^d \to [1, \infty)$, we were able to prove worst-case truncation bounds that directly give insight into the worst-case superposition dimension. We found that the important special case of isotropic and dominating-mixed smoothness is related to a low worst-case superposition dimension with error bounds for L_2 and L_∞ ANOVA truncation. The error bounds even suggested an independence of the spatial dimension for the worst-case error in many cases.

We were then interested in linking the ANOVA truncation together with the approximation by partial sums in the Lebesgue space $\mathrm{L}_2(\mathbb{D}^d, \omega^{(d)})$. To this end, we introduced a new form of index set, the grouped index set $\mathcal{I}_N(U)$ with bandwidths $\boldsymbol{N} \in \mathbb{N}$ and the set of ANOVA terms $U \subseteq \mathcal{P}([d])$. The fast evaluations of such partial sums on a number of nodes $\mathcal{X} \coloneqq \{\boldsymbol{x}_1, \boldsymbol{x}_2, \dots, \boldsymbol{x}_M\} \subseteq \mathbb{D}^d$ can always be interpreted as a matrix-vector multiplication for matrices of type

$$\boldsymbol{F}_{\mathcal{I}}^{\mathcal{X}} = \begin{pmatrix} \varphi_{\boldsymbol{k}_1}^{(d)}(\boldsymbol{x}_1) & \varphi_{\boldsymbol{k}_2}^{(d)}(\boldsymbol{x}_1) & \cdots & \varphi_{\boldsymbol{k}_n}^{(d)}(\boldsymbol{x}_1) \\ \varphi_{\boldsymbol{k}_1}^{(d)}(\boldsymbol{x}_2) & \varphi_{\boldsymbol{k}_2}^{(d)}(\boldsymbol{x}_2) & \cdots & \varphi_{\boldsymbol{k}_n}^{(d)}(\boldsymbol{x}_2) \\ \vdots & \vdots & \vdots & \vdots \\ \varphi_{\boldsymbol{k}_1}^{(d)}(\boldsymbol{x}_M) & \varphi_{\boldsymbol{k}_2}^{(d)}(\boldsymbol{x}_M) & \cdots & \varphi_{\boldsymbol{k}_n}^{(d)}(\boldsymbol{x}_M) \end{pmatrix}$$

with $(\varphi_{\boldsymbol{k}}^{(d)})_{\boldsymbol{k} \in \mathbb{Z}^d}$ being the orthonormal basis, and the index set $\mathcal{I} \coloneqq \{\boldsymbol{k}_1, \boldsymbol{k}_2, \dots, \boldsymbol{k}_n\} \subseteq \mathbb{Z}^d$. Depending on the basis functions $\varphi_{\boldsymbol{k}}$, index set $\mathcal{I}$, and the nodes $\mathcal{X}$, there are different fast algorithms available that produce a fast matrix-vector multiplication such as the fast Fourier transform (FFT), the non-equispaced fast Fourier transform (NFFT)

or the lattice fast Fourier transform, cf. Table 7.1. While the lattice FFT is applicable for high-dimensional functions, one has to be able to evaluate the function on a reconstructing rank-1 lattice. In our case of scattered data nodes, it is not applicable. Then we have the issue that the NFFT relies on a full grid index set and the curse of dimensionality quickly prevents its efficient application. We proposed the grouped transformations as an extension to the non-equispaced transformations that are able to harvest the advantages of the NFFT for grouped index sets $\mathcal{I}_N(U)$. The main idea was the decomposition of the high-dimensional matrix-vector multiplication into one low-dimensional multiplication for each ANOVA term in U by exploiting the connection between basis coefficients and ANOVA terms. Since all of these multiplications are independent of each other, they can be parallelized and the grouped transformation provide an efficient algorithm for this type of high-dimensional transformation. Since the NFFT and its counterpart for the cosine, the NFCT, are a main building block of the algorithm, we are for now restricted to bases built from the exponential function or the cosine. However, the algorithm can be extended to other bases. The algorithm is implemented in the publicly available Julia package *GroupedTransforms.jl*.

$\mathcal{X}$	$\mathcal{I}$	functions	algorithm	reference
equispaced	full grid	exponential	fast Fourier transform	[Bri88]
equispaced	full grid	cosine	fast Fourier transform (real part)	[Bri88]
scattered	full grid	exponential	non-equispaced fast Fourier transform	[PPST18]
scattered	full grid	cosine	non-equispaced fast cosine transform	[PPST18]
lattice	any	exponential	lattice fast Fourier transform	[Käm13]
Lissajou	any	cosine	lattice fast Fourier transform	[PV17]
scattered	grouped index set	exponential	grouped transformations	[BPS22]
scattered	grouped index set	cosine	grouped transformations	[BPS22]

Table 7.1: Fast algorithms to compute the multiplication of matrix $\boldsymbol{F}_{\mathcal{I}}^{\mathcal{X}}$ and a vector.

We combined all previous results to the ANOVA approximation method. Our given data is represented by scattered the data nodes $\boldsymbol{x}_1, \boldsymbol{x}_2, \dots, \boldsymbol{x}_M \in \mathbb{D}^d$ and the corresponding labels $y_1, y_2, \dots, y_M \in \mathbb{C}$.

Then we assume there is a continuous function in our Lebesgue space $\mathrm{L}_2(\mathbb{D}^d, \omega^{(d)})$ which fulfills $f(\boldsymbol{x}_i) \approx y_i$, $i = 1, 2, \ldots, M$. Applying our main assumption, i.e., we have a low superposition dimension, led to the truncation of the ANOVA decomposition with a superposition threshold and then the truncation of the series expansion of each term which yielded an approximand that is supported on a finite grouped index set. Depending on the specific problem, a sensible choice for the superposition threshold may have to be determined via cross-validation. While our approximand is supported on a finite index set, the basis coefficients are unknown and we determined approximations for them. To this end, we made use of regularized least-squares with iterative LSQR and applied the grouped transformations algorithm for the necessary matrix-vector multiplications. The regularization approach additionally allowed for the incorporation of a priori smoothness information if available. We analyzed the properties of the arising matrices and found that they are well-conditioned if the data nodes $\boldsymbol{x}_i$ are distributed according to the probability density of $\omega^{(d)}$ of the space $\mathrm{L}_2(\mathbb{D}^d, \omega^{(d)})$. However, we proposed multiple examples for systems that cover a number of scenarios such as the very common cases of uniformly distributed data or standard normal distributed data. In a application setting, one may perform well-known min-max normalization or Z-score normalization techniques and then assume such distributions. Bounds for the singular values of the Moore-Penrose inverse in the overdetermined case were obtained with high probability if there is sufficient oversampling. We showed that in our setting we require less oversampling than in the results of [KUV21, MU21].

An analysis of the global sensitivity indices of the initial approximand yielded a method to obtain structural information about the function. Through a number of techniques we suggested, e.g., attribute ranking or global sensitivity cut-off, one is able to reduce the number of involved ANOVA terms further. Moreover, this information may lead to interesting insights into the data. A refitting with the modified approximand, i.e., solving a new least-squares problem, may also bring improvement in the accuracy of the model by laying more emphasis on the important parts of the function. In the end, we obtained an

interpretable approximation of the function.

We analyzed the method and proved bounds on the worst-case L_2 error for functions from Sobolev type spaces and weighted Wiener spaces. While the bound for the Sobolev type spaces has a counterpart in the reproducing kernel Hilbert space setting of [MU21], the L_2 bound for the weighted Wiener spaces is a completely new result. While here the nodes can be drawn once for the entire class, one may also consider individual approximation errors where the nodes are drawn for each function. We have applied Bernstein's inequality, see [SC08, Chapter 6], to obtain such bounds for the L_2 and L_∞ errors. Since bounds on the L_∞ error in the worst-case setting have not yet been proven, we have used the individual bounds to still get results for this setting in Sobolev type spaces and weighted Wiener spaces. The ANOVA approximation method has been implemented in the publicly available Julia package *ANOVAapprox.jl*.

Experiments with synthetic data, i.e., the approximation of functions, showed that the method is able to determine sparsity in the ANOVA decomposition correctly and subsequently produce good approximations. We have considered examples in the periodic and the non-periodic setting. Specifically, we have used sums of products of B-splines as well as the well-known Friedman benchmark functions. The numerical results of the experiments with the Friedman 1 function showed that we are able to determine an approximation for this 10-dimensional function using as few as 200 nodes. Moreover, our attribute ranking as analysis tool yielded better results than experiments with mutual information estimation. A comparison to benchmark results with other well-known machine learning methods showed that we are able to outperform them for Friedman 1 and Friedman 2. Only for Friedman 3, we obtained a second place.

The experiments with publicly available real data sets also showed very promising results. Our method was in most cases able to outperform even ensemble machine learning methods such as gradient boosting machines. The insights from the data analysis proved significant, e.g., for the forest fires data set we were able to reduce the model to 3 important attributes yielding better approximation results than

all other models. The obtained structural information also delivers sensible results. Let us take the California housing data as an example. Here, we detected a two-dimensional interaction between latitude and longitude forming the geographical location. The information obtained by the attribute ranking also fits with the intuitive notion, e.g., what quantities influence the house price.

The idea of the ANOVA approximation method has already been extended to hyperbolic wavelet regression, see [LPU21], and hyperbolic cross approximation. An interesting open problem is the L_∞ worst-case error which would require probabilistic bounds on the ℓ_1 operator norm of the Moore-Penrose inverse.

Bibliography

[Ada03] R. Adams. *Sobolev spaces*. Elsevier, Amsterdam, NL, 2003. (Cited on page 23.)

[Agg15] C. C. Aggarwal. *Data Classification: Algorithms and Applications*. CRC Press, Boca Ration, FL, US, 2015. (Cited on page 10.)

[BBC+94] R. Barrett, M. Berry, T. F. Chan, J. Demmel, J. Donato, J. Dongarra, V. Eijkhout, R. Pozo, C. Romine, and H. V. der Vorst. *Templates for the Solution of Linear Systems: Building Blocks for Iterative Methods*. SIAM, Philadelphia, PA, US, 1994. (Cited on page 99.)

[BD73] F. F. Bonsall and J. Duncan. *Complete Normed Algebras*. Springer, Berlin, Heidelberg, DE, 1973. (Cited on pages 23 and 27.)

[BDL11] P. Binev, W. Dahmen, and P. Lamby. Fast high-dimensional approximation with sparse occupancy trees. *J. Comput. Appl. Math.*, 235(8):2063 – 2076, 2011. doi: 10.1016/j.cam.2010.10.005. (Cited on pages 17 and 155.)

[Bel72] R. E. Bellman. *Dynamic Programming*. Princeton University Press, Princeton, NJ, US, 1972. (Cited on page 10.)

[BG04] H.-J. Bungartz and M. Griebel. Sparse grids. *Acta Numer.*,

13:147–269, 2004. doi: 10.1017/S0962492904000182. (Cited on pages 10, 12, and 21.)

[BG14] J. Baldeaux and M. Gnewuch. Optimal randomized multilevel algorithms for infinite-dimensional integration on function spaces with ANOVA-type decomposition. *SIAM J. Numer. Anal.*, 52(3):1128–1155, 2014. doi: 10.1137/120896001. (Cited on pages 12 and 21.)

[BGM09] G. Beylkin, J. Garcke, and M. Mohlenkamp. Multivariate regression and machine learning with sums of separable functions. *SIAM J. Sci. Comput.*, 31:1840–1857, 2009. doi: 10.1137/070710524. (Cited on pages 17 and 155.)

[BH95] W. L. Briggs and V. E. Henson. *The DFT. An Owner's Manual for the Discrete Fourier Transform*. SIAM, Philadelphia, PA, US, 1995. (Cited on page 67.)

[BHP20] F. Bartel, R. Hielscher, and D. Potts. Fast cross-validation in harmonic approximation. *Appl. Comput. Harmon. Anal.*, 49(2):415–437, 2020. doi: 10.1016/j.acha.2020.05.002. (Cited on page 104.)

[Bjö96] Å. Björck. *Numerical Methods for Least Squares Problems*. SIAM, Philadelphia, PA, US, 1996. (Cited on pages 13 and 99.)

[BKUV17] G. Byrenheid, L. Kämmerer, T. Ullrich, and T. Volkmer. Tight error bounds for rank-1 lattice sampling in spaces of hybrid mixed smoothness. *Numer. Math.*, 136:993–1034, 2017. doi: 10.1007/s00211-016-0861-7. (Cited on pages 22 and 29.)

[Boh17] B. Bohn. *Error Analysis of regularized and unregularized Least-Squares Regression on discretized Function Spaces*. Dissertation, Institut für Numerische Simulation, Universität Bonn, 2017. (Cited on pages 14 and 116.)

[BPS22] F. Bartel, D. Potts, and M. Schmischke. Grouped transformations in high-dimensional explainable ANOVA approximation. *SIAM J. Sci. Comput. (accepted)*, 2022, ArXiv e-prints 2010.10199. (Cited on pages 13, 15, 19, 66, 71, 103, 105, 141, 142, and 185.)

[Bri88] E. O. Brigham. *The Fast Fourier Transform and Its Applications*. Prentice Hall, Englewood Cliffs, NJ, US, 1988. (Cited on pages 12, 65, and 185.)

[Buh03] M. D. Buhmann. *Radial Basis Functions*. Cambridge University Press, Cambridge, UK, 2003. doi: 10.1017/cbo9780511543241. (Cited on page 10.)

[CDW14] P. G. Constantine, E. Dow, and Q. Wang. Active subspace methods in theory and practice: Applications to kriging surfaces. *SIAM J. Sci. Comput.*, 36(4):A1500–A1524, 2014. doi: 10.1137/130916138. (Cited on page 12.)

[CEHW17] P. G. Constantine, A. Eftekhari, J. Hokanson, and R. A. Ward. A near-stationary subspace for ridge approximation. *Comput. Methods Appl. Mech. Engrg.*, 326:402–421, 2017. doi: 10.1016/j.cma.2017.07.038. (Cited on page 12.)

[CJJ12] R. Chitta, R. Jin, and A. K. Jain. Efficient kernel clustering using random Fourier features. In *2012 IEEE 12th International Conference on Data Mining*. IEEE, 2012. doi: 10.1109/icdm.2012.61. (Cited on page 12.)

[CK04] M. Capiński and P. E. Kopp. *Measure, Integral and Probability*. Springer, London, UK, 2004. doi: 10.1007/978-1-4471-0645-6. (Cited on pages 23 and 24.)

[CKNS20] R. Cools, F. Y. Kuo, D. Nuyens, and I. H. Sloan. Fast component-by-component construction of lattice algorithms for multivariate approximation with POD and SPOD weights. *Math. Comp.*, 90(328):787–812, 2020. doi: 10.1090/mcom/3586. (Cited on pages 10 and 29.)

[CM07] P. Cortez and A. Morais. A Data Mining Approach to Predict Forest Fires using Meteorological Data. In *New Trends in Artificial Intelligence, 13th EPIA 2007 - Portuguese Conference on Artificial Intelligence*, pages 512–523, Guimarães, PT, 2007. APPIA. (Cited on pages 169, 170, 171, and 172.)

[CMO97] R. Caflisch, W. Morokoff, and A. Owen. Valuation of mortgage-backed securities using Brownian bridges to reduce effective dimension. *J. Comput. Finance*, 1(1):27–46, 1997. doi: 10.21314/jcf.1997.005. (Cited on pages 11, 21, 39, 52, and 108.)

[CN07] R. Cools and D. Nuyens. An overview of fast component-by-component constructions of lattice rules and lattice sequences. *PAMM*, 7:1022609–1022610, 2007. doi: 10.1002/pamm.200700919. (Cited on page 11.)

[DG14] J. Dick and M. Gnewuch. Infinite-dimensional integration in weighted Hilbert spaces: Anchored decompositions, optimal deterministic algorithms, and higher-order convergence. *Found. Comput. Math.*, 14(5):1027–1077, 2014. doi: 10.1007/s10208-014-9198-8. (Cited on page 47.)

[DG17] D. Dua and C. Graff. UCI machine learning repository, 2017. URL `http://archive.ics.uci.edu/ml`. (Cited on pages 17, 169, 171, 175, and 176.)

[DSWW06] J. Dick, I. H. Sloan, X. Wang, and H. Woźniakowski. Good lattice rules in weighted Korobov spaces with general weights. *Numer. Math.*, 103(1):63–97, 2006. doi: 10.1007/s00211-005-0674-6. (Cited on page 29.)

[DTU18] D. Dũng, V. N. Temlyakov, and T. Ullrich. *Hyperbolic Cross Approximation*. Advanced Courses in Mathematics – CRM Barcelona. Birkhäuser, Cham, CH, 2018. (Cited on pages 27, 29, 37, and 126.)

[FSV12] M. Fornasier, K. Schnass, and J. Vybiral. Learning functions of few arbitrary linear parameters in high dimensions. *Found. Comput. Math.*, 12(2):229–262, 2012. doi: 10.1007/s10208-012-9115-y. (Cited on page 12.)

[GE03] I. Guyon and A. Elisseeff. An introduction to variable and feature selection. *J. Mach. Learn. Res.*, 3:1157–1182, 2003. (Cited on page 158.)

[GH10] M. Griebel and M. Holtz. Dimension-wise integration of high-dimensional functions with applications to finance. *J. Complexity*, 26(5):455–489, 2010. doi: 10.1016/j.jco.2010.06.001. (Cited on pages 12 and 21.)

[GH14] M. Griebel and J. Hamaekers. Fast discrete Fourier transform on generalized sparse grids. In *Sparse Grids and Applications - Munich 2012*, Lect. Notes Comput. Sci. Eng. 97, pages 75–107. Springer, Cham, CH, 2014. doi: 10.1007/978-3-319-04537-5_4. (Cited on pages 10, 22, and 29.)

[GHHR17] M. Gnewuch, M. Hefter, A. Hinrichs, and K. Ritter. Embeddings of weighted Hilbert spaces and applications to multivariate and infinite-dimensional integration. *J. Approx. Theory*, 222:8–39, 2017. doi: 10.1016/j.jat.2017.05.003. (Cited on page 47.)

[GKN+14] I. G. Graham, F. Y. Kuo, J. A. Nichols, R. Scheichl, C. Schwab, and I. H. Sloan. Quasi-Monte Carlo finite element methods for elliptic PDEs with lognormal random coefficients. *Numer. Math.*, 131(2):329–368, 2014. doi: 10.1007/s00211-014-0689-y. (Cited on pages 22 and 29.)

[GKN+18] I. G. Graham, F. Y. Kuo, D. Nuyens, R. Scheichl, and I. H. Sloan. Circulant embedding with QMC: analysis for elliptic PDE with lognormal coefficients. *Numer. Math.*, 140(2):479–511, 2018. doi: 10.1007/s00211-018-0968-0. (Cited on pages 22 and 29.)

[GKNW18] A. D. Gilbert, F. Y. Kuo, D. Nuyens, and G. W. Wasilkowski. Efficient implementations of the multivariate decomposition method for approximating infinite-variate integrals. *SIAM J. Sci. Comput.*, 40(5):A3240–A3266, 2018. doi: 10.1137/17m1161890. (Cited on page 47.)

[GKS10] M. Griebel, F. Y. Kuo, and I. H. Sloan. The smoothing effect of the ANOVA decomposition. *J. Complexity*, 26(5):523–551, 2010. doi: 10.1016/j.jco.2010.04.003. (Cited on pages 47 and 50.)

[GKS16] M. Griebel, F. Y. Kuo, and I. H. Sloan. The ANOVA decomposition of a non-smooth function of infinitely many variables can have every term smooth. *Math. Comp.*, 86(306):1855–1876, 2016. doi: 10.1090/mcom/3171. (Cited on pages 12, 21, and 47.)

[GPT20] M. Goyal, M. Pandey, and R. Thakur. Exploratory analysis of machine learning techniques to predict energy efficiency in buildings. In *8th International Conference on Reliability, Infocom Technologies and Optimization (Trends and Future Directions) (ICRITO)*. IEEE, 2020. doi: 10.1109/icrito48877.2020.9197976. (Cited on pages 169 and 170.)

[Gri06] M. Griebel. Sparse grids and related approximation schemes for higher dimensional problems. In *Foundations of Computational Mathematics (FoCM05), Santander 2005*, pages 106–161, Cambridge, UK, 2006. Cambridge University Press. (Cited on pages 11, 21, and 45.)

[Gu13] C. Gu. *Smoothing Spline ANOVA Models*. Springer, New York, NY, US, 2013. doi: 10.1007/978-1-4614-5369-7. (Cited on page 39.)

[HÖ4] W. Hörmann. *Automatic Nonuniform Random Variate Generation*. Springer, Berlin, Heidelberg, DE, 2004. doi: 10.1007/978-3-662-05946-3. (Cited on page 33.)

[Heg03] M. Hegland. Adaptive sparse grids. *ANZIAM J.*, 44:C335–C353, 2003. doi: 10.21914/anziamj.v44i0.685. (Cited on page 10.)

[Hoc88] J. Hocking. *Topology*. Dover Publications, New York, NY, US, 1988. (Cited on page 26.)

[Hol11] M. Holtz. *Sparse grid quadrature in high dimensions with applications in finance and insurance*. Lecture Notes in Computational Science and Engineering 77. Springer, Berlin, Heidelberg, DE, 2011. doi: 10.1007/978-3-642-16004-2. (Cited on pages 11, 21, 39, and 52.)

[HS52] M. Hestenes and E. Stiefel. Methods of conjugate gradients for solving linear systems. *J. Res. Nat. Bur. Standards*, 49:409–436, 1952. (Cited on page 99.)

[HSS+21] A. Hashemi, H. Schaeffer, R. Shi, U. Topcu, G. Tran, and R. Ward. Generalization bounds for sparse random feature expansions. *ArXiv e-prints 2103.03191*, 2021. (Cited on pages 12, 108, 169, 170, and 176.)

[HTF13] T. Hastie, R. Tibshirani, and J. Friedman. *The Elements of Statistical Learning - Data Mining, Inference, and Prediction*. Springer, New York, NY, US, 2013. (Cited on pages 10, 106, and 167.)

[Käm13] L. Kämmerer. Reconstructing hyperbolic cross trigonometric polynomials by sampling along rank-1 lattices. *SIAM J. Numer. Anal.*, 51:2773–2796, 2013. doi: 10.1137/120871183. (Cited on pages 10, 65, and 185.)

[KKP] J. Keiner, S. Kunis, and D. Potts. NFFT 3.5, C subroutine library. `http://www.tu-chemnitz.de/~potts/nfft`. Contributors: F. Bartel, M. Fenn, T. Görner, M. Kircheis, T. Knopp, M. Quellmalz, M. Schmischke, T. Volkmer, A. Vollrath. (Cited on pages 13, 65, and 70.)

[KKP09] J. Keiner, S. Kunis, and D. Potts. Using NFFT3 - a software library for various nonequispaced fast Fourier transforms. *ACM Trans. Math. Software*, 36:Article 19, 1–30, 2009. doi: 10.1145/1555386.1555388. (Cited on pages 13, 65, and 70.)

[KLT21] Y. Kolomoitsev, T. Lomako, and S. Tikhonov. Sparse grid approximation in weighted Wiener spaces. *ArXiv e-prints 2111.06335*, 2021. (Cited on pages 23, 27, 116, and 125.)

[KM15] Y. Kokkinos and K. G. Margaritis. Multithreaded local learning regularization neural networks for regression tasks. In *Engineering Applications of Neural Networks*, pages 129–138. Springer, Cham, CH, 2015. doi: 10.1007/978-3-319-23983-5_13. (Cited on pages 169, 170, 178, and 179.)

[KMU16] T. Kühn, S. Mayer, and T. Ullrich. Counting via entropy: new preasymptotics for the approximation numbers of Sobolev embeddings. *SIAM J. Numer. Anal.*, 54(6):3625–3647, 2016. doi: 10.1137/16m106580x. (Cited on pages 23, 27, and 29.)

[KN16] F. Y. Kuo and D. Nuyens. Application of quasi-Monte Carlo methods to elliptic PDEs with random diffusion coefficients: A survey of analysis and implementation. *Found. Comput. Math*, 16(6):1631–1696, 2016. doi: 10.1007/s10208-016-9329-5. (Cited on pages 22 and 29.)

[KNP+17] F. Y. Kuo, D. Nuyens, L. Plaskota, I. H. Sloan, and G. W. Wasilkowski. Infinite-dimensional integration and the multivariate decomposition method. *J. Comput. Appl. Math.*, 326:217–234, Dec. 2017. doi: 10.1016/j.cam.2017.05.031. (Cited on pages 12, 21, and 47.)

[KPV15] L. Kämmerer, D. Potts, and T. Volkmer. Approximation of multivariate periodic functions by trigonometric polynomials based on rank-1 lattice sampling. *J. Complexity*, 31:543–576, 2015. doi: 10.1016/j.jco.2015.02.004. (Cited on pages 10, 22, and 29.)

[KSG04] A. Kraskov, H. Stögbauer, and P. Grassberger. Estimating mutual information. *Phys. Rev. E*, 69(6), 2004. doi: 10.1103/physreve.69.066138. (Cited on pages 10 and 160.)

[KSS12] F. Y. Kuo, C. Schwab, and I. H. Sloan. Quasi-Monte Carlo finite element methods for a class of elliptic partial differential equations with random coefficients. *SIAM J. Numer. Anal.*, 50:3351 – 3374, 2012. doi: 10.1137/110845537. (Cited on pages 22 and 29.)

[KSWW09] F. Y. Kuo, I. H. Sloan, G. W. Wasilkowski, and H. Woźniakowski. On decompositions of multivariate functions. *Math. Comp.*, 79(270):953–966, 2009. doi: 10.1090/s0025-5718-09-02319-9. (Cited on pages 39, 40, 41, 45, and 46.)

[KUV21] L. Kämmerer, T. Ullrich, and T. Volkmer. Worst case recovery guarantees for least squares approximation using random samples. *Constr. Approx.*, 54:295–352, 2021. doi: 10.1007/s00365-021-09555-0. (Cited on pages 13, 96, 100, 102, 116, 119, and 186.)

[LO06] R. Liu and A. B. Owen. Estimating mean dimensionality of analysis of variance decompositions. *J. Amer. Statist. Assoc.*, 101(474):712–721, 2006. doi: 10.1198/016214505000001410. (Cited on pages 11, 12, 21, 39, 47, 51, and 52.)

[LPU21] L. Lippert, D. Potts, and T. Ullrich. Fast hyperbolic wavelet regression meets ANOVA. *ArXiv e-prints 2108.13197*, 2021. (Cited on pages 14, 116, 129, and 188.)

[LTOS19] Z. Li, J.-F. Ton, D. Oglic, and D. Sejdinovic. Towards a unified analysis of random Fourier features. In *Proceedings of the 36th International Conference on Machine Learning*, K. Chaudhuri and R. Salakhutdinov, eds., Proceedings of Machine Learning Research 97, pages 3905–3914. PMLR, 2019. (Cited on page 12.)

[MLH03] D. Meyer, F. Leisch, and K. Hornik. The support vector machine under test. *Neurocomputing*, 55(1):169 – 186, 2003. doi: 10.1016/S0925-2312(03)00431-4. (Cited on pages 17, 141, 155, 156, 158, 161, and 163.)

[MSM18] G. Montavon, W. Samek, and K.-R. Müller. Methods for interpreting and understanding deep neural networks. *Digit. Signal Process.*, 73:1–15, 2018. doi: 10.1016/j.dsp.2017.10.011. (Cited on page 10.)

[MU21] M. Moeller and T. Ullrich. L_2-norm sampling discretization and recovery of functions from RKHS with finite trace. *Sampl. Theory Signal Process. Data Anal.*, 19(2):13, 2021. doi: 10.1007/s43670-021-00013-3. (Cited on pages 13, 96, 100, 101, 102, 116, 119, 120, 186, and 187.)

[Nev79] P. G. Nevai. Orthogonal polynomials. *Mem. Amer. Math. Soc.*, 18(213):v+185, 1979. doi: 10.1090/memo/0213. (Cited on page 101.)

[Nie92] H. Niederreiter. *Random Number Generation and Quasi-Monte Carlo Methods*. CBMS-NSF Regional Conference Series in Applied Mathematics. SIAM, Philadelphia, PA, US, 1992. doi: 10.1137/1.9781611970081. (Cited on pages 12 and 21.)

[NK14] J. A. Nichols and F. Y. Kuo. Fast CBC construction of randomly shifted lattice rules achieving $O(n^{-1+\delta})$ convergence for unbounded integrands over $\mathbb{R}^s$ in weighted spaces with POD weights. *J. Complexity*, 30(4):444–468, Aug. 2014. doi: 10.1016/j.jco.2014.02.004. (Cited on pages 33 and 35.)

[NP20] R. Nasdala and D. Potts. Transformed rank-1 lattices for high-dimensional approximation. *Electron. Trans. Numer. Anal.*, 53:239–282, 2020. doi: 10.1553/etna_vol53s239. (Cited on pages 33 and 35.)

[NW08] E. Novak and H. Woźniakowski. *Tractability of Multivariate Problems*. European Mathematical Society, Zürich, CH, 2008. (Cited on page 10.)

[ORA16] L. Oneto, S. Ridella, and D. Anguita. Tikhonov, Ivanov and Morozov regularization for support vector machine learning. *Mach. Learn.*, 103(1):103–136, 2016. doi: 10.1007/s10994-015-5540-x. (Cited on page 104.)

[Owe13] A. B. Owen. *Monte Carlo Theory, Methods and Examples*. Art B. Owen, Stanford, CA, US, 2013. URL `https://artowen.su.domains/mc/`. (Cited on pages 11 and 40.)

[Owe19] A. Owen. Effective dimension of some weighted pre-Sobolev spaces with dominating mixed partial derivatives. *SIAM J. Numer. Anal.*, 57(2):547–562, 2019. doi: 10.1137/17m1158975. (Cited on page 57.)

[PPST18] G. Plonka, D. Potts, G. Steidl, and M. Tasche. *Numerical Fourier Analysis*. Applied and Numerical Harmonic Analysis. Birkhäuser, Cham, CH, 2018. doi: 10.1007/978-3-030-04306-3. (Cited on pages 12, 13, 31, 65, 70, 79, and 185.)

[PS82] C. C. Paige and M. A. Saunders. LSQR: An algorithm for sparse linear equations and sparse least squares. *ACM Trans. Math. Software*, 8:43–71, 1982. doi: 10.1145/355984.355989. (Cited on pages 13 and 99.)

[PS21a] D. Potts and M. Schmischke. Approximation of high-dimensional periodic functions with Fourier-based methods. *SIAM J. Numer. Anal.*, 59(5):2393–2429, 2021. doi: 10.1137/20m1354921. (Cited on pages 12, 14, 18, 21, 22, 40, 66, 71, 95, 117, 141, and 142.)

[PS21b] D. Potts and M. Schmischke. Interpretable approximation of high-dimensional data. *SIAM J. Math. Data Sci.*, 3(4):1301–1323, 2021, 2103.13787. doi: 10.1137/21M1407707. (Cited on pages 18, 71, 95, 106, 141, and 169.)

[PS22a] D. Potts and M. Schmischke. Learning multivariate functions with low-dimensional structures using polynomial bases. *J. Comput. Appl. Math.*, 403:113821, 2022. doi: 10.1016/j.cam.2021.113821. (Cited on pages 14, 18, 22, 40, 71, 95, 102, and 141.)

[PS22b] D. Potts and M. Schmischke. Interpretable transformed ANOVA approximation on the example of the prevention of forest fires. *Front. Appl. Math. Stat.*, 8:795250, 2022. doi: 10.3389/fams.2022.795250. (Cited on pages 19, 33, 95, 106, and 169.)

[PV16] D. Potts and T. Volkmer. Sparse high-dimensional FFT based on rank-1 lattice sampling. *Appl. Comput. Harmon. Anal.*, 41:713–748, 2016. (Cited on pages 17, 141, and 142.)

[PV17] D. Potts and T. Volkmer. Multivariate sparse FFT based on rank-1 chebyshev lattice sampling. In *International Conference on Sampling Theory and Applications (SampTA)*. IEEE, 2017. doi: 10.1109/sampta.2017.8024341. (Cited on pages 141 and 185.)

[PVG+11] F. Pedregosa, G. Varoquaux, A. Gramfort, V. Michel, B. Thirion, O. Grisel, M. Blondel, P. Prettenhofer, R. Weiss, V. Dubourg, J. Vanderplas, A. Passos, D. Cournapeau, M. Brucher, M. Perrot, and E. Duchesnay. Scikit-learn: Machine learning in Python. *J. Mach. Learn. Res.*, 12:2825–2830, 2011. (Cited on page 160.)

[RFA99] H. Rabitz and O. F. Alis. General foundations of high dimensional model representations. *J. Math. Chem.*, 25:197–233, 1999. doi: 10.1023/A:1019188517934. (Cited on pages 11, 21, and 39.)

[Ros14] B. C. Ross. Mutual information between discrete and continuous data sets. *PLoS ONE*, 9(2):e87357, 2014. doi: 10.1371/journal.pone.0087357. (Cited on pages 10 and 160.)

[RR08] A. Rahimi and B. Recht. Random features for large-scale kernel machines. In *Advances in Neural Information Processing Systems 20*, J. Platt, D. Koller, Y. Singer, and S. Roweis, eds., Red Hook, NY, US, 2008. Curran Associates. URL `https://proceedings.neurips.cc/paper/2007/file/013a006f03dbc5392effeb8f18fda755-Paper.pdf`. (Cited on page 12.)

[Sam19] W. Samek. *Explainable AI : interpreting, explaining and visualizing deep learning*. Springer, Cham, CH, 2019. (Cited on page 10.)

[SB] M. Schmischke and F. Bartel. GroupedTransforms.jl Julia Package. doi: 10.5281/zenodo.5654702. (Cited on page 91.)

[SC08] I. Steinwart and A. Christmann. *Support Vector Machines*. Springer, New York, NY, US, 2008. (Cited on pages 10, 14, 129, and 187.)

[Scha] M. Schmischke. ANOVAapprox.jl Julia Package. doi: 10.5281/zenodo.5657977. Contributor: F. Bartel. (Cited on page 110.)

[Schb] M. Schmischke. NFFT3.jl Julia Package. doi: 10.5281/zenodo.5656757. Contributors: F. Bartel, T. Riemer. (Cited on pages 70 and 91.)

[Sch18] M. Schmischke. Nonequispaced fast Fourier transform (NFFT) interface for Julia. *ArXiv e-prints 1810.09891*, 2018. (Cited on page 70.)

[SJ94] I. H. Sloan and S. Joe. *Lattice Methods for Multiple Integration*. Clarendon Press Oxford University Press, Oxford, NY, US, 1994. (Cited on page 10.)

[Sob90] I. M. Sobol. On sensitivity estimation for nonlinear mathematical models. *Matem. Mod.*, 2:112–118, 1990. (Cited on pages 12, 51, and 52.)

[Sob01] I. M. Sobol. Global sensitivity indices for nonlinear mathematical models and their Monte Carlo estimates. *Math. Comput. Simulation*, 55(1-3):271–280, 2001. doi: 10.1016/s0378-4754(00)00270-6. (Cited on pages 12, 51, and 52.)

[Sut18] R. Sutton. *Reinforcement Learning: An Introduction*. The MIT Press, Cambridge, MA, US, 2018. (Cited on page 32.)

[SW01] I. H. Sloan and H. Woźniakowski. Tractability of multivariate integration for weighted Korobov classes. *J. Complexity*, 17:697–721, 2001. doi: 10.1006/jcom.2001.0599. (Cited on page 27.)

[TA06] S. W. Taylor and M. E. Alexander. Science, technology, and human factors in fire danger rating: the Canadian experience. *Int. J. Wildland Fire*, 15(1):121, 2006. doi: 10.1071/wf05021. (Cited on page 172.)

[Tor] L. Torgo. Regression data sets. `https://www.dcc.fc.up.pt/~ltorgo/Regression/DataSets.html`. (Cited on pages 17, 169, 178, and 179.)

[Tre06] F. Treves. *Topological Vector Spaces, Distributions and Kernels*. Courier Corporation, Mineola, NY, US, 2006. (Cited on page 24.)

[Tre20] L. Trefethen. *Approximation theory and approximation practice*. SIAM, Philadelphia, PA, US, 2020. (Cited on page 31.)

[Tro11] J. A. Tropp. User-friendly tail bounds for sums of random matrices. *Found. Comput. Math.*, 12(4):389–434, 2011. doi: 10.1007/s10208-011-9099-z. (Cited on pages 13, 96, 100, and 102.)

[Vil85] A. Villani. Another note on the inclusion $L^p(\mu) \subseteq L^q(\mu)$. *Am. Math. Mon.*, 92(7):485, 1985. doi: 10.2307/2322503. (Cited on page 24.)

[Wen04] H. Wendland. *Scattered Data Approximation*. Cambridge University Press, Cambridge, UK, 2004. doi: 10.1017/cbo9780511617539. (Cited on page 10.)

[Wer18] D. Werner. *Funktionalanalysis*. Springer, Berlin, Heidelberg, DE, 8 edition, 2018. (Cited on pages 22 and 25.)

[WH11] C. F. J. Wu and M. S. Hamada. *Experiments - Planning, Analysis, and Optimization*. John Wiley & Sons, New York, NY, US, 2011. (Cited on pages 12 and 108.)

[XSSW21] Y. Xie, B. Shi, H. Schaeffer, and R. Ward. Shrimp: Sparser random feature models via iterative magnitude pruning. *ArXiv e-prints 2112.04002*, 2021. (Cited on page 12.)

[YL06] M. Yuan and Y. Lin. Model selection and estimation in regression with grouped variables. *J. R. Stat. Soc. Ser. B Stat. Methodol.*, 68(1):49–67, 2006. doi: 10.1111/j.1467-9868.2005.00532.x. (Cited on page 105.)

[YLM+12] T. Yang, Y.-F. Li, M. Mahdavi, R. Jin, and Z.-H. Zhou. Nyström method vs random Fourier features: A theoretical and empirical comparison. In *Proceedings of the 25th International Conference on Neural Information Processing Systems (NIPS'12)*, Vol. 1, page 476–484, Red Hook, NY, US, 2012. Curran Associates. (Cited on page 12.)